THE ASTROPHYSICAL JOURNAL

An International Review of Spectroscopy and Astronomical Physics

FOUNDED IN 1895 BY GEORGE E. HALE AND JAMES E. KEELER

VOLUME 108

JULY–NOVEMBER 1948

THE UNIVERSITY OF CHICAGO PRESS
CHICAGO, ILLINOIS

CAMBRIDGE UNIVERSITY PRESS, LONDON

PUBLISHED JULY, SEPTEMBER, NOVEMBER, 1948

COMPOSED AND PRINTED BY THE UNIVERSITY OF CHICAGO PRESS
CHICAGO, ILLINOIS, U.S.A.

CONTENTS

NUMBER 1

NUMBER 2

NUMBER 3

VOLUME 108 NUMBER 1

THE ASTROPHYSICAL JOURNAL

AN INTERNATIONAL REVIEW OF SPECTROSCOPY AND ASTRONOMICAL PHYSICS

JULY 1948

THE UNIVERSITY OF CHICAGO PRESS
CHICAGO, ILLINOIS, U.S.A.

July 1948 Vol. 108, No. 1

THE ASTROPHYSICAL JOURNAL

AN INTERNATIONAL REVIEW OF SPECTROSCOPY AND ASTRONOMICAL PHYSICS

The Astrophysical Journal is published bimonthly by the University of Chicago at the University of Chicago Press, 5750 Ellis Avenue, Chicago, Illinois, during July, September, November, January, March, and May. ¶The subscription price is $12.00 a year; the price of single copies is $3.00. Orders for service of less than a full year will be charged at the single-copy rate. ¶Postage is prepaid by the publishers on all orders from the United States and its possessions, Argentina, Bolivia, Brazil, Chile, Colombia, Costa Rica, Cuba, Dominican Republic, Ecuador, Guatemala, Haiti, Republic of Honduras, Mexico, Morocco (Spanish Zone), Nicaragua, Panama, Paraguay, Peru, Rio de Oro, El Salvador, Spain (including Balearic Islands, Canary Islands, and the Spanish Offices in Northern Africa; Andorra), Spanish Guinea, Uruguay, and Venezuela. ¶Postage is charged extra as follows: for Canada and Newfoundland, 42 cents on annual subscriptions (total $12.42); on single copies, 7 cents (total $3.07); for all other countries in the Postal Union, 96 cents on annual subscriptions (total $12.96), on single copies 16 cents (total $3.16). ¶Patrons are requested to make all remittances payable to The University of Chicago Press, in United States currency or its equivalent by postal or express money orders or bank drafts.

The following is an authorized agent:

For the British Empire, except North America and Australasia: The Cambridge University Press, Bentley House, 200 Euston Road, London, N.W. 1, England. Prices of yearly subscriptions and of single copies may be had on application.

Claims for missing numbers should be made within the month following the regular month of publication. The publishers expect to supply missing numbers free only when losses have been sustained in transit, and when the reserve stock will permit.

Business correspondence should be addressed to The University of Chicago Press, Chicago 37, Illinois.

Communications for the editors and manuscripts should be addressed to: W. W. Morgan, Editor of THE ASTROPHYSICAL JOURNAL, Yerkes Observatory, Williams Bay, Wisconsin.

Line drawings and photographs should be made by the author, and all marginal notes such as co-ordinates, wave lengths, etc., should be included in the cuts. It will not be possible to set up such material in type.

One copy of the corrected galley proof should be returned as soon as possible to the editor, Yerkes Observatory, Williams Bay, Wisconsin. Authors should take notice that the manuscript will not be sent to them with the proof.

The cable address is "Observatory, Williamsbay, Wisconsin."

The articles in this journal are indexed in the *International Index to Periodicals*, New York, N.Y.

Applications for permission to quote from this journal should be addressed to The University of Chicago Press, and will be freely granted.

Entered as second-class matter, July 31, 1940, at the Post-Office at Chicago, Ill., under the Act of March 3, 1879.
Acceptance for mailing at special rate of postage provided for in United States Postal Act of October 3, 1917, Section 1103, amended February 28, 1925.

[PRINTED IN U.S.A.]

THE ASTROPHYSICAL JOURNAL

AN INTERNATIONAL REVIEW OF SPECTROSCOPY AND ASTRONOMICAL PHYSICS

VOLUME 108 JULY 1948 NUMBER 1

THE SYSTEM OF ALGOL

OLIN J. EGGEN

Washburn Observatory

Received April 16, 1948

ABSTRACT

Seventeen photoelectrically determined epochs of minimum light obtained by Stebbins and Huffer between 1919 and 1942 and one minimum observed in 1947 by the author are discussed. These observations, together with the long series of minima available since discovery of this eclipsing star, indicate that the system contains four stars; (1) and (2) the brighter and fainter components of the eclipsing pair, $P = 2.867$ days; (3) a component with orbital period of 1.873 years; and (4) a component with orbital period of 188.4 years. The preliminary elements for the orbit of the longest period are $P = 188.4$ years, $e = 0.25$, $T = 1841.60$, $\omega = 87°$, and $a \sin i = 37 \times 10^8$ km. The photoelectric minima confirm the 1.873-year variation found spectroscopically by McLaughlin, but require slight alterations to the orbital elements; that is, $e = 0.14$, $\omega = 90°$, $T = 1903.20$, and $a \sin i = 78 \times 10^6$ km.

In addition to the variation of the eclipsing period caused by the 1.873- and 188.4-year orbital motions, the presence of a variation with a period of 32 years is confirmed. If this variation is ascribed to apsidal motion in the close pair created by tidal effects within the eclipsing system, then the mean central density of the eclipsing components is characterized by $K = 0.0036$, that is, a polytrope of index 3.8. The total mass of the system, 11 $\odot$, is found to be distributed as follows: $m_1 = 5.0\ \odot$, $m_2 = 1.0\ \odot$, $m_3 = 1.2\ \odot$, and $m_4 = 3.8\ \odot$.

From observations made by Dr. Stebbins in six colors at both maximum and minimum light, it is found that the fainter eclipsing component has the color of a subgiant F8 star with a visual absolute magnitude of +2.5 mag., making it quite similar to the fainter components of such systems as TX Ursae Majoris, U Cephei, and U Sagittae. No evidence of light from the third component is found, which fact is compatible with the assumption that it is a dG star of luminosity normal for its mass, $m_3 = 1.2\ \odot$. The fourth component apparently has the characteristics of a white dwarf.

Algol has been known as a variable star since 1670, when Montanari not only noted the variation in light but actually observed it at minimum brightness on November 8 of that year.[1] The general character of the light-variation was first established by Goodricke[2] in 1783. He found that the successive minima occurred at intervals of about $2^d\ 20^h\ 49^m$. Goodricke is usually credited with having first offered the explanation that the light-variation was caused by the eclipses of Algol by a dark star; but it is often overlooked that he offered this suggestion as an alternative to the rotation of a spotted star. The star has been the subject of such a large amount of literature that it would be impossible to present here a full reference list, but a summary of the knowledge up to 1935 may be found in R. G. Aitken's book, *The Binary Stars*.[3]

[1] A. Porro, *A.N.*, **127**, 41, 1891.

[2] *Phil. Trans. R. Soc.*, **73**, 482, 1783.

[3] New York: McGraw-Hill Book Co., 1935.

PERIOD

Approximately 80 years after the discovery of the variability of Algol in the period of 2.87 days, F. Argelander[4] demonstrated the existence of fluctuations in the period. The first thorough discussion of these fluctuations was made by S. C. Chandler[5] in 1888. He proposed to explain the alternate anticipations and retardations of Algol's eclipses on the basis of a light-equation resulting from the motion of the eclipsing stars in a large orbit about a center of mass common to them and to a third body. He found that this third star had a period of 130 years in an orbit of such size that light required 350 minutes to cross it. He also found, superposed upon this large variation in the departure of the predicted epochs of minimum light in the eclipsing pair, two other undulations with periods of 37 and 17 years and amplitudes of 18 and 3 minutes, respectively.

An alternative to Chandler's hypothesis was put forward by F. Tisserand[6] in 1895. Although similar considerations had been rejected by Chandler during the course of his investigation, as being insufficient, the form proposed by Tisserand was extremely plausible, namely, a rotation of the line of apsides caused by polar flattening of the stars and the presence of a slight amount of eccentricity in the orbit. This idea was carried forward in the next major investigation of the period of Algol by J. Hellerich.[7] From consideration of all minima then available, he derived the expression

$$\text{Minimum} = \text{JD } 2378497.7588 + 2^{d}.86731077\,E$$

$$(P = 158 \text{ years}) \qquad + 0^{d}.1266 \sin 0^{\circ}.01786\,(E - 176),$$

$$(P = 32 \text{ years}) \qquad + 0^{d}.0119 \sin 0^{\circ}.08762\,(E - 188).$$

Chandler's period for the third body is then increased to 158 years, and the 37-year period is reduced to 32 years; the 17-year period does not appear in Hellerich's solution.

Fifteen years later a new solution was made by K. Ferrari,[8] using the observed minima which had become available after 1919. Ferrari found that he could best represent the observations by the expression

$$\text{Minimum} = \text{JD } 2378497.7563 + 2^{d}.87631085\,E$$

$$(P = 158 \text{ years}) \qquad + 0^{d}.1294 \sin 0^{\circ}.01799\,(E - 289),$$

$$(P = 32 \text{ years}) \qquad + 0^{d}.0125 \sin 0^{\circ}.08455\,(E + 32),$$

$$(P = 55 \text{ years}) \qquad + 0^{d}.0061 \sin 0^{\circ}.05155\,(E - 892).$$

The first and second periodic terms remain essentially unchanged from Hellerich's study, but a new term with a period of 55 years and amplitude of 9 minutes has been added.

The present discussion of the period is based upon a series of photoelectric determinations of the times of minima, begun by Dr. Stebbins in 1919 and continued by Stebbins and Huffer at the Washburn Observatory through 1942. These observations cover the interval 1919–1942 well enough, especially when they are supplemented by a few photoelectric determinations made by W. M. Smart[9] and J. S. Hall.[10] The photoelectric minima for 1919, 1920, and 1921 have been previously published,[11] but all the photoelectric minima used are given in Table 1.

[4] *Bonn-Beob.*, **7**, 353, 1869.
[5] *A.J.*, **7**, 165, 1888; **22**, 39, 1901.
[6] *C.R.*, **120**, 125, 1895.
[7] *A.N.*, **209**, 227, 1919.
[8] *A.N.*, **253**, 225, 1934.
[9] *M.N.*, **97**, 402, 1937.
[10] *Ap. J.*, **90**, 449, 1939.
[11] J. Stebbins, *Pub. A.A.S.*, **4**, 331, 1923.

Ferrari's article contains normal minima up to 1934. The residuals from these normals, when they are compared with the linear elements,

$$\text{Minimum} = \text{JD } 2378497.7867 + 2^{d}.86731077\,E\,, \qquad (1)$$

and the residuals from the photoelectric observations listed in Table 1 from the same elements are plotted in Figure 1. It is obvious that the periodic variation of the largest amplitude cannot be regarded as of purely sinusoidal form. Rather, the curve suggests a light-equation in a large elliptical orbit, the companion star being near apastron at the present time. The solid curve, plotted in Figure 1, was computed from the elements

$$P = 188.4 \text{ years}\,, \qquad e = 0.25\,,$$

$$T = 1841.60 = 5{,}300\,E, \qquad \omega = 87^{\circ}\,,$$

$$a \sin i = 0^{d}.1380 = 24 \text{ A.U.} = 37 \times 10^{8} \text{ km}\,.$$

To find the true period of the eclipsing pair, we would logically start by removing the long-period variation with the use of the foregoing elliptical elements. However, although

TABLE 1

PHOTOELECTRIC MINIMA OF ALGOL

1 No.	2 t	3 E'	4 O−C₁	5 Phase	6 O−C₂	7 O−C₃	8 Remarks
1	2422321.5947	0	+0ᵈ0050	0ᵖ966	+0ᵈ0050	+0ᵈ0025	
2	22619.7866	104	− .0039	.400	− .0025	+ .0005	
3	22986.8075	232	+ .0006	.929	+ .0036	+ .0014	
4	23715.1018*	486	− .0031	.099	+ .0021	− .0005	
5	24477.8073	752	− .0035	.113	+ .0017	+ .0001	
6	24847.6881	881	− .0063	.651	− .0019	+ .0005	
7	25163.0986	991	− .0005	.118	+ .0027	+ .0011	
8	25303.5921	1040	− .0055	.411	− .0028	+ .0003	
9	25588.8582	1136	− .0016	.737	− .0002	+ .0004	
10	25917.2037	1254	+ .0007	.219	+ .0005	+ .0007	
11	26272.7512	1378	+ .0011	.737	− .0008	− .0001	
12	26674.1750	1518	+ .0008	.326	− .0027	− .0006	
13	27107.1454	1669	+ .0065	.908	+ .0017	− .0002	
14	27313.5904	1741	+ .0049	.256	− .0003	+ .0006	Smart
15	28113.5689	2020	+ .0024	.433	− .0027	+ .0005	Hall
16	28434.7110	2132	+ .0052	.897	+ .0009	− .0008	
17	28483.4560	2149	+ .0058	.972	+ .0017	− .0007	Smart
18	28821.7917	2267	− .0017	.465	− .0046	− .0012	Hall
19	29552.9550*	2522	− .0038	.534	− .0033	.0000	
20	30639.6721	2901	+ .0009	.117	+ .0057	+ .0040	
21	32451.8152	3533	+0.0007	0.779	+0.0033	+0.0032	

* Only minima Nos. 4–19 were used in the discussion, as explained in the text.

NOTES TO TABLE 1

4. Residuals from the linear ephemeris. Min. = JD 2422321.5897 + 2ᵈ86731525 E. Plotted in Fig. 2.
5. Phase in the 1.873-year orbit counted from 1902.70. To obtain the corresponding phases from McLaughlin's elements, these are to be reduced by 0ᵖ09.
6. Residuals after removing the effects of the expression, Deviation = −0ᵈ0055 sin 0°.145 E, as shown in Fig. 2.
7. Final residuals.
8. All minima are by Stebbins and Huffer unless otherwise noted.

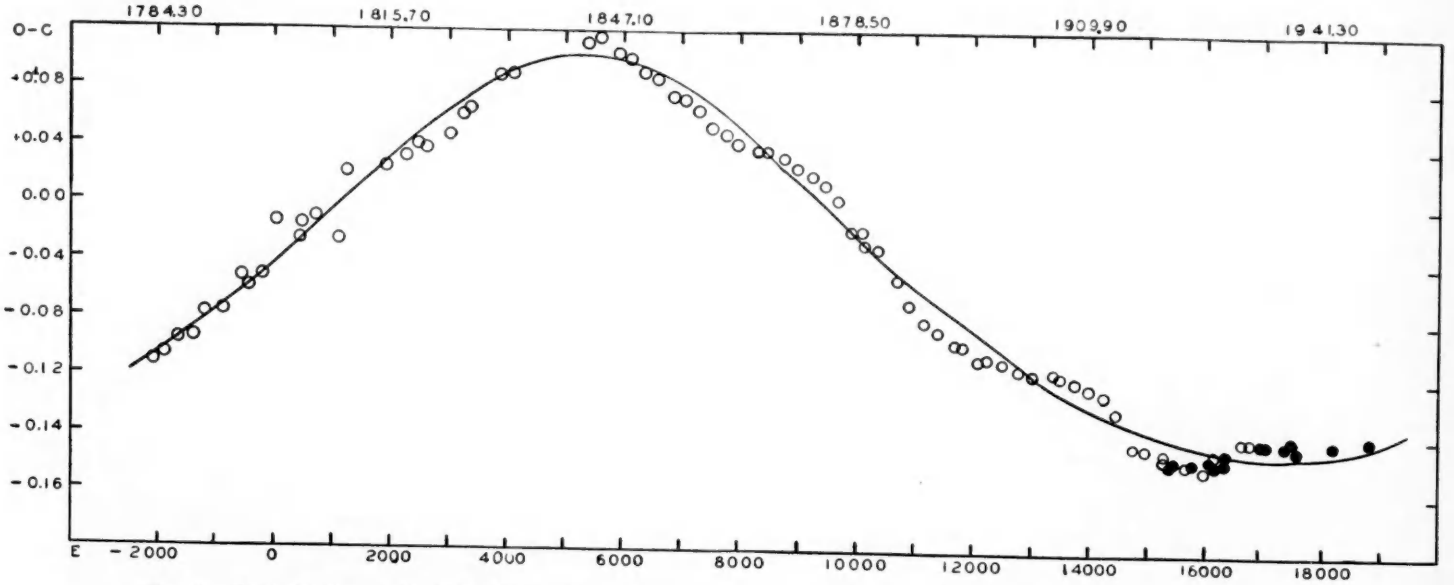

FIG. 1.—The light-time residuals for the normal minima given by Ferrari. The photoelectric minima are represented by filled circles

these elements are probably as well established as those for most visual binaries, the remaining uncertainty prevents using them for the elimination of the long-period variation with the precision necessary for the subsequent discussion. As can be seen from Figure 1, in an attempt to satisfy all the observations prior to 1840, the period may have been made too long. On the other hand, the fact that the single 1947 minimum stands above the computed curve, whereas, from the trend of the other observations, it would be expected to fall below, may be only the effect of the other fluctuations in the system. Furthermore, the 32-year period, detected by both Hellerich and Ferrari, and similar

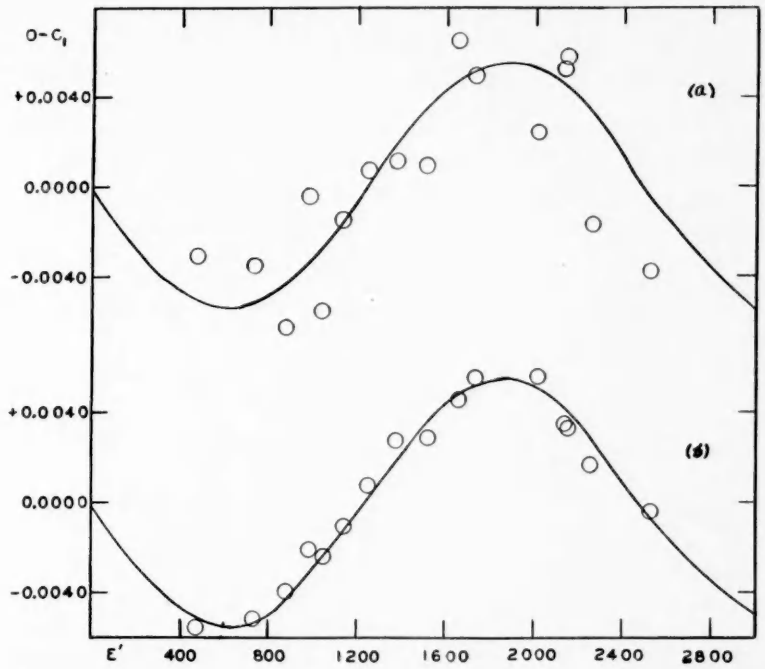

FIG. 2.—*a*) Plot of residuals $O-C_1$ computed from the elements, Minimum = JD 2422321.5897 + $2^d86731525\ E'$. The computed curve represents the term, Deviation = $-0^d0055 \sin 0°.145\ E'$ (period = 19.5 years).

b) Same as *a*, with the exception that the observations have been corrected for motion in the 1.873-year orbit.

to Chandler's 37-year variation, must be accounted for. The effect of this term can be easily seen in the sinusoidal variation of the residuals in Figure 1 about the computed curve. Unfortunately, this variation is appreciably distorted, a fact especially evident in observations made prior to 1900; and, as was true of the 188.4-year variation, it is not yet possible to disentangle it completely from the 55-year term found by Ferrari and other purely secular variations with which it appears to be confounded.

In view of the impossibility, at present, of totally removing the effects of the 32- and 55-year variations, we must investigate the possibility of minimizing these effects before discussing the photoelectric minima. From Figure 1, where the photoelectric results are plotted as filled circles, it is evident that if we restrict ourselves to the observations between 1923 and 1939—that is, minima 4–19 in Table 1—we may regard the motion in the 188-year orbit as nearly linear. Moreover, the 17-year sequence of photoelectric minima falls between one trough and the following crest of the 32-year sinusoidal variation.

Column 4 of Table 1 contains the residuals, O − C_1, left from the observed photoelectric minima when compared with the linear ephemeris

$$\text{Minimum} = \text{JD } 2422321.5897 + 2^d.86731525\,E' . \quad (2)$$

These residuals are plotted in Figure 2, *a*. The computed curve was determined by graphical means to give the best fit to the observations. This curve is represented by the expression

$$\text{Deviation} = -0^d.0055 \sin 0^\circ.145\,E'$$

and serves only as an interpolation formula for removing the neglected effects of the 32-year variation. When the observations are corrected by this expression, there remain

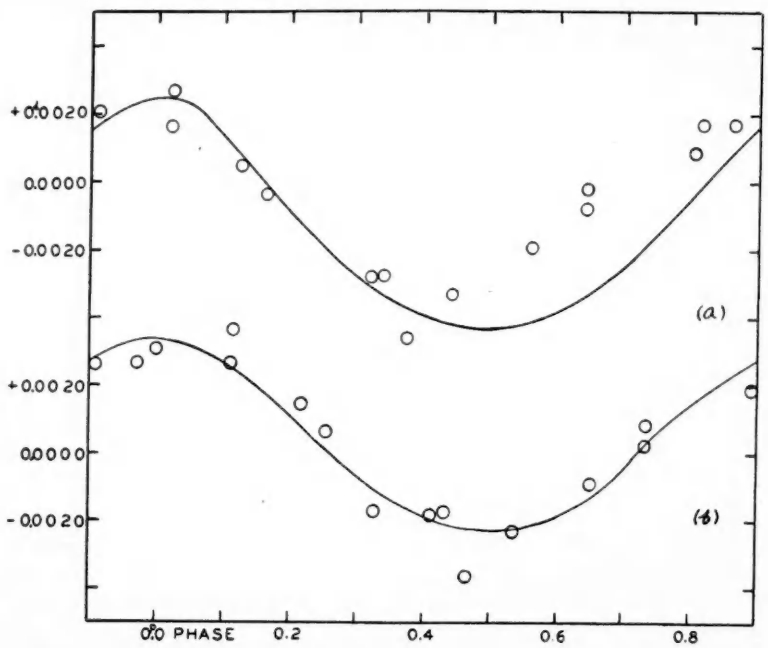

FIG. 3.—*a*) Plot of the residuals, O−C_2, of Table 1. The computed curve is based upon McLaughlin's spectroscopic elements for the 1.873-year variation.

b) Same as *a*, with the exception that the computed curve is based on the elements for the 1.873-year variation derived from the light-times alone.

the residuals O − C_2 given in column 6 of Table 1. There are left for investigation the effects of the light-time in the 1.873-year orbit covered by the eclipsing system and the additional companion detected by D. McLaughlin.[12] The presence of this companion was found from the periodic variation in the velocity of the center of mass of the eclipsing components, and a similar effect upon the epoch of eclipses can be anticipated. Figure 3, *a*, shows a plot of O − C_2 assembled on the 1.873-year period. The smooth curve is computed from McLaughlin's spectroscopic elements. The trend of the residuals appears to confirm the presence of the third body with an orbital period of 1.873 years, but some changes in the elements are necessary to remove the systematic deviations from

[12] *Pub. Obs. U. Michigan*, **6**, 20, 1934.

the computed curve. New elements, derived from the times of minima alone and compared with those found by McLaughlin, are shown in the accompanying tabulation. The

	McLaughlin (Spectroscopic)	Eggen (Light-Time)
P	1.873 years	1.873 years (assumed)
e	0.25	0.14
T	1903.38	1903.20
ω	93°	90°
$a \sin i$	88×10^6 km	78×10^6 km

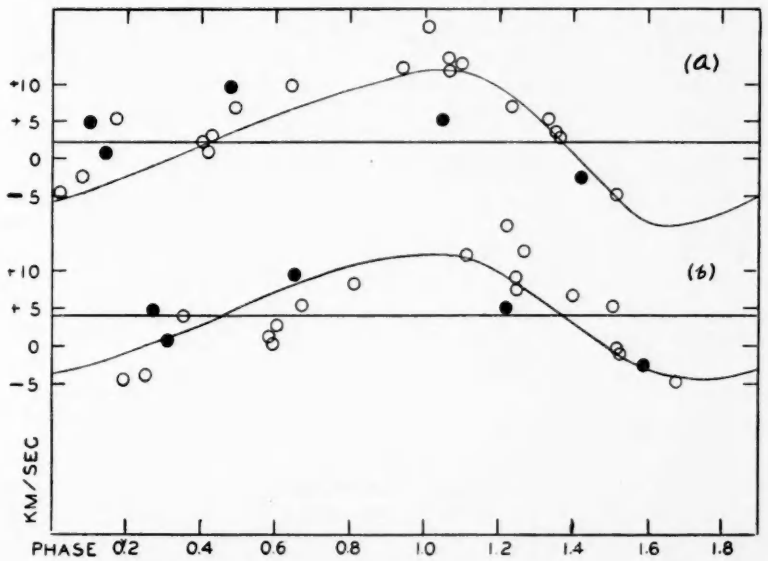

FIG. 4.—*a*) Radial velocities of the center of mass of the eclipsing pair listed by McLaughlin. The phases are computed, and the smooth curve derived, from McLaughlin's spectroscopic elements for the 1.873-year orbit. The filled circles represent observations rejected by McLaughlin.

b) Same as *a*, but the phases and computed curve are from the elements derived from the light-times alone.

residuals, O − C$_2$, are plotted in Figure 3, *b*, as in Figure 3, *a*, but the computed curve of Figure 3, *b*, is based on the new elements. Figure 2, *b*, contains a plot of the residuals O − C$_2$ after correction for the effects of the 1.873-year motion.

The velocities of the center of mass of the eclipsing system, listed by McLaughlin,[12] are plotted in Figure 4. The computed curve in Figure 4, *a*, is that of McLaughlin's spectroscopic elements; that in Figure 4, *b*, is based on the elements derived here from the light-times. McLaughlin has applied systematic corrections to the observations of Schlesinger,[13] +4.0 km/sec; Vogel,[14] +5.0 km/sec; and McLaughlin, +1.3 km/sec. The systematic corrections found necessary to bring all observations into alignment from the present elements are −4.0, +5.0, and 0.0 km/sec, respectively, for the same observers. The filled circles in Figure 4 represent the observations of Vogel and Scheiner and those

[13] *Pub. Allegheny Obs.*, **1**, 25, 1908.

[14] *A.N.*, **123**, 289, 1890.

of Belopolsky[15] for the epoch 1893.73, all of which were rejected by McLaughlin in his solution for the elements. McLaughlin also found a systematic trend in the residuals which pointed to the existence of a fourth body, but this cannot be identified with the fourth body responsible for the large variation in the period of 188.4 years, discussed above. This systematic trend of the velocity residuals is removed by the elements derived here from the light-times alone. The star is still under observation at Ann Arbor,[16] and further refinement of the orbit of the third body can await these results. The essential thing is that the presence of this third star is fully confirmed by the photometric data.

Summing our present knowledge of the periods of Algol, we find two variations, of periods 188.4 and 1.873 years, which may be attributed to orbital motion. There remain the 32-year-period fluctuation, which has persisted through all investigations, and the 55-year term, detected by Ferrari. W. J. Luyten[17] has discussed the theoretically expected fluctuations in the period, taking into account the apsidal motion and nodal regression in the close pair as a result of both the perturbations by the third body and the tidal distortions of the eclipsing components themselves. He finds that, if the 32-year variation is a result of apsidal motion caused by tidal effects within the system, its amplitude would lead to an eccentricity of the short-period orbit of 0.014. Following H. N. Russell,[18] this would lead to a central density of the system characterized by the parameter $K = 0.0036$ corresponding to a mean polytrope of index 3.8. However, if the 55-year variation in the period is to be attributed to this cause, the eccentricity in the short-period orbit would be 0.007, and $K = 0.0021$. The variation upon which the larger K depends appears to be the most definitely established, but neither value can be ruled out by the present photometric data. The period of the apsidal motion resulting from perturbations of the eclipsing system by the third body is found by Luyten to be of the order of 360,000 eclipsing orbital periods and can, in the present discussion, be safely neglected.

TABLE 2

PHOTOMETRIC ELEMENTS OF THE ECLIPSING SYSTEM

$k = 0.85$	$r_1 = 0.207$
$\alpha_0 = 0.700$	$r_2 = 0.244$
$L_1 = 0.925$	$\cos i = 0.144$
$L_2 = 0.075$	

After 150 years of observation, it is still not possible to predict future epochs of minimum light of Algol with any great accuracy, as is evident from the residuals $O - C_3$ for the minima of 1942 and 1947 (Nos. 20 and 21 in Table 1), which fall outside the interval considered here. The best that can be done at present is to adopt the last photoelectric minimum with the period of expression (2): that is

$$\text{Minimum} = \text{JD } 2432520.6303 + 2.86731525\,E\,.$$

The characteristics of the eclipses and the ordinary photometric elements of the close pair are quite well established. The values, in the usual notation, found by J. Stebbins,[19] are in Table 2. Z. Kopal[20] has recently derived new elements from a light-curve, composed of the combined observations of Stebbins[19] and Smart[9] and including the effects of limb darkening and tidal distortion on the light-curve within minima. However, since

[15] *Pulkowa Mitt.*, **4**, 171, 1911.

[16] L. Goldberg, *A.J.*, **53**, 145, 1948.

[17] *Zs. f. Ap.*, **15**, 97, 1938.

[18] *Ap. J.*, **90**, 642, 1939; also T. E. Sterne, *M.N.*, **99**, 415, 1939; and S. Chandrasekhar, *M.N.*, **93**, 451, 1933.

[19] *Ap. J.*, **53**, 105, 1921.

[20] *Ap. J.*, **96**, 399, 1942.

these two curves show differences in the depths of the minima, this procedure is somewhat risky. The results obtained by Kopal, however, differ only slightly from those given in Table 2, which we shall adopt for the present purpose.

We now assume four masses in the system of Algol to be designated as follows:

1 = Brighter star of the eclipsing system, period = 2.867 days,
2 = Fainter star of the eclipsing system, period = 2.867 days,
3 = Component with orbital period of 1.873 years,
4 = Component with orbital period of 188.4 years.

In addition to the effects of the orbital motion of these four components, the period of the eclipsing pair is subject to two other variations, with periods of 32 and 55 years. The period and amplitude of the 32-year variation are quite well established, and its cause is tentatively ascribed to apsidal motion in the eclipsing pair.

With the orbital dimensions and periods here derived for the four components, it is possible to obtain an estimate of the distribution of mass within the system. The mass function of the close pair, from spectroscopic elements given by McLaughlin,[12] is

$$f = \frac{(m_2^3 \sin^3 i)}{(m_1 + m_2)^2} = 0.0256 \odot .$$

Since the spectrum of but one component is visible, we must resort to indirect means to obtain the ratio of masses. McLaughlin has carried out an extensive study of the limb-effect, that is, the effect of the rotation of the partially eclipsed star on the spectrum observed within primary minimum. He found certain asymmetries in this effect which "have rather violently shaken the author's [McLaughlin's] faith in the rotation as a means of determining the dimensions of eclipsing variables."[12] These asymmetries are tentatively ascribed to a blending of the lines of the bright star and the third body or to the presence of extra lines as a result of the passage of light from the bright star through the atmosphere of the fainter one. Fortunately, there remains still another means of obtaining the mass-ratio of the close pair. Struve and Elvey[21] have derived the rotational velocity of component 1 from the "dish-shaped" contours of the *Mg* 4481 line in the spectra taken in full light. They derive the value $V_e = 60$ km/sec with an estimated maximum range of 15 km/sec. They also observed the limb-effect within minimum and found that it leads to a somewhat smaller rotational velocity than do the observations at full light. However, the rotational velocity from their observations of the limb-effect is larger than that derived by McLaughlin from spectra of lower dispersion. They conclude that the finite resolving power of the spectrograph obliterates the deepest point of the spectral line so that, by increasing the dispersion still further, the measured effect should bring the equatorial velocities derived by the two methods into better agreement. In view of these considerations, we shall adopt the value derived by Struve and Elvey from the observations at full light, that is $V_e = 60$ km/sec. If we now assume synchronism between the orbital and the rotational velocities of component 1, this rotational velocity corresponds to a radius of 2.3×10^6 km. Moreover, from the photometric solution, this radius is known to be 0.21 times the radius of the relative orbit, so the latter should amount to 10.9×10^6 km. On the other hand, the radius of the absolute orbit of component 1 is found by McLaughlin to be 1.8×10^6 km. Combining these two values, we find $m_1 = 5\ m_2$, which, when substituted in the mass function of the eclipsing system, gives $m_1 = 5.0 \odot$ and $m_2 = 1.0 \odot$.

The mass function of the third component and the eclipsing pair is found to be $f = 0.040 \odot$, using the elements derived from the light-times. Before we may use this value for obtaining the mass of the third component, we necessarily must know the inclination of the third orbit. A provisional determination of the astrometric orbit by Alden[22] led

[21] *M.N.*, **91**, 670, 1931.

[22] *Pub. A.A.S.*, **5**, 250, 1924.

to $i = 58°$. A later value, $i = 78°$, attributed to A. Thomas, is quoted by Kopal.[20] Thomas,[23] still later, states only ". . . . the semi-axis major of the long-period orbit [1.873 years] is of about the same size as the parallax and the inclination of the orbit is high." He finds an absolute trigonometric parallax of $0''.033 \pm 0''.003$. The trigonometric parallax given in Schlesinger's parallax catalogue[24] is $0''.031 \pm 0''.004$. Because of the difficulty of the astrometric measures and the presence of the still larger, 188.4-year motion, these values for the inclination must be used with caution. There are so few multiple systems known for which orbital elements have been well enough determined that it is not possible to draw any general conclusions concerning the relative orientations of the orbital planes. However, for the present purpose, we shall adopt 75° as the inclination of the third orbit, as indicated by the meager astrometric data, with the caution that the resulting mass, $m_3 = 1.2\ \odot$, may be only a minimum value.

The available evidence for the hypothetical fourth component is much more doubtful, but the elements derived here, together with the same assumption for the inclination of the orbital plane as for the third component, give a mass $m_4 = 3.8\ \odot$. The resulting total mass of the system is then approximately $11\odot$. Anticipating the discussion to follow concerning the total light of the system, we are forced to assume that if the presence of the fourth component is to be accepted, then, to explain the photometric results, the

TABLE 3

SIX COLORS OF ALGOL

JD 243+		Phase	U	V	B	G	R	I
0611.8917.....	β–α	+21^h.44	−1^m.028	−0^m.342	+0^m.012	+0^m.312	+0^m.678	+1.025
0610.9546.....	β–α	+ 0.32	+0.232	+0.880	+1.172	+1.417	+1.690	+1.917
0611.0118.....	β–α	− 1.06	−0.016	+0.646	+0.952	+1.217	+1.510	+1.777
.....	β–dG6	+21.44	−1.27	−0.96	−0.44	−0.04	+0.47	+0.92
.....	α–dG6	.....	+0.09	−0.28	−0.11	−0.02	+0.13	+0.21

star must possess a luminosity similar to a white dwarf and must contribute no appreciable light to the system. Adopting the parallax, $\pi = 0''.032$, for the system, we find the maximum possible separation in the wide pair to be $2''.5$, a much smaller value than the separation of similar stars such as the companions to Sirius and 40 Eridani.

SIX-COLOR OBSERVATIONS

In 1942 Dr. Stebbins observed Algol in six colors, twice at maximum and twice near minimum light with the six-color photometer[25] on the 60-inch reflector at Mount Wilson, and he has turned the results over to me for discussion. The photoelectric minimum determined 1 month later at Madison fixes accurately the phases of the observations. The differences in magnitude between β and α Persei in all six colors, to three decimals, are given in Table 3. The colors in the fourth and fifth lines of Table 3 are referred to the mean of B, G, and R for each star. The observations on 2 nights near maximum of β have been combined into one at average phase 21.44 hours. The step-by-step, rather involved, discussion of the six-color observations is tabulated in Table 4. The various lines of this table contain the following information:

1. The designation of the colors.
2. The reciprocal wave lengths.

[23] *Pub. A.A.S.*, **10**, 261, 1943.

[24] F. Schlesinger, *General Catalogue of Stellar Parallaxes* (New Haven: Yale University Observatory, 1935).

[25] J. Stebbins and A. E. Whitford, *Mt. W. Contr.*, No. 712; *Ap. J.*, **102**, 100, 1945.

3. Δm's for Algol between phases 21^h44 and 0^h32.
4. Δm of line 3 reduced to fractional light of the system.
5. The intensities of line 4, rectified by the expression

$$l_r = \frac{(l+c)+2b}{l+b},$$

where b and c are the coefficients in the expression $l = 1 - b\cos\theta - c\cos 2\theta$, b expressing the reflection effect and c the ellipticity of figure of the components. Using Milne's formulae for the reflection effect, Russell[26] has shown that

$$b = 0.347\left(\frac{E_2L_1}{E_1}\,r_1^2 - \frac{E_1L_2}{E_2}\,r_2^2\right)\sin i,$$

$$c = \left\{0.073\left(\frac{E_2L_1}{E_1}\,r_2^2 - \frac{E_1L_2}{E_2}\,r_1^2\right) - \tfrac{1}{2}\,(C_1L_1 + C_2L_2)\right\}\sin^2 i,$$

TABLE 4

SOLUTION FOR SIX COLORS OF COMPONENTS 1 AND 2

1	U	V	B	G	R	I	Colors
2.....	2.83	2.37	2.05	1.75	1.39	0.97	$1/\lambda$
3.....	1^m260	1^m222	1^m160	1^m105	1^m012	0^m892	$m_\beta(+0^h32) - m_\beta(+21^h44)$
4.....	0.313	0.324	0.344	0.361	0.394	0.440	$l(+0^h32)$
5.....	0.316	0.338	0.386	0.414	0.454	0.496	$l_r(+0^h32)$
6.....	1^m012	0^m988	0^m940	0^m905	0^m832	0^m752	$m_\beta(-1^h06) - m_\beta(+21^h44)$
7.....	0.394	0.402	0.421	0.434	0.464	0.500	$l(-1^h06)$
8.....	0.396	0.414	0.456	0.482	0.517	0.546	$l_r(-1^h06)$
9.....	0.706	0.697	0.688	0.686	0.685	0.684	$\alpha(+0^h32)$
10.....	0.624	0.617	0.609	0.608	0.607	0.606	$\alpha(-1^h06)$
11.....	0.969	0.949	0.892	0.854	0.797	0.737	$L_1(+0^h32)$
12.....	0.968	0.949	0.893	0.852	0.796	0.749	$L_1(-1^h06)$
13.....	0.968	0.949	0.892	0.853	0.796	0.743	L_1 (mean)
14.....	0.032	0.051	0.108	0.146	0.204	0.257	L_2+2b
15.....	0.030	0.039	0.062	0.087	0.136	0.203	L_2
16.....	3^m81	3^m52	3^m02	2^m65	2^m16	1^m73	$m_2 - m_\beta(+21^h44)$
17.....	$+1^m20$	$+0^m91$	$+0^m41$	-0^m04	-0^m45	-0^m88	Line 15 referred to (B+G+R)/3
18.....	-1^m27	-0^m96	-0^m44	-0^m04	$+0^m45$	$+0^m92$	Obs. colors of $\beta(21^h44)$
19.....	-0^m07	-0^m05	-0^m03	0^m00	$+0^m02$	$+0^m04$	Colors of component 2
20.....	$+0^m04$	$+0^m06$	$+0^m12$	$+0^m17$	$+0^m25$	$+0^m32$	$m_1 - m_\beta(+21^h44)$
21.....	-0^m14	-0^m12	-0^m06	-0^m01	$+0^m07$	$+0^m14$	Line 21 referred to (B+G+R)/3
22.....	-1^m41	-1^m08	-0^m50	-0^m05	$+0^m54$	$+1^m06$	Colors of component 1

where the E's are the luminous efficiencies of the radiation from the facing hemispheres of the components and the C's are the photometric ellipticities of the stars. The geometrical elements were taken from Table 2 and are assumed to be invariant with wave length. The E's were computed from Planck's formula for each color, with $T_1 = 12{,}500°$ and $T_2 = 6000°$. Figure 5 shows the predicted values, smooth curve, and available observed values for b. The deviation of the well-determined value at 4500 A from the computed curve undoubtedly results from the inadequacy of the black-body simplifications in the

[26] *Ap. J.*, **102**, 1, 1945.

violet end of the spectrum. We have interpolated the U and V values for b, used in the rectification, from the trend of the observed values alone. The observed ellipticities vary widely but are all small, and the computed values have been used for all colors.

6. Same as line 3 for phase -1.06 hour.
7. Same as line 4 for phase -1.06 hour.
8. Same as line 5 for phase -1.06 hour.

9 and 10. The values of the photometric depths of the eclipse at the various wave lengths based on the value $\alpha_0 = 0.700$ at 4500 as given in Table 3. The variation with wave length is governed by the same considerations as those given for the reflection effect in line 5. The values for the ultraviolet points are the most uncertain, in view of the scarcity of available material concerning radiation from beyond the Balmer limit.

11 and 12. The fractional light of the system, L_1, due to component 1, computed from the values in lines 5 and 8 by the expression $L = (1 - l_r)/\alpha$.

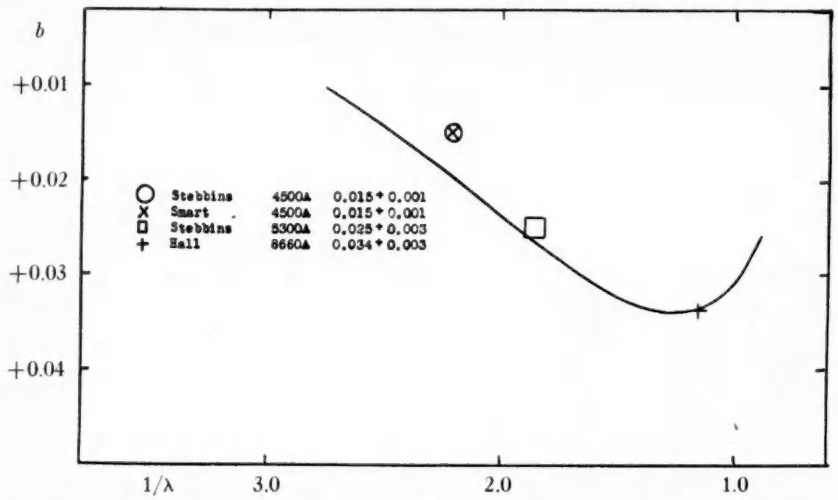

FIG. 5.—The values for the coefficient of the reflection effect, b, computed from black-body considerations (*smooth curve*), and the observed values.

13. Mean values of L_1 from lines 11 and 12. A check on our result is offered by the value of L_1 given in Table 2, determined by Stebbins at an effective wave length of 4500 A. We find, interpolating for $1/\lambda = 2.22$, $L_1 = 0.923$ as compared to 0.925 given in Table 2.

14. The light of component 2 plus the light reflected from component 2. We are here anticipating a later conclusion that only the light of the eclipsing system is observed.

15. The light of the companion freed of reflected light.

16. Δm's between the light of the system at 21.44 hours and the light of component 2. Taking the effective wave length of visual light as 5300 A and the visual magnitude of Algol at phase 21.44 hours as 2.2 mag., then $m_v(2) = 5^m.0$. Adopting for the parallax of the system $\pi = 0''.032$, we find $M_v(2) = +2^m.5$.

17. Δm's of line 16 referred to $(B + G + R)/3$.
18. Observed colors of components 1 and 2 at phase 21.44 hours.
19. Colors of component 2.
20. Δm's between Algol at phase 21.44 hours and the light of component 1 .
21. Δm's of line 20 referred to $(B + G + R)/3$.
22. Colors of component 1.

In Table 5 we have gathered the resulting colors of the two components and com-

pared them with known colors of similar stars. The colors of 31 Comae match those of component 2 quite well. The agreement in the ultraviolet is, in part, accidental, for this point is very sensitive to the values of a and b used in the reductions. Indeed, the argument may be applied in reverse; that is, the agreement in the ultraviolet with the run of the other colors is verification of our adopted values for a and b. The star 31 Comae is classified as F8 III by W. W. Morgan.[27] Its absolute visual magnitude is +2.3 according to the Mount Wilson observers,[28] which agrees well with the value +2.5 mag. found for component 2. The available data concerning the masses and luminosities of secondary

TABLE 5

COLORS OF ALGOL 1 AND 2 COMPARED WITH SIMILAR STARS

Star	Sp.	U	V	B	G	R	I	V−I
17 Tau	B7	-1^m38	-1^m03	-0^m49	-0^m05	$+0^m54$	$+1^m08$	-2^m11
υ Her	B8	−1.26	−1.00	−0.46	−0.05	+0.52	+1.06	−2.06
Mean		−1.32	−1.02	−0.48	−0.05	+0.53	+1.07	−2.08
Algol 1	B8	−1.41	−1.08	−0.50	−0.05	+0.54	+1.06	−2.14
31 Com	gF8	−0.13	−0.07	−0.02	0.00	+0.01	+0.06	−0.13
Algol 2		−0.07	−0.05	−0.03	0.00	+0.02	+0.04	−0.09

TABLE 6

ALGOL COMPARED WITH SIMILAR ECLIPSING SYSTEMS

Star	Period	Sp.	M_v	m	ρ	Authority
U Sge 1	3^d381	B9	-0^m4	6.7⊙	0.15⊙	Joy, *Ap. J.*, **71**, 349, 1930
U Sge 2		gG2	+1.8	1.2	.01	
TX UMa 1	3.063	B9	0.0	3.0	.20	Huffer and Eggen, *Ap. J.*, **105**, 217, 1947
TX UMa 2		gF2	+2.6	0.9	.01	Hiltner, *Ap. J.*, **101**, 108, 1945
U Cep* 1	2.493	B8	−0.2	3.5	.21	Dugan, *Princeton Contr.*, No. 5, 1920
U Cep 2		gG2	+2.0	1.1	0.02	Struve, *Ap. J.*, **99**, 222, 1944
Mean 1		B9	−0.2	4.3	0.18	
Mean 2		gF8	+2.2	1.1	0.01	
Algol 1		B8	−0.2	5.0	0.16	
Algol 2		(gF8)	+2.5	1.0	0.01	

* As a result of peculiar asymmetries in the velocity-curves of U Cephei, the values assigned to the masses of the components are particularly uncertain (Z. Kopal, *Harvard Bull.*, No. 914, 1940).

components of eclipsing systems similar to Algol are collected in Table 6. The absolute magnitude of component 1 of the Algol system was derived in the same manner as that for component 2 explained above. Taking the means of the values for three systems—U Sagittae, TX Ursae Majoris, and U Cephei—we find good agreement with special type, absolute magnitude, and mass of the Algol eclipsing system.

DISCUSSION

Thus far we have assumed that all the observed light of the system is contributed by the eclipsing components alone. One consequence of this assumption is that light-

[27] *Ap. J.*, **104**, 245, 1946. [28] W. S. Adams *et al.*, *Mt. W. Contr.*, No. 511; *Ap. J.*, **81**, 57, 1935.

curves made in different wave lengths should show, after allowance is made for the effect of limb darkening, equal photometric depths of the primary eclipse, α_0. We have adopted $\alpha_0 = 0.700$ at 4500 A in Table 4. From Stebbins' observations with the selenium photometer[29] we find rectified depths of primary and secondary minima to be, respectively, 0.620 and 0.055 in light-units. Stebbins, also with the selenium cell,[29] found the difference in magnitude between Algol and α Persei to be 0.14 mag. at phase 21.44 hours. From the six-color observations, for which α Persei was also used for comparison, we find that this value would obtain at 5300 A. Comparison of the 1910 selenium observations at phases 0.32 and -1.06 hours, counted from mid-primary eclipse, with the present results also indicate 5300 A as the effective wave length of the selenium photometer. Using the value of $k = 0.85$ in Table 2 and $\alpha_0 = 1 - \lambda_1 + (1 - \lambda_2)/Q$, we find $\alpha_0 = 0.695$. Also, interpolating in line 12 of Table 4 at 5300 A, we obtain $L_1 = 0.872$ and $\alpha_0 = (1 - \lambda_1)/L_1 = 0.709$. The mean, $\alpha_0 = 0.702$, is in excellent agreement with the adopted value of $\alpha_0 = 0.700$ at 4500 A. Hall[10] has also obtained a light-curve of Algol, using α Persei as a comparison star. Interpolating in the six-color wave lengths for Hall's magnitude differences between Algol and α Persei at phases 21.44, 0.32, and -1.06 hours, we find conflicting values for the effective wave length of his observations. These interpolated values range from 9000 A near maximum light to 8400 A for both phases within eclipse. Moreover, Hall also determined this magnitude difference, at phase 21.4 hours, to be 0.325 ± 0.006 mag. at 5500 A. From the six-color data, this value would obtain at 5800 A. Some of the difficulty, in the longer wave lengths, is undoubtedly caused by the fact that the difference in magnitude between β and α Persei is varying most rapidly with wave length in this region, and the interpolation over the rather wide range between the I and R points of the six-color observations is somewhat precarious. From the infrared observations, Hall finds $k = 0.79$ and $\alpha_0 = 0.683$. He estimates the probable error in k to be 10 per cent, which will affect α_0 by an amount of about the same order of magnitude.

We therefore have found no appreciable influence of the light of the third component, but a small percentage increase in the light of the system in the infrared could easily have escaped detection. If we postulate a dG star for component 3, the observational evidence is satisfied. We have found that the mass of this star is approximately that of the sun, and, on the assumption of its dwarf nature, it will therefore be approximately 2 mag. fainter than component 2. Furthermore, what little light it might contribute to the system would then be distributed with wave length in an almost identical manner as component 2, making its detection all the more unlikely.

The evidence against the presence of any contribution of light from the fourth component is still stronger, which fact, together with the large value found for the mass, $m_4 = 3.8\ \odot$, precludes the possibility that it is either a main-sequence star or itself a binary composed of two main-sequence stars. On the other hand, its large mass and apparently low luminosity suggest that it may be a white dwarf. No white dwarf with a mass as large as that assigned to m_4 is known at present, the upper limit of white-dwarf masses, predicted by the current theories,[30] being $5.75\ \odot\ \mu_e^{-2}$, where μ_e is the "molecular weight." Values determined for μ_e range from 1.3 to 2.0, giving limiting masses of 1.5–3.4 $\odot$, respectively. The lack of knowledge concerning the inclination of the orbital plane introduces the largest factor of uncertainty into the mass derived for m_4. However, if the masses derived here for the components of Algol seem largely hypothetical, they can at least be considered closer to the truth than can Vogel's classical values of $\frac{4}{9}$ and $\frac{3}{9}\ \odot$ for the eclipsing system.

I am indebted to Dr. Joel Stebbins for making available his photoelectric determinations of the epochs of minima and the six-color observations, as well as for much helpful advice during the course of this investigation.

[29] *Ap. J.*, **21**, 185, 1910.

[30] G. P. Kuiper, *Coll. internat. d'ap.* (Paris, 1941).

THE SYSTEM OF 44 i BOOTIS

OLIN J. EGGEN
Washburn Observatory
Received April 16, 1948

ABSTRACT

Two series of photoelectric observations of the combined light of this triple system are discussed, one series by Stebbins and Huffer in 1930 and the other by the author in 1947. Approximate photometric elements are derived from the 1930 light-curve. A difference in the total light of the system at the two maxima is found from the 1930 observations; and also a peculiar distortion of the light-curve at maximum, suspected in the 1930 results, is confirmed by the 1947 observations.

A combination of the photometric and spectroscopic elements yields masses of 1.0 ⊙ and 0.5 ⊙ for the eclipsing components. These masses are at variance with the near-equality of luminosity of the stars, inferred from the depths of the minima and the relative intensities of the spectral lines. This apparent violation of the mass-luminosity relation is characteristic of the W Ursae Majoris type systems and is perhaps due to the presence of large amounts of reflected light within the system which permits the secondary component to be seen only by reflection. This hypothesis is supported by the relatively small orbital inclinations derived for most of these systems.

A combination of the spectrographic, visual, and photometric orbits of the triple system shows the brighter visual component, $m = 1.0 \odot$, and $M_v = +4^m.63$, and the brighter eclipsing component, $m = 1.0 \odot$, and $M_v = +4^m.6$, to be very similar to the sun.

It is found that the change in period of the eclipsing system is not entirely due to motion in the visual orbit. An examination of the well-studied W Ursae Majoris type systems indicates that intrinsic changes in the period may be characteristic of these stars.

The visual binary now known as 44 i Bootis was discovered by W. Herschel in 1781. On the discovery night he entered in his observing book:

> Aug. 17 [1781]. Double, considerably unequal. Both W [white]. With 227 [power] they seem almost to touch or at most $\frac{1}{4}$ diameter of S [southernmost star] asunder; with 460, $\frac{1}{2}$ or $\frac{3}{4}$ diameter of S. This is a fine object to try a telescope, and a miniature of alpha Geminorum.[1]

The most recent discussion of the observations of this important double star is the one published by K. Aa. Strand[2] in 1937. His final elements, which we shall adopt throughout the ensuing discussion, are

$$P = 219.5 \text{ years}, \qquad a = 3''.609,$$

$$T = 1790.0, \qquad i = 83°.46,$$

$$e = 0.42, \qquad \omega = 58°.85.$$

The fainter component of the visual pair was found by members of the Mount Wilson staff to have a spectrum resembling that of W Ursae Majoris,[3] a short-period variable star the spectrum of which is characterized by rotationally broadened lines. J. Schilt,[4] from plates taken with the 60-inch reflector at Mount Wilson in 1926, found the star to be a variable as suspected and with a period of something more than a quarter of a day. It is of some interest to note that the variation of one or both components had been previously suspected by several observers of the visual pair. These early observations are summarized by Miss Agnes Clerke.[5]

[1] *Phil. Trans. R. Soc.*, **72**, 216, 1790.

[2] *Ann. Leiden*, **18**, 98, 1937.

[3] W. S. Adams *et al.*, *Mt. W. Contr.*, No. 199; *Ap. J.*, **53**, 53, 1921.

[4] *Mt. W. Contr.*, No. 316; *Ap. J.*, **64**, 215, 1926.

[5] *Nature*, **39**, 55, 1888.

In 1929, G. P. Kuiper[6] investigated the photographs of the visual pair taken by Hertzsprung in 1915 and 1919 and by Münch in 1922 and 1926 and confirmed the variability found by Schilt. There have been several investigations of the light-variations of the fainter component of the visual double, including a photographic study by Plaut[7] at Leiden in 1939, a photoelectric study by Shapley and Calder of Harvard in 1937,[8] a two-color study by Nikonov in 1940,[9] and an unpublished photoelectric investigation by Stebbins and Huffer at the Washburn Observatory in 1930. These last observations, which have been turned over to me for discussion, and an additional series of observations by myself in 1947 form the basis of the present investigation.

TABLE 1

COMPARISON STARS FOR 44 i BOOTIS

HR		R.A. (1900)	Decl. (1900)	m_v	Sp.
5618	44 i Boo	15^h00^m5	+48° 3′	4.86	G2–G2
5581	.....	14 53.0	+50 3	5.68	F5
5635	.....	15 3.4	+54 56	5.21	G2

TABLE 2

CONSTANCY OF THE COMPARISON STARS

JD	5635>5581	Residual	No.	Observer*	JD	5635>5581	Residual	No.	Observer*
2426040...	0^m012	-0^m010	16	S	2426068...	0^m026	$+0^m004$	16	S
44...	.025	+ .003	12	H	74...	.023	− .001	18	S
47...	.020	− .002	18	S	88...	.027	+ .005	10	S
54...	.020	− .002	12	H	89...	0.025	+0.003	8	S
55...	.021	− .001	18	S					
63...	0.023	+0.001	16	H	Mean.	0.022	±0.003	142	.....

* S = Stebbins; H = Huffer.

The Washburn observations of 1930 consist of measures made of the combined light of the visual pair on 10 nights. The two comparison stars used are described in Table 1. A neutral shade-glass was necessary on the variable to equalize the light. A test of the constancy of the comparison stars is given in Table 2. For some reason, the result on the first night is discordant by 0.01 mag., but the two stars may be considered constant. The normal differences of magnitude, in the sense of HR 5581 being brighter than 44 i Bootis, are given in Table 3, where the phases are computed from the elements

$$\text{Minimum} = \text{JD } 2426058.8554 + 0^d26780708\,E\,, \qquad (1)$$

and n indicates the number of sets, of three observations each, comprising each normal. These normals are plotted in Figure 1.

There is some doubt as to the difference in magnitude between the components of the visual pair at maximum light of the eclipsing system; but for the present purpose, in order to secure approximate photometric elements, the value 0.76 mag. in photographic

[6] *B.A.N.*, No. 165, 1929.

[7] *B.A.N.*, No. 3 1, 1939.

[8] *Harvard Bull.*, No. 907, p. 13, 1937.

[9] *Bull. Abastumani Ap. Obs.*, **4**, 1, 1940.

light, given by Schilt, has been adopted. The normal magnitudes, after the observations were reduced to the light of the eclipsing system alone, are given in the third column of Table 3. The light of the uneclipsed stars was found to vary as

$$l = 1.0000 - 0.0383 \sin\theta - 0.0296 \cos\theta - 0.2302 \cos^2\theta ,$$
$$\pm 0.0019 \quad \pm 0.0014 \qquad \pm 0.0024 \qquad \pm 0.0056$$

with the resulting probable error of a single normal between minima of ± 0.005 mag. or ± 0.002 mag. referred to the total light of the visual components. For purposes of comparison, (1) the mean photoelectric light-curve determined by Shapley and Calder in

TABLE 3

NORMAL MAGNITUDES OF 44 i BOOTIS

Phase	Obs. Δm	Corr. Δm	O−C	Phase	Obs. Δm	Corr. Δm	O−C
0P000	−0m050	+0m530	0m000	0P491	−0m012	+0m376	−0m001
.020	− .043	+ .500	+ .008	.526	− .004	+ .345	+ .003
.040	− .027	+ .436	− .013	.558	+ .018	+ .265	+ .006
.067	− .004	+ .456	+ .005	.590	+ .047	+ .165	− .004
.089	+ .001	+ .326	− .003	.618	+ .068	+ .096	− .009
.108	+ .028	+ .233	.000	.641	+ .078	+ .065	− .004
.130	+ .040	+ .188	.000	.672	+ .095	+ .012	.000
.165	+ .058	+ .128	.000	.697	+ .102	− .009	+ .001
.187	+ .068	+ .096	− .007	.715	+ .110	− .033	+ .003
.211	+ .074	+ .077	+ .004	.743	+ .113	− .043	+ .011
.245	+ .085	+ .042	− .011	.772	+ .113	− .043	+ .008
.277	+ .079	+ .061	− .005	.803	+ .102	− .009	− .002
.304	+ .077	+ .068	+ .018	.831	+ .080	+ .058	− .006
.333	+ .077	+ .068	.000	.871	+ .058	+ .128	+ .005
.361	+ .059	+ .125	+ .009	.898	+ .045	+ .171	+ .007
.396	+ .048	+ .161	+ .009	.920	+ .022	+ .250	+ .003
.420	+ .031	+ .219	− .009	.949	− .004	+ .345	+ .018
.446	+ .016	+ .272	+ .013	0.974	−0.040	+0.488	−0.005
0.466	−0.002	+0.338	−0.004				

1935 and (2) the photographic curve determined by Plaut in 1939 were reduced with the same assumption as to the magnitude difference in the visual pair, 0.76 mag., as was adopted for the reduction of the 1930 Washburn curve.

(1) $$l = 1.0000 - 0.0035 \sin\theta - 0.0227 \cos\theta - 0.2270 \cos^2\theta ;$$
$$\pm 0.0019 \quad \pm 0.0023 \qquad \pm 0.0038 \qquad \pm 0.0096$$

(2) $$l = 1.0000 - 0.0200 \cos\theta - 0.2362 \cos^2\theta .$$
$$\pm 0.0031 \quad \pm 0.0040 \qquad \pm 0.0100$$

It is interesting to note in this connection that an analysis of the light between the minima observed by Schilt,[3] for which the intensity of the photographic images of the eclipsing system alone were measured, gives

(3) $$l = 1.0000 - 0.0143 \cos\theta - 0.2145 \cos^2\theta .$$
$$\pm 0.0087 \quad \pm 0.0092 \qquad \pm 0.0228$$

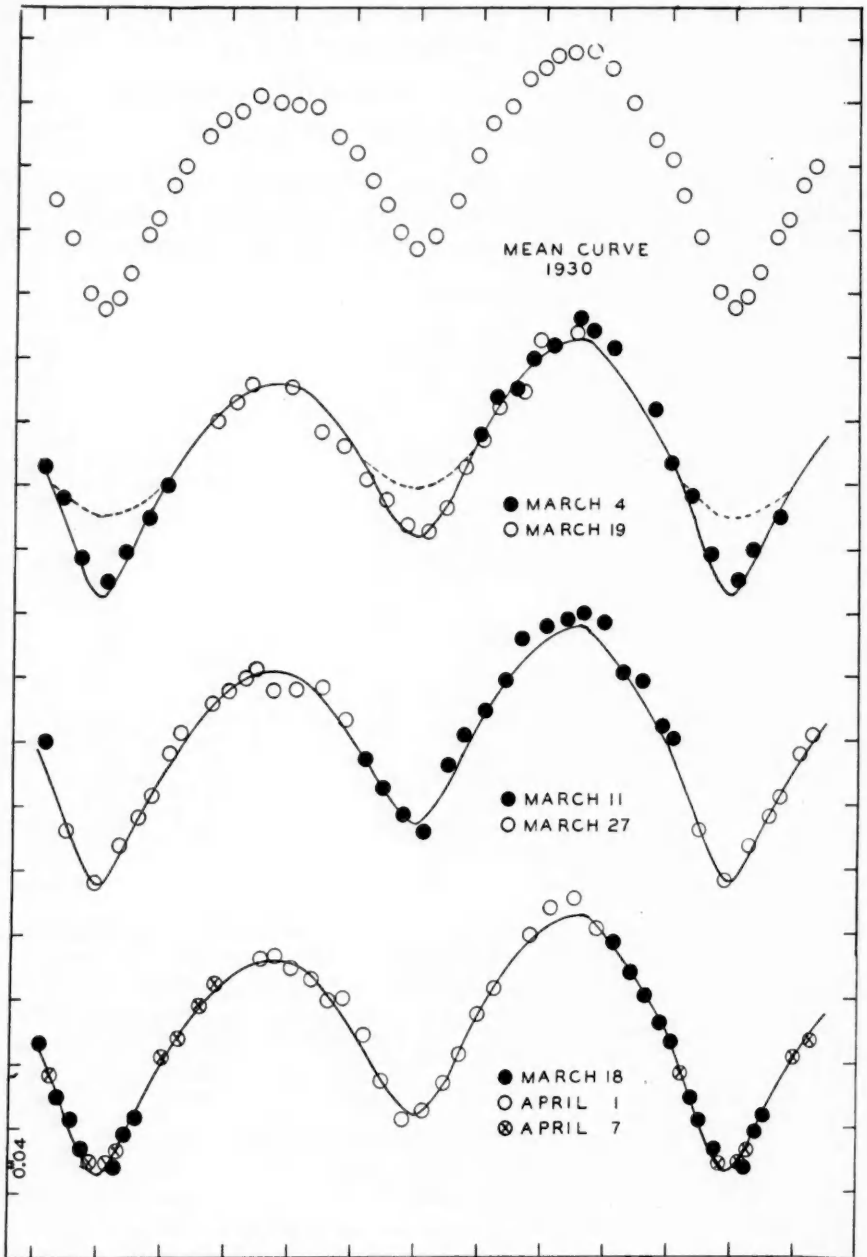

FIG. 1.—Light-curves of 44 i Bootis for 1930

After rectification, the Washburn light-curve shows two unequal minima with light-losses of $1 - \lambda_1 = 0.124$ and $1 - \lambda_2 = 0.088$. After a coefficient of limb darkening of 0.8 was assumed for each component, solutions were made with several values for k, the ratio of radii. Plotting the sums of the squares of the mean deviations of the normals from each of the computed curves revealed a range of indeterminancy of k between two values of 0.9, with the larger and smaller star alternately being also the brighter. For values of k outside this range, the computed curves leave relatively larger residuals from the normals of Table 3. The end-values of the ratio of radii in the apparent range of indeterminancy yield luminosity ratios of 0.55 and 0.80. From inspection of the intensity of the spectral lines, Popper[10] adopts the luminosity ratio 0.6 and states that the true value certainly lies between 0.5 and 0.85. Also from intensity measures in the spectrum, Petrie[11] finds this ratio to be 0.94 ± 0.04.

We have computed the photometric elements in Table 4 from the extreme values for k derived above, as well as for the intermediate assumption of equally large components. The absolute dimensions are based on Popper's spectroscopic elements. The elements in

TABLE 4

ELEMENTS OF 44 i BOOTIS

Ratio of radii	k	0.90	1.00	1.11
Fractional luminosity of component 1	L_1	0.56	0.58	0.64
Fractional luminosity of component 2	L_2	0.44	0.42	0.36
Semi-major axis (1)	a_1	0.36	0.38	0.38
Intermediate semi-axis (1)	b_1	0.35	0.37	0.37
Polar semi-axis (1)	c_1	0.34	0.35	0.35
Semi-major axis (2)	a_2	0.41	0.38	0.34
Intermediate semi-axis (2)	b_2	0.34	0.33	0.31
Polar semi-axis (2)	c_2	0.27	0.30	0.29
Inclination of the orbital plane	i	61°.6	63°.6	63°.6
Mass ratio	m_2/m_1	0.50	0.50	0.50
Mean radius in terms of the sun (1)	R_1	0.66	0.71	0.70
Mean radius in terms of the sun (2)	R_2	0.64	0.68	0.63
Mass in terms of the solar mass (1)	m_1	1.0	1.0	1.0
Mass in terms of the solar mass (2)	m_2	0.5	0.5	0.5
Assumed coefficient of darkening (1 and 2)	u	0.8	0.8	0.8

Table 4 must be regarded as but crude approximations not only because of the indeterminancy inherent in such shallow eclipses but also because of probable inadequacy of the simple theory used to derive them. The points of greatest interest in Table 4 are the near-contact of the two stars and the incompatibility of the mass and luminosity ratios with the standard mass-luminosity relation.

Also of interest is the difference in the magnitude of the system at the two maxima. In Figure 2 are plotted the photoelectric observations by Nikonov at both 8000 A and 4250 A, and the photoelectric observations of Shapley and Calder. The zero-point of the solid curve, representing the Washburn observations, has been adjusted to force agreement of the secondary maximum with the other curves. This adjustment also gives agreement at both minima, whereas the primary maximum falls 0.03 mag. too low. The reality of this phenomenon is demonstrated in Figure 1, where observations made on individual nights are plotted. The solid curves in Figure 1 represent the mean curve of Table 3. In the discussion of the Harvard curves of 1935–1936, Shapley and Calder found:[8] "In 1935 the first maximum was slightly, but most certainly higher than the secondary maximum;

[10] *Ap. J.*, **97**, 394, 1943.

[11] Presented in a paper at the seventy-sixth meeting of the American Astronomical Society and kindly communicated by the author in advance of publication.

in 1936 the reverse may have been the situation but the observations are too meager to justify stressing this evidence of variation in the light-curve." They also found the primary minimum 0.01 mag. deeper and the secondary 0.02 mag. shallower in 1936 than in 1935. The observations plotted in Figure 2 represent their mean curve. Not shown in Figure 2 is the excellent photographic curve determined by Plaut, who found equal maxima and amplitudes of minima agreeing well with the photoelectric results. Popper's spectroscopic results indicate a circular orbit. The Washburn and 1935 Harvard curves give $e \cos \omega = 0.00$. From much more meager material the 1936 Harvard curve gives $e \cos \omega = -0.02$. Nikonov's curves, which are of relatively low weight for the determination of times of minima, indicate $e \cos \omega = 0.0$ within their rather large probable error. Although the presence of a small amount of eccentricity is not ruled out, an attempt to account for the irregularities in the height of the maxima of the light-curves by means

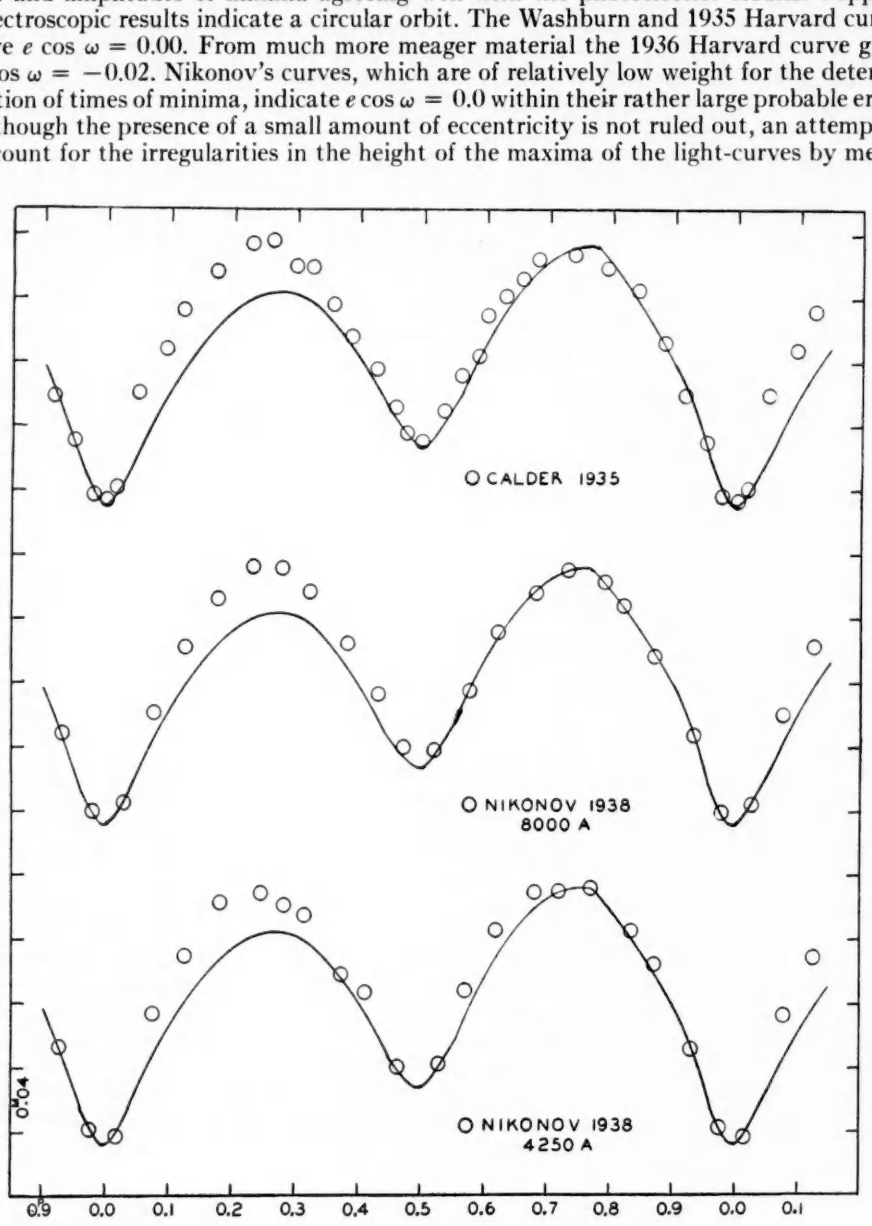

FIG. 2.—Observed light-curves of 44 i Bootis

of an apsidal motion does not appear feasible with the presently available material. However, it may be recalled that very similar asymmetries have been observed for β Lyrae. Stebbins,[12] using a rubidium cell, found the maximum following the primary minimum of this star to be 0.02 mag. lower than the other maximum, and Huffer,[13] with a potassium cell, found the maxima of equal brightness. Moreover, Smart,[14] also using a potassium cell, agreed with Stebbins in finding the first maximum about 0.02 mag. fainter. In an attempt to explain these asymmetries, Kuiper[15] has formulated a theory of "contact binaries," that is, binaries with common atmospheric envelopes. From this theory he concludes: (1) Contact binaries with unequal components are unstable; (2) matter streams from the more massive to the less massive component as long as the masses are unequal; and (3) the difference in magnitude between the components is abnormally large for the mass ratio. The elements in Table 4 show that the nearly equal photometric radii of the components each approximate 0.4 of the distance between centers. Moreover, our neglect of such effects as the gravity-darkening, which should be appreciable in this system, will produce radii which are an underestimation of the true values. Indeed, this fact is undoubtedly a partial cause of the abnormally high densities found for the W Ursae Majoris stars in general. It is possible, therefore, that the eclipsing system of 44 i Bootis constitutes a "contact binary" in which the equalization of the masses by the streaming of matter from the more massive to the least massive is still in process, the masses at the present time being in the ratio of 2 to 1. However, the difficulty remains that the ratio of luminosities inferred from the depths of the eclipses, as well as from the ratio of intensities of the spectral lines of the two components, is abnormally *small* for a mass ratio of 2—an effect just contrary to that expected from the theory of contact binaries as formulated by Kuiper.

The absolute visual magnitude of the brighter component has been determined, spectroscopically, at Victoria,[16] Mount Wilson,[17] and the Norman Lockyer[18] observatories. The mean value is $M_v = +4.63 \pm 0.13$. Taking Kuiper's value,[19] 0.63 mag., for the magnitude difference between the visual components at maximum of the eclipsing system in visual light, we then find the absolute visual magnitude of the eclipsing system, at mean maximum, to be +5.26 mag. The resulting spectroscopic parallax is 0".073, as compared with the trigonometric value of 0".078 $\pm$ 0".008.[19] If we designate the brighter visual companion by 1 and the brighter and fainter components of the eclipsing system by 2 and 3, respectively, then, from the elements of the visual orbit as determined by Strand, we find the total mass of the system, $m(1 + 2 + 3) = 2.53\odot$. From Table 4 we have $m_2 = 1.0\odot$ and $m_3 = 0.5\odot$, leaving $m_1 = 1.0\odot$.

An inspection of Figures 1 and 2 shows an apparent deformation of the maximum near phase 0^p.3. A search through the literature of the W Ursae Majoris stars revealed similar distortions in most well-determined light-curves of variables of this type.[20] In an attempt to test the reality of this phenomenon, a new series of observations of 44 i Bootis was undertaken in 1947 with the photomultiplier photometer, constructed by Dr. Whitford and used in connection with a recording milliameter permitting continuous recording of the light-changes. These observations, made on 7 nights of excellent sky transparency, are presented in Figure 3. The solid curves in Figure 3 represent the mean curve from the 1930 observations. The star HR 5581, described in Table 1, was used for comparison purposes, with additional check measures made on HR 5635. The observa-

[12] *Lick Obs. Bull.*, **8**, 186, 1915.

[13] *Pub. Washburn Obs.*, **15**, 209, 1931.

[14] *M.N.*, **95**, 647, 1935.

[15] *Ap. J.*, **93**, 29, 1941.

[16] R. K. Young and W. E. Harper, *Pub. Dom. Ap. Obs.*, **3**, 3, 1927.

[17] W. S. Adams *et al.*, *Mt. W. Contr.*, No. 511; *Ap. J.*, **81**, 58, 1935.

[18] W. B. Rimmer, *Mem. R.A.S.*, **62**, 113, 1923.

[19] *Ap. J.*, **88**, 429, 1938.

[20] E.g., E. Woodward, *Harvard Circ.*, No. 446, 1942.

tions of the comparison stars are grouped in Table 5, and it is evident that, as in 1930, they may be considered constant. The observational procedure was to make 1- to 2-minute tracings on the variable star, alternated with similar exposures to the comparison star, except that longer exposures were made on the variable when rapid changes became evident.

The deformity of the light-curve at maximum light, suggested in the previous results, is fully confirmed by the 1947 observations. Furthermore, this deformity appears to be the source of the apparent variation in the relative intensities at the two maxima dis-

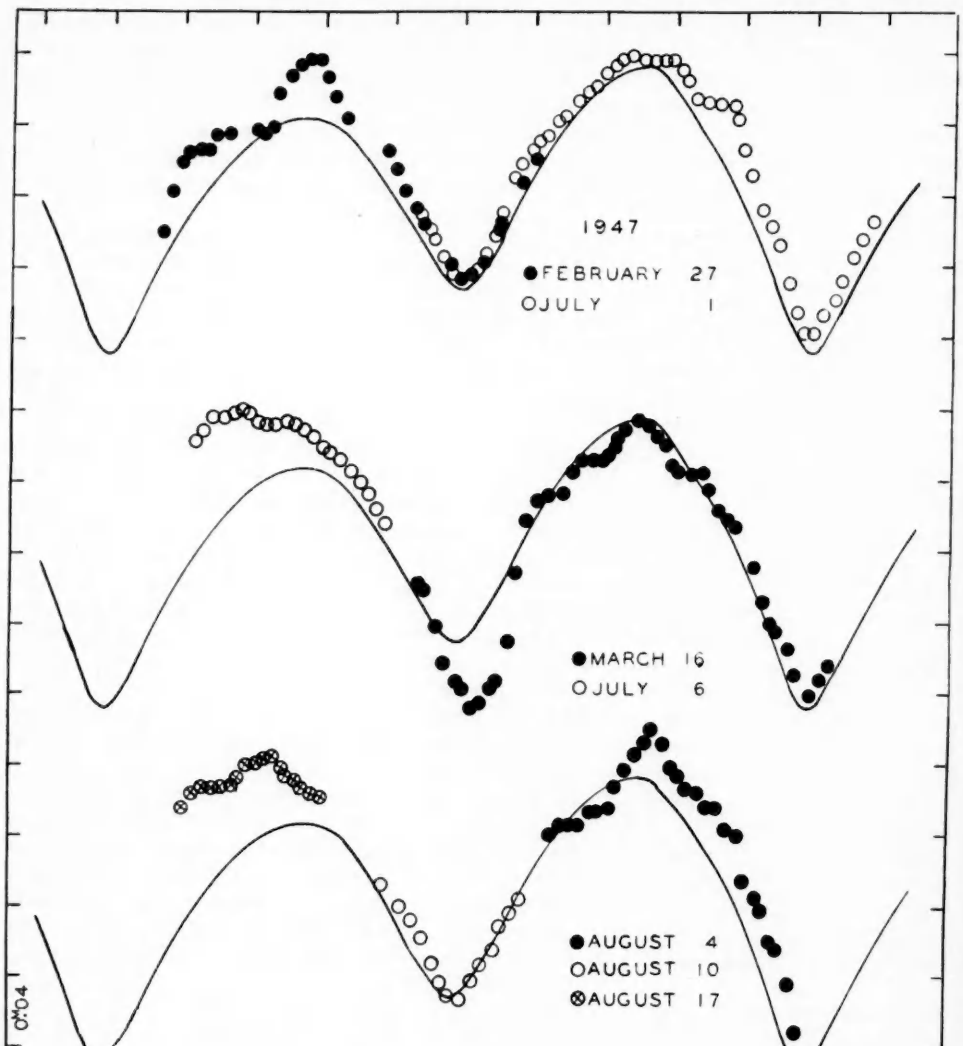

FIG. 3.—Light-curves of 44 i Bootis for 1947

cussed above. This is especially evident in the long runs made on February 27, March 16, and August 4, 1947, which show a nearly constant, premaximum intensity of the same order of magnitude as the apparently stunted primary maximum observed in 1930.

The explanation of the light-variations of this variable is complicated further by the peculiar secondary minimum observed on March 16. Both minima were observed on this night, and the faintness of the secondary minimum is well established. Furthermore, as is evident from Figure 3 and Table 6, this same secondary minimum is also considerably displaced from the normal $0^P.5$ position of the other secondary minima, whereas the primary minimum, observed the same night, appears to occur at the normal phase.

TABLE 5

CONSTANCY OF THE COMPARISON STARS

JD	5635 > 5581	Residual	No.
2432368	$0^m.068$	$0^m.000$	10
369	.066	+ .002	8
373	.067	+ .001	6
374	.069	− .001	7
376	.068	.000	10
402	0.069	−0.001	13
Mean	0.068	±0.0008	43

TABLE 6

NEW EPOCHS OF MINIMA OF 44 i BOOTIS

PRIMARY		SECONDARY	
JD	O−C	JD	O−C
2432339.7838	$+0^d.0286$	2432344.8455	$+0^d.0282$
2432369.7778	+ .0280	2432361.7221	+ .0329
2432373.7953	+ .0284	2432362.7892	+ .0288
2432380.7585	+0.0286	2432374.7332	+0.0290
Mean	$+0^d.0284 \pm 0^d.0002$	Mean*	$+0^d.0287 \pm 0^d.0003$

* Omitting the value for March 16, JD 2432361.

Previous investigators of this system have felt that, if the minima were accurately timed to approximately the year 1950, it would be possible to derive the mass function of the visual components from the variation in the period of the eclipsing system. Plaut,[7] using the minima available in 1939, found that $m_1/(m_1 + m_2 + m_3) = 0.4$, identical with the result which we have derived above by other means; but, even after he had corrected the observed epochs of minima for motion in the long-period orbit, using this mass-function, there remained a systematic deviation from a constant period.

Table 6 contains the minima determined in 1947, together with the residuals from the elements in equation (1). The computed epochs of secondary minima are for $e = 0.00$. The well-determined epochs of primary minima which have become available since 1916 are shown in Table 7.

The residuals of Table 7 are plotted in Figure 4. Similar computations were made,

using other values for the parallax and mass function; but no combination was found that appreciably changes the curvature shown in Figure 4. Unfortunately, there are no minima available to me between 1939 and 1947; but Popper,[10] in computing the phases for his spectroscopic observations, found not only that the period given by Plaut had run off in the same sense as that found here but that the increase was also evident over the 3-year interval covered by his observations. The epoch of minimum attributed to Popper in Table 7 is obtained from his spectrographic results.

Of the known W Ursae Majoris systems, there are six which have been sufficiently observed to test the constancy of their periods, namely: 44 i Bootis, $P = 0^d.26$; SW Lacertae,[20] $P = 0^d.32$; W Ursae Majoris,[20] $P = 0^d.33$; U Pegasi,[21] $P = 0^d.37$; and AK Herculis,[20] $P = 0^d.42$. All six have been found to have varying periods, and such explana-

TABLE 7

MINIMA OF 44 i BOOTIS

1 JD	2 O−C₁	3 O−C₂	4 O−C₃	5 Type and Authority
2421113.2588....	0ᵈ0000	0ᵈ0000	0ᵈ0000	pv; Hertzsprung, *B.A.N.*, No. 165, 1929
23204.4933....	− .0129	− .0157	− .0125	pv; Kuiper, *B.A.N.*, No. 165, 1929
24646.9724....	− .0172	− .0212	− .0135	pg; Schilt, *Ap. J.*, **64**, 215, 1926
25398.4398....	− .0189	− .0244	− .0156	pg; Osterhoff, *B.A.N.*, No. 321, 1939
25733.4699....	− .0180	− .0266	− .0137	pg; Osterhoff, *B.A.N.*, No. 321, 1939
26058.8554....	− .0181	− .0238	− .0146	pe; Huffer, *Pub. A.A.S.*, **6**, 365, 1930
27587.5035....	− .0214	− .0262	− .0169	vs; Plaut, *B.A.N.*, No. 321, 1939
27948.7741....	− .0243	− .0289	− .0198	pe; Calder, *Harvard Bull.*, No. 907, 1938
28635.4351....	− .0238	− .0283	− .0196	pg; Plaut, *B.A.N.*, No. 321, 1939
30152.5752....	− .0178	− .0235	− .0143	sp; Popper, *Ap. J.*, **97**, 407, 1943
32380.7583....	0.0000	0.0000	0.0000	pe; Eggen, present study

NOTES FOR TABLE 7

1. Epoch.
2. Residuals of the uncorrected minima from the linear elements: Minimum = JD 2421113.2588 + $0^d.26780832\ E$.
3. Residuals from the elements: Minimum = JD 2421113.1486 + $0^d.26780754\ E$ after the epochs are corrected for motion in the long-period orbit, using Strand's elements and assuming a negative sign for the inclination of the orbital plane. $\pi = 0''.073$, and $m_1/(m_1 + m_2 + m_3) = 0.40$.
4. Residuals from the elements: Minimum = JD 2421113.3690 + $0^d.26780910\ E$ after correcting the minima as in 3, except that the inclination of the orbital plane is here assumed to be positive.
5. Source of minima and method of observation.

tions as long-period orbital motion and apsidal motion have been invoked to account for them. Although the sample is small and it may be argued that it requires more observations to prove the constancy, than it does to prove the variability, of a period, it appears that period changes may be a characteristic of this type of system. In the theory of contact binaries proposed by Kuiper, he finds that the period of such a system would be affected by (1) mass transfer from one component to the other; (2) loss of mass and momentum by ejection of matter; and (3) pressure at the interface between the two components. The effects of characteristics 1 and 2 are to decrease the period, and the effect of point 3 is a slow regression of the line of apsides, the period of which is largely dependent upon the degree of contact. Kuiper concludes that the only mechanism available to explain an increase in the period is a sudden decrease in the diameter of the star; but in this case the increase of period would be only temporary.

In view of these considerations, it does not appear possible at the present time to segregate the change in period of the eclipsing system resulting from the long-period

[21] E. Woodward and F. Recillas, *A.J.*, **51**, 101, 1944.

orbital motion from those changes due to purely intrinsic causes and in this way to determine the mass function of the visual pair. In fact, the mass function 0.4, determined above in a different way, appears to be well established, and the problem may be reversed. Moreover, because of the presence of these intrinsic changes in the period, we are not able to fix the sign of the inclination in the visual orbit with any great certainty, although from Figure 4 we would select the positive value as being the most likely.

As we have already pointed out, the elements of the eclipsing system of 44 i Bootis, given in Table 4, must be considered as only crude approximations to the true values.

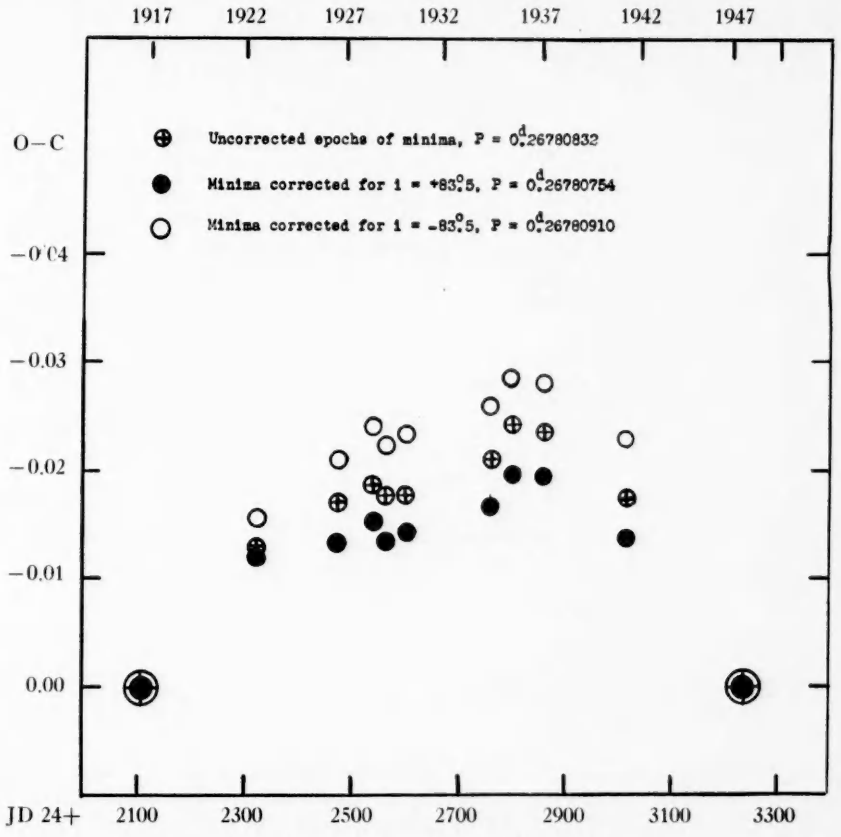

FIG. 4.—Variation of the period of 44 i Bootis

Before more definitive results can be obtained, the simple theory used in deriving these elements must be modified to explain: (1) the deformation of the two maxima of the light-curve; (2) the deepening and the displacement of the secondary minimum observed on March 16, 1947; (3) the intrinsic variation of the period; and (4) the apparent violation of the mass-luminosity relation. There is every evidence that these effects are not characteristic of 44 i Bootis alone but are also to be found in all the W Ursae Majoris systems. The variation of the period of these systems has already been discussed, as has the deformation of maximum light which is evident in many published photographic curves of variables of this type. It might be mentioned that I have already detected this deformation in an unpublished series of observations of W Ursae Majoris itself, made in 1947 in a similar manner to that described here for 44 i Bootis. Also, the apparent viola-

tion of the mass-luminosity relation appears to be another characteristic of these variables. In Table 8 are gathered the relevant data for systems which have been subjected to spectroscopic study. From the masses alone, the mass-luminosity relation would require the magnitudes of the components of these systems to differ by 2–3 mag. Moreover, the light-curves show nearly equal minima, and the fact that two spectra are observable at all is a contradiction. Therefore, we must assume that the masses and/or the luminosities are vitiated by some neglected effects or else that the mass-luminosity relation breaks down for the components of these systems. Some of these anomalies might be explained as resulting from the large reflection effect to be expected in such close systems. If we were to assume that the detection of the spectra of the fainter components were possible only because of the light reflected from the close primary stars, then most

TABLE 8

ELEMENTS OF TYPICAL W URSAE MAJORIS TYPE SYSTEMS

Star	Period	Sp.	i	L	R	m	M_v	Source
44 i Boo 1	0^{d}27	G2*	63°	0.58	0.7⊙	1.0⊙	+4.6	Popper, *Ap. J.*, **97**, 393, 1944
44 i Boo 2	.....	G2	.....	.42	0.7	0.5	+5.0	Eggen, present study
YY Eri† 1	.32	G5	.....	.....	.....	.....	.....	Struve, *Ap. J.*, **106**, 96, 1947
YY Eri 2	.....	G5	.....	.....	.....	‡	.....	
W UMa 1	.33	F8	75	.60	0.7	0.8	.....	Adams, *Ap. J.*, **49**, 189, 1919
W UMa 2	.....	F8	.....	.40	0.6	0.5	.....	Huffer, *Ap. J.*, **79**, 369, 1934
AH Vir† 1	.41	K0	83	.65	1.2	1.4	.....	Chang, *Ap. J.*, **107**, 96, 1948
AH Vir 2	.....	K0	.....	.35	0.7	0.6	.....	
ER Ori 1	.42	G2	71	.52	0.6	0.5	.....	Struve, *Pub. A.S.P.*, **58**, 34, 1944
ER Ori 2	.....	G2	.....	.48	0.6	0.3	.....	
S Ant 1	0.65	A8	62	.67	1.7	0.8	.....	Joy, *Ap. J.*, **64**, 293, 1926
S Ant 2	.....	A8	.....	0.33	1.3	0.4	.....	

* Classification by Joy and quoted by Wyse.

† Struve and Chang have found that the brighter, more massive components of YY Eri and AH Vir are eclipsed at secondary minima; but it is premature to discuss the significance of these results until accurate light-curves of the variables are available.

‡ $m_1 \sin^3 i = 0.72\odot$; $m_2 \sin^3 i = 0.47\odot$.

of the difficulty with the mass-luminosity relation could be explained. If the secondary component appears nearly as bright as the primary, as a result of this large reflection or even of the heating, effect, then the near-equality of the two eclipses is to be expected. Furthermore, the presence of such a large reflection effect would help explain the variation in the relative intensities of the spectral lines observed by Struve[22] and Chang[23] in the systems of YY Eridani and AH Virginis, respectively. The values given in Table 8 for the inclinations of the orbital planes provide another, indirect argument for the presence of a large amount of reflected light within the system. The preponderance of relatively small inclinations would be expected from photometric solutions of light-curves without first removing the excess light. Rather small values for the inclinations are quite common to these systems, those of the well-studied stars mentioned previously in connection with the change in period, for which no spectroscopic data are available, being[24] SW Lacertae, $i = 73°$; VW Cephei, $i = 63°$; U Pegasi, $i = 73°$; and AK Herculis, $i =$

[22] *Ap. J.*, **106**, 96, 1947.

[23] *Ap. J.*, **107**, 96, 1948.

[24] E. Woodward, *Harvard Circ.*, No. 447, 1942.

60°. Observations of the light-variations of these systems in several colors appear to be the best test of this hypotheses.

Similarly, observations in several colors should also throw more light on the nature of the deformed maximum in the light-curves of Figure 3. This effect is possibly connected with the presence of a large amount of reflected light, but either nonsynchronism of orbital and rotational periods or nonuniform reflecting surfaces would also be required. In addition, the recent possible detection of "flares" and "spots" on the eclipsing variable AR Lacertae by G. Kron[25] may provide a basis for similar explanation of the anomalies observed in 44 i Bootis.

Therefore, we conclude that spectroscopic and photometric elements of 44 i Bootis in particular and of the W Ursae Majoris stars in general should be regarded with suspicion. On the other hand, further study of these systems should provide much information regarding the evolution of binary systems. Moreover, the shortness of their periods and the presence of exaggerated reflection and ellipticity effects makes these variables excellent proving grounds for the theories to be applied to more normal systems.

I am indebted to Dr. A. E. Whitford, who designed and constructed the photoelectric photometer at the Washburn Observatory. The latest improvements of the photometer were made possible by a grant to Dr. Joel Stebbins from the Gould Fund of the National Academy of Sciences. The debt due Dr. Stebbins not only for making available the 1930 series of observations of 44 i Bootis but also for the benefits of his advice and experience cannot adequately be expressed.

[25] *Pub. A.S.P.*, **59**, 261, 1947.

THE ECLIPSING VARIABLE AO CASSIOPEIAE

FRANK BRADSHAW WOOD
Steward Observatory, University of Arizona
Received November 29, 1947

ABSTRACT

The eclipsing variable AO Cassiopeiae was observed photoelectrically at the Steward Observatory during the winter of 1946–1947. The observed minima fell about five hours later than the predicted times; new light-elements have been determined.

Satisfactory representation of the light between eclipses requires the use of terms in cos 2θ, sin θ, and sin 2θ. Comparison with earlier observations shows that the light-curve varies from year to year but indicates that the variation is confined to the sin θ and sin 2θ terms.

Limiting solutions have been carried out. The system consists of a pair of supergiants, with a combined mass of approximately sixty times that of the sun. Absolute dimensions, computed with the aid of Pearce's spectrographic elements, are given in Table 4.

The eclipsing system AO Cassiopeiae[1] is of considerable astrophysical interest. It is one of the few known class O eclipsing binaries. Both spectra have been measured, and the spectrographic orbit is available; the components are among the most massive stars known. The stars are highly distorted, and the light-variation is attributable largely to this distortion; the shape of the light-curve varies from year to year.

The variable velocity of this star was first discovered at Mount Wilson.[2] Shortly thereafter, Adams and Stromberg[3] published a velocity-curve and orbital solution based on measures of the brighter component. The light-variation was detected independently by Guthnick[4] and by Stebbins.[5] Further photometry was done by Guthnick and Pavel,[6] by Gussow,[7] and by Bennett.[8] Pearce[9] has made the most exhaustive study of the star to date. His spectrographic orbit is based on velocity-curves of both components. He further derived elements from Guthnick's 1919–1920 light-curve and determined the absolute dimensions of the system. Color measures have been made by Stebbins, Huffer, and Whitford[10] in both their two-color and their six-color photometry. All the foregoing photometry is photoelectric.

I. EPOCH AND PERIOD

The observed minima are listed in Table 1. The times are in Julian days, with the decimal of the day expressed in Greenwich mean time measured from noon. Because of the small light-variation, times of minimum are taken only from the mean curves; Nos. 4 and 5 are heliocentric; the others are not specified by the observer. Fortunately, the average heliocentric correction during the observing season is only +0.001 day, so that the minima from the mean curves will not be affected appreciably by its neglect. The residuals are based on Pearce's elements:

$$\text{Primary Minimum} = \text{JD } 2424002.564 + 3^{d}.52341\,E\,.$$

[1] BD+50°46; HD 1337; Boss 46; HR 65; PD 134; Groomb 35.

[2] *Annual Report of the Director of the Mount Wilson Observatory*, 1916.

[3] *Ap. J.*, **47**, 329, 1918; *Mt. W. Contr.*, No. 149.

[4] *Beob. Zirk.*, **1**, 12, 1919; *A.N.*, **211**, 391, 1920. [5] *Pub. Washburn Obs.*, **15**, 62, 1928.

[6] *A. N.* **215**, 395, 1921; *Atti d. pont. Accad. rom. d. Nouvi Lincei*, Session of May 20, 1923.

[7] *A.N.*, **237**, 321, 1930. [8] *A.J.*, **47**, 104, 1938. [9] *Pub. Dom. Ap. Obs., Victoria*, **3**, 275, 1926.

[10] *Pub. Washburn Obs.*, **15**, 224, 1934; *Ap. J.*, **91**, 26, 1940; **98**, 24, 1943; **102**, 318, 1945.

These elements satisfy both the spectrographic and the photometric work through 1928. The 1946–1947 measures, however, show the minima occurring more than 5 hours later than predicted. A plot of the residuals shows that they cannot be fitted satisfactorily by a constant period; they are most simply fitted by assuming a sudden change of period shortly before Bennett's observations. New light-elements are determined as

$$\text{Primary Minimum} = \text{JD } 2432191.189 + 3^d.52355\,E\,. \qquad (1$$

These should prove satisfactory for prediction in the near future.

II. THE OBSERVATIONS

The present study is based on 182 photoelectric observations taken between November, 1946, and February, 1947, with the 36-inch reflector and the photoelectric photometer of the Steward Observatory. The photometer is essentially that described by Roach.[11] The only major change is the substitution of a Western Electric tube, type D-96475, for the FP-54, with the corresponding necessary changes in the balanced circuit.

TABLE 1

OBSERVED MINIMA

No.	Epoch	Observed	O−C	Wt.	Authority
1	− 508	2422212.675	+0^{d}003	3	Guthnick*
2	− 288	2987.822	.000	1	Gussow† from observations of Guthnick and Pavel‡
3	+ 218	4770.667	.000	1	Gussow†
4	+ 964	7399.159	+ .028	3	Bennett§
5	+2324	2432191.189	+0.220	3	Wood

* *Beob. Zirk.*, **1**, 12, 1919; *A.N.*, **211**, 391, 1920.
† *A.N.*, **237**, 321, 1930.
‡ *A.N.*, **215**, 395, 1921; *Atti d. pont. Accad. rom. d. Nuovi Lincei*, Session of May 20, 1923.
§ *A.J.*, **47**, 104, 1938.

The observations are listed in Table 2. Times are in Julian days, decimals of a day being measured from Greenwich mean noon and reduced to the sun. The magnitude differences have been corrected for differential extinction; they are accompanied in some cases by letters which have the following significance: "a," clear 1; "b," clear 2; "c," clear 3; "f," clouds; "x," low smoke; "y," strong wind. The phases are from the elements given in equation (1). The comparison star, *a*, is BD+47°50 (B9). It was checked nightly against BD+51°62 (B3). The probable error of an individual observation from the theoretical curve is ±0.013 mag. This is unexpectedly large and will be considered more fully in the discussion of results.

III. THE SOLUTION

The solution is complicated by the lack of symmetry of the light-curve; the third quarter is almost 0.03 mag. brighter than the first quarter. A sine-term correction rectifies this, but the curve is still not symmetrical. Because Bennett had found that his observations were well represented by ellipticity variation alone, without eclipses, an attempt was made to fit the present curve in the same manner. On this assumption the lack of symmetry is accounted for by the variation of the light with $(v + w)$ in an elliptical orbit, instead of with θ. However, quantitative attempts to fit the curve on this hypothesis failed completely.

[11] *Ap. J.*, **88**, 305, 1938.

TABLE 2

OBSERVATIONS

Time JD 2430000+	$v-a$	Phase	Time JD 2430000+	$v-a$	Phase
2131.6433	+0^{m}175a	+0^{d}3547	2157.5998	+0^{m}231	+1^{d}6453
.6527	+ .134	+0.3641	.6084	+ .239	+1.6549
.6613	+ .160	+0.3727	.6179	+ .261	+1.6644
.6726	+ .162	+0.3840	.6294	+ .262	+1.6759
2135.6102	+ .143a	+0.7980	.6394	+ .267	+1.6859
.6224	+ .087	+0.8102	.6485	+ .251	+1.6950
.6313	+ .123	+0.8191	.6575	+ .247	+1.7040
.6394	+ .117	+0.8272	.6687	+ .232	+1.7152
.6477	+ .111	+0.8355	.6784	+ .246	+1.7249
.6618	+ .105	+0.8496	.6848	+ .259	+1.7353
.6704	+ .117	+0.8582	2169.6473	+ .155bx	+3.1232
.6795	+ .127	+0.8673	.6579	+ .151	+3.1338
2143.7036	+ .261a–f	+1.8443	.7299	+ .170	+3.2058
2144.6938	+ .114a	+2.8345	2170.5834	+ .126a	+0.5357
.7077	+ .143	+2.8484	.5959	+ .129	+0.5482
.7220	+ .138	+2.8627	.6063	+ .130	+0.5586
.7359	+ .132	+2.8766	.6179	+ .129	+0.5702
.7550	+ .134ab	+2.8957	.6288	+ .119	+0.5811
.7692	+ .159	+2.9099	.6397	+ .124	+0.5920
2145.6743	+ .163a	+0.2915	.6513	+ .108	+0.6036
.6861	+ .185	+0.3033	.6702	+ .121	+0.6225
.6971	+ .202	+0.3143	.6803	+ .121	+0.6326
.7073	+ .184	+0.3245	.6906	+ .118	+0.6429
.7177	+ .190	+0.3349	.7069	+ .103	+0.6592
.7287	+ .172	+0.3459	.7166	+ .123	+0.6689
.7399	+ .212	+0.3571	.7293	+ .113	+0.6816
.7504	+ .181	+0.3676	2174.5937	+ .163ax	+1.0225
2146.6484	+ .210ab–f	+1.2656	2189.6462	+ .216ay	+1.9808
2151.6102	+ .086ax	+2.7038	2190.6195	+ .160a	+2.9541
.6217	+ .079	+2.7153	.6325	+ .142	+2.9671
.6345	+ .072	+2.7281	.6489	+ .145	+2.9835
.6605	+ .052	+2.7541	.6715	+ .134	+3.0061
.6754	+ .055	+2.7690	2191.5791	+ .154a	+0.3901
.6865	+ .071	+2.7801	.5980	+ .143	+0.4090
.7106	+ .146	+2.8042	.6154	+ .163	+0.4264
.7231	+ .099	+2.8167	.6277	+ .134	+0.4387
.7568	+ .081	+2.8504	.6390	+ .158	+0.4500
.7700	+ .102	+2.8636	2191.6502	+ .153	+0.4612
2153.6665	+ .140a	+1.2366	.6721	+ .135	+0.4831
.6792	+ .163	+1.2493	.6838	+ .130	+0.4948
.6927	+ .181	+1.2628	2195.5850	+ .103b	+0.8724
.7059	+ .162	+1.2764	.5946	+ .119	+0.8820
.7203	+ .171	+1.2908	.6046	+ .104	+0.8920
.7338	+ .189	+1.3043	.6160	+ .127	+0.9034
.7462	+ .182	+1.3167	.6265	+ .115	+0.9139
.7579	+ .163	+1.3284	.6708	+ .104	+0.9582
.7911	+ .199	+1.3616	.6838	+ .104	+0.9712
.8095	+ .185	+1.3802	.6946	+ .127	+0.9820
2155.6058	+ .190ax	+3.1759	.7054	+ .133	+0.9928
.6164	+ .211	+3.1865	2196.5893	+ .191bx	+1.8767
.6255	+ .187	+3.1956	.5999	+ .210	+1.8873
.6359	+ .222	+3.2060	.6104	+ .254	+1.8978
.6756	+ .188	+3.2457	.6195	+ .193	+1.9069
.6884	+ .232	+3.2585	.6298	+ .194	+1.9172
.6979	+ .214	+3.2680	.6410	+ .170	+1.9284
.7104	+ .216	+3.2805	.6526	+ .240	+1.9400
.7207	+ .210	+3.2908	.6660	+ .210	+1.9534
2157.5790	+ .231ax	+1.6255	.6765	+ .230	+1.9639
.5889	+0.251	+1.6354	.6868	+0.210	+1.9742

TABLE 2—*Continued*

Time JD 2430000+	$v-a$	Phase	Time JD 2430000+	$v-a$	Phase
2196.6989	+0^{m}232	+1^{d}9863	2210.6154	+0^{m}217	+1^{d}8085
.7117	+ .232	+1.9991	.6267	+ .232	+1.8198
2201.5985	+ .235a	+3.3624	.6382	+ .230	+1.8313
.6093	+ .246	+3.3732	.6490	+ .220	+1.8421
.6238	+ .236	+3.3877	.6615	+ .225	+1.8546
.6363	+ .249	+3.4002	2211.5900	+ .137c	+2.7832
.6636	+ .239	+3.4275	.6146	+ .066	+2.8078
.6861	+ .252	+3.4500	2212.6254	+ .186ax	+0.2951
.6999	+ .248	+3.4638	.6368	+ .202	+0.3065
.7118	+ .255	+3.4757	.6463	+ .204	+0.3160
2206.6017	+ .194bx	+1.3185	.6567	+ .201	+0.3264
.6132	+ .232	+1.3300	2231.6022	+ .231c	+1.6541
2207.6222	+ .122ax	+2.3390	.6174	+ .254	+1.6689
.6317	+ .117	+2.3485	.6298	+ .231	+1.6813
.6418	+ .095	+2.3586	2232.6081	+ .075bx	+2.6600
.6525	+ .129	+2.3693	.6181	+ .094	+2.6700
.6621	+ .106	+2.3789	2235.5985	+ .184b	+2.1273
.6736	+ .134	+2.3904	2236.5893	+ .197ax	+3.1177
.6889	+ .126	+2.4057	.5978	+ .184	+3.1262
2208.5890	+ .235ax	+3.3058	.6064	+ .189	+3.1348
.6002	+ .228	+3.3170	.6160	+ .192	+3.1444
.6099	+ .214	+3.3267	2238.5896	+ .240bx	+1.5944
.6215	+ .220	+3.3383	.5983	+ .262	+1.6031
.6318	+ .217	+3.3486	.6061	+ .262	+1.6109
2209.6020	+ .070ax	+0.7952	.6141	+ .230	+1.6189
.6120	+ .096	+0.8051	2239.5947	+ .104ax	+2.5995
.6214	+ .095	+0.8145	.6048	+ .105	+2.6096
.6320	+ .101	+0.8251	.6137	+ .091	+2.6185
.6417	+ .133	+0.8348	2240.5900	+ .272ax	+0.0713
.6521	+ .093	+0.8452	.5970	+ .256	+0.0783
.6625	+ .126	+0.8556	.6036	+ .274	+0.0849
2210.6028	+0.215c	+1.7959	.6109	+0.249	+0.0922

A satisfactory representation of the light-variation between eclipses is given by

$$l_c = 0.9284 - 0.0578 \cos 2\theta - 0.0118 \sin \theta + 0.0150 \sin 2\theta \,. \qquad (2)$$

The cos 2θ term represents the variation due to ellipticity of figure of the stars. An alternate rectification has a smaller term in sin 2θ and a term in cos θ. This latter term is of opposite sign to the usual reflection correction. While this satisfies the observations between eclipses, rectification of the minima by it shows a primary of appreciable depth and no secondary at all. This is flatly contradictory to the spectrographic evidence, which requires eclipses of comparable depth. Several rectifications intermediate between these two were also tested. Those permitted by the spectrographic data failed to fit satisfactorily the observations between minima. The rectification given by equation (2) is therefore adopted.

Inspection of the light-curve illustrated in Figure 1 indicates that the solution is nearly indeterminate from photometric data alone. A graphical solution confirms this prediction. The velocity-curve shows that the brighter component is eclipsed at primary; and, from the spectra, Pearce estimates the ratio of luminosities of the components as 2.6. By the use of the above and the observed depths of the minima, two limiting solutions have been made. They are given in Table 3 as "Solution 1" and "Solution 2." For both, the degree of darkening, $x = 0.6$, is assumed. Pearce and the Mount Wilson observers agree in classifying the spectrum of the secondary as nearly the same as that of the primary. This near-equality indicates a surface-brightness ratio of nearly 1.0 and suggests that the true dimensions are probably much nearer those given in Solution 1.

The absolute dimensions of the system are listed in Table 4. The data in the first column are computed from the photometric elements of Solution 1, Table 3, and the spectrographic elements of Pearce:

$$m_1 \sin^3 i = 17.6 \odot , \qquad m_2 \sin^3 i = 16.4 \odot , \qquad a \sin i = 21{,}935{,}000 \text{ km} .$$

In the second column the absolute dimensions have been corrected for the reflection effect; details of this correction are given in the discussion.

Table 5 gives the computed light-curve. The elements of Solution 1 are again used.

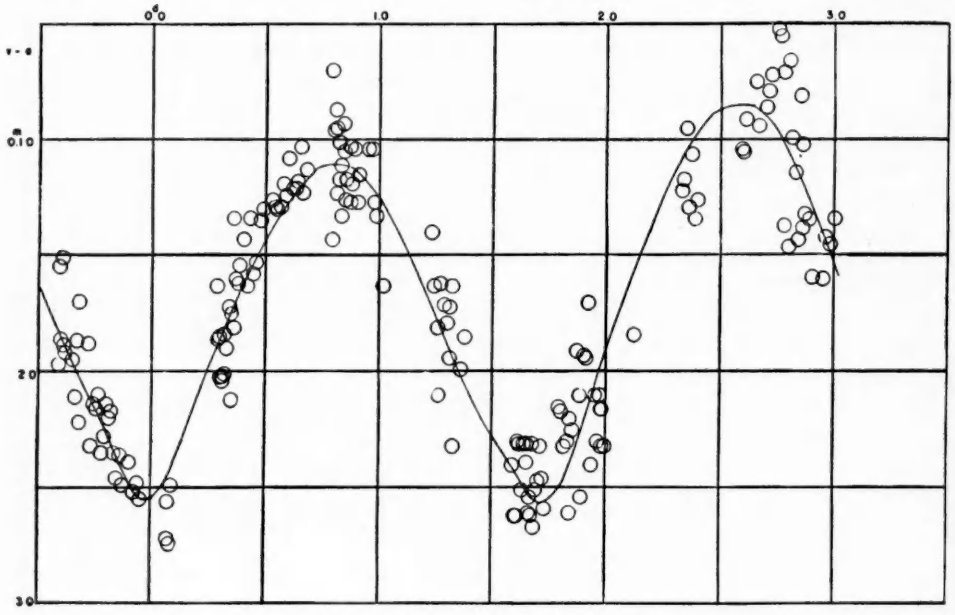

FIG. 1.—Light-curve of AO Cassiopeiae

IV. DISCUSSION

The discussion falls naturally into three parts: (1) the comparison of the various photometric curves; (2) the comparison of the absolute dimensions with those found by Pearce; and (3) the reliability of the results in view of the above comparisons.

1. A comparison of the light-curves obtained by various observers shows plainly that the curve is not constant from year to year. Careful consideration of these fluctuations is necessary before trust can be put in elements derived from any one curve.

Bennett's 1933 observations form a symmetrical curve, in marked contrast to the others. These observations, however, can be fitted by a curve computed by the use of the elements of Solution 1, Table 3, and the coefficient of cos 2θ given in equation (2). The disagreement between the 1946–1947 observations and those of 1933 lies solely in the presence of the sin θ and sin 2θ terms in the present set. Bennett's 1934–1935 observations agree with neither of these. However, they are fitted by the same computed curve if a correction, $-0.0150 \sin \theta$, is added to the computed points. Gussow's observations of 1925–1928 agree with the 1934–1935 set when the former are reduced to PD 129. Bennett also reduced Guthnick's 1921 curve to heliocentric phase and PD 129 and found agreement with his 1934–1935 observations. (Reduction to PD 129 is necessary, since the comparison star used by Guthnick and by Gussow was found by Guthnick to be variable.) Guthnick's 1919–1920 curve is more difficult to fit. His use of a variable compari-

son star may be partially responsible. However, this variation was small, and an attempt was made to correct for it. Addition of sin θ and sin 2θ terms to the eclipse and eccentricity elements used in this discussion gives an acceptable fit to the observations. Other factors may be affecting the light-curve; the significant point is that the fit cannot be improved by changing the eclipse elements or the ellipticity coefficient.

Thus, despite the variations in the light-curve from year to year, all the observations to date can be fitted by the eclipse elements of Solution 1 and an additional variation given by

$$l_c = 0.9284 - 0.0578 \cos 2\theta + x \sin \theta + y \sin 2\theta . \quad (3$$

TABLE 3

SUMMARY OF RESULTS

BD No.	+50°46
R.A. 1900	0^h12^m5
Dec. 1900	+50°53′
Spectral types	O8.5n–O8.5n
Maximum	5^m91*
Primary Minimum	6.08
Secondary Minimum	6.08
Comparison star, BD	+47°50
Initial epoch, JD	2432191.189
Period	3^d52355

* Using the HD magnitude of the comparison star.

Partial Eclipse. Transit Eclipse at Primary.

SOLUTIONS FOR DEGREE OF DARKENING 0.6

	Solution 1	Solution 2
Length of eclipse	0^d4464	0^d4404
Phase of secondary	$\frac{1}{2}P$	$\frac{1}{2}P$
$1-\lambda^{oe}$	0.0189	0.0154
$1-\lambda^{tr}$	0.0189	0.0300
a_v^{oe}	0.068	0.055
a_v^{tr}	0.058	0.051
k	0.643	0.876
L_1†	0.722	0.722
L_2†	0.278	0.278
J_b/J_f	1.07	1.99
i‡	56.9	55.5
a_b	0.411	0.379
a_f	0.264	0.332
b/a	0.930	0.923

† From the spectrographic data.

‡ Corrected for polar flattening.

The coefficients x and y often vary from year to year, but they apparently do not affect the cos 2θ term. The accuracy of the solution depends strongly upon the accuracy with which the ellipticity coefficient is determined. The value -0.0578 may be considered as satisfactory for the various photometric curves.

2. The masses of the components are found to be about 80 per cent, the radii 65 per cent, and the densities almost 400 per cent of the values given by Pearce. The disagreement is caused by the larger inclination and the smaller value of r_1 found in the present investigation. This discrepancy, in turn, is largely due to the deeper minima found by Pearce. Since the depths of the minima depend so strongly upon the rectification for ellipticity, the value of the ellipticity coefficient is the significant factor. Pearce had available only

Guthnick's 1919–1920 light-curve. This has the weirdest shape of any of the curves and is therefore probably the least satisfactory for determination of elements. The discussion of Part I indicates that the ellipticity coefficient there given may be accepted with reasonable confidence.

In making his solution, Pearce used the spectrographic values of e and ω. Study of the asymmetric light-curves shows that the apparent displacement of the secondary minimum is due to the sin 2θ term rather than to an actual displacement of the time of eclipse.

TABLE 4

ABSOLUTE DIMENSIONS

	Using Pearce's Spectrographic Elements	Corrected for Reflection Effect		Using Pearce's Spectrographic Elements	Corrected for Reflection Effect
m_1	29.9 ⊙	31.2 ⊙	ρ_2	0.034 ⊙	0.034 ⊙
m_2	27.9 ⊙	28.6 ⊙	L_1		317,000 ⊙
a_1	15.5 ⊙	15.7 ⊙	L_2		131,000 ⊙
a_2	9.9 ⊙	10.1 ⊙	$M_{(bol)1}$		-9^m1
ρ_1	0.0097 ⊙	0.0100 ⊙	$M_{(bol)2}$		-8^m1

TABLE 5

COMPUTED CURVE

Phase	$v-a$	Phase	$v-a$	Phase	$v-a$
0^d0000	$+0^m255$	1^d3212	$+0^m192$	2^d2022	$+0^m138$
0.0529	+ .250	1.4682	+ .222	2.3491	+ .105
0.0763	+ .245	1.5455	+ .233	2.4959	+ .087
0.1096	+ .237	1.5739	+ .237	2.6427	+ .086
0.1253	+ .233	1.5915	+ .241	2.7895	+ .103
0.1409	+ .229	1.6218	+ .247	2.9363	+ .135
0.1713	+ .219	1.6522	+ .251	3.0831	+ .173
0.1879	+ .215	1.7089	+ .257	3.2300	+ .208
0.2132	+ .206	1.7618	+ .255	3.3004	+ .220
0.2963	+ .190	1.8146	+ .247	3.3357	+ .228
0.4404	+ .157	1.8714	+ .231	3.3523	+ .232
0.5873	+ .128	1.9018	+ .221	3.3827	+ .239
0.7341	+ .112	1.9321	+ .211	3.3983	+ .243
0.8809	+ .112	1.9497	+ .205	3.4140	+ .246
1.0277	+ .129	1.9781	+ .196	3.4473	+ .252
1.1745	+0.158	2.0554	+0.176	3.4707	+0.254

Bennett's curves, which require no sin 2θ term, show a centrally located secondary. The spectrographic eccentricity is small (0.037); there is no real photometric evidence for its presence. The present solution assumes a circular orbit. Assumption of ellipticity, at all events, has in this case a negligible effect upon the computed elements.

A more serious difficulty in Pearce's derived elements lies in the large value of the radii of the components relative to the radius of the orbit. From considerations of dynamical stability, it is possible to compute the maximum size of the components of a binary system. The only assumptions involved are the Roche model and a circular orbit. Such a computation has been carried out by the author with a formula developed by Moulton.[12] (A discussion and details are given in *Princeton Contr.*, No. 21, pp. 36–37, 1946.) For equal masses the largest permissible value of the shorter equatorial radius of

[12] *Celestial Mechanics* (new ed.; New York: Macmillan Co., 1914), chap. viii.

either component is 0.373—far below the value found by Pearce in any of his solutions. Pearce's elements, therefore, cannot be those of a stable system. This conclusion agrees with that previously reached by Kuiper[13] in his study of the system. The elements of Table 3 lie slightly within the limits of stability.

The present solution is therefore to be preferred to that of Pearce for two reasons: (1) it is based on considerably more observational evidence than was available in 1926, and (2) the derived elements are those of a dynamically stable system.

In his extensive study of the empirical mass-luminosity relation, Kuiper[14] pointed out that the reflection effect must be taken into account in the determination of the masses and gave tables for computing the necessary corrections. The absolute dimensions thus corrected are listed in the second column of Table 4.

3. The system consists of a pair of supergiants. The absolute dimensions given are probably reasonably trustworthy. While they depend upon the spectrographic estimate of relative intensity, Pearce has shown that errors in this estimate have but small effect upon the absolute dimensions of this system. The exact amount of limb darkening to be expected in a type O star is not known; again, however, an error in the assumed darkening has in this case only a slight effect upon the computed dimensions. For example, a solution using the same depths of minima but assuming 0.2 darkening finds 30.9 $\odot$ for the mass of the larger component; the value listed in Table 4 is 31.2 $\odot$.

The value of A_2, the coefficient of cos 2θ, computed from the elements of the system by the method of Russell[15] is -0.0573. The value found from the light-curve is -0.0578. As the computed value depends strongly upon the assumed degree of darkening, this indicates that 0.6 is a good approximation of the limb darkening of a class O star. The ellipticities computed from the elements of the system are $\epsilon_1 = [(a - b)/a] = 0.081$, $\epsilon_2 = 0.025$. Almost 90 per cent of the between-eclipse variation is due to the larger component.

The value of ± 0.013 mag. found for the probable error of an individual observation from the theoretical curve really represents the combination of three effects. First, there is the actual scatter of the observations. This is small on many nights, but on others, owing to the presence of wispy and almost undetectable smoke, it is disappointingly large. Observations taken on such nights were, of course, given low weight in making the solution. Second, it seems that the shape of the light-curve cannot be completely represented without the use of higher-order terms than those used in equation (2). This is not surprising in a distorted system, but the observations do not justify a more complete investigation. Finally, the observations show occasional irregular fluctuations from night to night. When these are present, they are of the order of 0.02 mag. The comparison-check-star measures on these nights indicate that the cause of these lies in the variable.

In conclusion, it should be noted that further photometric observation of this system is still highly desirable. The star is being retained in the Steward Observatory photoelectric program, but observation elsewhere would be by no means an unnecessary duplication of effort. Because of the frequent fluctuation from year to year, it is important to cover the entire light-curve in one observing season.

This investigation was made possible by the grant of a National Research Fellowship by the National Academy of Sciences. Observing assistants were paid in part by a grant from the Penrose fund of the American Philosophical Society and in part by the Steward Observatory. I am indebted to Professor Edwin F. Carpenter for placing the Steward Observatory equipment at my disposal and for valuable advice and assistance in getting the photometer into operating condition after its wartime inactivity, and to Professor Newton L. Pierce for access to the card catalogue of eclipsing binaries. For reading the manuscript and making helpful suggestions, I am indebted to Professor Henry Norris Russell, Professor Carpenter, and Professor Pierce.

[13] *Ap. J.*, **88**, 501, 1938. [14] *Ibid.*, pp. 472 ff. [15] *Ap. J.*, **102**, 1, 1945.

AN ANALYTICAL METHOD FOR THE DETERMINATION OF THE INTERMEDIARY ORBIT OF AN ECLIPSING VARIABLE

S. L. PIOTROWSKI
Harvard College Observatory
Received December 20, 1947

ABSTRACT

Analytical procedures are developed for a determination of the intermediary elements of an eclipsing binary system, together with their mean errors, by a least-squares analysis of the light-changes. In contrast to the general solution for the differential corrections, the present method requires very little preknowledge of the elements. In principle, it is an extension of the method proposed earlier by Kopal. Its essential features are (*a*) an introduction of the corrections to the provisionally accepted depths of the minima as unknowns into the basic equations of condition; (*b*) an introduction of the appropriate system of weights of the equations of condition; (*c*) an introduction into the equations of the corrections to the maximum light and of the assumed degree of darkening; (*d*) a full allowance for the combined effects of errors of the photometric observations and of the finite speed of convergence of underlying successive approximations on the precision of the solution. As a result, the present method permits us to deduce, from the observed photometric data, the best possible (in the sense of the principle of least squares) set of elements of an eclipsing system whose components are regarded as spheres or prolate ellipsoids.

Statement of the problem.—There are three more or less distinct stages in the process of determination of the orbit of an eclipsing binary: the preliminary, the intermediary, and the final. In the first—preliminary—stage we try to ascertain the kind of eclipse (i.e., whether it is an occultation or a transit), as well as the approximate sizes of the components. In the intermediary stage we aim at a best-possible representation of the observations with the aid of a *simplified* model, consisting of two similar prolate ellipsoids whose disks are darkened toward the limb according to the simple cosine law. It is only when we have a set of really good intermediary elements, know the degree of their determinacy, and, in addition, are in possession of information concerning the mass-ratio of the components that we can decide to what extent we should allow for the photometric effect of various orders of distortions of both components, their gravity darkening, etc.

There are several fast methods of obtaining preliminary information about the system under consideration. The most successful and best known of them are associated with the names of Russell and Shapley.[1] In the case of a total (annular) eclipse a crude estimate of the ratio of radii k from the duration of eclipse and the depths of the minima is often sufficient to carry us immediately to the intermediary stage.

As soon as we propose, however, to determine the elements giving the *best representation* of observations and to find the *uncertainty* of these elements, all slide-rule and graphical methods become inadequate. With the accuracy attainable by modern photoelectric observations (of the order of 0.001 mag. or even better) the graphical plot, on the scale which would disclose the dispersion of individual normal points from a mean freehand curve, would necessitate the use of several dozen square yards of paper. Graphical methods of the preliminary stage, using fixed points of the light-curve, ascribe arbitrarily definite weights to different parts of the curve, and, as a result, they can often lead to erroneous conclusions about the determinacy of a solution. A mere inspection of the deviations of the individual observations from the theoretical light-curve can disclose very little about the uncertainty of the solution. Moreover, the less determinate the solution, the easier it is to obtain a representation of observations with some theoretical light-curve. A reasonably complete determination of the range over which the elements

[1] *Ap. J.*, **35**, 315; **36**, 239 and 385, 1912. A revised edition of tables necessary for a convenient application of these methods is being prepared by J. E. Merrill.

involved (at least four) can be varied without appreciable spoiling of the representation of observations is clearly very laborious.

Evidently, the best that we could do in the intermediary stage would be an application of the method of differential corrections. If we are, however, to avoid the recomputation of the matrix of coefficients, a good knowledge of all elements and some idea regarding the determinacy of the solution is prerequisite. It has, furthermore, been pointed out by Kopal[2] that, unless the components are almost in contact, the photometric perturbations arising from higher-order distortions can be computed with the aid of the intermediary elements, added with changed signs to the observed light-intensities, and then the regular least-squares solution for differential corrections can be performed. Unless, therefore, we are willing to compute the differential coefficients twice, it may often be convenient to defer the full-dress least-squares solution until the final stage.

The method developed in this paper proposes an adequate substitution for the general least-squares solution in the intermediary stage. It is fully analytical and leads to the determination of intermediary elements, together with their mean errors, also by the method of least squares but in such a way that, contrary to the general solution for the differential coefficients, very little information about the elements is prerequisite. In principle it is an extension of the method proposed by Kopal.[3] Its essentially new feature consists in the introduction, as unknowns into the equations of the problem, of the corrections to the provisionally accepted depths of the minima. The last point deserves a more detailed consideration.

Whichever method for determining the orbital elements of an eclipsing variable we employ, we have to accept certain values for the depths of minima before we can start with computations. As a rule, we determine the depths of minima from the freehand curves. There would be nothing objectionable in such a procedure if these depths were subjected, in the course of computation, to corrections resulting from the strict application of the equations of the problem to the observational data. But this has so far never been done. With the exception of a full-dress least-squares solution—for which, however, a good knowledge of all the elements is prerequisite—the depths of minima are mostly kept fixed during the analysis. This amounts to biasing the values of certain functions of the elements from the outset by an element of arbitrariness always inherent in drawing the "best-fitting" freehand curves. Moreover, if one's aim is to specify the accuracy of the photometric elements, no practicable way (short of the general differential corrections) has thus far been devised to account for the uncertainty of the depths of minima. We can, to be sure, repeat the whole determination of elements with altered depths of minima; but this is no method in itself and would multiply excessively the computer's work. Moreover, the net result would still be unsatisfactory, as we could not in this way get the mean errors of the depths themselves.

Partial eclipses.—Let us first consider the case of partial eclipses. We have the fundamental equation of the problem

$$\cos^2 i + \sin^2 i \sin^2\theta = r_1^2 [1 + kp(k, \alpha)]^2 , \tag{1}$$

where i denotes the inclination of the plane of relative orbit to the line of sight; θ, the phase angle computed from the mid-eclipse; r_1, the radius of the larger component; $k = r_2/r_1$, the ratio of the radii of the two stars. Furthermore, α denotes the loss of light expressed in terms of the light eclipsed at the moment of the inner contact, and p is a known (tabulated) function of k and α.[4] We suppose, for the sake of simplicity, that we

[2] Private communication.

[3] *An Introduction to the Study of Eclipsing Variables* (Cambridge: Harvard University Press, 1946), pp. 53 ff., 62 ff.

[4] For a complete set of such tables cf. Zessewitsch, *Bull. Inst. Astr. U.S.S.R. Acad. Sci.* No. 45, 1939, and Nc. 50, 1940.

are dealing with spherical stars and circular orbit. It will, however, be clear from what follows that the results admit of an easy generalization to the case of ellipsoidal stars and eccentric orbits as well. Let l_i denote the observed light-intensity of the ith normal point expressed in terms of the total light of the system outside eclipses. If λ denotes the fractional intensity of light at the bottom of the minimum which we propose to analyze, we have for the ith point

$$\alpha_i = \frac{1 - l_i}{1 - \lambda}\,\alpha_0 \equiv n_i \alpha_0 , \tag{2}$$

where α_0 denotes the maximum value of α and n_i is the proportional loss of light for the normal point considered. The depths of primary and secondary minimum are connected by the equation

$$\alpha_0 = 1 - \lambda_{oc} + (1 - \lambda_{tr})\,Q(k, \alpha_0) , \tag{3}$$

where Q is a known function of (k, α) and of the coefficients of limb darkening of both components, and $1 - \lambda_{oc}$ and $1 - \lambda_{tr}$ denote the maximum losses of light during the occultation and transit. Whether the primary minimum corresponds to an occultation or to a transit can be decided only in the further course of calculations. Following Kopal's[3] treatment of the problem, we write equation (1) down for the moment of conjunction; it reduces to

$$\cos^2 i = r_1^2 [1 + k p(k, \alpha_0)]^2 . \tag{4}$$

Subtracting equation (4) from equation (1), we obtain, for the ith observed normal point,

$$(p_1^2 - p_0^2)\,x + 2(p_i - p_0)\,y = \sin^2\theta_i , \tag{5}$$

where

$$p_i \equiv p(k, n_i\alpha_0) , \qquad p_0 \equiv p(k, \alpha_0) ,$$

$$x = r_1^2 k^2 \csc^2 i , \qquad y = r_1^2 k \csc^2 i .$$

If we change the accepted depth of primary minimum $1 - \lambda$ by $d(1 - \lambda)$, all normal points in the $(n, \sin^2\theta)$-plane will be shifted along the n-axis by an amount equal to

$$-\,n_i \frac{d(1 - \lambda)}{1 - \lambda} .$$

To this change of n there corresponds a change of $\sin^2\theta$ equal to

$$\frac{d \sin^2\theta}{dn} \times -\,n_i \frac{d(1 - \lambda)}{1 - \lambda} .$$

The left-hand side of equation (5) gives the value of $\sin^2\theta$ corresponding to the unchanged depths of minimum. In order to account for the change in the depth equal to $d(1 - \lambda)$, we have to add to the left-hand side of equation (5) the quantity

$$-\,n_i \frac{d \sin^2\theta}{dn} \frac{d(1 - \lambda)}{1 - \lambda} ;$$

thus we obtain

$$(p_1^2 - p_0^2)\,x + 2(p_i - p_0)\,y - n_i \frac{d \sin^2\theta}{dn} \frac{d(1 - \lambda)}{1 - \lambda} = \sin^2\theta_i . \tag{6}$$

Weighting of the equations.[5]—Equations (6) are linear in the unknowns x, y, and $d(1 - \lambda)$ and can be solved for them by the method of least squares. Before we proceed,

[5] Cf. Piotrowski, *Ap. J.*, **106**, 472, 1947.

however, to apply this method to a system of equations of the form (6), the individual equations of condition must be properly weighted. The errors of observation affect directly the n_i's in the left-hand sides of equations (6), whereas the phases can be regarded as error free because of the high exactitude with which the time of observation is usually known. Nevertheless, we can very easily shift these errors to the right-hand sides of equations (6). We can, namely, suppose that equations (6) hold *exactly* for the n_i's affected with errors, *provided* that the values of $\sin^2\theta$ on the right-hand sides are "corrected" by the quantity $(d\sin^2\theta/dn)dn_i$. If we now drop this "correction," we see that equations (6) can be regarded as having the coefficients of the unknowns unaffected by errors and the right-hand sides affected by errors proportional to

$$\frac{d\sin^2\theta}{dn}\,dn\,.$$

Denoting by dm the error in the stellar magnitude, we have

$$\frac{d\sin^2\theta}{dn}\,dn=\frac{d\sin^2\theta}{dn}\frac{dn}{dl}\frac{dl}{dm}\,dm=-\frac{d\sin^2\theta}{dn}\frac{1}{1-\lambda}\,l\,dm\,;$$

and thus

$$\sqrt{w_i}=-\frac{1-\lambda}{l}\frac{dn}{d\sin^2\theta}\,, \tag{7}$$

where w_i is the weight of the ith equation (6). The factor $1-\lambda$ is constant for the given minimum and can therefore be omitted whenever we treat one minimum alone. When, however, equations (6) are applied simultaneously to both minima—and it should be stressed that this is what should be done—we should remember its existence. The value of $dn/d\sin^2\theta$ occurring in the expression for $\sqrt{w}$ can be taken with sufficient accuracy directly from the freehand curve. It may, however, be noted that, when at a certain stage of approximation the preliminary values of the elements are known, use can be made of the formula

$$\frac{d\sin^2\theta}{dn}=\frac{d\sin^2\theta}{d\alpha}\frac{d\alpha}{dn}=2y\alpha_0(1+kp)\frac{\partial p}{\partial\alpha}. \tag{8}$$

The factor $1/l$ in equation (7) should be omitted whenever the errors are equal on the light-intensity scale.[6] In what follows we shall, however, consider the errors to be equal on the magnitude scale (as seems frequently to be the case) and shall multiply equations (6) by $\sqrt{w_i}$ as given by equation (7). We thus obtain

$$\sqrt{w_i}(p_i^2-p_0^2)\,x+2\sqrt{w_i}(p_i-p_0)\,y+\frac{n_i}{l_i}\,d(1-\lambda)=\sqrt{w_i}\sin^2\theta_i\,. \tag{9}$$

It is essential to make it quite clear just what we mean by shifting the errors from the observed brightnesses—which are really affected by them—to the phases which are sensibly error free. Using geometrical language, our aim—strictly speaking—is to "draw" the theoretical light-curve so as to minimize the sum of the squares of the distances from the observed points to the points, on the curve, with the same phase. By multiplying equations (6) with the square roots of weights taken inversely proportional to $(d\sin^2\theta)/dn$ and solving them by the method of least squares, we shall minimize the sum of the squares of distances measured in the same direction as previously—measured, however, not from the curve itself but from the tangent to the curve drawn in the point with the observed brightness. When the errors of photometric observations are small, the considered distance between the curve and the tangent is a small quantity of the second

[6] Cf., *ibid.*, n. 3.

order. The neglect of this quantity is the price which we must pay for being able to "draw"—from the outset and with only very crude knowledge of the parameter k—the light-curve in conformity with the principle of the least squares. If the errors are large, the use of any refined analytical method is out of place. It should be kept in mind that, from the moment when we have multiplied equations (6) by the square roots of the proposed weights, the n_i's in p_i's, though computed from erroneous brightnesses, must be formally treated as exactly known quantities.

Thus far we have tacitly assumed that the light of the system outside eclipses is known exactly. Let us denote this light by l_m. By definition, we have set l_m to be unity. The light-intensities l_i of normal points during the eclipses were, in fact, set equal to l_i'/l_m, where l_i' denotes the actually observed light-intensity. A change of dl_m in l_m introduces a change equal to $-(l_i'/l_m)(dl_m/l_m)$ in l_i. If we put $dl_m/l_m = dU$, we get

$$dl_i = -l_i dU \ .$$

To the change of l_i specified by the last equality there corresponds a change of n_i equal to $l_i dU/(1-\lambda)$, and this quantity should be treated as was $-n_i[d(1-\lambda)/(1-\lambda)]$ before. We thus obtain an additional term in equation (9) equal to $-dU$. The total correction to the amplitude of the minimum depends on this correction of our unity of light. It is therefore often desirable to introduce the correction $(d\lambda)$ of the minimal light (with light-unity kept unchanged) and the correction of the light-unity dU as independent unknowns. Substituting in equation (9) $d(1-\lambda)$ from the relation

$$d(1-\lambda) = -(d\lambda) + \lambda dU$$

and adding the term $-dU$, we obtain the fundamental equation of condition in the form

$$\sqrt{w_i}(p_i^2 - p_0^2)\, x + \sqrt{w_i} 2(p_i - p_0)\, y - \frac{n_i}{l_i}(d\lambda) + \left[\frac{n_i - 1}{l_i}\right] dU = \sqrt{w_i}\sin^2\theta_i \,. \quad (10)$$

The factor $1/l_i$ should be omitted whenever the errors are equal on the light-intensity scale.[6] As a rule, the eclipses extend only over a small fraction of the whole period, and therefore the information about maximum light, which we can get only from the observations relative to the eclipses, will contribute little to our knowledge of the maximum light as obtained from observations outside eclipses. Nevertheless, it may be advisable to transpose the terms with dU to the right-hand sides of equations of condition and of the normal equations and thus introduce dU as an undetermined parameter into the final solution. Knowing the uncertainty (mean error) of the maximum light from the observations pertaining to full light, we can easily compute the uncertainty introduced into the determination of the elements by the uncertainty in the light-unity.

We proceed now to solve equation (9) or equation (10) together with equation (3) in a way identical in principle with the one described by Kopal.[3] We start by making a rough estimate (from the durations or depths of both minima or otherwise) of k and denote this trial value by K. We insert K, together with a value of a_0 obtained from equation (3), in the coefficients of x and y in equation (9) and solve equation (9) by the method of least squares. If the correction to the depth of the minimum $d(1-\lambda)$ comes out appreciable, we add it to $1-\lambda$, recompute the n_i's, and proceed to improve k, by iteration or otherwise, until $x/y = k$ becomes equal to K. As a rule, there should rarely be a need of computing the n_i's for the second time. For reasons of simplicity we have thus far limited our discussion to the primary minimum alone. In dealing with actual eclipsing systems, it should, however, be borne in mind that equation (9) should be applied to both minima simultaneously. For a secondary minimum, $d(1-\lambda)$ denotes, of course, the correction of the depth of the secondary. A shallow secondary minimum will, to be sure, add very little—if anything—to the determination of x and y; but its inclusion bears essentially on the determination of $d(1-\lambda_{sec})$. The following procedure may often

be advantageous when we limit ourselves to the determination of the amplitude only, from a shallow secondary minimum. Let us denote by $n_{\theta i}$ the function of r_i, k, i, and θ_i determined by the equations

$$\cos^2 i + \sin^2 i \sin^2 \theta_i = r_1^2 [1 + kp(k, \alpha)]^2 ,$$

$$n_{\theta i} = \frac{\alpha(r_1, k, i, \theta_i)}{\alpha(r_1, k, \imath, 0)} .$$

Obviously, the equations of condition can be written in the form

$$n_{\theta i}[(1-\lambda) + d(1-\lambda)] = \frac{l_m + dl_m - l_i'}{l_m + dl_m} = 1 - l_i + l_i dU .$$

Substituting in the last equation $d(1-\lambda) = -(d\lambda) + \lambda dU$ and neglecting small quantities of the second order, we get

$$n_{\theta i}(1-\lambda) - n_{\theta i}(d\lambda) + (n_{\theta i} - 1)\, dU = 1 - l_i \tag{11}$$

or

$$n_{\theta i}\{1 - [\lambda + (d\lambda)]\} + (n_{\theta i} - 1)\, dU = 1 - l_i . \tag{12}$$

Equations (11) and (12), as they stand, refer to the case of equal errors on the light-intensity scale. If the errors are equal on the magnitude scale, they should be multiplied by $1/l_i$. For a shallow secondary minimum, we can neglect the difference of shape between the primary and the secondary minimum. If we know with any reasonable accuracy the moment of the mid-secondary minimum, we can substitute it in equations (12) written down for all $1 - l_i$ observed during this minimum $n_{\theta i}$ from the well-observed curve of the primary minimum and determine the amplitude of the secondary by the method of least squares. Very often we shall have to put $dU = 0$.

A special case presents itself when, owing to the errors of observation, any of the n_i's may have a small negative value for some normal point near the beginning of the eclipse. Neither p nor $\sqrt{w}$ is defined for negative values of n. In such a case we can make use of equation (11), which is valid for all phases. Let us define $\sqrt{w_i}$ (for simplicity the case of equal errors on the light-intensity scale is considered) with the aid of the relation

$$n_{\theta i}(1-\lambda) = \sqrt{w_i}(\sin^2 \theta' - \sin^2 \theta_i) ,$$

where θ' is the phase of the first contact (we assume that $\theta_i < \theta'$). This definition of $\sqrt{w_i}$ means that the approximate value of the derivative $dn/d \sin^2 \theta$ occurring in the expression for $\sqrt{w_i}$ was taken from the light-curve as equal to the ratio of the change of n to the change of $\sin^2 \theta$ over the whole interval θ_i to θ'. Let us now introduce $n_{\theta i}(1-\lambda)$ from the last equation into equation (11) and replace $\sin^2 \theta'$ by its expression in functions of x, y, and p_0; we obtain

$$\sqrt{w_i}(1 - p_0^2)\, x + \sqrt{w_i} 2(1 - p_0)\, y - n_{\theta i}(d\lambda) + (n_{\theta i} - 1)\, dU = \sqrt{w_i} \sin^2 \theta_i + 1 - l_i . \tag{13}$$

The value of $n_{\theta i}$ in the coefficients of $(d\lambda)$ and dU can, with sufficient accuracy, be taken from the mean light-curve as n corresponding to $\theta = \theta_i$.

Total eclipses.—We proceed now to the case of a total eclipse. In such a case all elements can be determined from the analysis of one minimum alone. Instead of equation (10) we shall have

$$\sqrt{w_i}(p_i^2 - 1)\, x + 2\sqrt{w_i}(p_i + 1)\, y + \sqrt{w_i}\, z - \frac{n_i}{l_i}(d\lambda) + \left(\frac{n_i - 1}{l_i}\right) dU = \sqrt{w_i} \sin^2 \theta_i , \tag{14}$$

where z denotes the $\sin^2\theta$ at the beginning of totality. Equations (14) make use of the observations corresponding to the partial phases only. We have therefore to add to equations (14) one more equation of condition, viz., the equation relating to the normal points falling between the second and third contact. If the number of such normal points is N, if the mean value of their light-intensity is l_0, and if equations (14) are weighted according to equation (7), this additional equation will be

$$\frac{1}{\lambda}\sqrt{N}\,(d\lambda) = \frac{1}{\lambda}\sqrt{N}\,(l_0 - \lambda)\,.$$

Most often we accept $\lambda = l_0$, and therefore the right-hand side of the last equation will be zero. The factor $1/\lambda$ must again be omitted if errors are equal on the light-intensity scale.

A case similar to that of $n_i < 0$, discussed previously, can arise in connection with a total eclipse if, because of errors of observations, n_i happens to be a little greater than 1 for a normal point near the beginning of totality. Proceeding as we did for $n_i < 0$, we find that, for such a normal point, the equation of condition can be written in the form

$$\sqrt{w_i}\,z - n_{\theta i}\,(d\lambda) + (n_{\theta i} - 1)\,dU = \sqrt{w_i}\sin^2\theta_i + \lambda - l_i\,, \tag{15}$$

where the derivative $dn/d\sin^2\theta$ contained in the expression for $\sqrt{w_i}$ should be taken from the mean light-curve as the ratio of the change of n to the change of $\sin^2\theta$ over the whole interval θ_i to θ'' (θ'' being the phase of the second contact, $\theta_i > \theta''$). If the errors are equal on the magnitude scale, the factor $1/l_i$ should be introduced in the coefficients of $(d\lambda)$ and dU and in the term $\lambda - l_i$.

Annular eclipses.—For an annular eclipse equations (14) hold good for all phases of the eclipse. The quantity $1 - \lambda$ in this case corresponds, however, to the moment of internal tangency, not to the conjunction.

Errors of the elements.—For both partial, as well as total, eclipses the mean errors of the unknowns obtained from the least-squares solution do not represent the total mean errors of these quantities. The reason is the relation $K = k$, by which we judged the degree of the achieved approximation. The value of $k = x/y$ is subject to error and so is, in consequence, K, which occurs in the coefficients of the equations of condition. This additional source of error affects, in practice, only x, y (and z). It is clear a priori that $d(1 - \lambda)$ will depend relatively little on the particular set of elements that we are using to "draw" the theoretical curve. The total errors of x and y can be found in the following way.[7] We obtain from the solution of normal equations x and y as functions of K and of the right-hand sides of equations (10) or equations (14)—let us denote them by L_i; we have thus

$$\begin{aligned} x &= F\,(K, L_1, L_2, \ldots, L_n)\,, \\ y &= G\,(K, L_1, L_2, \ldots, L_n)\,. \end{aligned} \tag{16}$$

Now the condition $k = K$ means that we substitute x/y for K in F and G. With this substitution we get, by differentiation of equations (16),

$$\begin{aligned} \frac{\partial x}{\partial L_i} &= \frac{1}{y^2}\frac{\partial x}{\partial K}\frac{\partial x}{\partial L_i}\,y - \frac{\partial y}{\partial L_i}\,x + \frac{\partial F}{\partial L_i}\,, \\ \frac{\partial y}{\partial L_i} &= \frac{1}{y^2}\frac{\partial y}{\partial K}\frac{\partial x}{\partial L_i}\,y - \frac{\partial y}{\partial L_i}\,x + \frac{\partial G}{\partial L_i}\,; \end{aligned} \tag{17}$$

[7] The results expressed by equations (19) and (20) have already been stated by the writer (*ibid.*). Their present derivation is, however, novel and considered superior to the writer's earlier treatment of the subject.

and, solving equations (17) for $\partial x/\partial L_i$ and $\partial y/\partial L_i$, we have

$$\left(y-\frac{\partial x}{\partial K}+k\frac{\partial y}{\partial K}\right)\frac{\partial x}{\partial L_i}=\left(y+k\frac{\partial y}{\partial K}\right)\frac{\partial F}{\partial L_i}-k\frac{\partial x}{\partial K}\frac{\partial G}{\partial L_i},$$
$$\left(y-\frac{\partial x}{\partial K}+k\frac{\partial y}{\partial K}\right)\frac{\partial y}{\partial L_i}=\frac{\partial y}{\partial K}\frac{\partial F}{\partial L_i}+\left(y-\frac{\partial x}{\partial K}\right)\frac{\partial G}{\partial L_i}. \tag{18}$$

We easily see that

$$y-\frac{\partial x}{\partial K}+k\frac{\partial y}{\partial K}=y\left(1-\frac{\partial k}{\partial K}\right).$$

The total error of x—let us denote it by Δx—is equal to

$$\sum_i \frac{\partial x}{\partial L_i}\,\delta L_i,$$

and an analogous relation exists for Δy. The expressions

$$\sum_i \frac{\partial F}{\partial L_i}\,\delta L_i \quad \text{and} \quad \sum_i \frac{\partial G}{\partial L_i}\,\delta L_i$$

are the errors of x and y whose root-mean-square values we have found from the least-squares solution. Let us denote them by $(\delta x)_K$ and $(\delta y)_K$, respectively. Multiplying both equations (18) by δL_i and performing the summation over all i's, we get

$$\Delta x=(\delta x)_K+\frac{\partial x}{\partial K}\frac{1}{1-\frac{\partial k}{\partial K}}\frac{(\delta x)_K-k(\delta y)_K}{y},$$
$$\Delta y=(\delta y)_K+\frac{\partial y}{\partial K}\frac{1}{1-\frac{\partial k}{\partial K}}\frac{(\delta x)_K-k(\delta y)_K}{y}. \tag{19}$$

In the case of total eclipse we have, in addition,

$$\Delta z=(\delta z)_K+\frac{\partial z}{\partial K}\frac{\Delta x-k\Delta y}{y}. \tag{20}$$

The derivatives $\partial k/\partial K$, $\partial x/\partial K$, $\partial y/\partial K$, as well as $\partial z/\partial K$, can be evaluated numerically quite easily, as we had to make at least two hypotheses on K when solving equations (10) and (14). With the aid of formulae (19) and (20) we have expressed the total errors of x, y, and (z) as linear functions of $(\delta x)_K$, $(\delta y)_K$, and $(\delta z)_K$. In order to find the mean error of any element, we have to express this error as a linear function of $(\delta x)_K$, $(\delta y)_K$, $(\delta z)_K$, and $\delta d(1-\lambda)$ and apply the formula for the error of a linear function as given in any textbook on the theory of the least-squares method.[8] Unless the iteration or trial-and-error process, basic to the application of the present method, converges very slowly, the additional errors just discussed (i.e., the terms factored by $[\partial x/\partial K]/[1-\partial k/\partial K]$, $[\partial y/\partial K]/[1-\partial k/\partial K]$, and $\partial z/\partial K$ in equations [19] and [20]) will be negligible. Actually, they arise because of the slowness of convergence of successive approximations. If, however, the intrinsic determinacy of the ratio of radii is small, the denominator $1-\partial k/\partial K$ may come close to zero, and the neglect of the terms factored by $(1-\partial k/\partial K)^{-1}$ would give us far too optimistic a picture of the accuracy of the solution.

Ellipsoidal stars.—As was pointed out previously, all results admit of an easy generalization to the case of ellipsoidal stars. On the assumption that the system consists of two

[8] E.g., E. T. Whittaker and G. Robinson, *The Calculus of Observations* (London: Blackie & Son, 1932), pp. 242 ff.

similar prolate ellipsoids, we rectify the brightnesses for ellipticity and, eventually, for the reflection effect.[9] In the case of partial eclipses, instead of equation (10) we shall have

$$\sqrt{w_i}\,[p_1^2(1 - z\cos^2\theta_i) - p_0^2(1 - z)]\,x' + \sqrt{w_i}2\,[p_i(1 - z\cos^2\theta_i) - p_0(1 - z)]\,y' - \frac{n_i}{l_i}(d\lambda) + \left[\frac{n_i - 1}{l_i}\right]dU = \sqrt{w_i}\sin^2\theta_i,$$

where $z = 2\epsilon\sin^2 i$, ϵ is the geometrical ellipticity, and between x' and y' and the parameters x and y, used in the case of spherical stars, we have the relations

$$x = \frac{x'^2}{x' + zy'^2}; \qquad y = \frac{x'y'}{x' + zy'^2}.$$

The equations for the case of total (annular) eclipses can be obtained from those valid for spherical stars in a similar way; the reader is referred to Kopal's treatment of the subject.[10]

General remarks.—The general procedure by which we have introduced into the equations of the problem the correction of the provisionally accepted value of a certain element, E, can be summarized as follows: We have, for each normal point,

$$H(n, x, y, z, E + dE) = \sin^2\theta(n),$$

where H is a known function of elements. Now we expand H in a power series in dE and drop all terms with second and higher powers of dE. Then we replace the value of $\partial H/\partial E$ by $(d\sin^2\theta/dn)(\partial n/\partial E)$. The resulting system of equations is solved for x, y, z, and dE. This procedure can be easily applied to determine the corrections to the assumed values of the coefficients of limb darkening. It suffices to remark that $n = \alpha/\alpha_0$, and the α's are simple functions of limb darkening. Let us denote by the subscript 1 the quantities referring to the larger body and by the subscript 2 those pertaining to the smaller one. Furthermore, let the superscripts U and D in the α's signify that these quantities have been taken from uniform and darkened tables, respectively. The subscript i in α signifies that this value of α corresponds to the ith normal point; α_i is a function of p_i and k. Similarly, α_0 is a function of p_0 and k, the zero subscript corresponding to the moment of deepest eclipse—or, in the case of a total (annular) eclipse, to the moment of internal tangency. Furthermore, let $x_1 = 2u_1/(3 - u_1)$ and $x_2 = 2u_2/(3 - u_2)$, where u denotes the coefficient of limb darkening. The terms factoring the corrections dx_1 and dx_2 are, then, for a transit,

$$\frac{1 - \lambda}{\alpha_{01}[1 - x_1 + \frac{3}{2}\Phi(k)]}\,\frac{n_i}{l_i}\left[\frac{\frac{3}{2}\Phi(k)\,\alpha_{i1}^D - \alpha_i^U}{n_i} - \frac{3}{2}\Phi(k)\,\alpha_{01} + \alpha_0^U\right],$$

while for an occultation they are

$$\frac{1 - \lambda}{\alpha_{02}}\,\frac{n_i}{l_i}\left[\frac{\alpha_{i2}^D - \alpha_i^U}{n_i} - (\alpha_{02}^D - \alpha_0^U)\right],$$

where $\Phi(k)$ is a tabulated function of k.[4] The factor $1/l_i$ should be omitted if the errors are equal on the light-intensity scale.[6]

When we apply the general method of differential corrections,[11] the uncertainty of the maximum light of the system should be duly accounted for. Let L_1 denote the luminosity of the component undergoing eclipse, f the fractional loss of light of this component at

[9] Cf. Russell, *Ap. J.*, **102**, 1, 1945; **104**, 153, 1946.

[10] Kopal, *op. cit.*, p. 197.

[11] Cf. *ibid.*, chap. iv.

any moment within eclipse, L_2 the luminosity of the eclipsing component, and l the brightness of the system. We have

$$l = L_1 + L_2 - fL_1 .$$

As a rule, the brightness, l, is expressed in terms of the maximum brightness, l_m. Denoting by l' the brightness actually observed, we have $l = l'/l_m$. Now we assume, by definition, *either* that always $L_1 + L_2 = 1$ *or* that L_1 and L_2 are expressed, by definition, in terms of l_m. These two definitions are *not* equivalent, because l_m is an observed quantity. If we accept, by definition, $L_1 + L_2 = 1$ and $\Delta L_1 = -\Delta L_2$, the equations of condition of the method of differential corrections will be of the form

$$\frac{l'}{l_m + \Delta l_m} = 1 - fL_1 - f\Delta L_1 - L_1 \Delta f .$$

Putting $l - (1 - fL_1) = \Delta l$ and $\Delta l_m / l_m = \Delta U$, we can re-write the foregoing equation as follows:

$$\Delta l = l\Delta U - f\Delta L_1 - L_1 \Delta f . \qquad (21)$$

From observations outside eclipses we have $\Delta U = 0$, with a certain mean error. As was discussed previously in more detail, it may be advisable to keep ΔU in equation (21) undetermined and to find, in the final solution, which amount of uncertainty is introduced into the elements by the fact that ΔU is equal to zero only within a certain mean error. If we accept l_m as our unit of light, we shall have, instead of equation (21),

$$\Delta l = \Delta L_1 + \Delta L_2 - f\Delta L_1 - L_1 \Delta f ;$$

and, from observations of uneclipsed light, $\Delta L_1 + \Delta L_2 = 0$, with a certain mean error. It is a matter of preference which definition we choose. We should remember, however, that the form of the equations of condition depends on our choice.

Numerical example.—In order to illustrate the application of the fundamental equation (9) to a numerical case, let us consider the following (fictitious) example. Let us take an eclipsing system consisting of uniformly bright stars with $k = 0.7$, $r_1 = 0.2$, the amplitude of the primary (occultation) 1.5 mag. (thus $1 - \lambda = 0.7488$), the depth of the secondary 0.0741, and $\alpha_0 = 0.9$. From the above data I have calculated phases and losses of light for four points corresponding to $\alpha = 0.045$, 0.315, 0.585, and 0.855. It is clear that, having "observed" only these four points during the primary minimum, no freehand curve could tell us much about its depth. The reader may notice that the observation nearest the bottom of the curve is still 0.15 mag. brighter than the true minimum light. As the amplitude of the primary I accepted 1.45 mag., a value too small by 0.05 mag. With the loss of light corresponding to 1.45 mag. = 0.7370, I computed the n_i's for the mentioned four "observed" points. The weights were calculated from equations (7) and (8). Starting with $K = 0.7$ and α_0 (resulting from eq. [3] with the erroneous $1 - \lambda = 0.7370$) equal to 0.8882, I found, from the least-squares solution of a system of equations of the form (9), $k = 0.707$ and $d(1 - \lambda) = +0.0116$, and hence the corrected amplitude was 1.499 mag., the true value being 1.5 mag. Even with $K = 1$, which is rather far from the true 0.7, the least-squares solution of equation (9) still leads to the corrected amplitude 1.504 mag., which is only 0.004 mag. in error. It can be mentioned that, without the term $(n_i/l_i)d(1 - \lambda)$ in equation (9), we get (with the erroneous amplitude 1.45 mag.) $k = 0.613$—a value considerably too small.

In conclusion, the writer considers it a pleasure to express his appreciation to Dr. Harlow Shapley for an opportunity of working at the Harvard College Observatory, where the foregoing study was carried out. He wishes also to acknowledge his indebtedness to Dr. Zdeněk Kopal for valuable discussions of the problem and his careful preview of the manuscript.

REMARKS ON THE DETERMINATION OF INTERMEDIARY ORBITS OF ECLIPSING BINARY SYSTEMS

ZDENĚK KOPAL
Center of Analysis, Massachusetts Institute of Technology
and
Harvard College Observatory
Received May 3, 1948

ABSTRACT

A theory of intermediary orbits of eclipsing binary systems is further developed in three different directions. First, the formulae for evaluating the differential correction Δa_0 simultaneously with C_1, C_2, and $\Delta(1-\lambda)$ are established. It is shown that the correction Δa_0 is practically indeterminate for partially eclipsing systems but that it can be expressed as a combination of $\Delta(1-\lambda_a)$ and $\Delta(1-\lambda_b)$; and these should be solved for simultaneously from the observational data pertaining to both minima.

In the second part of this paper, formulae are developed for computation of the derivatives dC_1/dK and dC_2/dK prerequisite for the specification of errors with which the individual geometrical elements are defined by the observations. The proposed process makes full use of the data previously available and requires but little additional work.

In the third part a similar method is outlined for computation of the derivatives dC_1/du and dC_2/du which, in turn, permit us to ascertain the rates of change of the individual geometrical elements corresponding to a small change in the adopted degree of limb darkening.

Piotrowski's beautiful and penetrating analysis[1] of the problem of intermediary orbits of eclipsing binary systems and of the errors with which the geometrical elements of an eclipsing variable are defined by its light-curve covers the subject in so thorough a manner that little remains to be added if the eclipses are total (or annular). When, however, the eclipses happen to be partial, certain supplementary considerations may be pointed out.

I

Consider, for instance, the effects, upon a determination of the geometrical elements, caused by an error $\Delta(1-\lambda)$ in the assumed value of the loss of light of the minimum under investigation. This error will vitiate systematically all fractional losses of light, a, in two distinct ways: first, by affecting all values of n and, second, by affecting a_0, which, for partially eclipsing systems, represents an additional unknown to be determined by orbital analysis. Only the first source of error, i.e., the effects of $\Delta(1-\lambda)$ upon n, has been considered by Piotrowski. In what follows, we shall complete his analysis by investigating the other.

In order to do so, let us start from the fundamental equation of our problem[2]

$$\begin{aligned} &H = \sin^2\theta\,, \\ &H \equiv (p^2 - p_0^2)C_1 + 2(p - p_0)C_2\,, \\ &p \equiv p(k, a)\,, \qquad p_0 \equiv p(k, a_0)\,, \\ &a = n a_0\,, \qquad n = \frac{1-l}{1-\lambda}\,. \end{aligned} \tag{1}$$

[1] *Ap. J.*, **108**, 36, 1948. The writer is indebted to Dr. Piotrowski for an opportunity to study the text of his paper in advance of publication.

[2] Cf. the writer's *Introduction to the Study of Eclipsing Variables* (Cambridge: Harvard University Press, 1946), chap. iii, pp. 62 ff. Unless specifically explained or stated to the contrary, the notations of the *Introduction* will hereafter be used.

It can, furthermore, be proved[3] that, if the eclipse under consideration is an occultation (smaller star eclipsed),[4]

$$a_0' = 1 - \lambda_a + \frac{1 - \lambda_b}{k^2 Y}, \tag{2.0}$$

while if it is a transit (larger star eclipsed),

$$a_0'' = \left(\frac{Y}{Y_0}\right)(1 - \lambda_a) + \frac{1 - \lambda_b}{k^2 Y_0}, \tag{2.1}$$

where λ_a and λ_b denote the fractional luminosity of the system at the respective maximum eclipse, and

$$Y = \frac{(1 - x_b)\, a^U(k, p_0) + \frac{3}{2}\Phi(k)\, x_b a_b^D(k, p_0)}{(1 - x_a)\, a^U(k, p_0) + x_a a_a^D(k, p_0)}, \tag{3}$$

Y_0 being the value that Y would assume at the moment of internal tangency (when $p_0 = -1$), i.e.,

$$Y_0 = 1 - x_b + \tfrac{3}{2} x_b \Phi(k). \tag{3.1}$$

In these equations,

$$\Phi(k) = \frac{2}{3}\frac{q^D}{k^2}$$

denotes a known function of k, which has been tabulated by Zessewitsch.[5]

Suppose, now, that, in estimating the depth $1 - \lambda$ of the minimum under investigation,[6] an error of $\Delta(1 - \lambda)$ was made. Furthermore, let the function H, evaluated with the erroneous value of $1 - \lambda$, be denoted by H_0. In order to determine $\Delta(1 - \lambda)$ and its effect upon the determinacy of other elements, we expand H in a Maclaurin series of the form

$$H_0 + \frac{\partial H_0}{\partial(1 - \lambda)}\Delta(1 - \lambda) + \frac{\partial H_0}{\partial a_0}\Delta a_0 + \ldots = \sin^2\theta, \tag{4}$$

where, remembering that $C_1/C_2 = k$, we find

$$\frac{\partial H_0}{\partial(1 - \lambda)} = -\frac{2n a_0 C_2}{1 - \lambda}\{1 + kp\}\frac{\partial p}{\partial a}, \tag{5}$$

and

$$\frac{\partial H_0}{\partial a_0} = 2nC_2(1 + kp)\frac{\partial p}{\partial a} - 2C_2(1 + kp_0)\frac{\partial p_0}{\partial a}. \tag{6}$$

Now Piotrowski[1] has shown that the fundamental equation (1) appropriate to any observed loss of light should be multiplied by the square root, $\sqrt{w}$, of its intrinsic weight

$$\sqrt{w} = -(1 - \lambda)\frac{dn}{dH_0} = -\frac{1 - \lambda}{2a_0 C_2(1 + kp)\frac{\partial p}{\partial a}} \tag{7}$$

[3] Cf. *Ibid.*, chap. ii, pp. 32 ff.

[4] The quantity Y was not used as such in the *Introduction*, but its usefulness occurred later. It is related with Q as defined by eq. (45) of the *Introduction* by $k^2 Y = 1/Q$.

[5] *Bull. Astr. Inst. U.S.S.R. Acad. Sci.*, No. 50, Table 5, p. 307, 1940.

[6] Whenever, in what follows, the values of λ are used without subscripts, it is understood that they apply equally to either occultations or transits. The same is true of a_0 when used without accents.

before their solution for the unknown constants C_1 and C_2 is performed. If we multiply equations (5) and (6) by equation (7), we find, with Piotrowski, that

$$\sqrt{w}\,\frac{\partial H_0}{\partial(1-\lambda)} = n\,; \tag{8}$$

but, in addition,

$$\sqrt{w}\,\frac{\partial H_0}{\partial a_0} = \frac{1-\lambda}{a_0}\left\{\sqrt{\left(\frac{w}{w_0}\right)} - n\right\}, \tag{9}$$

where $\sqrt{w_0}$ denotes the square root of the intrinsic weight at the moment of maximum eclipse.

When the explicit forms (8) and (9) of the respective coefficients are inserted in equation (4), an equation is obtained containing C_1, C_2, $\Delta(1-\lambda)$, and Δa_0 as unknowns, from which it would seem that a correction Δa_0 to the assumed value of the maximum obscurations could be determined from equation (4) simultaneously with the other unknowns and wholly on its own merits (i.e., without any reference to eqs. [2]). This is indeed possible in theory but not, unfortunately, in practice because of the numerical smallness of the expression on the right-hand side of equation (9) and its strong correlation with the coefficient of C_1 in equation (4). The expression on the right-hand side of equation (9), namely, vanishes not only at the beginning of the eclipse ($\sqrt{w} = n = 0$) and at the moment of maximum obscuration ($\sqrt{[w/w_0]} = n = 1$) but also around $p = -p_0$ during the partial phases. An inclusion of Δa_0 as an additional unknown to be determined simultaneously with C_1, C_2, and $\Delta(1-\lambda)$ by a least-squares solution of the equations of condition of the form (4) leads, consequently, to so drastic a loss of weight of the whole solution that such a procedure appears to be futile even with the best light-curves now available.[7] This is no new feature of the problem but merely a new aspect of a well-known fact that a determination of the geometrical elements of partially eclipsing systems from one minimum alone remains still impracticable.

If, however, the depths of both minima have been observed,[8] the situation is thoroughly altered because equations (2) are then available to eliminate Δa_0 from equation (4) by

[7] In order to illustrate the situation by a specific example, the writer would like to quote a few actual figures obtained in the course of a solution for an intermediary orbit of Algol, based on essentially the same observational data as those used in his previous study of the Algol system (*Ap. J.*, **96**, 399, 1942), which certainly constitutes one of the best light-curves available for any eclipsing system. Whereas, when advantage was taken of our knowledge of the depth of the secondary minimum and equation (2.0) was used to evaluate a_0, the intermediary solution (with $K=0.95$ and $u=0.55$ assumed) led to

$$\begin{aligned} C_1 &= 0.0526 \pm 0.0010 \text{ (p.e.)}, \\ C_2 &= 0.0554 \pm 0.0002, \\ \Delta(1-\lambda_0) &= -0.0027 \pm 0.0012, \end{aligned}$$

yielding $k = 0.949 \pm 0.018$ (p.e.), the inclusion of Δa_0 among the unknowns led to

$$\begin{aligned} C_1 &= 0.0320 \pm 0.0171 \text{ (p.e.)}, \\ C_2 &= 0.0526 \pm 0.0023, \\ \Delta(1-\lambda_0) &= -0.0035 \pm 0.0014, \\ \Delta a_0 &= 0.26 \pm 0.22, \end{aligned}$$

yielding $k = 0.61 \pm 0.35$ (p.e.)! The fit to the observations is just about equally good in either case. This would be the degree of determinancy of the orbital solution from the primary minimum alone, if nothing whatever were known about the secondary minimum.

[8] In order to forestall any possible misunderstanding, let it be stressed that this does *not* require the secondary minimum to be deep. What matters is that an absolute (not proportional) error in its determination be small. A knowledge that the secondary minimum is quite insensible, but that its amplitude cannot exceed, say, 0.01 mag., is just as valuable for fixing the value of a_0 as if the depth of this minimum were, say, 0.10 ± 0.01 mag. In this latter case, a_0 would merely respond more to any change of k than in the former, which may slow down the convergence of the approximations. It is only when we know *nothing whatever* about the secondary minimum—whether it is shallow or deep—that the determination of orbits of partially eclipsing systems becomes well-nigh hopeless.

expressing it in terms of $\Delta(1-\lambda_a)$ and $\Delta(1-\lambda_b)$. From equations (2) it follows, therefore, that

$$\Delta\alpha_0' = \Delta(1-\lambda_a) + \frac{\Delta(1-\lambda_b)}{k^2 Y}, \tag{2.01}$$

while

$$\Delta\alpha_0'' = \left(\frac{Y}{Y_0}\right)\Delta(1-\lambda_a) + \frac{\Delta(1-\lambda_b)}{k^2 Y_0}. \tag{2.11}$$

Inserting these in equation (4), we find that under these circumstances equation (4), properly weighted, can be re-written as

$$\sqrt{w}H_0 + \left\{\frac{n(1-\lambda_b)}{\alpha_0' k^2 Y} + \frac{1-\lambda_a}{\alpha_0'}\sqrt{\left(\frac{w}{w_0}\right)}\right\}\Delta(1-\lambda_a) + \frac{1-\lambda_a}{\alpha_0' k^2 Y}\left\{\sqrt{\left(\frac{w}{w_0}\right)} - n\right\}\Delta(1-\lambda_b) = \sqrt{w}\sin^2\theta \tag{4.1}$$

if the eclipse giving rise to the minimum under investigation is an occultation, and as

$$\sqrt{w}H_0 + \left\{\frac{n(1-\lambda_a)}{\alpha_0''\left(\frac{Y_0}{Y}\right)} + \frac{1-\lambda_b}{\alpha_0'' k^2 Y_0}\sqrt{\left(\frac{w}{w_0}\right)}\right\}\Delta(1-\lambda_b) + \frac{1-\lambda_b}{\alpha_0''\left(\frac{Y_0}{Y}\right)}\left\{\sqrt{\left(\frac{w}{w_0}\right)} - n\right\}\Delta(1-\lambda_a) = \sqrt{w}\sin^2\theta \tag{4.2}$$

if it is a transit.

In either case, the respective equations of condition for each minimum contain explicitly both $\Delta(1-\lambda_a)$ and $\Delta(1-\lambda_b)$ as unknowns. The correction to the depth of the minimum under investigation is always a well-determined quantity, and its coefficient is numerically not very different from n; the correction to the depth of the other minimum is, however, notoriously indeterminate.[9] However, if we combine the equations of condition of the form (4.1) and (4.2) appropriate for both minima into a single set and solve them simultaneously, well-determined corrections to the depths of both minima can be obtained. There is probably little need to stress that this should always be done.

We may add that, when the eclipse becomes total and α_0 is therefore exactly equal to 1, equations (2) show that, for a fixed value of k, the depths of the two minima are interrelated, so that

$$\Delta(1-\lambda_a) = -\frac{\Delta(1-\lambda_b)}{k^2 Y_0}. \tag{10}$$

If we insert this in equations (4.1) and (4.2), these equations reduce to the form given by Piotrowski. Equations (4.1) and (4.2) are then completely independent, and the corrections to the depths of the alternate minima can be solved for separately. For partially eclipsing systems this is, however, not the case and should never be done.

II

A great merit of Piotrowski's investigation was to point out the role of the derivative dk/dK in the determination of errors of the individual geometrical elements and its

[9] The reason for this is not too hard to find. An error in the assumed depth of the minimum under investigation affects systematically all values of n, and the corresponding errors in α affect all p's, but not p_0; its effect upon the differences $p - p_0$ or $p^2 - p_0^2$ may therefore become appreciable. An error in the assumed depth of the other minimum will affect only α_0 and, through it, both p and p_0 alike—so that its effect on the differences $p - p_0$ or $p^2 - p_0^2$ is very minor indeed.

effect on the convergence of the iterative process of solution of the fundamental equation (1) in general. Since, by definition, $k = C_1/C_2$, it follows by differentiation that

$$\frac{dk}{dK} = \frac{1}{C_2}\frac{dC_1}{dK} - \frac{k}{C_2}\frac{dC_2}{dK}. \tag{11}$$

In order to ascertain this quantity, Piotrowski suggests carrying out the whole orbital solution for two assumed values of K_1 and K_2 and determining the derivatives dC_1/dK and dC_2/dK from the differences of C_1 and C_2 computed under the two assumptions. Such a process would not only just about double the computer's work, but the approximate values of the derivatives obtained in this way would pertain to the ratio of the radii halfway between K_1 and K_2, which do not necessarily envelop k. Moreover, the approximate values of the derivatives deduced solely from the first differences may be seriously in error in regions where the variation of C_1 and (or) C_2 with K is rapid. In what follows, however, the present writer would like to point out that correct values of the derivatives dC_1/dK and dC_2/dK can be determined, in the course of an orbital solution, with a minimum of repetitive work along the following lines.

Let us return again to our fundamental equation (1) and consider what happens when we vary the value of K. It is obvious that the values of C_1 and C_2 must be altered so as to counter the change of p with K because, if the light-curve is to pass through the same points, the right-hand side of equation (1) must remain the same. This statement can be mathematically expressed as

$$\frac{dH}{dK} = 0, \tag{12}$$

which represents an implicit form of the equation for determining dC_1/dK and dC_2/dK. On performing the actual differentiation, we find that

$$(p^2 - p_0^2)\frac{dC_1}{dK} + 2(p - p_0)\frac{dC_2}{dK} = 2C_2\left\{\frac{dp_0}{dK}(1 + kp_0) - \frac{dp}{dK}(1 + kp)\right\}. \tag{12.1}$$

The computation of the derivatives of p with respect to K requires some care. We have, in general,

$$\frac{dp}{dK} = \left(\frac{\partial p}{\partial K}\right)_a + \left(\frac{\partial p}{\partial a}\right)_K \frac{\partial a}{\partial K}; \tag{13}$$

and, on using equations (2), remembering that $a = na_0$, and ignoring, for simplicity, the minor variation of Y with k, we find

$$\frac{\partial a}{\partial K} = -\frac{2n(1 - \lambda_b)}{K^3 Y}. \tag{14}$$

On the other hand, differentiating partially the identity $p \equiv p[k, a(k, p)]$, we find that

$$\left(\frac{\partial p}{\partial K}\right)_a = -\left(\frac{\partial p}{\partial a}\right)_K \left(\frac{\partial a}{\partial K}\right)_p. \tag{15}$$

Inserting equations (14) and (15) in equation (13) and multiplying by the intrinsic weight (7) (in which we shall ignore the difference between K and k which is supposed to be small), we find that the explicit form of equation (12) for determining the required derivatives of C_1 and C_2 with respect to K ultimately becomes

$$\sqrt{w}(p^2 - p_0^2)\left[\frac{1}{C_2}\frac{dC_1}{dK}\right] + 2\sqrt{w}(p - p_0)\left[\frac{1}{C_2}\frac{dC_2}{dK}\right] = \frac{4(1 - \lambda_b)}{YK^3}\left\{\sqrt{\left(\frac{w}{w_0}\right)} - n\right\} + 2\left\{\left(\frac{\partial a_0}{\partial K}\right)_n \sqrt{\left(\frac{w}{w_1}\right)} - \left(\frac{\partial a}{\partial K}\right)_p\right\}. \tag{12.2}$$

The reader should notice that the coefficients of the unknowns on the left-hand side of this equation are exactly the same as those in the fundamental equation (1) for determining C_1 and C_2, so that it is only the absolute term on the right-hand side of equation (12.2) which must be evaluated anew for each one of our equations of condition before a solution for the derivatives can be made. Since, moreover, the corresponding numerical values of $\sqrt{w}$ and n are also available at this stage, the only new quantities needed are the derivatives $\partial\alpha/\partial K$, whose values can be extracted with the greatest of ease from the tabular differences of Zessewitsch's tables. A determination of the derivatives dC_1/dK and dC_2/dK by means of equation (12.2) is much more accurate and really takes much less time than the one based on a comparison of two completely independent solutions for two different starting values of K. Moreover, if we proceed by way of equation (12.2), we can ascertain not only the most probable values of the required derivatives but also the uncertainty within which these derivatives are defined by the available observational evidence.

The process by which an intermediary orbit of an eclipsing binary system can be determined with a minimum amount of work may therefore be outlined as follows:

1. Assume a plausible value of K and carry through a customary solution for C_1 and C_2 leading to $C_1/C_2 = k$.

2. Solve equation (12.2) for dC_1/dK and dC_2/dK and then evaluate dk/dK by means of equation (11).

3. The true value of k (i.e., the one for which the assumed K and the resulting k would be identical)—let us denote it by $\bar{k}$—then follows from

$$\bar{k} = K - \frac{K - k}{1 - \frac{dk}{dK}}. \tag{16}$$

4. The true (barred) values of C_1 and C_2 such that $\bar{C}_1/\bar{C}_2 = \bar{k}$ are then given by

$$\begin{aligned} \bar{C}_1 &= C_1 + \frac{dC_1}{dK}(\bar{k} - K), \\ \bar{C}_2 &= C_2 + \frac{dC_2}{dK}(\bar{k} - K); \end{aligned} \tag{17}$$

and these should be used to compute the true geometrical elements of a system in the customary manner.

III

As a corollary to the foregoing considerations, another simple generalization of the theory of intermediary orbits may be developed, which should enable us to gain insight into the dependence of the computed elements on the assumed degree of darkening. As is well known, the light-curves of partially eclipsing systems do not, in general, lend themselves to a determination of the limb darkening of the component undergoing eclipse, but a certain amount of it must be assumed from the general physical evidence (spectrum, color) before the orbital solution can proceed. Since this assumed coefficient of darkening, u, might often be subject to later revision, it is desirable to know the extent to which the geometrical elements of a system may depend on our particular choice of u, and the manner in which these elements would individually respond to a given small change of u. One way of finding this out would be a repetition of a solution with several trial values of u and a comparison of the outcome; but such a way is no method in itself and would clearly be very laborious. In what follows we shall describe a methodical way for investigating the dependence of the individual geometrical elements upon the adopted value of u, which again requires only a minimum amount of additional work.

Let us start again from our fundamental equation (1) and consider the consequences

of a small change of u on its left-hand side. All p's will change, but so must C_1 and C_2 in order to keep the resultant light-curve the same. This amounts to a requirement that

$$\frac{dH}{du} = 0 , \tag{18}$$

or, explicitly,

$$(p^2 - p_0^2)\frac{dC_1}{du} + 2(p - p_0)\frac{dC_2}{du} = 2C_2\left\{\frac{dp_0}{du}(1 + kp_0) - \frac{dp}{du}(1 + kp)\right\} . \tag{18.1}$$

Now, by the same rules of implicit differentiation that we used to obtain equation (15), it follows that

$$\frac{dp}{du} = -\frac{\partial p}{\partial a}\frac{\partial a}{\partial u} . \tag{19}$$

Inserting this into equation (18.1) and multiplying the latter by the intrinsic weight (7), we eventually find that

$$\sqrt{w}(p^2 - p_0^2)\left[\frac{1}{C_2}\frac{dC_1}{du}\right] + 2\sqrt{w}(p - p_0)\left[\frac{1}{C_2}\frac{dC_2}{du}\right] = 2\left\{\frac{\partial a_0}{\partial u}\sqrt{\left(\frac{w}{w_0}\right)} - \frac{\partial a}{\partial u}\right\} . \tag{18.2}$$

The reader should again notice that the coefficients of the unknowns on the left-hand side of equation (18.2) are exactly the same as those in the fundamental equation (1), so that the only new quantity to be evaluated is the absolute term on the right-hand side of equation (18.2). Moreover, the partial derivatives $\partial a/\partial u$ occurring in it have recently been tabulated by Irwin and published in a recent issue of this *Journal*.[10] With the aid of these tables, the evaluation of the absolute terms of the equations of condition of the form (18.2) should be very simple indeed.

Once these equations have been solved and the most probable values of the derivatives dC_1/du and dC_2/du obtained, the derivatives of the fractional radii, r_a and r_b, of the smaller and the larger star, and of the orbital inclination i with respect to u can be obtained as follows. We have, by definition,

$$C_1 = r_a^2 \csc^2 i ,$$

$$C_2 = r_a r_b \csc^2 i ,$$

and

$$\cos i = r_b(1 + kp_0) .$$

Hence, by a differentiation,

$$\begin{aligned}
\frac{1}{C_2}\frac{dC_1}{du} &= \frac{2}{r_b}\frac{dr_a}{du} - \frac{2k}{\sin i}\frac{d\sin i}{du} , \\
\frac{1}{C_2}\frac{dC_2}{du} &= \frac{1}{r_a}\frac{dr_a}{du} + \frac{1}{r_b}\frac{dr_b}{du} - \frac{2}{\sin i}\frac{d\sin i}{du} , \\
\frac{\partial p_0}{\partial a}\frac{\partial a_0}{\partial u} &= \frac{p_0}{r_a}\frac{dr_a}{du} + \frac{1}{r_a}\frac{dr_b}{du} - \frac{\tan i}{r_a}\frac{d\sin i}{du} .
\end{aligned} \tag{20}$$

The left-hand sides of these equations being known, the rates of change of r_a, r_b, and $\sin i$ corresponding to a given small change in u can readily be evaluated from equations (20).

It is a pleasure to record that the ideas presented in this paper crystallized during discussions with Professor Henry Norris Russell at the Neighbors Meeting in Princeton, April, 1948.

[10] *Ap. J.*, **106**, 380, Tables 4 (occultation) and 8 (transit), 1947.

PRELIMINARY SOLUTIONS FOR ECLIPSING BINARIES FROM ACCURATE OBSERVATIONS

HENRY NORRIS RUSSELL
Princeton University Observatory
Received May 3, 1948

ABSTRACT

When the observations are of high precision, much time and labor may be saved by making a preliminary solution of Piotrowski's equations based on the minimum number (four) of well-observed data. A second approximation may be made, if necessary, from four normal places. Differential corrections may then be derived by Irwin's or Piotrowski's method. Equations are given for the rapid solution of the preliminary problem by means of the ψ-functions.

1. Dr. Piotrowski[1] has done a service to students of eclipsing binaries by recognizing that the accuracy of modern photoelectric observations may surpass the limits of graphical methods. When "square yards of paper" would be required, these methods would demand such meticulous care that they would lose their convenience, and graphical interpolation might be of inadequate precision. The problem then resembles that presented by an asteroid, rather than by a visual binary.

In such a case the observations may best be handled in a "planetary" fashion—determining a preliminary orbit so as to represent exactly a minimum number of observations, or normals, and comparing the resulting ephemeris with the others. These elements may then be improved by appropriate methods, until they justify a definitive correction by least squares. Piotrowski's equations are directly available for this purpose. We assume, as he does, that the observations have been rectified for ellipticity and reflection and that a value for the limb darkening may be adopted.

2. For a partial eclipse, four elements must be determined, and four observations are required. Taking two at the bottoms of the minima and the others as any two good observations at well-separated points on the slope of the principal minimum, the data are as follows:

θ	0°	180°	θ_1	θ_2
l	λ_1	λ_2	l_1	l_2

We may start, as he does, with an assumed value of K and find α_0 for the primary eclipse from the depths of the minima, or by assuming α_0 and finding K. In either case, p_0 is determined and the observations give

$$(p_i^2 - p_0^2)\, x + 2\,(p_i - p_0)\, y = \sin^2 \theta_i \qquad (i = 1,\ 2)\,. \quad (1)$$

Solving for x and y, $k = x/y$. Trials starting with other values of K (or α_0) lead to the solution, for which $k = K$.

This is precisely Piotrowski's method (with two equations of condition and with $d\lambda = 0$). The resulting values of x, y, k, and α_0 represent the four selected data exactly. The exploratory investigation to find preliminary elements may thus be made with a minimum of labor. These elements will not be the best possible, but their errors will be small if the observations are good, unless a solution from photoelectric data alone is indeterminate or nearly so. In such a case $1 - (dk/dK)$ is zero or small (Piotrowski, eq. [19]). The pairs of corresponding values of k and K obtained in the preliminary trials suffice to determine this quantity, detect the difficulty at an early stage, and avoid waste of time on unprofitable calculations.

If the solution is reasonably determinate, the value of $\sin^2 \theta$ may be calculated for all the

[1] *Ap. J.*, **108**, 36, 1948.

observations by equation (1). If the residuals are systematic, a better approximation may be made by forming new normal places—still four in number—and re-solving by the same method.

Just as for a planet, the residuals from the ephemeris will run much more smoothly with the time (apart from accidental errors) than the original co-ordinates, and observations covering a greater interval can be combined into stronger normals. Improved values of λ may be found by plotting l against $\sin^2\theta$ and extrapolating to $\sin^2\theta = 0$, using the computed curve as a guide. Only small values of $\sin^2\theta$ are involved, and the plot may be made on a very open scale without wasting paper.

This second approximation should give a close fit to the whole run of the observations, provided that the observations are really good and the photometric perturbations small.

3. If the elements are to be determined from a total eclipse alone, three quantities must be found from these observations during the partial phases. Piotrowski's equation (14), omitting the small corrections, gives

$$(p_i^2 - 1)\,x + 2\,(p_i + 1)\,y + z = \sin^2\theta_i \qquad (i = 1, 2, 3)\,. \quad (2)$$

Observations near the top, middle, and bottom of the slope always give a definite solution (though with enough loss of weight during the solution to make it important to have the numerical coefficients accurate). The second approximation is simpler here, since λ is strongly determined and needs no change.

For annular eclipses, the value of l at the moment of internal contact, which Piotrowski calls λ, is practically impossible to estimate from the observations with the accuracy here desired. The introduction of $d\lambda$ into the equations leads to an extremely serious loss of weight in a least-squares solution, however numerous and well distributed the observations may be.

Here the writer strongly recommends the use of the method for partial eclipses—taking the depth of the secondary into account, starting with an assumed value of $a_0(>1)$ at the middle of the annular eclipse, and determining K from the depths and k from the points on the slope, as above.

4. Corrections by least squares to the elements thus found will be definitive only if the photometric perturbations have been calculated and applied, or shown to be insensible. A computer with ample means for numerical work may, however, desire to see how close a fit may be obtained if the perturbations are disregarded.

In any case Piotrowski's equation (10) or equation (14) may be applied to determine differential corrections, introducing dx, dy, and dz on one side and $d\sin^2\theta\,(O - C)$ on the other; or one may set $dx = ydk + kdy$. Such a solution demands much less numerical work than one in which x, y, and z themselves appear. In the second, the absolute terms are of the order of $\sin^2\theta$; in the first, of $d\sin^2\theta$, which in the case considered will be smaller by a factor of 30 or more. All the calculations must be made to two more significant figures in the second case, and the coefficients of the equations of condition must be known with corresponding accuracy—as must the factors $dn/d\sin^2\theta$ which enter into the weights (eq. [7]).

These can hardly be determined from a freehand curve with the desired accuracy. A curve computed from the elements undergoing correction has been provided during the calculation of $d\sin^2\theta$. This should give weights accurate enough for the solution for dx, dy, and dz, but hardly for x, y, and z. The adopted values of $dn/d\sin^2\theta$ should, of course, be those corresponding to the (accurately known) values of θ. This is important near the external and internal contacts, where the weighting depending on the value of l meets with difficulties.

The writer doubts seriously whether this form of the equations of condition has at present any advantage over the usual one which employs residuals in l instead of in $\sin^2\theta$. Irwin's detailed tables[2] then save a great deal of work in setting up the equations

[2] *Ap. J.*, **106**, 380, 1947.

of condition. They have also the advantage of giving directly the corrections to the usual elements and their probable errors. For a total eclipse, Piotrowski's unknowns are simply related to the usual elements: $d\lambda = dL_1$; $dU = (dL_1 + dL_2)/(L_1 + L_2)$; $K = x/y$; $r_1^2 \csc^2 i = y^2/x$. At internal contact $r_1^2(1 - k)^2\csc^2 i = \cot^2 i + z$; whence $\cot^2 i = y^2/x - 2y + x - z$. But for a partial eclipse, $\cos^2 i$ and L_1 are connected with r_1, k, λ_1, and λ_2 by complicated equations, and the determination of their probable error is laborious.

5. Piotrowski and Kopal's method for the essential preliminary solution from four points is of great value. So long as Zessewitsch's tables were the only accurate ones available, their equations involving the p-functions had no competition.

A more rapid solution (analytically merely a transformation of the other) may be made with Merrill's[3] tables of ψ-functions (which have an interval of 0.05 in k and 0.02 in α). For any eclipse, total, partial, or annular,

$$\sin^2\theta = A + B\psi\,(k,\ \alpha)\,,$$

where A and B are connected by simple relations with r_1, k, and i.

For a total eclipse, the observations give λ_1, l_1, θ_1, etc. Then $\alpha = (1 - l)/(1 - \lambda)$, and

$$\frac{\sin^2\theta_1 - \sin^2\theta_3}{\sin^2\theta_2 - \sin^2\theta_3} = \frac{\psi\,(k,\ \alpha_1) - \psi\,(k,\ \alpha_3)}{\psi\,(k,\ \alpha_2) - \psi\,(k,\ \alpha_3)}. \tag{3}$$

The first member is known; the second may be computed for tabular values of k, and the solution found.

For partial and annular eclipses, α_0 is assumed and K found from the depths of the minima. Then $\theta_3 = 0$; $\alpha_3 = \alpha_0$;

$$\frac{\sin^2\theta_1}{\sin^2\theta_2} = \frac{\psi\,(k,\ \alpha_1) - \psi\,(k,\ \alpha_0)}{\psi\,(k,\ \alpha_2) - \psi\,(k,\ \alpha_0)}; \tag{4}$$

and k is found as above. Trials with other values of α_0 lead to the solution $k = K$.

These equations are available for occultations or transits and for any limb darkening, if the appropriate tables are used.

In all cases A and B may be found at once. The value of $\sin^2\theta$ corresponding to any α may then be found by direct interpolation in the ψ-table, and that of α for a given θ by inverse interpolation, and the corresponding residuals determined. It may be noted that, if $\alpha_2 = 0.6$, $\alpha_3 = 0.9$, the second member of equation (3) is $1 + \psi(k, \alpha_1)$, while if $\alpha_1 = n\alpha_0$, $\alpha_2 = \frac{1}{2}\alpha_0$, that of equation (4) is $\chi(k, \alpha_0, n)$. Hence the methods here presented are simple generalizations of those proposed in 1912, available for any given points of the variation rather than for those at specified levels. When readings from the light-curve are more accurate than the individual normals in the vicinity, the older forms are preferable; otherwise the new.

In the writer's opinion, a preliminary solution by some such method, specifically adapted to the problem, should always precede one which involves differential corrections. How much time should then be spent on improving the first approximation by relatively simple methods depends upon the available computing facilities and the experience and taste of the computer. The smaller and less systematic the residuals left by this improved solution, the better basis it will be for a least-squares adjustment.

The writer is greatly indebted to the courtesy of Dr. Piotrowski, through Dr. Kopal, for the opportunity to study his work in manuscript and to present these comments at the time of its publication. The notation of his paper has here been followed, to facilitate comparison.

It is a pleasure also to thank Dr. Kopal for stimulating discussion and for the privilege of seeing his "Remarks" on the same topic in manuscript.

[3] Now in process of publication.

SPECTROSCOPIC AND PHOTOMETRIC OBSERVATIONS OF A FAINT WOLF-RAYET SPECTROSCOPIC BINARY*

W. A. HILTNER
Yerkes and McDonald Observatories
Received May 6, 1948

ABSTRACT

Spectrographic and photometric observations of a faint Wolf-Rayet spectroscopic binary with a period of 2.1267 days are presented. The velocity-curve of the Wolf-Rayet component has a semi-amplitude of 290 km/sec. The light-curve shows shallow minima, with the primary one occurring when the early-type companion is eclipsed. The light-curve shows an anomaly at that phase when the Wolf-Rayet component is approaching the observer. The system is 0.045 mag. too faint at this phase.

INTRODUCTION

The Wolf-Rayet star under discussion was discovered at the Leander McCormick Observatory[1] and has been observed both spectroscopically and photometrically at the McDonald Observatory. Three slit spectrograms taken in 1945 indicated that the star was a spectroscopic binary[2] with a large amplitude. Additional spectrograms were obtained with low dispersion as time permitted. The period and amplitude resulting from the spectrographic observations were such that it seemed advisable to investigate the system for light-variation. Observation with a photoelectric photometer in August and September, 1947, gave a well-defined light-curve with a pronounced anomaly.

SPECTROGRAPHIC OBSERVATIONS

The spectrum of this Wolf-Rayet binary has been described and illustrated previously.[3] The spectral class is WN5. In all, seventy spectrograms were obtained from October, 1945, to September, 1947, for the determination of the velocity-curve. With the exception of one spectrogram, the dispersion employed was 200 A/mm at λ 4686. Only *He* II 4686 can be accurately measured on spectrograms of this dispersion, and consequently the velocity-curve illustrated in Figure 1 is based exclusively on this line. The individual observations, as well as the normal points, are plotted. Only the normal velocity points are recorded in Table 1, for it seems that the period of 2.1267 days is well established.

One spectrogram was taken with quartz optics, and on this spectrogram the higher members of the Balmer series can be seen as weak diffuse absorption lines. It is possible that these absorption lines arise in the atmosphere of the companion star, as has been the case in similar binary systems.[4]

PHOTOMETRIC OBSERVATIONS

The photometric observations were made with a photoelectric photometer employing a 1P21 photomultiplier. The output from the multiplier was measured, without further amplification, by a sensitive galvanometer with a period of 6 seconds. A star of approximately the same magnitude and color (comparison No. 3 on Fig. 2) and within 6 minutes of arc of the variable was used as a comparison star. It was checked against a second star

* *Contributions from the McDonald Observatory, University of Texas*, No. 153.

[1] A.N. Vyssotsky, W. J. Miller, S.J., and Miriam E. Walther, *Pub. A.S.P.*, **57**, 314, 1945. (1945) $\alpha = 22^h7^m6; \delta = +57°26'$; $M \sim 12.5$ pg. The chart reproduced here (Fig. 2) was kindly provided by Dr. Vyssotsky.

[2] W. A. Hiltner, *Pub. A.S.P.*, **58**, 215, 1946. [3] *Ibid.* [4] See, e.g., *Ap. J.*, **101**, 356, 1945.

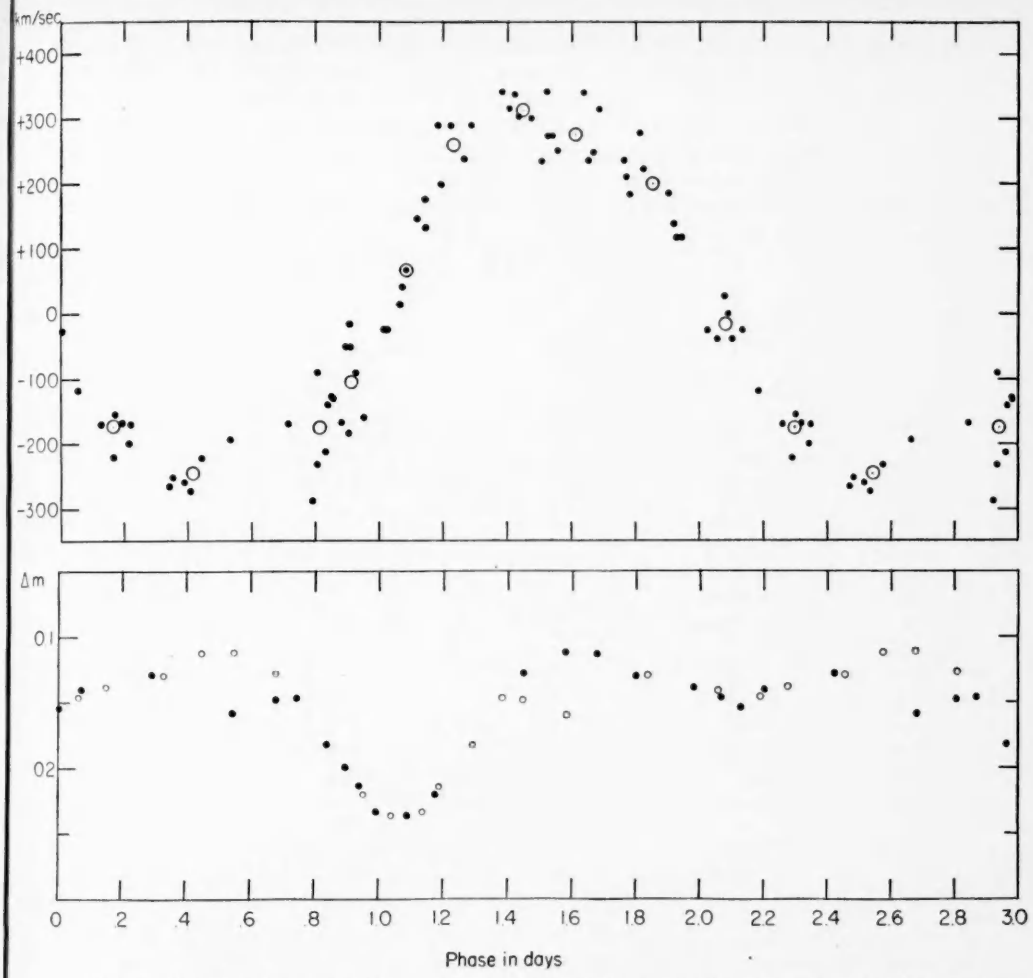

FIG. 1.—The velocity- and light-curves of a faint Wolf-Rayet star. The upper curve is the velocity-curve based on measurements of *He* II 4686 only. Open circles represent normal observations and solid dots individual plates. The lower curve is the photoelectric light-curve. The solid dots indicate normal points, and the open circles are the reflected normal points.

TABLE 1

NORMAL RADIAL VELOCITIES

Phase	Vel. *He* II 4686 (Km/Sec)	Phase	Vel. *He* II 4686 (Km/Sec)	Phase	Vel. *He* II 4686 (Km/Sec)	Phase	Vel. *He* II 4686 (Km/Sec)
0.167.....	−172	0.912...	−103	1.452...	+311	1.855...	+199
0.414.....	−246	1.086...	+ 67	1.611...	+276	2.082...	− 17
0.814.....	−174	1.233...	+260				

(comparison No. 2 on Fig. 2) on 15 nights; and, if we assume constant light for the two comparison stars, the computed probable error of a single observation (three deflections on the variable and three on the comparison) is ± 0.004 mag. This probable error is slightly larger than that obtained when a color filter is employed, for it has been the experience of the author that more accurate and, of course, more significant observations can be obtained if the wave-length region is restricted. At present the photometer is equipped with three filters which give effective wave lengths from λ 3550 to λ 5300. Also,

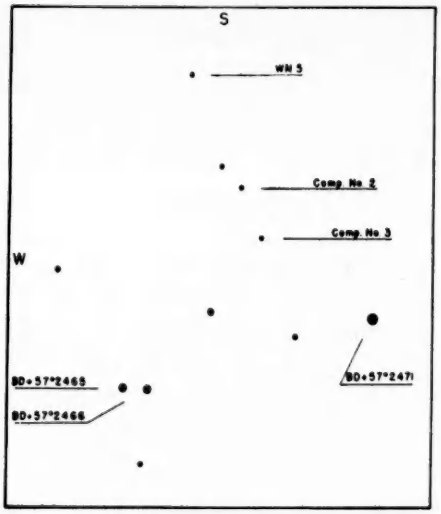

FIG. 2.—Field of WN5

TABLE 2

NORMAL PHOTOMETRIC OBSERVATIONS

Phase	WN Anon − Comp. No. 3 (Δm)	Phase	WN Anon − Comp. No. 3 (Δm)	Phase	WN Anon − Comp. No. 3 (Δm)
0.001	+0.154	0.836	+0.182	1.448	+0.128
.075	+ .140	0.893	+ .199	1.578	+ .112
.295	+ .128	0.937	+ .213	1.677	+ .113
.543	+ .158	0.991	+ .233	1.800	+ .130
.679	+ .148	1.088	+ .236	1.981	+ .139
0.743	+0.146	1.173	+0.220	2.065	+0.147

a direct-coupled amplifier and a Brown Electronic-Strip Chart Recorder has replaced the galvanometer.

Only the normal observations are recorded in Table 2 and also plotted in Figure 1. The normals consist of approximately six single observations and have a probable error of approximately ± 0.002 mag.

DISCUSSION

The light- and velocity-curves of this binary system in which one component is a Wolf-Rayet star of the nitrogen sequence are well determined. The velocity-curve sug-

gests slight departures from a sinusoidal one. These departures, if real, must not be considered as definitive evidence for a noncircular orbit but may give further evidence that the radial-velocity measurements of *He* II 4686 do not give the true radial velocity of the center of mass of the Wolf-Rayet component.

The light-curve of this system, although disappointing, at first, because of the shallow eclipses, is, in reality, an especially interesting one. The primary eclipse, 0.125 mag., occurs when the companion star is eclipsed; and secondary minimum, 0.042 mag., occurs when the Wolf-Rayet component is eclipsed. This agrees well with the general picture of a Wolf-Rayet star surrounded by an electron envelope.

TABLE 3

INDIVIDUAL OBSERVATIONS

Date (1947)	Phase	Δm
Sept. 18	0.518	+0.157
18	.523	+ .153
18	.525	+ .153
16	.562	+ .162
16	.565	+ .162
16	0.568	+0.164

The light-curve in Figure 1 shows the reflected normal points as well as the observed normal points. This is done in order to show an anomaly at phase 0.5. At this phase the system is 0.045 mag. too faint. The reality of this phenomenon is well established, for the normal point at phase 0.54, which is the mean of two different nights, consists of individual observations, listed in Table 3, which are in good agreement. The system becomes abnormally faint after phase 0.4, reaching a minimum at phase 0.55 and then increasing to its normal brightness at phase 0.74. The evidence is not definitive that the phenomenon is repeating, since the system was observed at phases 0.5–0.6 on only two nights, separated by one cycle. However, it should be pointed out that on September 17, the intermediate night (phase 1.5–1.6), the system was normal in brightness.

Further discussion of this system will be postponed until the photometric observations of the binary system CQ Cephei, another eclipsing binary with one Wolf-Rayet component, are completed.

THE RADIAL VELOCITY OF RR LYRAE*

O. STRUVE AND A. BLAAUW
Yerkes and McDonald Observatories
Received March 23, 1948

ABSTRACT

Measurements of radial velocity were made on spectrograms secured between June 3 and July 15, 1947. The velocity-curve was found to oscillate in time with a period of approximately 75 cycles, or 42 days. On June 5 and again on July 17 the velocity-curve was retarded by approximately $0.024P$, this being the maximum retardation observed. Halfway between, or approximately on June 26, the velocity-curve was advanced by about $0.024P$, this being the maximum advance observed. The principal period, P, is 0.567 day. At the times of maximum retardation the hydrogen lines appeared in emission near the phase of median increasing brightness. The dates of greatest retardation and greatest advance of the velocity-curve agree with those determined by Walraven from the light-curve.

Individual velocity-curves were derived for six groups of phase intervals, groups I and VI coinciding approximately with the dates of maximum retardation and groups III and IV coinciding approximately with the date of maximum advance. The velocity-curves in these six groups show only minor changes in shape. Most pronounced is a high, peaked maximum of velocity in groups I and VI, as shown by the hydrogen lines, $H\gamma$, $H\delta$, and $H\zeta$. Other minor differences in the velocity-curves corresponding to the six groups have been described and are considered as being probably real.

The spectral types were determined for all plates by means of a sequence of standard stars. The results show that the earliest type, A2, as estimated from the metallic lines and *Ca* II 3933, occurs about 0.05 day earlier than minimum radial velocity. The latest spectral type, between A8 and F1, occurs about 0.15 day earlier than maximum radial velocity. There is some indication that the spectral type had a larger range in groups I, II, and perhaps VI than in groups III, IV, and V.

A series of 390 spectrograms of RR Lyrae was obtained at the McDonald Observatory between June 3 and July 15, 1947, with the Cassegrain spectrograph attached to the 82-inch reflector. This instrument was equipped with two quartz prisms and a camera, 500 mm in focal length. The average linear dispersion was 40 A/mm. The purpose of this work was to investigate whether the velocity-curve changes in conformity with the 41-day period of fluctuation in the character of the short-period light-curve.[1] Our previous knowledge of the velocity-curve rests entirely upon the work of R. F. Sanford.[2]

Table 1 lists the wave lengths of the star lines and comparison lines which were chosen from a preliminary list of about twice as many star lines. Table 3 shows a comparison of the radial velocities obtained from 13 plates measured by both authors. The entries in this table represent the mean velocities from all star lines, uncorrected for the motion of the earth and for the curvature of the lines. These values are therefore not directly comparable to those of Table 2. The mean difference is

$$\text{Blaauw} - \text{Struve} = +0.5 \pm 0.6 \text{ km/sec} .$$

Hence there is no systematic difference between the observers.

Table 2 lists all the radial velocities, corrected to the sun. The column marked "All

* *Contributions from the McDonald Observatory, University of Texas*, No. 150.

[1] This investigation is the outcome of a conference at the Leiden Observatory in the fall of 1946. Miss H. A. Kluyver and Dr. P. Th. Oosterhoff proposed a joint study of the photometric and spectrographic properties of RR Lyrae (see also *B.A.N.*, **10**, 251, 1947), and Dr. J. H. Oort, director of the Leiden Observatory, arranged to have the star observed photoelectrically by Dr. T. Walraven. He also arranged to give leave of absence to Dr. A. Blaauw, of the Leiden Observatory, who was then appointed as research assistant at Yerkes and McDonald and collaborated with Mr. Struve in the measurement and discussion of the spectrographic material. The spectrograms were all obtained by Mr. Struve, who has already published two notes on the *H* emission lines which he found at median increasing brightness (*Pub. A.S.P.*, **59**, 192, 1947; *A.J.*, **53**, 108, 1948). About two-thirds of the radial-velocity measurements were made by Mr. Blaauw, the rest by Mr. Struve. The discussion was carried through jointly. Dr. Walraven very kindly furnished the results of his photoelectric work, in advance of publication, and it is due to this circumstance that the two series of data can be tied together. Dr. Detre, of Budapest, who had made an earlier comprehensive study of the light-curve, supplied valuable additional information.

[2] *Ap. J.*, **67**, 319, 1928; **69**, 240, 1929; **81**, 149, 1935.

Table 1

List of Star Lines and Comparison Lines

Element	λ	Element	λ	Element	λ
C*	3677.63	C	3827.82	Sr II	4077.71
H21	3679.36	C	3834.22	Hδ	4101.74
C	3679.92	H9	3835.39	C	4118.55
H20	3682.81	C	3841.05	Fe I	4143.73
H18	3691.56	Si II + Fe I	3856.22	C	4202.03
C	3694.01	C	3856.37	Sr II	4215.52
H17	3697.15	C	3865.53	Ca I	4226.73
C	3701.09	Fe I	3878.34	Fe II	4233.16
H15	3711.97	H8	3889.05	C	4260.48
C	3716.45	C	3895.66	Fe I	4271.48
H14	3721.94	C	3899.71	Ti II	4289.84
C	3727.62	Fe I	3902.95	C	4307.91
C	3743.36	C	3902.95	Sc II	4314.09
V II + Fe I	3745.63	C	3906.48	Sc II + Fe I	4325.39
Ti II	3761.58	Ti II	3913.46	C	4325.76
C	3767.10	C	3920.26	C	4337.05
H 11	3770.63	C	3930.30	Hγ	4340.47
C	3787.88	Fe I	3930.31	C	4375.93
C	3795.00	Ca II	3933.67	C	4383.55
H 10	3797.90	C	3956.68	Ti II	4394.95
C	3805.34	C	4005.25	C	4415.12
Fe I	3815.82	Fe I	4045.82	Mg II	4481.23
C	3815.84	Fe I	4063.60	C	4494.57
Fe I	3820.43	C	4071.74	C	4528.62

*Comparison Line

TABLE 2

Radial Velocities of RR Lyrae

Plate CQ	Date 1947	U.T.	Phase Uncorr.	Phase Corr.	Mean of all Lines*	Mean of H_γ, H_δ H_ζ	Mg II 4481	H_γ	Ca II 3933	Spectral Type Ca II+ metal	Spectral Type H
5323	June 3	5:54	0.659	.634	-67.5	-72.7	-58.3	-77.1	-79.1	A6	F2
24	3	6:21	0.692	.667	-66.6	-74.3	----	-77.1	-54.7	A5	F2
25	3	6:55	0.733	.708	-85.4	-86.8	-37.6	-99.9	-94.3	A6	F2
26	3	7:30	0.776	.751	-66.3	-83.3	-54.4	-73.7	-67.0	A6	F2
27	3	8:06	0.822	.797	-60.7	-66.3	-58.4	-77.2	-57.8	A8	F3
28	3	8:43	0.866	.841	-57.3	-63.4	-21.6	-50.2	-54.8	A8	F3
29	3	9:22	0.913	.888	-59.7	-54.1	-25.7	-50.3	-67.1	A8	F4
30	3	10:09	0.971	.946	-77.9	-74.8	-54.5	-69.7	-76.2	A8	F3
31	3	10:54	1.026	.001	-56.6	-49.9	-21.6	-42.6	-73.1	A8	F3
33	4	7:51	2.566	.539	-93.7	-90.4	----	-96.7	-88.5	A5	F1
34	4	8:22	2.605	.578	-85.1	-89.5	-86.7	-96.7	-85.5	A5	F1
35	4	8:54	2.644	.617	-83.8	-86.7	----	-103.7	-91.7	A7	F2
36	4	9:29	2.686	.659	-80.1	-87.5	-74.8	-100.3	-79.5	A7	F2
37	4	10:06	2.732	.705	-77.9	-75.3	-13.9	-75.1	-103.9	A8	F1
38	4	10:47	2.782	.755	-66.9	-77.2	+ 2.7	-81.1	-70.4	A8	F2
41	5	5:53	4.186	.158	-45.9	-43.6	-21.8	-69.8	----	A8	F3
42	5	6:16	4.214	.186	-36.0	-55.6	+32.0	-47.0	-48.9	F0	F3
43	5	6:38	4.241	.213	-39.9	-47.3	-45.9	----	----	--	--
44	5	6:59	4.267	.239	-39.1	-32.3	-58.6	-42.8	-58.0	F0	F3
45	5	7:20	4.293	.265	-53.9	-37.1	-50.0	-20.1	-45.9	A7	--
46	5	7:41	4.318	.290	-73.8	-24.3	-70.8	-16.0	-73.4	A3	A6
47	5	8:04	4.346	.318	-86.6	-87.5	-95.6	-85.1	-91.7	A4	F0
48	5	8:28	4.376	.348	-92.3	-99.4	----	-88.6	-107.0	A3	A9
49	5	8:52	4.405	.377	-98.9	-115.8	-58.8	-108.0	-107.1	A3	A9
51	5	9:41	4.465	.437	-99.8	-112.3	-99.7	-119.1	-107.1	A3	A9
52	5	10:05	4.495	.467	-98.0	-119.2	-54.8	-126.7	-104.0	A3	F0
58	6	5:48	5.945	.917	-54.8	-53.5	+39.6	-58.9	-91.7	F0	F5
59	6	6:31	5.998	.970	-65.6	-68.2	-42.0	-77.5	-52.0	F0	F5
60	6	7:12	6.047	.019	-50.7	-43.6	+14.9	-39.5	-49.0	F0	F5
61	6	7:53	6.096	.068	-53.3	-50.1	-62.9	-43.0	-46.0	F1	F5
62	6	8:30	6.142	.114	-45.4	-41.9	- 9.3	-22.3	-33.8	F1	F5
65	6	10:40	6.301	.273	-67.2	-34.8	-55.0	-24.1	-46.2	A3	--
66	6	11:05	6.333	.305	-78.6	-67.0	-95.9	-70.2	-70.6	A2	A9
73	7	5:43	7.702	.676	-77.1	-81.3	-66.9	-85.2	-85.7	A6	F0
74	7	6:17	7.744	.718	-74.3	-67.7	-50.1	-74.1	-91.8	A7	F1
75	7	6:53	7.788	.762	-62.2	-69.7	-22.0	-81.1	-73.5	A8	F1
76	7	7:33	7.838	.812	-62.1	-67.3	-38.2	-74.3	-67.6	A9	F3
77	7	8:14	7.887	.861	-62.4	-68.2	-26.2	-62.6	-61.5	A9	F5
86	8	6:09	9.498	.475	-100.5	-111.0	-83.1	-100.6	-88.9	A4	A9
87	8	6:31	9.526	.503	-90.2	-90.2	-63.1	-108.2	-101.1	A4	F0
88	8	6:57	9.558	.535	-91.0	-109.1	-79.2	-108.3	-104.3	A4	F1
89	8	7:28	9.595	.572	-86.8	-85.2	-87.2	-93.1	-86.0	A5	F1
90	8	8:00	9.634	.611	-76.5	-89.0	-34.4	-85.5	-86.0	A5	F1
91	8	8:32	9.674	.651	-84.4	-88.6	-50.3	-93.2	-86.1	A6	F1
92	8	9:02	9.709	.686	-79.6	-92.4	-42.5	-97.4	-92.2	A6	F2
93	8	9:32	9.746	.723	-73.1	-89.5	-30.4	-89.1	-28.1	A7	F2
5401vp**	9	4:52	11.168	.147	-54.0	-66.2	----	-50.9	----	--	--
02	9	5:47	11.235	.214	-41.3	-52.4	+14.5	-47.5	-52.8	A7	F3
03	9	6:13	11.267	.246	-46.8	-38.6	-14.3	-50.9	-37.2	A3	F8
04	9	6:32	11.290	.269	-52.6	-30.6	- 5.6	-43.3	-34.1	A2	F8

*Excluding H_γ, H_δ, H_ζ, Mg II 4481, but including Ca II 3933 and the higher members of the Balmer series.

**vp means very poor; p means poor

TABLE 2 (continued)

Plate CQ	Date 1947	U.T.	Phase Uncorr.	Phase Corr.	Mean of all Lines*	Mean of H_γ, H_δ	Mg II 4481	H_γ	Ca II 3933	Spectral Type Ca II+ metal	Spectral Type H
5405	June 9	6:47	11.310	.289	-63.3	-41.0	-59.1	-24.0	-46.3	A2	A9
06	9	7:10	11.338	.317	-83.4	-85.5	-124.2	-81.5	-73.9	A2	A9
07	9	7:38	11.371	.350	-94.0	-112.6	-124.2	-114.0	-95.2	A2	A8
08	9	8:01	11.400	.379	-105.6	-105.6	-67.4	-96.8	-104.5	A3	A7
09	9	8:21	11.424	.403	-97.7	-115.4	-96.2	-116.1	-101.4	A3	A8
10	9	8:41	11.449	.428	-101.3	-104.1	-108.3	-116.2	-95.4	A3	A9
11	9	9:02	11.474	.453	-96.9	-109.8	-108.3	-127.3	-104.6	A4	A9
27	10	5:39	12.989	.973	-45.3	-49.5	-38.7	-51.2	-64.9	F0	F5
28	10	6:26	13.047	.021	-41.3	-42.3	-34.6	-51.1	-40.4	F0	F5
29	10	7:11	13.102	.086	-45.6	-44.6	-46.6	-43.5	-49.6	F0	F5
30	10	7:54	13.155	.139	-47.1	-43.5	-52.7	-47.8	-49.7	F1	F5
31	10	8:37	13.208	.192	-45.4	-43.6	-38.7	-51.2	-49.0	F0	F5
32	10	9:14	13.254	.238	-46.1	-45.7	+10.1	-51.3	-43.7	F0	F5
33	10	9:38	13.282	.266	-47.3	-40.4	-59.5	-32.7	-43.7	A4	F4
34	10	9:54	13.301	.285	-90.5	-56.5	-87.6	-51.3	-74.2	A1	A9
46	11	6.06	14.787	.776	-69.1	-76.4	-55.5	-63.1	-74.2	A7	F4
47	11	6.50	14.841	.830	+60.7	-64.0	-22.6	-70.6	-74.1	A9	F5
48	11	7.39	14.901	.890	-53.9	-59.2	-34.8	-55.5	-65.0	A9	F5
49	11	8:24	14.956	.945	-51.4	-53.4	-22.8	-51.4	-52.9	F0	F5
50	11	8:58	14.998	.987	-44.1	-51.0	-30.9	-48.1	-53.0	F0	F6
51	11	9:34	15.043	.032	-41.5	-47.7	-39.0	-51.5	-37.8	F0	F6
60	12	5:21	16.496	.490	-102.7	-110.7	-100.6	-124.1	-104.9	A3	A9
61	12	5:58	16.542	.536	-94.7	-101.7	-124.6	-108.8	-101.7	A5	F0
62	12	6:38	16.590	.584	-90.7	-99.7	-112.5	-112.7	-89.5	A5	F0
63	12	7:23	16.646	.640	-78.5	-85.6	-71.8	-89.6	-92.7	A6	F2
64	12	8:07	16.699	.693	-80.6	-95.9	-83.8	-101.3	-95.7	A6	F3
65	12	8:49	16.750	.744	-71.7	-79.7	-51.1	-78.6	-68.4	A7	F5
66	12	9:31	16.803	.797	-62.3	-73.7	-59.8	-78.6	-77.5	A7	F5
67	12	10:15	16.856	.850	-57.9	-54.6	-31.1	-60.0	-68.5	F0	F5
70p**	13	5:14	18.252	.248	-65.2	-77.2	+13.8	-86.2	-34.9	--	--
71	13	7:12	18.396	.392	-101.4	-122.5	-137.5	-127.7	-111.1	A1	A8
72	13	7:47	18.439	.435	-105.8	-118.2	-120.8	-131.9	-105.1	A3	A8
73	13	8:22	18.483	.479	-94.3	-101.7	-92.1	-105.0	-99.0	A3	F0
74	13	9:02	18.530	.526	-94.5	-104.4	-84.1	-113.3	-99.0	A4	F0
75	13	9:42	18.580	.576	-88.0	-98.8	-80.1	-109.2	-92.9	A5	F1
76	13	10:19	18.626	.622	-79.3	-86.8	-64.1	-94.1	-83.9	A6	F2
77	13	10:54	18.668	.664	-76.1	-92.8	-88.2	-101.7	-87.0	A6	F3
82p	14	5:16	20.018	.018	-53.9	-59.3	-63.9	-63.5	-50.2	A9	F5
83p	14	6:13	20.088	.088	-47.3	-33.2	-19.1	-44.1	---	--	--
86	15	6:27	21.870	.873	-62.1	-65.5	- 2.7	-71.4	-71.8	A9	F5
87vp	15	7:17	21.930	.933	-42.5	-36.8	---	-36.8	---	--	--
88	15	8:07	21.992	.995	-48.5	-58.0	-27.5	-56.3	-47.5	F0	F6
89	15	8:52	22.046	.049	-50.1	-48.3	-31.5	-52.1	-41.4	F1	F6
90	15	9:43	22.110	.113	-48.2	-48.4	-60.4	-48.8	---	F1	F6
91vp	15	10:32	22.170	.173	-48.7	-67.4	-27.6	-67.4	---	--	--
96	16	5:47	23.585	.591	-84.5	-96.2	-56.2	-94.2	-96.2	A5	F3
97	16	6:28	23.634	.640	-79.4	-84.3	-56.3	-78.4	-90.2	A8	F5
98	16	7:03	23.678	.684	-75.0	-86.1	-60.3	-90.1	-87.2	F0	F5
99	16	7:34	23.715	.721	-76.6	-93.1	-47.6	-94.3	-84.1	A9	F4
5500	16	8:04	23.752	.758	-71.4	-71.1	-51.7	-79.2	-84.2	F0	F4
01	16	8:36	23.791	.797	-64.6	-75.4	-15.6	-75.7	-62.9	F0	F4
02	16	9:06	23.828	.834	-63.0	-67.9	-23.6	-79.2	-62.9	F0	F4
03	16	9:36	23.865	.871	-68.6	-70.1	-19.8	-79.9	-66.1	F0	F5
09	17	4:43	25.271	.279	-58.6	-44.2	-31.6	-50.5	-59.8	A2	F0
10	17	5:02	25.294	.302	-71.9	-60.7	-84.5	-64.0	-62.9	A2	F0
11	17	5:18	25.314	.322	-82.7	-83.7	-94.9	-77.5	-79.7	A1	A9
12	17	5:34	25.333	.341	-93.1	-97.8	-94.9	-106.1	-102.5	A1	A7
13	17	5:50	25.352	.360	-99.5	-114.4	-78.5	-119.3	-111.7	A1	A8
14	17	6:06	25.372	.380	-104.7	-113.4	-115.3	-124.5	-111.7	A2	A8
15	17	6:25	25.395	.403	-101.8	-124.3	-109.4	-113.2	-104.1	A2	A8

TABLE 2 (continued)

Plate CQ	Date 1947	U.T.	Phase Uncorr.	Phase Corr.	Mean of all Lines*	Mean of H_γ, Ho H_δ	Mg II 4481	H_γ	Ca II 3933	Spectral Type Ca II+ metal	Spectral Type H
5516	June 17	6:45	25.419	.427	-104.4	-113.4	-107.4	-113.5	-105.6	A2	A9
17	17	7:02	25.441	.449	-100.6	-117.4	-101.0	-121.1	-101.0	A2	F0
18	17	7:18	25.460	.468	-99.4	-118.5	-143.8	-120.8	-104.2	A3	F0
19	17	7:36	25.483	.491	-97.7	-106.9	-107.4	-111.4	-102.6	A3	F0
20	17	7:55	25.506	.514	-96.3	-108.1	-95.1	-119.1	-96.6	A3	F0
21	17	8:14	25.529	.537	-100.1	-107.6	-109.1	-113.6	-93.6	A4	F1
23vp	19	8:24	29.069	.083	-47.1	-106.1	-----	-106.1	-14.7	--	--
32	20	4:39	30.558	.575	-89.7	-96.0	-89.0	-99.0	-96.9	A6	F1
33	20	5:20	30.608	.625	-78.5	-91.2	-77.0	-99.0	-84.7	A6	F2
34	20	5:58	30.655	.672	-75.7	-89.3	-52.3	-95.0	-84.8	A7	F2
35	20	6:32	30.696	.713	-72.1	-85.0	-89.1	-87.4	-78.7	A9	F3
36	20	7:08	30.740	.757	-68.1	-76.3	-20.2	-87.4	-66.5	F0	F3
37	20	7:41	30.781	.798	-61.5	-71.2	-3.6	-68.2	-66.6	F0	F4
38	20	8:13	30.820	.837	-59.5	-68.4	-85.2	-76.4	-69.7	F1	F4
39	20	8:48	30.864	.881	-55.4	-62.2	-44.4	-61.2	-60.5	F1	F5
40p	20	9:28	30.911	.928	-65.4	-69.6	-4.3	-72.4	-66.7	F1	F5
41	20	10:16	30.971	.988	-52.0	-47.2	-28.4	-45.4	-66.7	F1	F6
42	20	10:57	31.021	.038	-49.9	-54.9	-20.6	-53.2	-57.8	A9	F4
49p	21	4:03	32.279	.297	-73.9	-57.1	-106.0	-57.1	-54.4	A3	F0
50	21	4:24	32.303	.321	-93.3	-65.4	-61.1	-64.7	-72.7	A2	A8
51	21	4:40	32.323	.341	-103.8	-91.9	-122.0	-76.4	-103.2	A2	A8
52	21	4:56	32.344	.362	-99.0	-111.4	-101.9	-128.9	-109.3	A1	A8
53	21	5:12	32.363	.381	-97.3	-110.1	-114.0	-117.9	-112.3	A1	A7
54	21	5:28	32.383	.401	-101.6	-106.9	-97.9	-114.4	-115.4	A2	A8
55	21	5:44	32.402	.420	-104.6	-110.8	-106.0	-114.4	-106.2	A3	A9
56	21	6:00	32.421	.439	-98.3	-109.2	-97.9	-110.3	-103.2	A3	A9
57	21	6:10	32.434	.452	-99.7	-117.3	-114.1	-121.4	-100.2	A4	F0
58	21	6:18	32.443	.461	-104.0	-106.5	-126.1	-99.3	-109.4	A4	F0
59	21	6:32	32.460	.478	-96.0	-105.3	-102.0	-106.2	-106.3	A5	F0
60	21	6:47	32.480	.498	-96.2	-105.9	-85.3	-121.4	-94.1	A5	F0
61	21	7:03	32.499	.517	-95.5	-102.4	-85.4	-102.9	-91.1	A5	F0
62	21	7:19	32.518	.536	-93.4	-100.3	-77.3	-95.2	-88.1	A6	F0
63	21	7:35	32.538	.556	-90.1	-103.1	-85.3	-110.4	-97.2	A6	F1
64	21	7:51	32.557	.575	-87.1	-109.3	-57.3	-118.1	-82.1	A7	F1
65	21	8:08	32.578	.596	-87.6	-97.7	-85.4	-106.3	-94.2	A7	F1
66p	21	8:24	32.598	.616	-76.0	-116.0	-65.3	-121.5	-94.2	A6	F0
67p	21	8:41	32.619	.637	-86.0	-72.5	-110.2	-61.4	-69.9	A7	F0
68p	21	9:00	32.642	.660	-73.5	-78.8	----	-76.6	-76.0	A7	F0
69p	21	9:20	32.667	.685	-81.0	-80.4	-77.1	-83.6	-97.4	A7	F0
70	21	9:48	32.700	.718	-68.6	-78.6	----	-95.4	-76.1	A7	F0
71	21	10:20	32.740	.759	-66.6	-79.0	-16.6	-76.7	-63.9	A8	F2
72	21	10:55	32.783	.801	-64.4	-75.6	----	-80.3	-60.9	A8	F4
78	22	5:40	34.161	.182	-41.3	-47.3	-89.4	-57.3	-30.2	A9	F2
79	22	6:23	34.214	.235	-43.8	-46.9	----	-45.6	-48.6	F0	F3
80	22	7:00	34.260	.281	-62.5	-43.1	-16.6	-45.6	-39.5	A4	A9
81	22	7:38	34.306	.327	-88.0	-61.9	-77.6	-53.3	-82.3	A3	A8
82	22	8:20	34.357	.378	-104.2	-102.2	-81.6	-114.8	-100.5	A3	A7
83	22	9:03	34.410	.431	-92.1	-89.8	-110.4	-83.7	-100.5	A2	A7
93	23	6:04	35.955	.978	-52.6	-58.3	-36.8	-65.1	-64.0	F0	F5
94	23	6:45	36.004	.027	-42.0	-44.8	-48.8	-42.3	-51.8	F0	F5
95	23	7:28	36.057	.080	-38.8	-44.2	-36.9	-42.4	-33.6	F0	F5
96	23	8:11	36.110	.133	-33.3	-38.3	-32.9	-30.7	-45.9	A9	F5
97	23	8:53	36.161	.184	-40.6	-38.1	+3.9	-34.9	-48.9	A9	F4
98	23	9:36	36.214	.237	-36.4	-46.1	-25.0	-35.0	-33.8	F0	F3
99	23	10:13	36.260	.283	-53.8	-49.3	----	-46.0	-49.0	A3	F0
5600	23	10:40	36.292	.315	-73.6	-68.3	-94.0	-57.8	-79.5	A3	F0
01p	23	11:04	36.322	.345	-88.2	-85.1	-110.8	-88.3	-88.8	A2	A9
05	24	5:00	37.640	.664	-73.4	-86.2	-134.7	-83.9	-106.8	A6	F1
06	24	5:43	37.693	.717	-75.0	-86.0	-98.4	-76.9	-70.2	A7	F1
07	24	7:50	37.848	.872	-45.1	-74.5	-37.1	-84.0	-9.4	A8	F1

TABLE 2 (continued)

Plate CQ	Date 1947	U.T.	Phase Uncorr.	Phase Corr.	Mean of all Lines*	Mean of H_γ, $H\delta$ $H\zeta$	Mg II 4481	H_γ	Ca II 3933	Spectral Type Ca II+ metal	Spectral Type H
5608p	June 24	8:32	37.901	.925	-72.8	-56.2	-29.0	-61.9	----	--	--
14p	25	3:26	39.289	.314	-86.3	-47.3	-57.8	-57.8	-73.4	A3	A9
15	25	3:49	39.318	.343	-86.2	-97.6	-130.7	-95.8	-106.9	A2	A7
16	25	4:15	39.349	.374	-105.2	-108.9	-89.9	-126.2	-110.0	A2	A7
17	25	4:38	39.378	.403	-99.3	-121.7	-106.7	-118.6	-113.0	A3	A7
18	25	4:54	39.397	.422	-104.6	-136.5	-106.7	-137.9	-97.8	A3	A9
19	25	5:10	39.416	.441	-101.1	-117.2	-89.9	-126.2	-103.9	A3	A9
20	25	5:27	39.438	.463	-96.4	-102.7	-93.9	-111.0	-116.1	A3	A9
21	25	5:46	39.460	.485	-91.9	-99.4	-61.8	-106.8	-100.8	A4	F0
23	25	6:11	39.492	.517	-95.5	-114.2	-114.8	-118.7	-85.7	A4	F0
24	25	6:33	39.519	.544	-90.4	-101.7	-70.0	-103.5	-97.9	A5	F1
25	25	6:58	39.549	.574	-88.1	-89.1	-41.3	-96.0	-94.9	A5	F1
26	25	7:27	39.584	.609	-78.5	-98.4	-53.3	-96.0	-88.9	A6	F1
27	25	7:59	39.625	.650	-74.6	-89.8	-74.1	-91.8	-82.8	A7	F2
30	25	8:59	39.697	.722	-70.6	-82.0	-66.1	-77.4	-76.8	A8	F3
31	25	9:44	39.753	.778	-58.3	-78.3	-33.3	-80.9	-73.7	A9	F4
32	25	10:35	39.815	.840	-53.6	-73.5	-82.2	-62.2	-55.4	F0	F5
33	26	5:03	41.172	.197	-45.3	-39.1	-53.7	-58.4	-43.5	A9	F5
34	26	5:48	41.228	.253	-41.7	-41.1	-8.8	-35.3	-40.2	A9	F4
35	26	6:26	41.274	.299	-71.7	-51.4	-41.4	-58.1	-64.6	A4	F4
36	26	6:52	41.306	.331	-86.7	-68.3	-78.2	-80.9	-79.8	A3	A9
37	26	7:12	41.331	.356	-99.4	-101.4	-107.0	-115.4	-98.1	A2	A7
38	26	7:31	41.353	.378	-100.4	-115.8	-94.4	-119.0	-107.4	A2	A7
39	26	7:49	41.376	.401	-101.9	-121.3	-90.3	-130.1	-107.4	A2	A8
40	26	8:07	41.398	.423	-96.2	-107.2	-66.3	-103.8	-104.3	A3	A8
41	26	8:26	41.420	.445	-105.1	-116.3	-90.3	-111.4	-110.4	A3	A8
42	26	8:44	41.443	.468	-98.6	-107.7	-70.3	-100.3	-98.2	A4	A8
51	27	6:16	43.026	.051	-53.9	-46.5	-21.5	-35.5	-55.6	A9	F4
52	27	7:02	43.082	.107	-44.2	-44.4	-45.6	-50.7	-37.3	A9	F5
53	27	7:48	43.139	.164	-56.8	-65.6	-111.3	-66.0	-80.1	A8	F5
54	27	8:34	43.195	.220	-49.5	-65.2	-33.6	-69.5	-43.5	A9	F4
55	27	9:14	43.245	.270	-52.8	-42.2	-94.7	-54.3	-46.7	A5	F1
56	27	9:42	43.278	.303	-71.7	-59.7	-62.5	-50.9	-68.0	A3	F0
57	27	10:02	43.303	.328	-99.7	-88.1	-90.6	-92.4	-92.4	A3	A9
58	27	10:24	43.329	.354	-102.5	-115.1	-103.5	-107.7	-104.7	A2	A8
59	27	10:45	43.356	.381	-106.1	-131.4	-144.3	-111.8	-120.0	A2	A7
60	27	11:05	43.380	.405	-106.0	-113.9	-119.4	-138.7	-116.9	A2	A7
65	28	5:57	44.767	.791	-56.0	-78.0	-55.8	-92.3	-49.7	A8	F3
66	28	6:37	44.817	.841	-55.2	-62.8	-53.8	-73.7	-46.7	A9	F5
67	28	7:17	44.864	.888	-50.2	-54.4	----	-62.7	-68.1	F0	F5
68	28	7:57	44.914	.938	-59.9	-66.4	-53.9	-73.8	-52.9	F0	F5
69p	28	8:37	44.963	.987	-44.6	-31.5	----	-31.6	-37.6	A9	F5
70p	28	9:17	45.012	.036	-38.0	-50.6	-13.2	-54.5	-19.4	A9	F5
71p	28	9:57	45.062	.086	-45.3	-63.7	----	-43.5	-46.9	A9	F4
77	30	4:42	48.204	.226	-45.1	-53.3	-50.0	-62.8	-53.0	A9	F4
78	30	5:17	48.246	.268	-47.4	-45.3	-78.9	-43.6	-56.1	A5	F3
79p	30	5:42	48.278	.300	-70.8	-47.6	----	-66.4	-59.2	A2	A8
80p	30	6:05	48.304	.326	-89.5	-107.8	-111.7	-107.8	-101.8	A2	A8
81	30	6:38	48.345	.367	-94.8	-113.0	----	-101.0	-98.9	A1	A8
82	30	9:29	48.555	.577	-78.3	-94.9	----	-101.2	-86.9	A4	F0
83	30	10:09	48.604	.626	-80.8	-87.4	----	-97.1	-74.7	A6	F1
84	30	10:52	48.657	.679	-79.3	-86.7	-34.4	-97.2	-102.2	A6	F2
87	July 1	6:34	50.106	.125	-47.6	-46.1	----	-36.4	-41.3	A8	F5
88	1	7:25	50.167	.186	-45.1	-45.2	----	-39.8	-47.4	A8	F5
89	1	8:08	50.220	.239	-46.3	-48.0	----	-55.0	-44.3	A8	F4
92p	1	9:16	50.303	.322	-92.6	-74.6	----	-82.1	-90.2	A2	A9
93	1	9:36	50.328	.347	-106.2	-100.8	-104.2	-104.9	-108.5	A2	A7
94	1	9:55	50.352	.371	-101.9	-113.9	-108.2	-123.6	-117.6	A2	A7
95	1	10:14	50.374	.393	-96.7	-112.3	-34.6	-116.8	-111.7	A3	A9
96	1	10:35	50.400	.419	-97.4	-119.9	-83.5	-120.2	-105.5	A3	A9

Table 2 (continued)

Phase CQ	Date 1947	U.T.	Phase Uncorr.	Phase Corr.	Mean of all Lines*	Mean of H_γ, $H\delta$ $H\zeta$	Mg II 4481	H_γ	Ca II 3933	Spectral Type Ca II+ metal	Spectral Type H
5697	July 1	10:59	50.430	.449	-95.7	-122.5	-132.3	-135.4	-102.4	A3	F0
5704	2	4:26	51.713	.730	-60.1	-69.0	-54.4	-74.3	-74.7	A7	F4
05	2	5:11	51.767	.784	-61.1	-70.8	-30.3	-76.7	-56.4	A9	F5
06	2	5:55	51.822	.839	-62.1	-72.3	-42.5	-74.4	-74.8	A9	F5
07	2	6:39	51.874	.891	-55.5	-59.3	---	-51.6	-65.8	A9	F5
08	2	7:22	51.928	.945	-50.5	-48.9	---	-47.6	-62.8	A9	F6
09	2	8:08	51.984	.001	-52.5	-55.3	---	-55.2	-59.8	A8	F5
10	2	8:55	52.043	.060	-47.5	-50.5	---	-47.6	-53.8	A8	F5
11	2	9:41	52.097	.114	-45.7	-53.5	---	-51.9	-53.8	A8	F5
12	2	10:25	52.152	.169	-47.7	-39.2	---	-32.6	-60.0	A8	F5
13	2	11:03	52.198	.215	-39.2	-39.7	-67.7	-44.4	-47.8	A8	F5
27	3	5:03	53.521	.535	-83.4	-95.0	-75.5	-97.4	-90.3	A5	F0
28	3	5:35	53.562	.576	-78.9	-92.4	-71.5	-93.2	-84.2	A5	F1
41	4	3:59	55.208	.220	-42.1	-43.1	---	-47.7	-47.7	A9	F5
42	4	4:31	55.246	.258	-51.6	-46.3	---	-47.8	-44.7	A5	F3
43	4	4:56	55.278	.290	-57.7	-38.3	-91.6	-32.5	-53.8	A3	F0
44	4	5:16	55.301	.313	-83.3	-47.5	-124.5	-25.0	-84.4	A3	F0
45	4	5:35	55.326	.338	-97.3	-95.8	-108.5	-90.0	-96.5	A3	A8
46	4	5:53	55.347	.359	-96.6	-88.4	-91.7	-97.6	-105.7	A3	A8
47	4	6:09	55.366	.378	-102.6	-109.5	-112.5	-123.8	-102.6	A3	A8
48	4	6:25	55.386	.398	-96.6	-105.4	-95.7	-105.2	-105.7	A3	A9
49	4	6:41	55.405	.417	-104.4	-109.1	-91.7	-112.8	-102.6	A3	A9
50	4	6:57	55.426	.438	-89.6	-100.0	-116.7	-93.6	-102.8	A4	F0
51	4	7:15	55.447	.459	-91.0	-102.2	-79.9	-108.8	-93.7	A5	F0
52	4	7:35	55.472	.484	-90.0	-109.1	79.9	-105.4	-99.8	A6	F0
53	4	7:55	55.497	.509	-87.6	-95.8	-59.8	-101.9	-96.7	A6	F1
54	4	8:18	55.525	.537	-82.7	- 97.9	-95.9	-105.4	-87.6	A6	F2
55	4	8:46	55.559	.571	-79.3	-93.8	-79.8	-90.1	-93.6	A5	F1
56	4	9:18	55.599	.611	-75.0	-89.8	-120.8	-93.7	-78.6	A7	F2
57	4	9:56	55.645	.657	-71.0	-85.6	-27.1	-90.3	-75.5	A7	F4
58	4	10:38	55.696	.708	-67.9	-81.8	-23.2	-82.8	-90.9	A8	F5
67	5	4:40	57.021	.030	-52.3	-50.1	-39.0	-44.5	-57.0	A8	F5
68	5	5:26	57.078	.087	-54.4	-50.3	-47.1	-48.0	-63.2	A8	F5
69	5	6:08	57.130	.139	-48.1	-46.3	----	-55.6	-57.1	A9	F5
70	5	6:44	57.175	.184	-52.0	-53.5	----	-48.2	-32.9	A8	F5
71	5	7:15	57.212	.221	-43.9	-52.0	-60.0	-64.1	-54.3	A8	F5
72	5	7:45	57.249	.258	-46.7	-42.0	-51.3	-40.6	-45.1	A4	F2
73	5	8:08	57.277	.286	-60.0	-44.5	-92.1	-44.8	-51.2	A2	F3
74	5	8:23	57.295	.304	-84.6	-30.0	-96.2	-37.3	-60.5	A2	--
75	5	8:37	57.312	.321	-91.7	-76.0	-84.2	-64.2	-91.0	A3	A8
76	5	8:51	57.330	.339	-95.8	-104.3	-51.4	-117.4	-103.1	A2	A7
77	5	9:07	57.349	.358	-99.0	-108.3	-100.9	-124.3	-109.2	A3	A9
78	5	9:23	57.369	.378	-100.3	-119.1	-141.7	-117.4	-112.3	A3	F0
79	5	9:39	57.388	.397	-101.1	-110.9	-68.1	-124.3	-109.2	A3	F0
80	5	9:55	57.407	.416	-93.9	-106.6	-----	-121.0	-97.1	A3	F0
81	5	10:11	57.427	.436	-95.0	-105.7	-60.2	-109.2	97.1	A3	F0
88	6	5:17	58.831	.837	-62.3	-70.3	-72.1	-75.2	-72.6	A7	F5
89	6	6:03	58.891	.897	-58.6	-57.0	----	-64.1	-66.5	A8	F5
90	6	6:46	58.940	.946	-56.8	-54.8	----	-60.2	-60.6	A8	F5
91	6	7:26	58.990	.996	-55.3	-57.4	----	-64.3	-54.5	A8	F5
92	6	8:07	59.039	.045	-53.6	-54.0	----	-45.0	-51.4	A8	F5
93	6	8:47	59.089	.095	-55.3	-51.0	----	-60.3	-45.4	A9	F5
5803	7	4:09	60.512	.513	-91.1	-98.3	-109.0	-109.2	-91.0	A5	F0
04	7	4:39	60.549	.552	-87.1	-98.8	-80.2	-109.2	-87.9	A6	F1
05	7	5:09	60.586	.589	-77.6	-79.9	-64.2	-75.4	-78.9	A6	F2
06	7	5:41	60.625	.628	-77.6	-88.3	-72.3	-86.5	-85.0	A7	F2
07	7	6:11	60.662	.665	-79.0	-81.7	-88.3	-94.1	-75.8	A8	F3
08	7	6:44	60.703	.706	-73.0	-78.2	-55.7	-79.7	-82.1	A8	F4
09	7	7:22	60.749	.752	-66.7	-72.3	----	-64.5	-79.1	A8	F5
10	7	8:02	60.798	.801	-63.3	-78.9	-55.7	-79.7	-66.9	A8	F4

TABLE 2 (continued)

Plate CQ	Date 1947	U.T.	Phase Uncorr.	Phase Corr.	Mean of all Lines*	Mean of H_{γ}, Hb H_{ζ}	Mg II 4481	H_{γ}	Ca II 3933	Spectral Type Ca II+ metal	Spectral Type H
5811	July 7	8:42	60.848	.851	-67.8	-67.9	----	-71.5	-60.9	A8	F4
12	7	9:27	60.902	.905	-58.0	-67.2	----	-75.7	-76.1	A8	F5
18	8	3:25	62.222	.224	-38.9	-47.4	----	-52.9	-45.4	A5	F4
19	8	4:06	62.273	.275	-58.7	-41.2	-51.6	-40.9	-57.6	A3	F1
20	8	4:30	62.303	.305	-91.1	-40.0	-105.2	-37.6	-76.0	A3	--
21	8	4:40	62.314	.316	-93.9	-84.8	----	-79.7	-88.2	A3	F0
22	8	4:50	62.326	.328	-85.6	-81.3	-92.5	-90.8	-88.2	A3	F0
23	8	5:00	62.338	.340	-88.7	-105.9	-109.3	-117.7	-91.3	A3	F0
24	8	5:11	62.352	.354	-97.7	-106.2	-92.5	-94.2	-97.3	A3	F0
25	8	5:21	62.365	.367	-94.5	-104.4	-113.3	-113.6	-100.4	A3	A9
26	8	5:31	62.377	.379	-102.1	-108.4	-96.5	-132.2	-91.3	A3	A9
27	8	5:41	62.389	.391	-94.7	-101.9	----	-102.5	-91.3	A3	A9
28	8	5:51	62.402	.404	-92.3	-110.5	-92.5	-128.8	-109.5	A3	A9
29	8	6:02	62.414	.416	-90.7	-103.2	-121.4	-117.8	-97.4	A3	A9
30	8	6:14	62.430	.432	-95.1	-113.5	-96.6	-109.5	-100.5	A2	A9
31	8	6:28	62.446	.448	-91.5	-108.6	-105.4	-113.7	-109.7	A3	F0
32	8	6:44	62.467	.469	-86.1	-103.7	-105.5	-98.6	-91.5	A3	F0
33	8	7:04	62.490	.492	-91.4	-106.6	-96.8	-113.8	-97.6	A4	F0
34	8	7:31	62.524	.526	-78.5	-86.1	-101.5	-94.5	-91.5	A5	F0
35	8	8:02	62.562	.564	-83.6	-94.1	-113.5	-98.6	-100.6	A5	F1
37	8	9:10	62.645	.647	-74.1	-89.3	-88.8	-91.1	-91.6	A6	A1
45	9	4:27	64.062	.060	-51.2	-59.0	-----	-75.8	-51.8	F0	F5
46	9	5:12	64.118	.116	-48.1	-48.5	-11.1	-48.9	-55.0	A9	F4
47	9	5:56	64.171	.169	-40.9	-42.2	----	-45.5	-67.2	A9	F4
48	9	6:27	64.210	.208	-36.8	-51.4	-30.5	-51.7	-47.5	A7	F4
49	9	6:46	64.233	.231	-48.5	-48.1	-13.9	-51.8	-56.7	A7	F3
50	9	7:03	64.254	.252	-40.6	-48.6	----	-44.2	-50.6	A4	F1
51	9	7:18	64.272	.270	-55.2	-49.7	----	-63.5	-47.6	A3	--
52	9	7:31	64.288	.286	-72.0	-31.1	-54.7	-32.4	-78.1	A1	--
53	9	7:42	64.302	.300	-73.8	-27.4	-54.7	-28.3	-68.9	A2	--
54	9	7:52	64.314	.312	-82.5	-72.7	-83.5	-40.0	-87.2	A3	A8
55	9	8:02	64.327	.325	-89.3	-84.3	----	-89.9	-102.5	A2	A8
56	9	8:12	64.339	.337	-97.3	-90.2	----	-108.5	-93.4	A2	A7
57	9	8:20	64.348	.346	-90.8	-100.8	-100.3	-105.1	-105.6	A2	A9
58	9	8:30	64.360	.358	-101.5	-109.3	-112.4	-105.1	-114.7	A2	A9
59	9	8:38	64.371	.369	-91.5	-106.6	-46.8	-105.1	-102.5	A2	A9
60	9	8:48	64.383	.381	-92.4	-104.6	-63.5	-123.7	-102.5	A2	A9
61	9	9:02	64.399	.397	-99.0	-110.1	-108.4	-123.7	-99.5	A2	A9
62	9	9:18	64.420	.418	-88.8	-100.1	-79.6	-108.5	-102.5	A3	A9
72	10	4:56	65.863	.857	-59.1	-60.8	-56.8	-63.6	-62.9	A7	F3
73	10	5:39	65.914	.908	-56.6	-59.8	-18.7	-55.3	-59.9	A9	F4
74	10	6:20	65.965	.959	-53.7	-61.8	-71.6	-51.9	-62.9	A9	F4
75	10	7:01	66.015	.009	-43.4	-52.8	-79.7	-44.4	-47.8	A9	F5
76	10	7:44	66.068	.062	-49.0	-52.2	-34.8	-63.7	-63.0	A8	F5
79	10	10:25	66.265	.259	-52.8	-37.8	----	-32.8	-44.9	--	--
80	10	10:43	66.288	.282	-50.1	----	----	----	----	--	--
81	10	11:01	66.309	.303	-85.6	-45.9	----	----	-81.5	A1	A9
82	10	11:17	66.329	.323	-90.9	-84.9	----	-67.4	-102.9	A1	A9
86	11	5:18	67.654	.643	-74.8	-88.8	-52.4	-103.3	-79.8	A5	F0
87	11	6:02	67.707	.696	-81.8	-71.7	----	-72.1	-92.0	A7	F2
91	12	3:40	69.298	.285	-63.2	-37.0	-43.1	-37.0	-35.8	--	--
92	12	3:52	69.312	.299	-74.6	-21.1	-71.9	-21.1	-57.1	A0	--
93	12	4:04	69.326	.313	-86.1	-63.9	-112.7	-67.4	-78.5	A2	F0
94	12	4:23	69.351	.338	-89.8	-97.7	-118.1	-103.3	-98.2	A3	A9
95	12	4:47	69.379	.366	-93.6	-103.0	-77.4	-114.5	-98.3	A3	A9
96	12	5:12	69.411	.398	-96.1	-109.1	-81.4	-118.7	-113.6	A3	A9
97	12	5:40	69.444	.431	-92.0	-106.5	-77.4	-122.1	-101.3	A3	A9
5898	12	6:09	69.480	.467	-99.6	-98.4	-97.5	-106.9	-92.2	A2	A9
5907	13	3:14	71.030	.011	-54.1	-62.9	-73.5	-76.6	-37.4	A9	F4
08	13	4:09	71.097	.078	-46.5	-60.1	-73.5	-38.6	-70.9	A9	F4

Table 2 (continued)

Plate CQ	Date 1947	U.T.	Phase Uncorr.	Phase Corr.	Mean of all Lines*	Mean of H_γ, H_δ H_ζ	Mg II 4481	H_γ	Ca II 3933	Spectral Type Ca II+ metal	Spectral Type H
5909	July 13	4:59	71.159	.140	-41.1	-40.2	----	-65.6	-68.0	A8	F3
10	13	5:46	71.216	.197	-40.9	-44.5	----	-42.1	-28.3	A8	F2
11	13	6:18	71.256	.237	-42.5	-49.7	----	-48.4	-42.3	A8	F3
12	13	6:36	71.277	.258	-41.5	-49.0	-76.3	-67.8	-33.1	A4	--
13	13	6:51	71.295	.276	-54.7	-47.0	-55.5	-47.0	-69.7	--	--
14	13	7:06	71.314	.295	-89.3	-76.2	-88.3	-71.2	-121.5	--	--
15	13	7:22	71.334	.315	-90.1	-136.2	----	-136.2	-54.5	A1	--
16	13	7:38	71.353	.334	-78.2	-96.0	----	-109.2	-106.3	A3	A9
17	13	7:54	71.373	.354	-85.6	-102.2	-129.2	-120.5	-88.1	A3	A9
18	13	8:18	71.403	.384	-94.5	-98.8	-138.7	-119.0	-98.6	A3	A9
19	13	8:46	71.436	.417	-97.6	-111.5	-114.6	-130.1	-101.7	A3	F0
20	13	9:14	71.471	.452	-96.0	-105.7	-73.8	-114.9	-95.6	A4	F0
21	13	9:44	71.508	.489	-91.4	-96.5	-69.9	-99.8	-98.8	A4	F0
27	14	3:20	72.802	.779	-66.5	-65.2	-44.9	-65.7	-74.2	A9	F4
28	14	4:00	72.851	.828	-63.3	-65.7	-65.6	-72.6	-62.0	A9	F5
29	14	4:42	72.902	.879	-56.3	-62.4	-36.9	-61.7	-62.1	A9	F5
30	14	5:28	72.959	.936	-45.9	-49.0	-16.2	-46.5	-43.8	F0	F6
31	14	6:12	73.012	.989	-51.1	-53.8	-8.2	-57.6	-71.3	A9	F5
32	14	6:58	73.068	.045	-45.4	-48.1	-53.1	-42.4	-56.1	A9	F5
33	14	7:44	73.124	.101	-46.3	-40.1	-21.1	-50.1	-44.0	A9	F5
34	14	8:26	73.176	.153	-40.9	-43.1	-29.1	-50.1	-37.9	A7	F5
35	14	9:03	73.221	.198	-37.5	-45.6	-12.4	-42.5	-31.8	A7	F5
36	14	9:31	73.257	.234	-48.4	-47.1	-53.3	-46.8	-53.3	A4	F3
37	14	9:50	73.280	.257	-45.2	-47.0	----	-42.6	-44.1	A2	--
38	14	10:04	73.296	.273	-59.0	-24.8	-74.1	-35.0	-59.3	A2	--
39	14	10:15	73.310	.287	-80.1	+26.5	----	+26.5	-59.3	A2	--
40	14	10:25	73.322	.299	-76.1	-43.2	-90.1	-54.4	-80.7	A3	A8
41	14	10:35	73.334	.311	-78.7	-91.9	----	-92.5	-77.7	A3	A9
42	14	10:45	73.347	.324	-85.7	-99.1	-115.0	-111.1	-86.9	A2	A9
43	14	10:55	73.359	.336	-94.9	-102.9	-33.3	-119.4	-93.0	A2	F0
44	14	11:05	73.371	.348	-104.4	-99.4	-86.2	-100.1	-102.1	A1	F0
45	14	11:15	73.384	.361	-92.8	-110.3	-127.0	-115.3	-102.1	A1	F0
46	14	11:25	73.396	.373	-91.4	-107.4	-90.2	-100.1	-93.0	A2	F0
50	15	3:15	74.559	.536	-81.2	-95.3	-81.9	-103.9	-101.8	A5	F2
51	15	4:05	74.620	.594	-79.6	-96.3	-65.8	-99.8	-92.7	A7	F4
52	15	5:00	74.688	.662	-74.7	-83.1	-114.8	-84.7	-83.6	A8	F5
53	15	6:00	74.762	.736	-74.2	-73.3	----	-66.0	-89.7	A8	F5
54	15	6:55	74.829	.803	-50.8	-59.1	----	-73.0	-59.3	A8	F5
55	15	7:41	74.885	.859	-54.8	-63.4	----	-69.7	-56.4	A9	F5
5956	15	8:22	74.936	.910	-53.2	-48.5	----	-50.4	-53.4	A8	F5

Lines" gives the mean velocities after the exclusion of $H\gamma$, $H\delta$, $H\zeta$, and *Mg* II 4481. The *Ca* II 3933 line was included in these means. The three *H* lines were excluded because Sanford[2] had found that they differ systematically from the other lines. We are indebted to Dr. Sanford for the information that the higher members of the Balmer series probably do not depart appreciably from the metallic lines. We have, therefore, included them in the means.

The phases were computed with the following formula:

$$\text{Phase} = 1.7641745\,[\text{JD} - 2{,}414{,}856.408] - \text{a whole number}.$$

This corresponds to a period of 0.56683735 day. The same formula was used by Walraven and also by Detre, so that their results and ours are directly comparable. The whole number subtracted from their phases is 30,843; this results in giving our first observation the cycle designation "zero."

TABLE 3

SYSTEMATIC DIFFERENCE BETWEEN OBSERVERS

Plate	Blaauw	No.	Struve	No.	Difference
5509	− 60.6	28	− 63.8	29	+3.2
10	− 76.3	22	− 79.2	27	+2.9
11	− 88.7	30	− 92.7	29	+4.0
12	− 97.0	34	−103.0	30	+6.0
13	−105.4	31	−108.1	30	+2.7
14	−112.4	28	−112.6	29	+0.2
15	−112.3	30	−109.2	28	−3.1
16	−112.7	28	−111.0	28	−1.7
17	−110.1	31	−107.1	29	−3.0
18	−110.4	31	−107.1	32	−3.3
19	−103.6	34	−106.8	32	+3.2
20	−104.7	35	−102.5	29	−2.2
21	−108.8	31	−105.9	28	−2.9

After about one-third of the material had been measured, a mean velocity-curve (similar to that in Fig. 1) was derived for those phases at which the velocity changes rapidly from about −40 to −100 km/sec, i.e., between phases 0.20 and 0.37. With the aid of this mean curve we next reduced the phases for the plates which fell between phases 0.20 and 0.37 to a uniform velocity of −70 km/sec (the procedure is explained below). If more than one plate in the same cycle occurred between the phase limits mentioned above, the mean of the reduced phases was taken. Next these means were plotted against the cycle number. A smooth curve drawn through these points is represented by the dotted line in Figure 2. The abscissae are our cycles, the ordinates are the reduced phases. There is a pronounced change within a period of about 75 cycles. At cycles 4 and 79 the velocity-curve was retarded relative to the mean phase, 0.290. Near cycles 35–40, the velocity-curve was advanced relative to the mean phase. We thus have here precisely the same phenomenon as is known to exist in the light-curve.

From the dotted curve in Figure 2, phase corrections were derived and applied to the phases computed by the formula mentioned above, in order to remove the relative phase shift of the velocity-curves for different cycles. For instance, a correction of +0.025 was applied to the phases of plates at cycle numbers about 40, and −0.025 to phases at cycle numbers about 5 and 75, whereas for cycles 22 and 62 the correction is zero. Thus, in the corrected system of phases, velocity −70 km/sec on the steep branch always occurs at about phase 0.290. These corrected phases are listed in Table 2, together with the ones

computed by the formula on page 60. After these phase corrections had been applied, a new mean velocity-curve was computed from all plates between corrected phases 0.200 and 0.380. The velocities used are those obtained from "all lines." Each good plate was assigned a weight of 1, each poor plate a weight $\frac{1}{2}$.

The new mean curve is represented by the normal points in Table 4 and by the curve in Figure 1. On this final curve new computations of the phase shifts were based. As an example, let us consider plate No. 5345: The original uncorrected phase was 0.293, and

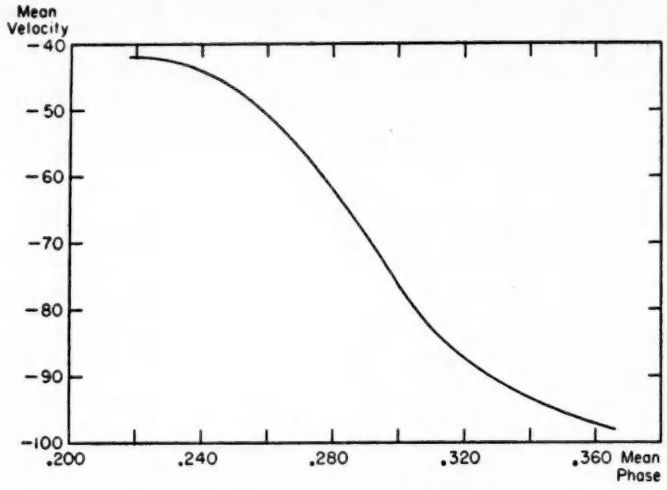

FIG. 1.—Mean velocity-curve of RR Lyrae for the descending branch

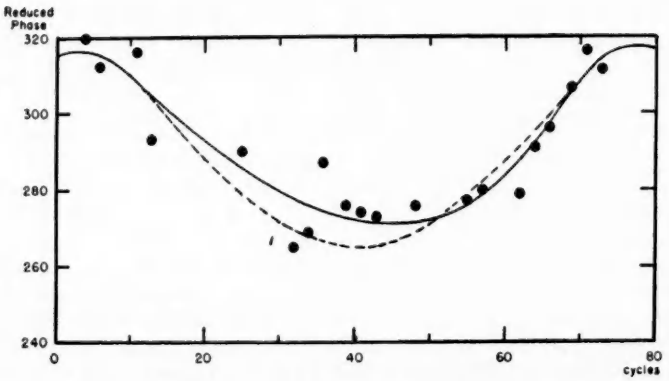

FIG. 2.—Phases at which the velocity on the descending branch was −70 km/sec

the velocity, from all lines, was −53.9 km/sec. From Figure 1 we read phase 0.266, corresponding to a velocity of −53.9 km/sec. Velocity −70.0 km/sec corresponds to phase 0.290. Hence plate No. 5345 gives a correction of 0.290 − 0.266 = 0.024 to the original phase, in order to reduce it to velocity −70 km/sec. The reduced phase is 0.293 + 0.024 = 0.317. In this manner we obtain four reduced phases for the four plates taken on June 5, which fall within the adopted interval. They differ because of errors of observations and possible slight changes in the shape of the true velocity-curve from the mean curve. The latter source of error is negligible. Hence we take the mean for June 5,

0.320, as representing the phase for that date, at which the velocity was −70 km/sec. The latter value is almost precisely the mean velocity of the variable and corresponds to the point of inflection in Figure 1.

In this manner we obtained the reduced phases for all dates at which we had measured at least two spectrograms within the adopted range. Figure 2 shows a plot of the results; they are represented by the drawn curve.

In Figure 3 we show the corresponding displacements of the light-curve as observed by Walraven. The abscissae are shown at the bottom in Julian Days. Our scale of cycles

TABLE 4

MEAN VELOCITY-CURVE

PHASE		MEAN VELOCITY	WEIGHT
Range	Average		
0.208–0.230	0.218	−41.9	9.0
.230– .260	.246	−45.5	16.5
.260– .290	.277	−60.1	20.0
.290– .320	.305	−79.8	23.5
.320– .350	.334	−92.1	25.5
0.350–0.380	0.366	−98.2	25.0

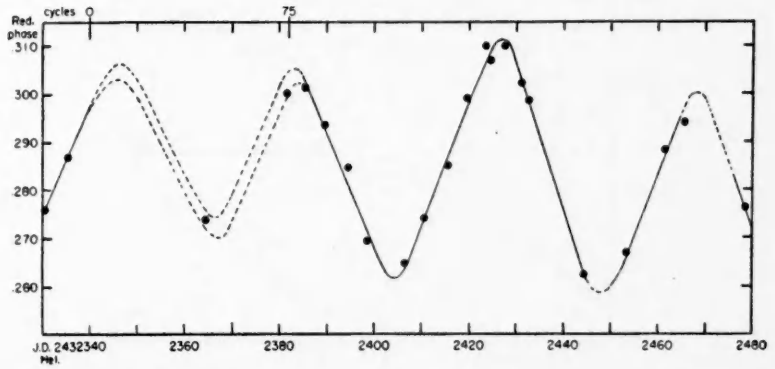

FIG. 3.—Displacements of the light-curve of RR Lyrae as observed by T. Walraven. The phases plotted correspond to the observed median ascending magnitudes.

is shown at the top. It is apparent that our curve in Figure 2 agrees in phase, and probably also in amplitude, with that of Walraven. The velocity-curve and the light-curve shift simultaneously back and forth. The two must be closely connected.

The material of Table 2 was next divided into six groups, as shown in the accompanying table. For each group we have computed the mean velocity-curves shown in Figures

Group	Cycles	Group	Cycles
I	0–13	IV	41–53
II	14–31	V	55–62
III	32–39	VI	64–74

4–7. Figure 4 shows for each of the six groups the average velocity-curve as obtained from all lines, except *Hγ*, *Hδ*, *Hζ*, and *Mg* II 4481. These curves are now lined up in

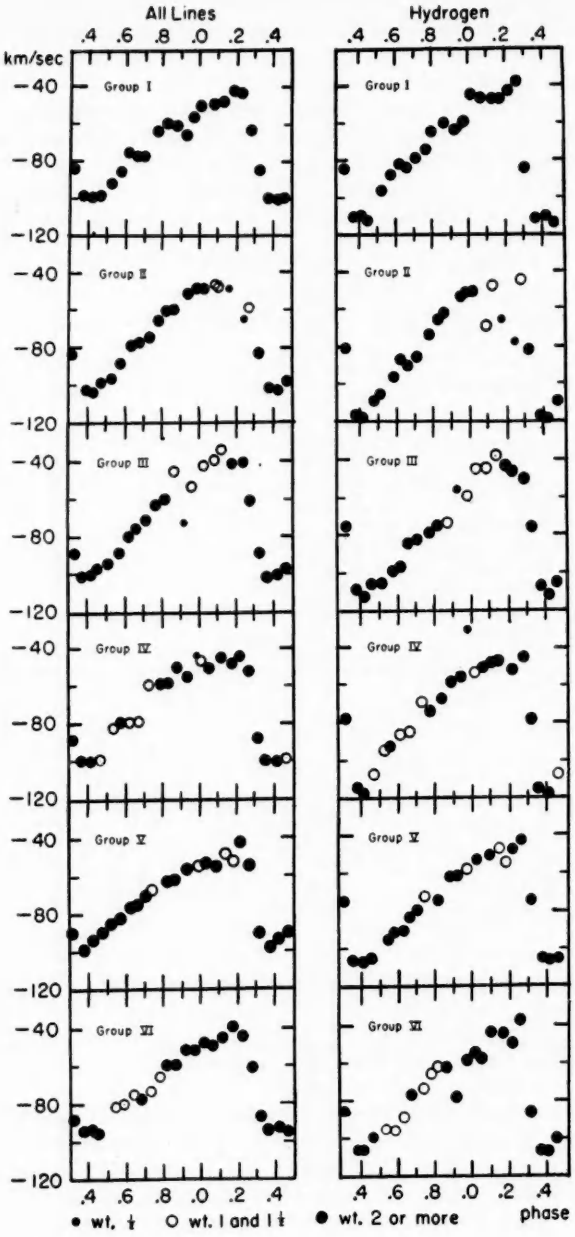

FIG. 4.—Velocity-curves of RR Lyrae

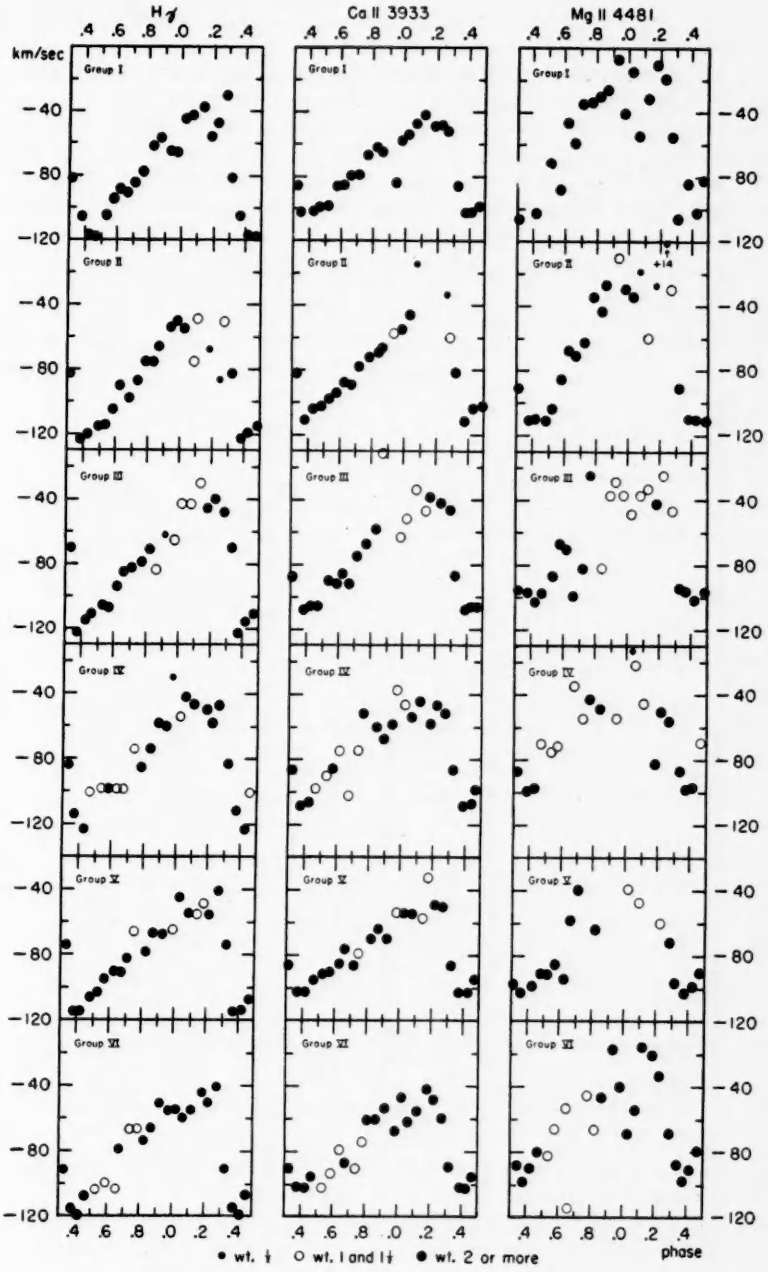

FIG. 5.—Velocity-curves of RR Lyrae

phase because we have used in forming the means the corrected phases of Table 2. If we examine the six velocity-curves as given by all lines, we notice that they agree in giving minimum radial velocity at phase 0.40. There is a strong suggestion that the total amplitude of the velocity-curves is not always the same, and there may also be a slight change in the asymmetry of the six curves. Examining, next, the six velocity-curves representing the means of the hydrogen lines $H\gamma$, $H\delta$, and $H\zeta$, we notice, first of all, that amplitudes of the curves are systematically larger than those given by the metallic lines and the higher members of the Balmer series. This agrees with Sanford's conclusion, except for

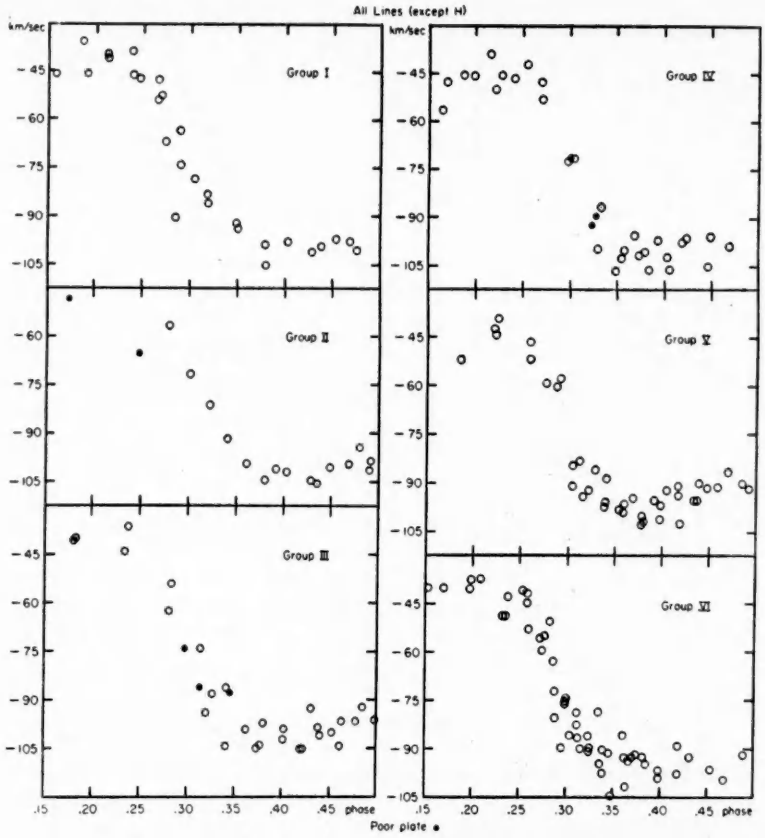

FIG. 6.—Individual observations on descending branch of velocity-curve

the fact that in his work $H\gamma$ rose to a higher maximum than the metallic lines, while the minima were about the same for $H\gamma$ and the metallic lines.

There is also a conspicuous change from group to group in the minimum velocity at phase 0.40. Reading off the best smoothed values, we obtain for the three H lines the minimum velocities shown in the accompanying tabulation. Figure 5 shows the mean

Group	Km/Sec	Group	Km/Sec
I	−112	IV	−118
II	−118	V	−108
III	−112	VI	−107

velocities averaged for small intervals of phase in the case of $H\gamma$, *Ca* II 3933, and *Mg* II 4481; of these, $H\gamma$ is particularly interesting. The minimum velocity reaches to nearly -120 km/sec in all six groups, while the maximum around -40 km/sec is almost identically the same as for the mean of the three hydrogen lines and the mean of all other lines. Hydrogen therefore shows a tendency to give larger velocities of approach at phase 0.40, and this tendency is greatest in $H\gamma$ and decreases toward the higher members of the Balmer series.

In Figures 6 and 7 we have shown the individual observations for all six groups between phases 0.15 and 0.50. This is the interval during which the velocity rapidly changes from its maximum value to its minimum value. Of interest is especially the steep appearance of all twelve curves. The observations are especially numerous between phases 0.35 and 0.45 because the variable is then near maximum brightness. It is instructive to list, in Table 5, the maxima and minima of the individual groups. It would appear that

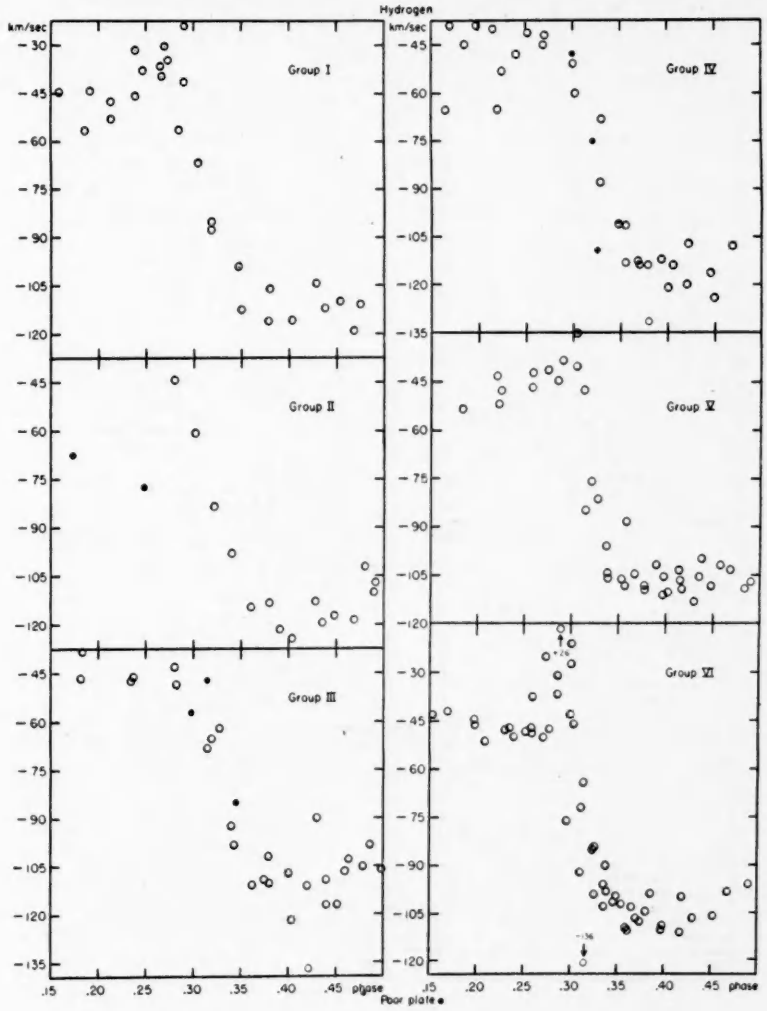

FIG. 7.—Individual observations on descending branch of velocity-curve

the intermediate groups II, III, and IV have deeper minima as measured in *H* and perhaps also in the means of all lines. However, at the same time there is a pronounced tendency, especially in the case of *H*, to show slightly lower maxima in the intermediate groups than in groups I and VI. The changes are not large and do not at all resemble the very conspicuous variations in the amplitude of the light-curve. Perhaps the only striking variation recorded in our observations is the peaked maximum of velocity, for *H*, at about phase 0.29, which is conspicuous in groups I and VI and which is certainly absent in groups III and IV. At this phase of 0.29, when the *H* lines of cycles I and VI reach their maximum radial velocity, the means from "all lines" reach the median velocity of −70 km/sec. There can be but little doubt that this phenomenon is real and is somehow connected with the 41-day cycle.

TABLE 5

MAXIMA AND MINIMA OF VELOCITY-CURVES

Group	All Lines		$H\gamma$		Group	All Lines		$H\gamma$	
	Max.	Min.	Max.	Min.		Max.	Min.	Max.	Min.
I	−40	−100	−30	−112	IV	−45	−100	−45	−120
II	.....	−102	.....	−120	V	−42	− 96	−42	−108
III	−40	−100	−45	−111	VI	−39	− 98	−25	−105

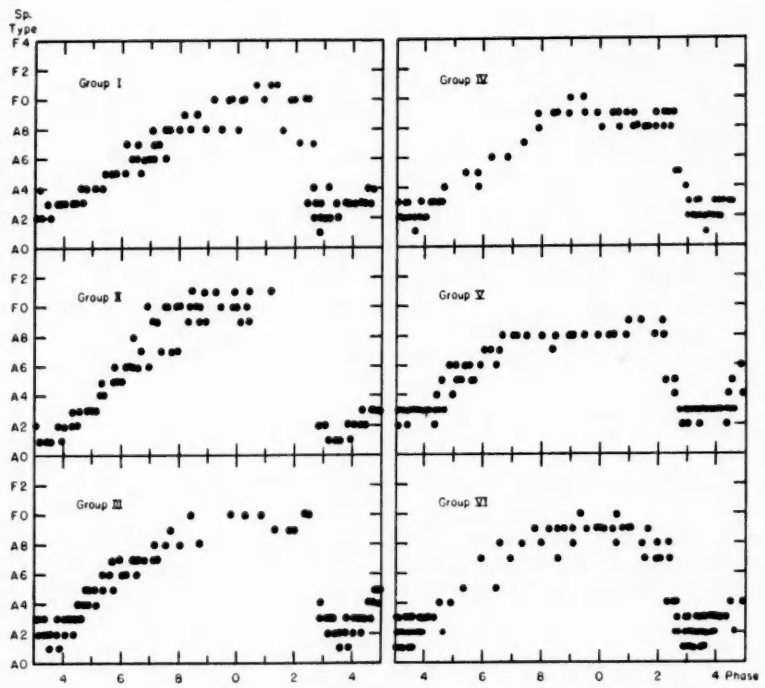

FIG. 8.—Spectral types of RR Lyrae as estimated from the metallic lines and *Ca* II 3933

The line *Mg* II 4481 is somewhat anomalous. It is faint on all plates, and we note especially that it remains surprisingly faint even near maximum light, when the spectral type is about A2. This line shows a large scatter in Figure 5. It is probable that at minimum light or maximum velocity it is blended with the lines *Fe* I 4482.26 and *Fe* I 4482.17. In α Canis Minoris the blend of these two *Fe* I lines produces on high-dispersion spectrograms a line of estimated intensity 7; the estimated intensity of the *Mg* II line is 11.[3] It is extremely probable that this blend accounts for the high maximum of the velocity-curve of *Mg* II 4481 in groups I, II, and VI.

The velocity-curves derived from the strong line *Ca* II 3933 agree remarkably well with those obtained from the other metallic lines. It is difficult to be certain of the changes in the amplitude of these individual curves, but they do not display anything unusual as compared to the curves from the means of all lines.

The spectrographic material will later be used for a detailed study of the line intensities. In the meantime, we have obtained estimates of the spectral type on each plate by comparing RR Lyrae with a set of standard stars chosen from the *Atlas of Stellar Spectra* by Morgan, Keenan, and Kellman. Table 2 lists in two columns the spectral type as estimated from the metallic lines and *Ca* II 3933 and, separately, that from the hydrogen lines. Our results agree closely with those published by Münch and Terrazas.[4] Figure 8 shows the variation in spectral type for each of the six groups. The earliest type at or near class A2 as estimated from the metallic lines and *Ca* II 3933, occurs near phase 0.35. This is a little earlier than the phase of minimum radial velocity, 0.40. The latest spectral type occurs near phase 0.00, which distinctly precedes the phase of maximum radial velocity. The curves of spectral type have broad maxima and narrow minima. This is also true of the velocity-curves, though to a less marked degree. There is a suggestion that the spectral class in groups I, II, and perhaps, VI reached a later type near phase 0.00 than in cycles IV and V. This may furnish an explanation for the otherwise peculiar variation in the velocity-curve as derived from *Mg* II 4481. The latter reached higher maxima in groups I, II, and VI than in cycles III, IV, and V. Since we were inclined to explain the high maxima of velocity as given by *Mg* II 4481 by an effect of blending with lines of *Fe* I which lie on the red side of the *Mg* line, we should expect that the result of the blending would produce a larger shift toward the red when the spectral type is late than when it is relatively early. Hence, if in groups I, II, and VI the spectral type at phase 0.00 was later than it was in groups III, IV, and V, the blending would be more pronounced in the first three groups than in the last three groups.

[3] J. W. Swensson, *Ap. J.*, **103**, 227, 1946.

[4] *Ap. J.*, **103**, 371, 1946.

RAPID VARIATIONS IN THE SPECTRUM OF RHO CASSIOPEIAE*

JESSE L. GREENSTEIN
Yerkes and McDonald Observatories
Received March 17, 1948

ABSTRACT

Spectra of ρ Cassiopeiae taken nightly in November, 1947, show that on at least one occasion, November 10, and possibly also on November 2, the spectrum showed large changes. On November 10 almost all lines were greatly weakened, especially those from zero volts excitation potential in *Fe* I, and from the molecule *AlO;* lines of *Mg* I and *H* were appreciably strengthened. The velocity changed from −60 to −12 km/sec. These changes had disappeared by November 11. An interpretation of the effects is possible if the extended atmosphere surrounding ρ Cas is normally supported by radiation pressure and if on November 10 an ionizing burst of radiation had permitted this extended envelope to start to collapse. Another striking peculiarity was observed on November 2, consisting of the complete disappearance of the continuous spectrum over a range of 500 A. If the phenomenon is real and not caused by a peculiar sensitivity distribution in the emulsion used, the absorption could be caused by the molecule *CaH*. A recent coudé plate shows that the spectral lines in ρ Cas are extremely wide and possibly asymmetric; the star shows at least double the turbulent broadening observed in the supergiant δ CMa.

INTRODUCTION

During the period November 2–19, 1947, spectra of ρ Cas were obtained every clear night at the McDonald Observatory. The dispersion was 30 A/mm in the violet, 40 A/mm at $H\beta$, and 100 A/mm at $H\alpha$. The films used (Eastman 103*a*-F) cover the range $H\beta$ to $H\alpha$ on every occasion; dense exposures and special exposures on IIa-O

TABLE 1

JOURNAL OF OBSERVATIONS

Plate	Date Nov., 1947	Plate	Date Nov., 1947	Plate	Date Nov., 1947	Plate	Date Nov., 1947
CG 6184....	2.2*	CG 6223....	5.3	CG 6256....	12.2	CG 6272....	16.3
6200....	3.2	6244....	8.1	6269....	13.2	6284....	18.4
6201....	3.3	6245....	10.0*	6270....	15.0	6290....	19.3
6213....	4.2	6247....	11.1	6271....	15.1	Cd 755....	24.2
6222....	5.3	6255....	12.1				

*The plates marked with an asterisk show some peculiarity.

emulsion reach to λ 4000. A journal of the observations is contained in Table 1. One underexposed 4-A/mm coudé plate was also obtained. According to A.A.V.S.O. observations, kindly supplied by Leon Campbell, the mean visual brightness was 5.3 mag. My own estimates at the telescope give 5.7 mag. on November 2 and about 5.4 for the balance of the period.

The spectrum and light (and possibly the color) of ρ Cas are variable; a discussion of the history of the slow changes has been made by Popper,[1] Keenan,[2] Thackeray,[3] and Morgan and Bidelman.[4] I shall discuss only those short-period changes observed during November, 1947; the "normal" spectrum with which I compare the altered spectra is

* *Contributions from the McDonald Observatory, University of Texas*, No. 151.

[1] *A.J.*, **52**, 129, 1946.

[2] *Ap. J.*, **106**, 295, 1947.

[3] *Nature*, **160**, 370, 1947.

[4] Unpublished data kindly communicated.

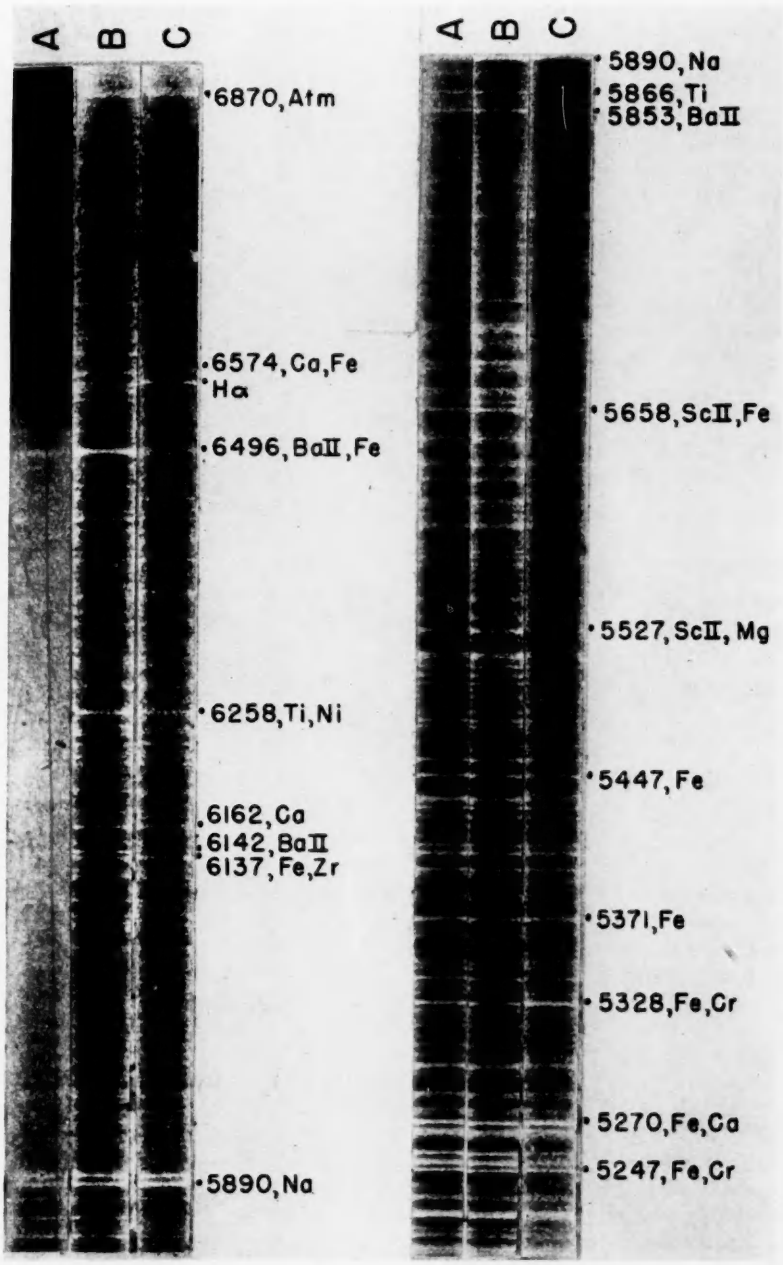

FIG. 1.—Spectra of ρ Cas; strip *A*, November 2; strip *B*, November 12; strip *C*, November 10, 1947. The gap in the November 2 spectrum, near λ 6300, may be due to the molecule *CaH*. Strip *C* shows the weakening of the lines on November 10, with the accompanying enhancement of *Hα*.

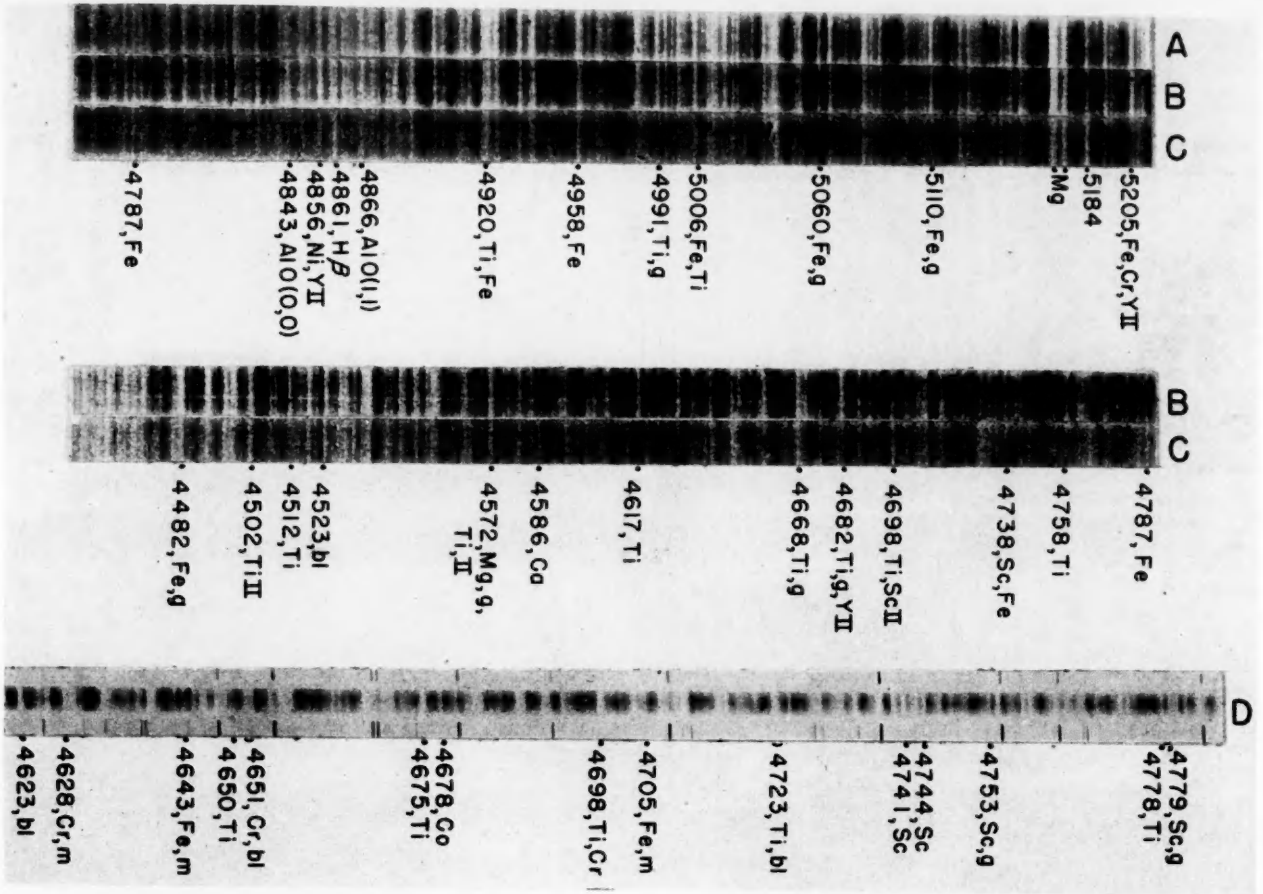

FIG. 2.—Spectra of ρ Cas; strips *A*, *B*, *C*. Lines marked *g* arise from the ground levels of the atom and are particularly weakened on November 10; the heads of the *AlO* band, with the general absorption of the band, also show large weakening in strip *C*. Strip *D* is an enlargement of a section of a McDonald coudé plate, original dispersion 4 A/mm. The spectrum is very complex, and the strength of the neutral lines, especially *Sc* I, resembles that in M stars. Lines marked *bl* are generally blends; those marked *m* arise from the highly excited nonmetastable levels and would not be strong if the dilution were great. The width of the marked, nearly unblended, lines (greater than 0.5 A in all cases) can be seen to be very great compared to that of the comparison lines. The broadening, and any possible asymmetries, must be due to motions in the envelope.

that obtained on November 12.1 and is illustrated in Figures 1 and 2 (strip *B*). The spectrum obtained on November 2.2 is shown in strip *A*, and that of November 10.0 in strip *C*. All other plates show spectra substantially identical with that of November 12.1; the peculiarities of November 2.2 were absent on November 3.2, and those of November 10.0 were absent on November 8.1 and 11.1. Such rapid changes in an enormously extended atmosphere are unexpected.

A brief description of the spectral features of the present "normal" phase is necessary. (Before the 1946 light-minimum, ρ Cas was a nearly normal supergiant F8 I*a* star, with a velocity of -43 km/sec.) I measured wave lengths on two plates, from $H\alpha$ to $H\beta$, and identified about three hundred and fifty lines. The blending is serious and the spectral region limited; shortward of $H\beta$ the spectrum is so complex that an extensive investigation with higher dispersion is required. Table 2 contains a list of the elements identified, together with the excitation potentials (E.P.) represented. For certain elements lines from the lowest levels, E.P. = 0, are greatly enhanced as compared to laboratory sources. Bidelman[5] has recently discussed the present "normal" spectrum and pointed out the

TABLE 2

ELEMENTS PRESENT IN ρ CASSIOPEIAE

Element	E.P. (Volts)	Remarks	Element	E.P. (Volts)	Remarks
H	10.2		*Cr* I	1–3	
Ca I	0–2.7	Strong	*Cr* II	3–3.8	?
Mg I	2.7–4.3	Strong	*Mn* I	0	
Si I	4.9	?	*Fe* I	0–4.4	Strong
Na I	0	Strong	*Fe* II	3.9	
Sc I	0–1.4	?	*Ni* I	1.7–4.2	Strong
Sc II	1.4		*Y* II	1.7	
Ti I	0–2.5	Strong	*Zr* I	0–1.4	
Ti II	1.6–3.0		*Ba* II	0–0.7	Strong
V I	0–1.1		*Al O*	0	
V II	2	?			

great strength of these lines, which are also strong in a supergiant K star. In many features ρ Cas now resembles a supergiant K star, except for the unexpected strength[2,5] of lines from highly excited levels, such as *H, Fe, Mg, Si, N, O*.

There is only slight evidence for velocity differences between the elements in this spectral region. I find a difference (*Ti* I − *Fe* I) = -7 km/sec and also that lines of low excitation potential, 0–2 volts, show a velocity 6 km/sec more negative than those from 2 to 4 volts. An inspection in a comparator showed that the mean velocity was large and negative on nearly all plates. From about seventy lines on CG 6255 (November 12) I find the velocity of -60 km/sec. For CG 6245 (November 10) the same lines give -12 km/sec; inspection of plates taken on November 8 and 11 show that they would have given a velocity near -60 km/sec.

Plate Cd 755, with a dispersion of 4 A/mm, covers the region λλ 4300–4950. Although underexposed, it provides some information on the contours of the lines. A short section is reproduced as strip *D*, Figure 2. Before its outburst, ρ Cas resembled δ CMa and probably had nearly similar line widths. At present its lines are nearly twice as wide; measured widths of nearly unblended lines range from 0.54 to 1.5 A, and in δ CMa from 0.24 to 0.8 A. The velocity range must be of the order of at least 50 km/sec in ρ Cas. The great widening cannot be due to rotation but may arise from turbulence or filamen-

[5] Unpublished, given at the December, 1947, meeting of the A.A.S., Columbus, Ohio.

tary prominence-like motions. Most unblended lines seem to be symmetrical, U-shaped, and very deep; other lines show apparent sharp cores superposed on asymmetric wings, longward or shortward. While such shadings are known in Pleione's expanding shell, their reality cannot be proved in ρ Cas because of the severe blending and the richness of the spectrum. It is interesting to find several lines of *Fe* I and *Cr* I which arise from high, excited, nonmetastable levels up to 3.5 volts. These lines show the wide profiles and the same negative velocities as do the low-level lines.

SPECTRAL CHANGES ON NOVEMBER 10

Plate CG 6245, November 10, shows almost all lines weakened, with only *H* and *Mg* I appreciably strengthened. Changes of line intensity were estimated in a comparator and recorded as δI (in the sense, CG 6245 *minus* CG 6255). These δI's are on an arbitrary scale but measure roughly the fractional change in line intensity. (Otherwise weak lines of intensity 1, for example, could not have $\delta I < -1$.) The scale is fairly uniform, with weak and strong lines showing about the same δI, if of similar origin. Table 3 contains

TABLE 3

CHANGES IN LINE INTENSITY BETWEEN NOVEMBER 12 AND NOVEMBER 10

Element	E.P. (Volts)	δI	Element	E.P. (Volts)	δI
Fe I	0	−5	*Na* I	0	−3
	1.5	−1.5	Ions	0–3	−2.5
	2.5	−0.2	*AlO*	0	−4
Ti I	0	−2.1	*Mg* I	2.7	+2
	2	−2.7	*H*	10.2	+3
	3	−0.7			

the well-observed values of δI for different elements. The two band heads of *AlO* and the resonance multiplet of *Fe* I($a^5D - z^7D^0$) show the largest effects; ions with low excitation potential, such as *Ba* II, also show large weakenings. It is this group of lines which is unusually strong[5] in ρ Cas. The δI's for *Fe* I clearly show an increase of excitation temperature on November 10; many high-level lines were unchanged or even strengthened, while the lines from 0 volts had the largest δI's. An alternative hypothesis would be that very large stratification exists; the 0- and 1-volt lines of *Fe* I would be normally produced in an outer envelope so cool and rarefied that no excited atoms are present. Then the change on November 10 could be interpreted as the temporary ejection or ionization of this envelope, leaving strong the higher-excitation lines which are produced in the normal reversing layer. This hypothesis does not account for the velocity change or for the strengthening of the *H* and *Mg* I lines.

The velocity on November 10, −12 km/sec, is more positive by 31 km/sec than that observed (−43 km/sec) before the large disturbances occurred in the spectrum. If the old velocity is actually that of the center of mass of the star, matter was actually collapsing toward the star on November 10. The collapse lasted for a time of the order of a day, and the change in radius, about 4×10^{11} cm, was negligible compared to the radius of the star, which is near 10^{13} cm, or of the envelope, which may be much larger. A tentative hypothesis to explain the present "normal" spectrum of ρ Cas, and the changes observed on November 10, may be suggested. The star is surrounded by a very extended, dominantly expanding envelope, supported by the radiation pressure on the

hydrogen atoms. Differential expansion may be present. Hydrogen is dominantly neutral and partially transfers its momentum to the other atoms. The envelope is so large that the outer parts have very low radiative and negligible collisional excitation. Then stratification would occur, as suggested by Keenan,[2] with only the low-level lines capable of absorbing in the outer parts of the envelope. Somewhere between November 8 and November 10 a burst of ionizing radiation partially ionized the hydrogen and increased the excitation of the entire envelope. The loss of radiation-pressure support permitted the outer envelope to start collapsing with the gravitational acceleration, g, which was large compared to the effective reduced acceleration g_{eff} (which included the radiation pressure and governed the "normal" equilibrium). We can estimate the gravitational acceleration from our observations. The collapse velocity of 31 km/sec was established (and again disappeared) within one day; since

$$v = gt\,, \tag{1}$$

we find $g \approx 36$ cm sec^{-2}. Now, if we adopt a luminosity of -6 mag., a mass of 30 $\odot$, and a radius of >160 $\odot$, we find the expected gravitational g to be $g < 30$ cm sec^{-2}. There is at least an order-of-magnitude agreement between the observed and the expected velocity of collapse. In solar prominences accelerations greater than that of gravity occur, because of electromagnetic attractive forces, which may also be present in the atmosphere of ρ Cas.

THE SPECTRUM ON NOVEMBER 2

The spectrum marked *A* on Figure 1, CG 6184, November 2, shows an extremely strong feature which runs from λ 5700 to λ 6600; between λ 6000 and λ 6450 the spectrum is almost completely wiped out, with a photographic density the same as that of the clear film. If interpreted as a molecular absorption band, it is degraded shortward; the head or heads would be near λ 6400, with successive vibrational sequences extending longward, while overlapping and highly developed rotational structure extends shortward. An alternative explanation is that the feature arises from a loss of sensitivity in this wave-length region due to a sensitization defect of the strip of film used. However, the long-wave cutoff of the spectrum is normal for the F emulsion. The region is about 10 mm long on the original film; no defects, except a thin longitudinal scratch, are visible or suspected (see top strip, Fig. 1). The iron comparison spectrum provides no information, since only a weak exposure had been made, and no lines are, or would be expected to be, visible longward of λ 5600. The film was cut to size from a 4 × 5 inch section, the other two strips of which were used at some time during the observing session; no other spectrum had a similar appearance. Since many strips of film were used for tube-photometer exposures, which would not reveal a loss of sensitivity in a limited spectral region, there is no complete proof of the absence of such a loss.

On the night of November 2 the star was suspected to be faint and quite red. This is supported by underexposure of the spectrum in the blue and a rapid decrease in intensity in the blue-green. We must reserve judgment on the reality of the existence of an absorption band near λ 6400. Its great extent, depth, lack of structure, rapid disappearance, and possible identification[6] are all unparalleled in normal stars. On CG 6184 no other spectral peculiarity was found from λ 4600 to λ 6600 except a general reddening of the star. Dr. P. Swings, of the Liége and McDonald Observatories, has suggested as a possible identification, the molecule *CaH*, which has a strong transition from its ground state, $B^2\Sigma - {}^2\Sigma$ in this region. The (0, 0) band origin is at λ 6346, with heads at λ 6382, λ 6389; the (1, 1) origin is at λ 6352 and the (2, 2) at λ 6358. The band is

[6] Dr. G. Herzberg has remarked that it is surprising that no head-structures are visible, if the band is a diatomic hydride; heavier or polyatomic molecules might give the broad diffuse structure seen.

degraded to the violet. The $A^2\Sigma - {}^2\Sigma$ transition heads lie near λ 7000 and would have appeared only as a weakening of the spectrum longward of the λ 6400 band. The *CaH* bands have been observed to be strong in sunspots[7] and in dwarf M stars.[8] They are weak or absent in a giant M star[9] and in other phases[3] of ρ Cas. The appearance of the feature on November 2 did not affect the strength of the *Ca* I lines; the only other molecule present, *AlO*, was also unchanged. All traces had disappeared by November 3, although a slight general depression of the λλ 6200–6500 region of the spectrum is suspected on all plates; the depression may, however, be a slight dip in the sensitivity-curve of the emulsion.

I am much indebted to Dr. W. P. Bidelman for discussions of the history, spectral features, and identifications in ρ Cas.

[7] Richardson, *Ap. J.*, **73**, 216, 1931; also Mount Wilson Sunspot Spectrum Map.

[8] Öhman, *Ap. J.*, **80**, 171, 1934.

[9] D. Davis, *Ap. J.*, **106**, 28, 1947.

ON THE INTERPRETATION OF THE CONTINUOUS SPECTRUM OF α LYRAE

ANNE B. UNDERHILL*
Yerkes Observatory
Received April 15, 1948

ABSTRACT

The observed spectral variation of the continuous spectrum of α Lyrae from λ 4040 to λ 9870 can be predicted satisfactorily from a model atmosphere in which the effective temperature is 10,080°, the electron pressure is 10^4, and the opacity is given by neutral hydrogen and the negative hydrogen ion.

It is of interest to compare the observed spectral variation of the continuous spectrum of an A0 star with that predicted from theory, for thereby the effective temperature and electron pressure in the stellar atmosphere may be deduced. This method of determining the temperature and electron pressure in a stellar atmosphere requires only the observation of relative fluxes at a number of wave lengths and is therefore free from the liabilities of the methods which require the measurement of absolute fluxes. Most interest attaches to the determination of the effective electron pressure, for spectroscopic evidence has already indicated that the effective temperature of an A0 star is close to 10,000°. We shall see that it is possible to differentiate between a model atmosphere with $p_e = 10^3$ and one with $p_e = 10^4$, both being at the same effective temperature.

The emergent flux in a stellar atmosphere can be predicted by a method outlined by Chandrasekhar and Münch[1] if κ_λ/κ is known at the effective optical depth of the continuum. Since the continuous absorption coefficient of hydrogen may be computed for any temperature from well-known formulae and since the continuous absorption due to H^- can be found from tables prepared by Chandrasekhar and Mrs. Breen,[2] $\kappa_\lambda/\bar{\kappa}$ can be readily computed. The emergent flux at a number of wave lengths has been computed, with the tables provided for that purpose by Chandrasekhar and Mrs. Breen,[3] for the following cases: H and H^- as sources of opacity, $T_e = 10{,}080°$, $p_e = 10^4$; H and H^- as sources of opacity, $T_e = 10{,}080°$, $p_e = 10^3$; H as source of opacity, $T_e = 14{,}000°$; H as source of opacity, $T_e = 16{,}800°$. In the two latter cases the neglect of H^- as a source of opacity would appear justifiable in view of the high temperature, for even at $T_e = 10{,}080°$ an electron pressure of 10^4 is required to make the absorption from H^- comparable to that from neutral hydrogen. When the opacity is due to H only, the ratio $\kappa_\lambda/\bar{\kappa}$ does not depend on the electron pressure. The effective optical depth of the continuum is assumed to be $\tau = 0.60$. The computed fluxes are expressed as magnitude differences from the flux at λ 5000 for comparison with the photographic measures of the continuous spectrum of α Lyrae by R. C. Williams[4] and as magnitude differences from the flux at λ 7880 for comparison with the photoelectric measurements of J. S. Hall and R. C. Williams.[5] Table 1 gives the computed relative fluxes and R. C. Williams' observations[4] in the range λλ 4040–6370. Table 2 gives the computed relative fluxes and the observations of Hall and Williams[5] in the range λλ 5390–9870. The data of Tables 1 and 2 are plotted in Figure 1.

We see from Figure 1 that the best agreement between theory and observation for

* This work was done during the author's tenure of a scholarship from the Canadian Federation of University Women.

[1] *Ap. J.*, **104**, 446, 1946.

[2] *Ap. J.*, **104**, 430, 1946.

[3] *Ap. J.*, **105**, 461, 1947.

[4] *Pub. Obs. U. Michigan*, **7**, 147, 1939.

[5] *Ap. J.*, **95**, 225, 1942.

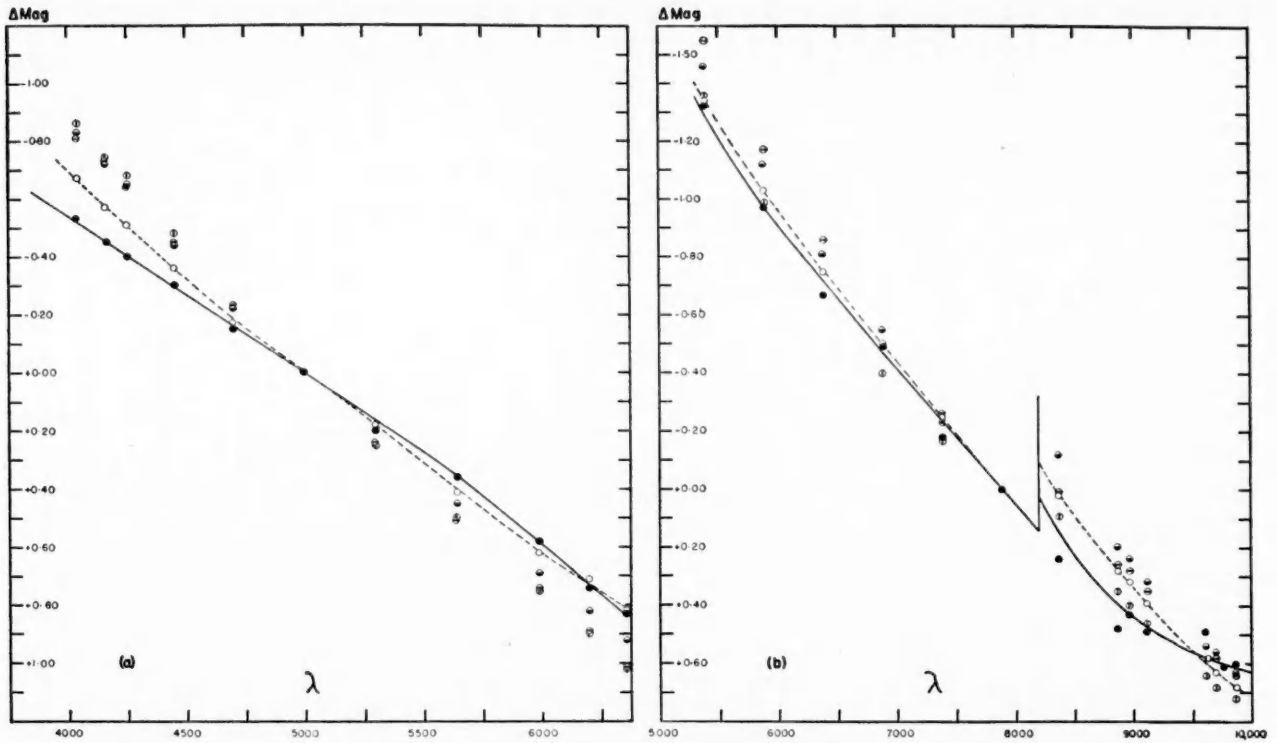

FIG. 1.—The continuous spectrum of α Lyrae. The observations of Williams and of Hall and Williams are plotted as filled circles. These points are joined by a solid line. The relative fluxes from the model with $T_e = 10{,}080°$, $p_e = 10^4$, H and H^- as sources of opacity are given by open circles; they are joined by a dotted line. The fluxes from the model with $T_e = 10{,}080°$, $p_e = 10^3$, H and H^-, are given by half-filled circles. The fluxes from the model with $T_e = 14{,}000°$ and pure H are given by circles with a horizontal bar. The fluxes from the model with $T_e = 16{,}800°$ and pure H are given by circles with a vertical bar. If a symbol cannot be seen at any wave length, it coincides with one of the other symbols plotted. In Figure 1, *b*, the Paschen limit is indicated by a vertical line.

both series of measurements is obtained with the model which has $T_e = 10{,}080°$, $p_e = 10^4$, and H and H^- as the sources of opacity. The discrepancies between observation and theory in the violet, $\lambda < 4400$ A (Fig. 1, *a*), and around λλ 8200–9000(Fig. 1, *b*) are probably due to the wings of the hydrogen lines suppressing the continuum in these regions. Reference to Williams' Figure 3[6] shows that the wings of the Balmer lines, $H\gamma$, $H\delta$, and $H\epsilon$, very nearly overlap in the region $\lambda < 4400$ A. Hall and Williams remark[5] that their measurements to the red of the Paschen jump are probably affected by the blended Paschen lines. The model with $T_e = 10{,}080°$, $p_e = 10^3$, and H and H^- as sources of opacity can be definitely ruled out as representing the atmosphere of α Lyrae, for it nowhere closely predicts the observed course of the continuous spectrum.

The models with only hydrogen as the source of opacity do not give an adequate representation of the continuous spectrum of α Lyrae. In the wave-length range (λλ 4040–

TABLE 1

RELATIVE FLUXES IN MAGNITUDE DIFFERENCES FROM THE FLUX AT λ 5000

λ	$T_e = 10{,}080°$ $p_e = 10^4$ H and H^-	$T_e = 10{,}080°$ $p_e = 10^3$ H and H^-	$T_e = 14{,}000°$ H Only	$T_e = 16{,}800°$ H Only	α Lyrae Observed by Williams
4040	−0.67	−0.83	−0.81	−0.86	−0.53
4170	− .57	− .72	−0.73	−0.74	− .45
4250	− .51	− .65	−0.64	−0.68	− .40
4450	− .36	− .44	−0.45	−0.48	− .30
4700	− .17	− .22	−0.23	−0.22	− .17
5000	+ .00	+ .00	+0.00	+0.00	+ .00
5300	+ .18	+ .20	+0.24	+0.25	+ .20
5645	+ .41	+ .45	+0.51	+0.50	+ .36
5990	+ .62	+ .69	+0.74	+0.75	+ .58
6200	+ .71	+ .82	+0.89	+0.90	+ .74
6370	+0.82	+0.92	+1.01	+1.02	+0.83

TABLE 2

RELATIVE FLUXES IN MAGNITUDE DIFFERENCES FROM THE FLUX AT λ 7880

λ	$T_e = 10{,}080°$ $p_e = 10^4$ H and H^-	$T_e = 10{,}080°$ $p_e = 10^3$ H and H^-	$T_e = 14{,}000°$ H Only	$T_e = 16{,}800°$ H Only	α Lyrae Observed by Hall and Williams
5390	−1.34	−1.46	−1.55	−1.36	−1.32
5890	−1.03	−1.12	−1.17	−0.99	−0.97
6390	−0.75	−0.81	−0.86	−0.67	−0.67
6880	−0.50	−0.55	−0.55	−0.40	−0.49
7390	−0.25	−0.26	−0.23	−0.17	−0.18
7880	+0.00	+0.00	+0.00	+0.00	+0.00
8370	+0.02	−0.12	+0.01	+0.09	+0.24
8870	+0.28	+0.20	+0.26	+0.35	+0.38
8970	+0.32	+0.24	+0.28	+0.40	+0.33
9120	+0.39	+0.32	+0.35	+0.46	+0.39
9620	+0.58	+0.54	+0.54	+0.64	+0.49
9700	+0.63	+0.56	+0.58	+0.68	+0.61*
9870	+0.68	+0.63	+0.64	+0.72	+0.60

* The observed value is at λ 9770.

[6] *Pub. Obs. U. Michigan*, **7**, 93, 1939.

6370) of Figure 1, *a*, the two models give practically the same result, for in this region the relative absorption coefficient of hydrogen at various wave lengths is not very sensitive to temperature. This agreement between the predicted relative fluxes illustrates the difficulty of determining a unique effective temperature for high-temperature stars from measurements in the usual photographic and visual region, if hydrogen is the only source of opacity. The wave-length range (λλ 5390–9870) of Figure 1, *b*, is centered around the Paschen jump. Here the relative value of the absorption coefficient is sensitive to temperature changes, and there is a difference between the results predicted for the model with $T_e = 14{,}000°$ and the model with $T_e = 16{,}800°$. In this wave-length range, agreement between observation and theory can be obtained from a pure hydrogen model at a sufficiently high temperature, as well as from a model at a lower effective temperature but with H and H^- as the sources of opacity. This is so because in this wave-length region the absorption coefficient of both H and H^- increases in a somewhat similar manner with increasing wave length. Consequently, the effect of H and H^- can be simulated for a short wave-length range by a pure H atmosphere at a sufficiently high temperature. That the pure hydrogen atmosphere at $T_e = 16{,}800°$ is not adequate to explain the observations is shown by the curves of Figure 1, *a*. The direction and amount of the systematic deviations of the predicted relative fluxes one from another at any wave length depends on the point of reference chosen. The computations show that the continuous spectrum of α Lyrae may be successfully predicted over the entire range of the observations by a model which has an effective temperature of 10,080° and an electron pressure of 10^4 and in which the opacity is given by neutral hydrogen and the negative hydrogen ion as required by physical theory.

RELATIVE *gf*-VALUES FOR LINES OF *Ni* I*

ROBERT B. KING
Mount Wilson Observatory
Received March 23, 1948

ABSTRACT

The relative *gf*-values for 134 lines in the spectrum of *Ni* I λλ 3012–3912 have been obtained from electric-furnace absorption spectra. All the lines arise from the three lowest terms, a^3F, a^3D, and a^1D. The furnace *gf*-values are compared with arc-intensity measurements published by other investigators.

The relative *gf*-values of 134 lines in 37 multiplets have been measured in the spectrum of neutral nickel (*Ni* I) by the electric-furnace, absorption-spectrum method described in earlier papers.[1,2]

The *Ni* I spectrum has three low-lying, overlapping terms—a^3F, a^3D, and a^1D—of excitation potentials between 0.0 and 0.4 volts. These terms, combining with the lowest odd terms between 3.1 and 4.5 volts E.P., give rise to the very strong lines between λ 2900 and λ 3900 which dominate the *Ni* I spectrum. The next lowest term, b^1D, has a much higher excitation potential of 1.7 volts. Upward transitions from b^1D and from the other even terms under 3.0 volts are relatively weak. Only a few lines arising from these transitions lie in the ultraviolet, and none has been observed in absorption. Relatively strong transitions occur from the lowest odd terms a^5D°, z^5G°, and z^5F°, but the excitation potentials of these terms are over 3.0 volts, and the lines have not been observed in absorption. The present measurements are, therefore, limited to lines from the three lowest terms, a^3F, a^3D, and a^1D, in the wave-length region λλ 3012–3912.

The observations were made at furnace temperatures between 1300° and 2400° C with the second order of the 15-foot concave-grating spectrograph and Eastman IV-O and Cramer Contrast plates.

The results of the measurements are in Table 1. The data in the first four columns are taken from the *Revised Multiplet Table*,[3] the arc intensities in the fourth column being eye estimates. The fifth column contains the relative *gf*-values derived from the furnace absorption-spectra measurements. The relative weights of these measurements are indicated by the letters, A, B, and C, following the system described in a recent paper on *gf*-values for *V* I.[4]

Quantitative measurements of relative line intensities in the arc spectrum of *Ni* I have been made in the Utrecht Physical Laboratory by Ornstein and Bouma[5] and by H. van Driel.[6] The list of Ornstein and Bouma includes over three hundred lines between λ 2800 and λ 4200, with many lines from transitions between high terms that were not observed in the furnace. Their published intensities were apparently not corrected for excitation temperature of the arc. A comparison of the arc intensities and furnace *gf*-values showed that the arc measurements of the stronger lines are affected by self-absorption or by self-reversal. The former—a curve-of-growth effect—is probably dominant because the arc measurements were made at low current (0.45 amp.), where

* *Contributions from the Mount Wilson Observatory, Carnegie Institution of Washington*, No. 746.

[1] R. B. and A. S. King, *Mt. W. Contr.*, No. 528; *Ap. J.*, **82**, 377, 1935.

[2] R. B. and A. S. King, *Mt. W. Contr.*, No. 581; *Ap. J.*, **87**, 24, 1938.

[3] C. E. Moore, *Princeton U. Obs. Contr.*, No. 20, 1945.

[4] R. B. King, *Mt. W. Contr.*, No. 731; *Ap. J.*, **105**, 376, 1947.

[5] *Phys. Rev.*, **36**, 679, 1930.

[6] Thesis, University of Utrecht, 1935.

TABLE 1

RELATIVE gf-VALUES FOR LINES OF Ni I

Mult. No.	Designation	J	λ	Estimated Arc Int.	Furnace gf	Wt.	Arc gf‡
(1)*	$a^3F-z^5D^\circ$	4–3	3749.045	8	8.0	A	.....
		3–2	3832.873	5	4.7	A	.....
		2–1	3885.87	P	0.84	B	.....
(2)	$a^3F-z^5G^\circ$	4–5	3724.733	15	47	A	.....
		3–4	3739.229	10	31	A	.....
		2–3	3792.337	5	8.4	B	.....
		4–4	3561.751	10	32	A	.....
		3–3	3669.241	12	31	A	.....
		2–2	3730.751	4	4.8	A	.....
		4–3	3498.19	P	0.25	A	.....
		3–2	3611.54	P	0.67	B	.....
(3)	$a^3F-z^5F^\circ$	4–5	3502.595	8	22	A	.....
		3–4	3602.281	15	86	B	70.6
		4–4	3437.280	30R	520	B	665
		3–3	3507.694	8	42	A	.....
		2–2	3577.240	2	2.1	A	.....
		4–3	3351.06	P	0.25	B	.....
		3–2	3467.502	12	85	B	98
		2–1	3548.185†	20r	(430)	A	(225)
(4)	$a^3F-z^5P^\circ$	3–2	3670.427	20	73	B	.....
		2–1	3664.095	20	129	B	.....
		2–2	3793.608	8	19.3	A	.....
(5)	$a^3F-z^3F^\circ$	4–4	3391.050	50R	604	B	754
		3–3	3571.869	50R	670	C	645
		2–2	3519.766	20R	510	B	347
		4–3	3409.578	8	42	A	.....
		3–2	3413.478	25R	420	B	.....
		3–4	3551.534	8	37	A	.....
		2–3	3688.415	15	88	A	.....
(6)	$a^3F-z^3D^\circ$	4–3	3369.573	80R	1540	B	2260
		3–2	3500.852	25R	520	B	464
		2–1	3483.774	25R	990	B	680
		3–3	3527.982	15	86	B	53
		2–2	3612.741	30R	460	A	300
		2–3	3641.641	4	4.0	A	.....
(7)	$a^3F-z^3G^\circ$	4–5	3232.963	25R	680	C	1380
		3–4	3371.993	15r	440	B	736
		2–3	3380.885	15r	370	B	.....
		4–4	3226.984	5	30	A	.....
		3–3	3282.696	8	48	A	.....
		4–3	3145.121	3	1.4	B	.....
(8)	$a^3F-z^1F^\circ$	4–3	3221.652	10r	133	A	.....
		3–3	3366.168	20r	390	B	386
		2–3	3469.486	15	185	B	125
(9)	$a^3F-z^1D^\circ$	3–2	3320.257	20r	390	A	366
		2–2	3420.741	5	10.4	A	.....
(10)	$a^3F-z^1P^\circ$	2–1	3249.440	6	29	A	.....

* Multiplet incompletely observed.

† Blend with a line in another Ni I multiplet; gf-value in parenthesis computed on the assumption that the furnace line is due entirely to transition indicated.

‡ From measurements by H. van Driel (Thesis, Utrecht, 1935).

TABLE 1—*Continued*

Mult. No.	Designation	J	λ	Estimated Arc Int.	Furnace gf	Wt.	Arc gf‡
(11)	$a^3F-y^3F^\circ$	4–4	3031.870	10r	147	B	.....
		3–3	3145.719	8	54	A	.....
		2–2	3184.367	8	79	A	.....
		4–3	3019.143	20R	326	B	.....
		3–2	3097.118	15r	320	A	.....
		3–4	3159.521	3	4.0	A	.....
		2–3	3235.753	4	6.4	A	.....
(12)*	$a^3F-y^3D^\circ$	3–2	3045.006	10r	160	A	.....
		2–1	3105.469	15r	340	A	.....
		3–3	3107.714	4	9.1	C	.....
		2–2	3129.314	7	44	A	.....
		2–3	3195.573	6	41	A	.....
(13)	$a^3F-z^1G^\circ$	3–4	3099.115	12r	270	A	.....
(15)	$a^3D-z^5D^\circ$	3–4	3912.979	5	1.4	B	.....
		1–2	3889.671	15	3.4	B	.....
		3–3	3778.063	5	4.3	A	.....
		1–1	3811.32	(2)	0.91	A	.....
		3–2	3674.06†	10	(18.0)	A	(67.0)
		2–1	3693.932	8	15.5	A	.....
		1–0	3772.530	6	6.1	A	.....
(16)	$a^3D-z^5G^\circ$	3–4	3587.931	12	46	B	37
		2–3	3609.314	15	87	B	81
		1–2	3661.951	8	14.5	A	.....
		3–3	3523.444	10	37	A	.....
		2–2	3553.483	7	20	A	.....
(17)	$a^3D-z^5F^\circ$	3–4	3461.652	125R	2400	B	3560
		2–3	3452.890	40R	1040	B	1350
		1–2	3513.933	15	145	B	97
		3–3	3374.221	15r	165	B	206
		2–2	3413.939	12r	180	A	.....
		1–1	3485.888	10	86	A	58
		3–2	3337.014	4	0.87	A	.....
		2–1	3387.466	3	0.88	A	.....
(18)	$a^3D-z^3P^\circ$	2–2	3524.541	200R	5500	B	5810
		2–1	3492.956	150R	3100	B	3970
		1–0	3510.338	80R	1400	C	1320
		2–2	3610.462	60R	510	B	600
		1–1	3597.705	50R	690	B	605
		1–2	3722.484	15	76	A	.....
(19)	$a^3D-z^3F^\circ$	3–4	3414.765	150R	4500	B	5270
		2–3	3515.054	150R	3600	B	5100
		1–2	3458.474	125R	3800	B	4360
		3–3	3433.558	70R	1300	B	1750
		2–2	3361.556	20R	330	B	341
		3–2	3286.946	8	33	A	.....
(20)	$a^3D-z^3D^\circ$	3–3	3392.992	100R	1800	B	2910
		2–2	3446.263	100R	2300	B	3130
		1–1	3423.711	50R	1370	B	1610
		3–2	3367.892	8	16.0	A	.....
		2–1	3328.714	5	5.0	B	.....
		2–3	3472.545	70R	1200	B	1710
		1–2	3548.185†	20R	(280)	A	(201)

TABLE 1—*Continued*

Mult. No.	Designation	J	λ	Estimated Arc Int.	Furnace gf	Wt.	Arc gf‡
(21)	$a^3D-z^3G^\circ$	3–4	3248.457	8	60	A	.....
		2–3	3234.649	10r	220	A	.....
		3–3	3165.508	3	3.9	B	.....
(22)	$a^3D-z^1F^\circ$	3–3	3243.058	25R	370	B	342
		2–3	3315.663	30R	540	B	262
(23)	$a^3D-z^1D^\circ$	3–2	3200.423	5	15.0	A	.....
		2–2	3271.118	10	51	A	.....
		1–2	3362.806	6	14.3	A	.....
(24)	$a^3D-z^1P^\circ$	2–1	3114.124	20R	250	B	.....
		1–1	3197.113	10r	129	A	.....
(25)*	$a^3D-y^3F^\circ$	3–4	3050.819	100R	4800	C	.....
		2–3	3101.554	100R	4700	C	.....
		1–2	3134.108	60R	4200	C	.....
		3–3	3037.935	60R	1900	C	.....
		2–2	3054.316	50R	1750	C	.....
(26)*	$a^3D-y^3D^\circ$	1–1	3057.638	50R	3300	C	.....
		2–3	3064.623	25R	640	A	.....
		1–2	3080.755	20R	420	B	.....
(30)*	$a^1D-z^5F^\circ$	2–3	3783.530	30R	610	B	614
		2–2	3736.813	15	200	A	.....
(31)*	$a^1D-z^3P^\circ$	2–1	3831.690	20	99	C	.....
(32)	$a^1D-z^3F^\circ$	2–3	3858.301	40r	1400	C	550?
		2–2	3674.15†	15	(250)	A	(141)
(33)	$a^1D-z^3D^\circ$	2–3	3807.144	35r	720	A	487
		2–2	3775.572	30r	570	B	347
		2–1	3634.941	12	33	B	.....
(34)	$a^1D-z^3G^\circ$	2–3	3523.074	4	6.6	A	.....
(35)	$a^1D-z^1F^\circ$	2–3	3619.392	150R	6000	C	7960
(36)	$a^1D-z^1D^\circ$	2–2	3566.372	100R	4000	C	4480
(37)	$a^1D-z^1P^\circ$	2–1	3380.574	80R	5200	B	4540
(38)	$a^1D-y^3F^\circ$	2–3	3365.766	15r	420	B	499
		2–2	3310.202	5	15.4	A	.....
39)	$a^1D-y^3D^\circ$	2–3	3322.310	15r	420	A	443
		2–2	3250.743	9	182	A	.....
		2–1	3225.020	10r	410	A	.....
(40)	$a^1D-y^1F^\circ$	2–3	3101.879	40R	5600	B	.....
(41)	$a^1D-y^1D^\circ$	2–2	3012.004	75R	8000	C	.....

self-reversal should be small. Strong lines from all the low terms (including a^1D_2) are affected; but, since the arc intensity at which the effect begins is directly proportional to the excitation potential of the lower term, it would appear that self-reversal also may be present. By the use of unaffected arc lines and furnace *gf*-values, an attempt was made to derive an excitation temperature for the arc by plotting the log $(I/\nu^3)/gf$ against the excitation potential of the upper state. The arc temperature derived by a least-squares solution for the slope of this plot was about 12,000° K. Unfortunately, the range available in excitation potential (less than 1.0 volt) was too small and the scatter of the points too large to give this value any useful significance. The writer had hoped that, if a reasonably good excitation temperature for the arc used by Ornstein and Bouma could be obtained in this manner, their measurements of arc intensities of high-level lines could be corrected for excitation temperature and might thus provide a significant extension to the *gf*-values measured in the furnace.

Van Driel's arc-intensity measurements were made on 50 lines, all of which were measured by the writer in the furnace absorption spectra. Van Driel corrected his data for self-absorption effects and also for an excitation temperature of 6400°K determined from *CN*-band intensities.[7] Since his results have not been published in a periodical and therefore have not had wide distribution, it seems worth while to include them in Table 1. Van Driel's arc intensities, corrected for frequency ($gf \sim I/\nu^3$) and Boltzmann distribution ($T = 6400°$ K), and adjusted to the furnace *gf*-value scale, are listed in the sixth column of Table 1. A determination of arc temperature from a comparison of van Driel's arc intensities (uncorrected for Boltzmann factor) and my furnace *gf*-values yielded a temperature of about 6500° K. While this value is in excellent agreement with that obtained by van Driel from the *CN* bands, it has little significance in view of the short range available in excitation potential and the relatively large individual differences between the arc and the furnace measurements. The mean individual difference between arc and furnace *gf*-values is about 24 per cent, which is rather extraordinarily large.[8] No significant systematic differences appear, except a tendency for the arc measurements of strong lines to be stronger and weak lines weaker than in the furnace. Because the accidental errors causing these discrepancies are felt to be largely in the furnace absorption-spectra data, which are inherently less precise than emission-spectra measurements and in this case perhaps due in part to the unusually large range in furnace temperatures (1100°) required for the measurements, the arc *gf*-values in Table 1 may preferably be used for the lines for which they exist.

Arc-intensity measurements have been compared by Ornstein and Bouma[5] and by van Driel[6] with theoretical multiplet and supermultiplet strengths. In both investigations agreement was poor even with the sum rule. A similar comparison by the writer, using furnace *gf*-values, also showed wide discrepancies. Only one multiplet, $a^3F - z^3G^\circ$, shows normal line-strengths; and divergences from the sum rule for lines within muliplets are large.

[7] Cf. J. A. Smit, *Physica*, **12**, 683, 1946.

[8] For the triplet system of *Ti* I, H. L. M. van Stekelenburg (Thesis, Utrecht, 1943) found an average difference between furnace and arc intensities of about 7 per cent.

ON THE RADIATIVE EQUILIBRIUM OF A STELLAR ATMOSPHERE. XXIV

S. CHANDRASEKHAR
Yerkes Observatory
Received April 30, 1948

ABSTRACT

In this paper the functional equations governing the X- and Y-functions (introduced in Paper XXII) are solved by an iteration process, starting with the "first approximation" $X^{(1)} = 1$ and $Y^{(1)} = e^{-\tau/\mu}$. The iteration of these functions leads to a "second approximation." The solutions in these approximations are then corrected by a semi-empirical method to satisfy, exactly, an integral property of the X- and Y-functions. It appears that, in this fashion, solutions for the X- and Y-functions, with an error probably not exceeding 1 per cent for $\tau < 0.5$, can be found. The construction of standard solutions in conservative cases is also considered. In an appendix (worked jointly with Mrs. Frances H. Breen) tables of the auxiliary functions, for use in conjunction with the exact solutions of Paper XXII, are provided.

1. *Introduction.*—In Paper XXII[1] we have shown how the various standard problems in the theory of radiative transfer in plane-parallel atmospheres of finite optical thicknesses can be reduced to the solution of one or more pairs of functional equations of the type

$$X(\mu) = 1 + \mu \int_0^1 \frac{\Psi(\mu')}{\mu + \mu'} [X(\mu) X(\mu') - Y(\mu) Y(\mu')] \, d\mu' \tag{1}$$

and

$$Y(\mu) = e^{-\tau/\mu} + \mu \int_0^1 \frac{\Psi(\mu')}{\mu - \mu'} [Y(\mu) X(\mu') - X(\mu) Y(\mu')] \, d\mu' , \tag{2}$$

where the characteristic function $\Psi(\mu)$ is an even polynomial in μ, satisfying the condition

$$\int_0^1 \Psi(\mu) \, d\mu \leqslant \tfrac{1}{2} , \tag{3}$$

and τ is the optical thickness of the atmosphere.[2]

For general values of τ the solution of equations (1) and (2) can be found only by an iteration process of the kind which was adopted, for example, in the evaluation of the H-functions.[3] However, in certain important applications of the theory, interest is mainly attached to small values of the optical thickness (of the order of 0.1 or 0.2). It will therefore be convenient if simple analytical representations of the solutions of equations (1) and (2) can be found which will be accurate enough for these applications. The importance of having such analytical representations has been emphasized by van de Hulst,[4] who has recently reconsidered the problem of diffuse reflection by an isotropically scattering atmosphere with a view to such applications.

Now for an isotropically scattering atmosphere the characteristic function is a constant ($= \frac{1}{2}\varpi_0$), and the solutions for the reflected and the transmitted intensities are expressed very simply in terms of the X- and Y-functions (cf. Paper XXII, Sec. II, §7,

[1] *Ap. J.*, **107**, 48, 188, 1948.

[2] In Papers XXI (*Ap. J.*, **106**, 152, 1947) and XXII the optical thickness of the atmosphere was denoted by τ_1. It is convenient to suppress the subscript 1 when, as in the present instance, there will be no occasion to refer to the radiation field in the interior.

[3] Cf. Papers XVI, XIX, and XXIII (*Ap. J.*, **105**, 435; **106**, 143, 1947; **107**, 216, 1948).

[4] *Ap. J.*, **107**, 220, 1948.

eqs. [178] and [179]). By analyzing the emergent radiations in terms of the light which has been scattered once, twice, etc., in the atmosphere and consistently arranging that, at each stage of the approximation, the solutions have the forms required by the exact theory as developed in Paper XXII, van de Hulst has shown that it is possible to write down relatively simple expressions which will adequately represent the solutions of equations (1) and (2) for the case

$$\Psi(\mu) = \text{Constant} = \tfrac{1}{2}\varpi_0 \qquad (4)^5$$

and valid for small values of τ. In the general case when no very simple meanings can be attached to the X- and Y-functions,[6] a more directly mathematical approach to the solution of equations (1) and (2) than was adopted by van de Hulst appears necessary. It is the object of this paper to develop such an approach and to present a method for solving equations (1) and (2) for suitably small values of τ.

2. *The first and the second approximation.*—Quite generally we may expect to solve equations (1) and (2) by an iteration process in which the nth iterates are obtained by evaluating the integrals on the right-hand sides of equations (1) and (2) in terms of the $(n-1)$th iterates. Thus

$$X^{(n+1)}(\mu) = 1 + \mu \int_0^1 \frac{\Psi(\mu')}{\mu+\mu'} [\, X^{(n)}(\mu)\, X^{(n)}(\mu') - Y^{(n)}(\mu)\, Y^{(n)}(\mu') \,]\, d\mu' \qquad (5)$$

and

$$Y^{(n+1)}(\mu) = e^{-\tau/\mu} + \mu \int_0^1 \frac{\Psi(\mu')}{\mu-\mu'} [\, Y^{(n)}(\mu)\, X^{(n)}(\mu') - X^{(n)}(\mu)\, Y^{(n)}(\mu') \,]\, d\mu' . \qquad (6)$$

The success of such an iteration scheme will largely depend on how well the first "trial" functions $X^{(1)}(\mu)$ and $Y^{(1)}(\mu)$ are chosen. The third or the fourth approximation in the method of solution of the earlier papers[7] of this series could, of course, be used; indeed, for the purposes of numerical iterations the approximate solutions (Paper XXII, eqs. [155]–[161]) in terms of characteristic roots and points of the Gaussian division are found to be quite satisfactory; for the purposes of analytical iterations, on the other hand, these solutions are not very satisfactory, as the resulting expressions are too inconvenient to handle. An alternative method which appears more suitable, particularly for small values of τ, is to start the iteration with the functions

$$X^{(1)}(\mu) = 1 \qquad \text{and} \qquad Y^{(1)}(\mu) = e^{-\tau/\mu} . \qquad (7)$$

The appropriateness of these functions in our present context arises from the fact that with these expressions for X and Y we essentially recover the formulae for the reflected and the transmitted light which have suffered a single scattering process in the atmosphere.

Iterating the functions (7) in accordance with equations (5) and (6), we have

$$X^{(2)}(\mu) = 1 + \mu \int_0^1 \frac{\Psi(\mu')}{\mu+\mu'} \left[1 - \exp\left\{ -\tau \left(\frac{1}{\mu} + \frac{1}{\mu'} \right) \right\} \right] d\mu' \qquad (8)$$

[5] Van de Hulst uses a in place of our ϖ_0.

[6] It should be noted in this connection that different source functions can give rise to the same laws for the angular distributions of the emergent radiations. Indeed, it is on this account that the functional equations governing the angular distributions of the emergent radiations are simpler to handle than are the equations governing the source functions themselves.

[7] Specifically, Paper XXI in this context.

and

$$Y^{(2)}(\mu) = e^{-\tau/\mu} + \mu \int_0^1 \frac{\Psi(\mu')}{\mu - \mu'} [\, e^{-\tau/\mu} - e^{-\tau/\mu'}] \, d\mu' . \tag{9}$$

Let

$$\Psi(\mu) = \sum_j a_j \mu^j . \tag{10}$$

(In actual fact, only even powers of μ can occur on the right-hand side, since the characteristic function is an even polynomial in μ.)

For $\Psi(\mu)$ of the form (10) we can clearly express $X^{(2)}(\mu)$ and $Y^{(2)}(\mu)$ in the forms

$$X^{(2)}(\mu) = 1 + \sum_j a_j F_{j+1}(\tau, -\mu) \tag{11}$$

and

$$Y^{(2)}(\mu) = e^{-\tau/\mu} \Big[1 + \sum_j a_j F_{j+1}(\tau, \mu) \Big] , \tag{12}$$

where

$$F_{j+1}(\tau, \mu) = \mu \int_0^1 \frac{\mu'^j}{\mu - \mu'} \left[1 - \exp \left\{ - \tau \left(\frac{1}{\mu'} - \frac{1}{\mu} \right) \right\} \right] d\mu' . \tag{13}$$

The functions $F_{j+1}(\tau, \mu)$ $(j = 0, 1, \ldots)$, defined as in equation (13), are the same as the functions

$$F_{j+1}(\tau, \mu) = \int_0^\tau e^{t/\mu} E_{j+1}(t) \, dt \tag{14}$$

introduced by van de Hulst (*op. cit.*). To see the identity of the definitions (13) and (14), write

$$s = \frac{1}{\mu} \quad \text{and} \quad s' = \frac{1}{\mu'} \tag{15}$$

in equation (13). We obtain

$$F_{j+1}(\tau, s) = \int_1^\infty \frac{ds'}{s'^{j+1}(s' - s)} [1 - e^{-\tau(s' - s)}] . \tag{16}$$

Since

$$\int_0^\tau e^{-t(s' - s)} dt = \frac{1}{s' - s} [1 - e^{-\tau(s' - s)}] , \tag{17}$$

we can re-write equation (16) in the form

$$F_{j+1}(\tau, s) = \int_1^\infty \frac{ds'}{s'^{j+1}} \int_0^\tau dt \, e^{-t(s' - s)} , \tag{18}$$

or, inverting the order of the integrations, we have

$$F_{j+1}(\tau, s) = \int_0^\tau dt \, e^{ts} \int_1^\infty \frac{ds'}{s'^{j+1}} \, e^{-ts'} ; \tag{19}$$

and this is in agreement with van de Hulst's definition.

For the problems considered in Paper XXII, the characteristic functions $\Psi(\mu)$ are, at most, of degree 2 in μ^2; consequently, the solutions of the various problems in the second approximation (and for small values of τ) can all be written down in terms of the functions F_n of the odd orders 1, 3, and 5. These functions, for various values of τ and μ, are tabulated in the appendix.

The further iteration of $X^{(2)}(\mu)$ and $Y^{(2)}(\mu)$ to obtain a third approximation does not seem practicable, since a large number of other transcendental functions are introduced. However, in § 4 we shall show how the solutions $X^{(2)}(\mu)$ and $Y^{(2)}(\mu)$ can be "corrected" to satisfy certain exact integrals of the problem by a procedure essentially equivalent to taking into account the third and higher orders of scattering in a semi-empirical fashion.

3. *The moments of* $X^{(2)}(\mu)$ *and* $Y^{(2)}(\mu)$.—For several purposes the moments (cf. Paper XXII, eqs. [10] and [11])

$$\alpha_n = \int_0^1 X(\mu)\,\mu^n d\mu\,, \qquad \beta_n = \int_0^1 Y(\mu)\,\mu^n d\mu\,,$$
$$x_n = \int_0^1 X(\mu)\Psi(\mu)\,\mu^n d\mu\,, \quad \text{and} \quad y_n = \int_0^1 Y(\mu)\Psi(\mu)\,\mu^n d\mu \tag{20}$$

of the functions $X(\mu)$ and $Y(\mu)$ are needed. In the second approximation of § 2, these moments can all be expressed in terms of the functions

$$G_{n,m}(\tau) = \int_0^1 F_n(\tau, -\mu)\,\mu^m \frac{d\mu}{\mu^2} = \int_1^\infty F_n(\tau, -s)\,\frac{ds}{s^m}$$

and

$$G'_{n,m}(\tau) = \int_0^1 e^{-\tau/\mu} F_n(\tau, \mu)\,\mu^m \frac{d\mu}{\mu^2} = \int_1^\infty e^{-\tau s} F_n(\tau, s)\,\frac{ds}{s^m}, \tag{21}$$

also introduced by van de Hulst. We clearly have

$$\alpha_n^{(2)} = \frac{1}{n+1} + \sum_j a_j G_{j+1,n+2}(\tau)\,,$$
$$\beta_n^{(2)} = E_{n+2}(\tau) + \sum_j a_j G'_{j+1,n+2}(\tau)\,, \tag{22}$$
$$x_n^{(2)} = \sum_j \frac{a_j}{j+n+1} + \sum_j \sum_k a_j a_k G_{j+1,k+n+2}(\tau)\,,$$

and

$$y_n^{(2)} = \sum_j a_j E_{j+n+2}(\tau) + \sum_j \sum_k a_j a_k G'_{j+1,k+n+2}(\tau)\,.$$

For the various problems considered in Paper XXII the functions $G_{n,m}$ and $G'_{n,m}$ (symmetrical in the indices n and m) are required for $m \geqslant n$ and $n = 1, 2, 3, 4$, and 5. These functions are also tabulated in the appendix.

4. *The correction of the approximate solutions.*—In Paper XXII (Sec. I, § 4) a number of integral properties of the functions X and Y were established. The most important of these is the relation (Paper XXII, eq. [32])

$$x_0 = 1 - \left[1 - 2\int_0^1 \Psi(\mu)\,d\mu + y_0^2\right]^{1/2}. \tag{23}$$

An alternative form of this relation is

$$[1 - (x_0 + y_0)]\,[1 - (x_0 - y_0)] = 1 - 2\int_0^1 \Psi(\mu)\,d\mu\,. \tag{24}$$

The approximate solutions of equations (1) and (2) obtained in the iteration scheme of § 2 will not, naturally, satisfy equation (24) exactly. We shall now show how, on this

account, we can make use of equation (24) to "correct" the approximate solutions. For this purpose, we shall write

$$\begin{aligned} X(\mu) &= X^{(n)}(\mu) + \Delta(\tau)\,\mu(1 - e^{-\tau/\mu}) \\ \text{and} \qquad Y(\mu) &= Y^{(n)}(\mu) + \Delta(\tau)\,\mu(1 - e^{-\tau/\mu}), \end{aligned} \tag{25}$$

and determine $\Delta(\tau)$ by requiring that x_0 and y_0, evaluated with the aid of the functions (25), satisfy the relation (24) exactly. This procedure of adding a correction term of the form $\Delta(\tau)\mu(1 - e^{-\tau/\mu})$ to both X and Y can, in a sense, be regarded as equivalent to assuming that the sources giving rise to the radiation which has been scattered more than n times in the atmosphere are uniformly distributed (cf. van de Hulst, *op. cit.*).[8] In conservative cases the procedure can also be described as a device by which we arrange for the flux integral to be satisfied exactly.

For $X(\mu)$ and $Y(\mu)$ defined as in equations (25), we have

$$\begin{aligned} x_0 &= x_0^{(n)} + \Delta(\tau)\int_0^1 \Psi(\mu)\,\mu(1 - e^{-\tau/\mu})\,d\mu \\ \text{and} \qquad y_0 &= y_0^{(n)} + \Delta(\tau)\int_0^1 \Psi(\mu)\,\mu(1 - e^{-\tau/\mu})\,d\mu, \end{aligned} \tag{26}$$

where $x_0^{(n)}$ and $y_0^{(n)}$ are the respective quantities evaluated with the functions $X^{(n)}$ and $Y^{(n)}$. Inserting equations (26) in equation (24), we obtain, after some minor rearranging of the terms,

$$\Delta(\tau) = \frac{1}{2\int_0^1 \Psi(\mu)\,\mu(1 - e^{-\tau/\mu})\,d\mu}\left\{1 - [x_0^{(n)} + y_0^{(n)}] - \frac{1 - 2\int_0^1 \Psi(\mu)\,d\mu}{1 - [x_0^{(n)} - y_0^{(n)}]}\right\}, \tag{27}$$

where it may be noted that, for $\Psi(\mu)$ given by equation (10),

$$\int_0^1 \Psi(\mu)\,\mu(1 - e^{-\tau/\mu})\,d\mu = \sum_j a_j \left\{\frac{1}{j+2} - E_{j+3}(\tau)\right\}. \tag{28}$$

In conservative cases equation (27) simplifies to

$$\Delta(\tau) = \frac{1 - [x_0^{(n)} + y_0^{(n)}]}{2\int_0^1 \Psi(\mu)\,\mu(1 - e^{-\tau/\mu})\,d\mu}. \tag{29}$$

As an illustration of the foregoing procedure of correcting the solutions $X^{(n)}$ and $Y^{(n)}$ ($n = 1$ and 2) consider the isotropic case (4) and the correction to the first approximation (7). In this case

$$x_0^{(1)} = \tfrac{1}{2}\varpi_0 \qquad \text{and} \qquad y_0^{(1)} = \tfrac{1}{2}\varpi_0 E_2(\tau), \tag{30}$$

[8] This remark should not be taken too literally, since, even in the simplest case of isotropic scattering, the solutions obtained by successive iterations of the equations for X and Y are not in strict 1:1 correspondence with the solutions obtained by including successively the higher orders of scattering. And, even apart from this, the method of correcting by the moment relation (24) is not exactly the same as distributing the sources for the higher orders of scattering uniformly through the atmosphere.

and

$$\Delta(\tau) = \frac{1}{\varpi_0[\frac{1}{2} - E_3(\tau)]}\left\{1 - \tfrac{1}{2}\varpi_0[1 + E_2(\tau)] - \frac{1-\varpi_0}{1 - \tfrac{1}{2}\varpi_0[1 - E_2(\tau)]}\right\}. \tag{31}$$

For the case $\varpi_0 = 1$ we have, in particular,

$$\Delta(\tau) = \frac{1 - E_2(\tau)}{1 - 2E_3(\tau)}. \tag{32}$$

Actual numerical comparisons show that the first approximation, corrected according to equations (25) and (31), differs from the second approximation,

$$\begin{aligned} X^{(2)}(\mu) &= 1 + \tfrac{1}{2}\varpi_0 F_1(\tau, -\mu) \\ \text{and} \qquad Y^{(2)}(\mu) &= e^{-\tau/\mu}[1 + \tfrac{1}{2}\varpi_0 F_1(\tau, \mu)], \end{aligned} \tag{33}$$

by less than 5 per cent for $\tau \leqslant 0.2$.[9] It will therefore appear that the second approximation, corrected in the manner we have indicated, will give entirely satisfactory representations for $\tau < 0.5$.

For $X^{(2)}(\mu)$ and $Y^{(2)}(\mu)$, given by equations (11) and (12), the moments $x_0^{(2)}$ and $y_0^{(2)}$ are (cf. eqs. [22])

$$\begin{aligned} x_0^{(2)} &= \sum_j \frac{a_j}{j+1} + \sum_j \sum_k a_j a_k G_{j+1,k+2} \\ \text{and} \qquad y_0^{(2)} &= \sum_j a_j E_{j+2} + \sum_j \sum_k a_j a_k G'_{j+1,k+2}. \end{aligned} \tag{34}$$

The resulting expression for $\Delta(\tau)$ is

$$\Delta(\tau) = \left[1 - \left\{\sum_j a_j\left(\frac{1}{j+1} + E_{j+2}\right) + \sum_j \sum_k a_j a_k (G_{j+1,k+2} + G'_{j+1,k+2})\right\} - \frac{1 - 2\int_0^1 \Psi(\mu)\, d\mu}{1 - \left\{\sum_j a_j\left(\frac{1}{j+1} - E_{j+2}\right) + \sum_j \sum_k a_j a_k (G_{j+1,k+2} - G'_{j+1,k+2})\right\}}\right] \div 2\left[\sum_j a_j\left(\frac{1}{j+2} - E_{j+3}\right)\right]. \tag{35}$$

In the conservative case the foregoing equation simplifies to

$$\Delta(\tau) = \frac{1 - \left\{\sum_j a_j\left(\frac{1}{j+1} + E_{j+2}\right) + \sum_j \sum_k a_j a_k (G_{j+1,k+2} + G'_{j+1,k+2})\right\}}{2\sum_j a_j\left(\frac{1}{j+2} - E_{j+3}\right)}. \tag{36}$$

[9] Thus, for the case $\varpi_0 = 1$ and $\mu = 1$, the corrected first approximation gives for X the values 1.16 and 1.26 for $\tau = 0.1$ and $\tau = 0.2$, respectively; on the uncorrected second approximation the corresponding values are 1.133 and 1.197. And van de Hulst estimates that the true values in these cases are probably 1.159 and 1.263.

As an illustration of the foregoing expressions, consider again the isotropic case. In this case the only nonvanishing a is

$$a_0 = \tfrac{1}{2}\varpi_0 ; \tag{37}$$

and equation (35) becomes

$$\Delta(\tau) = \Big[1 - \tfrac{1}{2}\varpi_0 \{ 1 + E_2 + \tfrac{1}{2}\varpi_0 (G_{12} + G'_{12}) \} - \frac{1-\varpi_0}{1 - \tfrac{1}{2}\varpi_0 \{ 1 - E_2 + \tfrac{1}{2}\varpi_0 (G_{12} - G'_{12}) \}} \Big] \frac{1}{\varpi_0 (\tfrac{1}{2} - E_3)} . \tag{38}$$

And for the case $\varpi_0 = 1$, we have

$$\Delta(\tau) = \frac{1}{4} \frac{1}{\tfrac{1}{2} - E_3} (2 - 2E_2 - G_{12} - G'_{12}) . \tag{39}$$

The foregoing expression for $\Delta(\tau)$ reduces to the correction factor $g(\tau)/\tau$ given by van de Hulst (*op. cit.*, eqs. [28] and [30]) if we replace $\frac{1}{2} - E_3(\tau)$ by τ as sufficiently accurate.

Finally, we may note that on the corrected second approximation the various moments are given by

$$\alpha_n - \alpha_n^{(2)} = \beta_n - \beta_n^{(2)} = \Delta(\tau) \left(\frac{1}{n+2} - E_{n+3} \right)$$

and

$$x_n - x_n^{(2)} = y_n - y_n^{(2)} = \Delta(\tau) \sum_j a_j \left(\frac{1}{j+n+2} - E_{j+n+3} \right), \tag{40}$$

where the quantities $\alpha_n^{(2)}$, etc., are given by equations (22).

5. *The standard solutions.*—In Paper XXII (Sec. I, theorem 5) we have shown that in conservative cases the solutions of equations (1) and (2) are not unique and that they form, instead, a one-parametric family. A member of this family which plays a particularly important role in the theory is the *standard solution*, defined by the property (Paper XXII, eqs. [64] and [65])

$$x_0^{(s)} = \int_0^1 X^{(s)}(\mu) \Psi(\mu)\, d\mu = 1 \qquad \text{and} \qquad y_0^{(s)} = \int_0^1 Y^{(s)}(\mu) \Psi(\mu)\, d\mu = 0 . \tag{41}$$[10]

Now if $X(\mu)$ and $Y(\mu)$ are particular solutions of equations (1) and (2) (in the conservative case), then the standard solutions can be derived from them by writing

$$\begin{aligned} X^{(s)}(\mu) &= X(\mu) + q\mu [X(\mu) + Y(\mu)] \\ \text{and} \qquad Y^{(s)}(\mu) &= Y(\mu) - q\mu [X(\mu) + Y(\mu)] \end{aligned} \tag{42}$$

and determining the constant q by conditions (10).[11] In this manner we find that

$$q = \frac{y_0}{x_1 + y_1} . \tag{43}$$

Since the approximate solutions constructed as in § 4 satisfy the moment condition $x_0 + y_0 = 1$ exactly, standard solutions can be constructed from them according to

[10] We have used a superscript s to distinguish the standard solutions from the rest.

[11] Since $x_0 + y_0 = 1$ in conservative cases, the two conditions $x_0 = 1$ and $y_0 = 0$ are equivalent.

equations (42) and with q given by equation (43). In the corrected second approximation we therefore have

$$q = \Big[\sum_j a_j E_{j+2} + \sum_j \sum_k a_j a_k G'_{j+1,k+2} + \Delta(\tau) \sum_j a_j \Big(\frac{1}{j+2} - E_{j+3}\Big)\Big] \div \Big[\sum_j a_j \Big(\frac{1}{j+2} + E_{j+3}\Big) + \sum_j \sum_k a_j a_k (G_{j+1,k+3} + G'_{j+1,k+3}) + 2\Delta(\tau) \sum_j a_j \Big(\frac{1}{j+3} - E_{j+4}\Big)\Big]. \quad (44)$$

Substituting for $\Delta(\tau)$ according to equation (36) in the numerator of the foregoing equation, we obtain the more symmetrical expression

$$a = \frac{1}{2}\Big[1 - \sum_j a_j \Big(\frac{1}{j+1} - E_{j+2}\Big) - \sum_j \sum_k a_j a_k (G_{j+1,k+2} - G'_{j+1,k+2})\Big] \div \Big[\sum_j a_j \Big(\frac{1}{j+2} + E_{j+3}\Big) + \sum_j \sum_k a_j a_k (G_{j+1,k+3} + G'_{j+1,k+3}) + 2\Delta(\tau) \sum_j a_j \Big(\frac{1}{j+3} - E_{j+4}\Big)\Big]. \quad (45)$$

The moments $\alpha_j^{(s)}$ and $\beta_j^{(s)}$ of the standard solutions are related to the moments α_j and β_j of the solutions from which they are derived by

$$\alpha_j^{(s)} = \alpha_j + q(\alpha_{j+1} + \beta_{j+1})$$

and

$$\beta_j^{(s)} = \beta_j - q(\alpha_{j+1} + \beta_{j+1}). \quad (46)$$

6. *The approximate solution for the conservative isotropic case.*—In Paper XXII we have shown that for the problem of diffuse reflection by an isotropically scattering atmosphere the solutions for X and Y appropriate to the problem are (Paper XXII, eqs. [180], [181], and [202])

$$X^*(\mu) = X^{(s)}(\mu) + Q\mu [X^{(s)}(\mu) + Y^{(s)}(\mu)]$$

and

$$Y^*(\mu) = Y^{(s)}(\mu) - Q\mu [X^{(s)}(\mu) + Y^{(s)}(\mu)], \quad (47)$$

where

$$Q = -\frac{\alpha_1^{(s)} - \beta_1^{(s)}}{[\alpha_1^{(s)} + \beta_1^{(s)}]\tau + 2[\alpha_2^{(s)} + \beta_2^{(s)}]}. \quad (48)$$

When the standard solutions are themselves derived from another set, $X(\mu)$ and $Y(\mu)$, the required solutions can be expressed in terms of these latter solutions in the forms

$$X^*(\mu) = X(\mu) + (Q+q)\mu [X(\mu) + Y(\mu)]$$

and

$$Y^*(\mu) = Y(\mu) - (Q+q)\mu [X(\mu) + Y(\mu)], \quad (49)$$

where, according to equations (46) and (48),

$$Q = -\frac{\alpha_1 - \beta_1 + 2q(\alpha_2 + \beta_2)}{(\alpha_1 + \beta_1)\tau + 2(\alpha_2 + \beta_2)} \quad (50)$$

the moments now referring to $X(\mu)$ and $Y(\mu)$.

Since (in this case)

$$q = \frac{y_0}{x_1 + y_1} = \frac{\beta_0}{\alpha_1 + \beta_1}, \tag{51}$$

we obtain from equations (50) and (51)

$$Q + q = \frac{\beta_0 \tau - (\alpha_1 - \beta_1)}{(\alpha_1 + \beta_1)\,\tau + 2\,(\alpha_2 + \beta_2)}. \tag{52}$$

The solutions $X^*(\mu)$ and $Y^*(\mu)$ appropriate to the problem of diffuse reflection are, therefore,

$$X^*(\mu) = X(\mu) + \frac{\beta_0 \tau - (\alpha_1 - \beta_1)}{(\alpha_1 + \beta_1)\,\tau + 2\,(\alpha_2 + \beta_2)}\,\mu\,[X(\mu) + Y(\mu)]$$

and (53)

$$Y^*(\mu) = Y(\mu) - \frac{\beta_0 \tau - (\alpha_1 - \beta_1)}{(\alpha_1 + \beta_1)\,\tau + 2\,(\alpha_2 + \beta_2)}\,\mu\,[X(\mu) + Y(\mu)].$$

If we now use in equations (53) the solutions in the corrected second approximation, we shall obtain solutions which will *exactly* satisfy both the integrals of the problem, namely, the flux and the K-integrals (cf. Paper XXII, eqs. [188] and [189]).[12]

I am indebted to Dr. van de Hulst for discussions on various aspects of scattering by planetary atmospheres.

APPENDIX

S. Chandrasekhar and Frances H. Breen

The practical use of the developments given in this paper will largely depend on the availability of tables of the various auxiliary functions in terms of which the solutions are expressed. In this appendix we shall therefore provide the necessary tables which may prove adequate for use in conjunction with the exact solutions given in Paper XXII. For this latter purpose, the functions $F_n(\tau, -\mu)$ and $e^{-\tau/\mu}F_n(\tau, \mu)$ of orders 1, 3, and 5 and the functions $G_{n,m}(\tau)$ and $G'_{n,m}(\tau)$ for $m \geqslant n$ and $n = 1, 2, 3, 4$, and 5 are needed. These functions are given in Tables 1 and 2 for values of the arguments which are probably sufficiently close for practical applications. (The tables can, in any case, be supplemented by the series expansions given in van de Hulst's paper.)

As the solutions given in this paper are intended only for small values of $\tau(< 0.5)$, it did not seem necessary to carry the tabulations beyond $\tau = 1.0$.

The formulae which were used in the computation of the various functions are given in van de Hulst's paper. But for convenience we note here the principal formulae.

The functions $F_1(\tau, -\mu)$ and $e^{-\tau/\mu}F_1(\tau, \mu)$ are given by

$$F_1(\tau, -\mu) = \mu\left[\log\left(\frac{1}{\mu} + 1\right) - e^{-\tau/\mu}E_1(\tau) + E_1\left(\frac{\tau}{\mu} + \tau\right)\right] \qquad (0 \leqslant \mu \leqslant 1),$$

$$e^{-\tau/\mu}F_1(\tau, \mu) = \mu\left[E_1(\tau) + e^{-\tau/\mu}Ei\left(\frac{\tau}{\mu} - \tau\right) - e^{-\tau/\mu}\log\left(\frac{1}{\mu} - 1\right)\right] \qquad (0 \leqslant \mu < 1),$$

and

$$e^{-\tau}F(\tau, 1) = e^{-\tau}(\gamma + \log\tau) + E_1(\tau),$$

[12] In this connection it is of interest to note that, by writing the reflected and the transmitted intensities in the forms given in Paper XXII, eqs. (178) and (179) (with $\varpi_0 = 1$), we can readily show that the flux and the K-integrals are equivalent to the conditions

$$\alpha_0 + \beta_0 = 2 \qquad \text{and} \qquad \tau = \frac{\alpha_1 - \beta_1}{\beta_0}.$$

And it may be verified that, with the solutions for X and Y in the forms given by eqs. (53), the latter condition is satisfied in virtue of the former.

TABLE 1

τ	μ	$F_1(-\mu,\tau)$	$F_3(-\mu,\tau)$	$F_5(-\mu,\tau)$	$e^{-\tau/\mu}F_1(\mu,\tau)$	$e^{-\tau/\mu}F_3(\mu,\tau)$	$e^{-\tau/\mu}F_5(\mu,\tau)$
	0	0	0	0	0	0	0
	0.010	0.023024	0.001958	0.000981	0.022045	0.001957	0.000980
	0.025	0.026166	0.002255	0.001129	0.025714	0.002254	0.001129
	0.050	0.027353	0.002367	0.001186	0.027116	0.002367	0.001186
	0.075	0.027766	0.002407	0.001205	0.027605	0.002406	0.001205
	0.1	0.027975	0.002427	0.001215	0.027854	0.002426	0.001215
	0.2	0.028294	0.002457	0.001230	0.028232	0.002457	0.001230
	0.3	0.028401	0.002467	0.001236	0.028360	0.002467	0.001236
0.005	0.4	0.028455	0.002472	0.001238	0.028424	0.002472	0.001238
	0.5	0.028488	0.002475	0.001240	0.028463	0.002475	0.001240
	0.6	0.028509	0.002477	0.001241	0.028489	0.002477	0.001241
	0.7	0.028525	0.002479	0.001241	0.028508	0.002479	0.001242
	0.8	0.028537	0.002480	0.001242	0.028521	0.002480	0.001242
	0.9	0.028546	0.002481	0.001242	0.028532	0.002481	0.001242
	1.0	0.028553	0.002481	0.001243	0.028540	0.002481	0.001243
	0	0	0	0	0	0	0
	0.010	0.033454	0.003135	0.001572	0.030347	0.003125	0.001568
	0.025	0.042319	0.004083	0.002048	0.040680	0.004078	0.002046
	0.050	0.046072	0.004489	0.002251	0.045170	0.004486	0.002250
	0.075	0.047432	0.004636	0.002325	0.046810	0.004634	0.002325
	0.1	0.048133	0.004712	0.002364	0.047659	0.004711	0.002363
	0.2	0.049214	0.004830	0.002422	0.048971	0.004829	0.002422
0.01	0.3	0.049582	0.004870	0.002443	0.049418	0.004869	0.002442
	0.4	0.049767	0.004890	0.002453	0.049644	0.004889	0.002453
	0.5	0.049879	0.004902	0.002459	0.049780	0.004902	0.002459
	0.6	0.049954	0.004910	0.002463	0.049871	0.004910	0.002463
	0.7	0.050007	0.004916	0.002466	0.049936	0.004915	0.002466
	0.8	0.050047	0.004920	0.002468	0.049985	0.004920	0.002468
	0.9	0.050078	0.004924	0.002470	0.050023	0.004923	0.002470
	1.0	0.050103	0.004926	0.002471	0.050054	0.004926	0.002471
	0	0	0	0	0	0	0
	0.010	0.042087	0.004266	0.002142	0.033934	0.004214	0.002124
	0.025	0.062645	0.006768	0.003402	0.057223	0.006733	0.003390
	0.050	0.073290	0.008093	0.004070	0.070022	0.008072	0.004063
	0.075	0.077453	0.008616	0.004333	0.075168	0.008601	0.004328
	0.1	0.079667	0.008894	0.004474	0.077868	0.008883	0.004470
	0.2	0.083167	0.009336	0.004696	0.082222	0.009329	0.004694
0.02	0.3	0.084384	0.009489	0.004774	0.083743	0.009485	0.004772
	0.4	0.085002	0.009567	0.004813	0.084517	0.009564	0.004812
	0.5	0.085376	0.009615	0.004837	0.084986	0.009612	0.004836
	0.6	0.085626	0.009646	0.004853	0.085301	0.009644	0.004852
	0.7	0.085806	0.009669	0.004864	0.085526	0.009667	0.004864
	0.8	0.085941	0.009686	0.004873	0.085696	0.009685	0.004873
	0.9	0.086046	0.009699	0.004880	0.085828	0.009698	0.004879
	1.0	0.086131	0.009710	0.004885	0.085934	0.009709	0.004885
	0	0	0	0	0	0	0
	0.010	0.044804	0.004674	0.002349	0.032150	0.004557	0.002308
	0.025	0.074335	0.008533	0.004298	0.064157	0.008438	0.004265
	0.050	0.092426	0.010989	0.005540	0.085759	0.010926	0.005518
	0.075	0.100023	0.012033	0.006068	0.095138	0.011987	0.006052
	0.1	0.104183	0.012607	0.006358	0.100338	0.012571	0.006346
	0.2	0.110924	0.013541	0.006831	0.108856	0.013522	0.006824
0.03	0.3	0.113315	0.013873	0.006999	0.111901	0.013860	0.006994
	0.4	0.114538	0.014044	0.007085	0.113465	0.014033	0.007082
	0.5	0.115282	0.014147	0.007137	0.114417	0.014139	0.007135
	0.6	0.115782	0.014217	0.007173	0.115057	0.014210	0.007170
	0.7	0.116141	0.014267	0.007198	0.115517	0.014261	0.007196
	0.8	0.116411	0.014304	0.007217	0.115864	0.014299	0.007215
	0.9	0.116622	0.014334	0.007232	0.116135	0.014329	0.007230
	1.0	0.116791	0.014357	0.007244	0.116352	0.014353	0.007242

TABLE 1-Continued

τ	μ	$F_1(-\mu,\tau)$	$F_3(-\mu,\tau)$	$F_5(-\mu,\tau)$	$e^{-\tau/\mu}F_1(\mu,\tau)$	$e^{-\tau/\mu}F_3(\mu,\tau)$	$e^{-\tau/\mu}F_5(\mu,\tau)$
	0	0	0	0	0	0	0
	0.010	0.045696	0.004821	0.002424	0.029468	0.004628	0.002356
	0.025	0.081341	0.009695	0.004891	0.066117	0.009508	0.004825
	0.050	0.106443	0.013316	0.006727	0.095670	0.013183	0.006680
	0.075	0.117698	0.014968	0.007566	0.109572	0.014868	0.007530
	0.1	0.124032	0.015860	0.008040	0.117540	0.015824	0.008012
	0.2	0.134552	0.017467	0.008834	0.130977	0.017423	0.008819
0.04	0.3	0.138358	0.018035	0.009123	0.135895	0.018005	0.009112
	0.4	0.140320	0.018328	0.009272	0.138443	0.018305	0.009263
	0.5	0.141518	0.018507	0.009363	0.140001	0.018489	0.009356
	0.6	0.142325	0.018628	0.009424	0.141052	0.018612	0.009418
	0.7	0.142905	0.018715	0.009468	0.141809	0.018701	0.009463
	0.8	0.143342	0.018781	0.009501	0.142380	0.018769	0.009497
	0.9	0.143684	0.018832	0.009527	0.142826	0.018821	0.009523
	1.0	0.143958	0.018873	0.009548	0.143185	0.018863	0.009545
	0	0	0	0	0	0	0
	0.010	0.045996	0.004875	0.002452	0.026979	0.004600	0.002354
	0.025	0.085630	0.010459	0.005283	0.065447	0.010155	0.005174
	0.050	0.116925	0.015186	0.007686	0.101593	0.014953	0.007603
	0.075	0.131828	0.017490	0.008859	0.119937	0.017309	0.008794
	0.1	0.140440	0.018833	0.009543	0.130799	0.018686	0.009491
	0.2	0.155087	0.021134	0.010715	0.149653	0.021051	0.010686
0.05	0.3	0.160488	0.021987	0.011150	0.156714	0.021929	0.011129
	0.4	0.163294	0.022431	0.011376	0.160406	0.022387	0.011360
	0.5	0.165014	0.022704	0.011515	0.162674	0.022668	0.011502
	0.6	0.166175	0.022888	0.011609	0.164209	0.022858	0.011598
	0.7	0.167011	0.023020	0.011676	0.165316	0.022994	0.011667
	0.8	0.167643	0.023121	0.011727	0.166153	0.023098	0.011719
	0.9	0.168137	0.023199	0.011767	0.166808	0.023179	0.011760
	1.0	0.168533	0.023262	0.011799	0.167334	0.023244	0.011793
	0	0	0	0	0	0	0
	0.010	0.046098	0.004894	0.002462	0.024873	0.004538	0.002333
	0.025	0.088290	0.010963	0.005542	0.063430	0.010521	0.005383
	0.050	0.124867	0.016690	0.008461	0.104712	0.016327	0.008331
	0.075	0.143271	0.019657	0.009976	0.127218	0.019368	0.009872
	0.1	0.154179	0.021436	0.010885	0.140976	0.021198	0.010799
	0.2	0.173163	0.024559	0.012481	0.165551	0.024421	0.012431
0.06	0.3	0.180296	0.025740	0.013085	0.174968	0.025644	0.013050
	0.4	0.184030	0.026360	0.013402	0.179935	0.026287	0.013375
	0.5	0.186327	0.026742	0.013597	0.183002	0.026682	0.013575
	0.6	0.187882	0.027001	0.013729	0.185084	0.026951	0.013711
	0.7	0.189004	0.027188	0.013825	0.186589	0.027144	0.013809
	0.8	0.189853	0.027329	0.013897	0.187728	0.027291	0.013883
	0.9	0.190517	0.027440	0.013954	0.188620	0.027406	0.013941
	1.0	0.191050	0.027529	0.013999	0.189338	0.027498	0.013988
	0	0	0	0	0	0	0
	0.010	0.046133	0.004901	0.002465	0.023116	0.004464	0.002307
	0.025	0.089955	0.011294	0.005712	0.060785	0.010699	0.005498
	0.050	0.130936	0.017899	0.009087	0.105840	0.017379	0.008899
	0.075	0.152621	0.021520	0.010941	0.132117	0.021095	0.010787
	0.1	0.165785	0.023749	0.012083	0.148685	0.023393	0.011953
	0.2	0.189217	0.027759	0.014138	0.179136	0.027549	0.014062
0.07	0.3	0.198228	0.029314	0.014935	0.191111	0.029178	0.014886
	0.4	0.202913	0.030124	0.015351	0.197425	0.030010	0.015310
	0.5	0.205833	0.030630	0.015611	0.201366	0.030538	0.015577
	0.6	0.207814	0.030974	0.015787	0.204049	0.030896	0.015759
	0.7	0.209247	0.031223	0.015915	0.205994	0.031156	0.015890
	0.8	0.210332	0.031412	0.016012	0.207467	0.031352	0.015990
	0.9	0.211181	0.031559	0.016087	0.208623	0.031506	0.016068
	1.0	0.211865	0.031678	0.016148	0.209553	0.031630	0.016131

TABLE 1-Continued

τ	μ	$F_1(-\mu,\tau)$	$F_3(-\mu,\tau)$	$F_5(-\mu,\tau)$	$e^{-\tau/\mu}F_1(\mu,\tau)$	$e^{-\tau/\mu}F_3(\mu,\tau)$	$e^{-\tau/\mu}F_5(\mu,\tau)$
	0	0	0	0	0	0	0
	0.010	0.046145	0.004903	0.002466	0.021635	0.004388	0.002278
	0.025	0.091003	0.011512	0.005827	0.057916	0.010755	0.005550
	0.050	0.135606	0.018871	0.009593	0.105555	0.018170	0.009337
	0.075	0.160311	0.023122	0.011775	0.135154	0.022533	0.011559
	0.1	0.175655	0.025804	0.013152	0.154390	0.025306	0.012970
	0.2	0.203569	0.030749	0.015694	0.190755	0.030448	0.015584
0.08	0.3	0.214445	0.032694	0.016694	0.205336	0.032480	0.016616
	0.4	0.220221	0.033731	0.017228	0.213164	0.033565	0.017167
	0.5	0.223801	0.034374	0.017559	0.218044	0.034239	0.017510
	0.6	0.226237	0.034813	0.017785	0.221376	0.034699	0.017743
	0.7	0.228002	0.035131	0.017948	0.223796	0.035032	0.017912
	0.8	0.229339	0.035372	0.018073	0.225633	0.035285	0.018041
	0.9	0.230388	0.035561	0.018170	0.227075	0.035483	0.018141
	1.0	0.231232	0.035713	0.018248	0.228237	0.035643	0.018222
	0	0	0	0	0	0	0
	0.010	0.046149	0.004904	0.002467	0.020367	0.004312	0.002248
	0.025	0.091667	0.011656	0.005902	0.055043	0.010729	0.005561
	0.050	0.139218	0.019653	0.010002	0.104275	0.018749	0.009668
	0.075	0.166668	0.024499	0.012494	0.136731	0.023720	0.012207
	0.1	0.184089	0.027632	0.014108	0.158453	0.026964	0.013861
	0.2	0.216464	0.033543	0.017154	0.200679	0.033131	0.017002
0.09	0.3	0.229300	0.035913	0.018377	0.217993	0.035618	0.018268
	0.4	0.236165	0.037186	0.019034	0.227371	0.036956	0.018949
	0.5	0.240438	0.037980	0.019444	0.233245	0.037792	0.019374
	0.6	0.243351	0.038522	0.019724	0.237269	0.038363	0.019665
	0.7	0.245466	0.038916	0.019927	0.240197	0.038778	0.019876
	0.8	0.247070	0.039215	0.020081	0.242423	0.039094	0.020036
	0.9	0.248329	0.039450	0.020202	0.244173	0.039341	0.020162
	1.0	0.249343	0.039639	0.020300	0.245584	0.039541	0.020264
	0	0	0	0	0	0	0
	0.010	0.046150	0.004904	0.002467	0.019263	0.004237	0.002219
	0.025	0.092088	0.011750	0.005952	0.052282	0.010651	0.005544
	0.050	0.142022	0.020283	0.010333	0.102306	0.019155	0.009914
	0.075	0.171944	0.025684	0.013116	0.137160	0.024690	0.012747
	0.10	0.191327	0.029257	0.014961	0.161161	0.028393	0.014640
	0.15	0.214651	0.033617	0.017213	0.191256	0.032946	0.016964
0.10	0.2	0.228096	0.036155	0.018526	0.209127	0.035611	0.018323
	0.3	0.242926	0.038973	0.019983	0.229234	0.038580	0.019837
	0.4	0.250914	0.040498	0.020773	0.240222	0.040191	0.020659
	0.5	0.255903	0.041453	0.021267	0.247139	0.041201	0.021173
	0.6	0.259314	0.042107	0.021605	0.251890	0.041894	0.021526
	0.7	0.261793	0.042582	0.021852	0.255355	0.042398	0.021783
	0.8	0.263676	0.042944	0.022039	0.257994	0.042781	0.021978
	0.9	0.265156	0.043228	0.022186	0.260069	0.043082	0.022132
	1.0	0.266348	0.043458	0.022305	0.261745	0.043326	0.022256
	0	0	0	0	0	0	0
	0.010	0.046151	0.004905	0.002467	0.018289	0.004164	0.002190
	0.025	0.092357	0.011813	0.005985	0.049685	0.010539	0.005509
	0.050	0.144206	0.020789	0.010600	0.099875	0.019422	0.010088
	0.075	0.176337	0.026702	0.013653	0.136687	0.025471	0.013192
	0.10	0.197558	0.030702	0.015722	0.162750	0.029618	0.015317
	0.15	0.223490	0.035667	0.018294	0.196129	0.034813	0.017975
0.11	0.2	0.238624	0.038597	0.019813	0.216280	0.037899	0.019552
	0.3	0.255467	0.041882	0.021517	0.239216	0.041374	0.021327
	0.4	0.264600	0.043672	0.022446	0.251862	0.043275	0.022297
	0.5	0.270326	0.044798	0.023031	0.259859	0.044471	0.022908
	0.6	0.274252	0.045572	0.023432	0.265371	0.045295	0.023329
	0.7	0.277108	0.046135	0.023725	0.269398	0.045894	0.023634
	0.8	0.279281	0.046564	0.023947	0.272470	0.046351	0.023868
	0.9	0.280990	0.046901	0.024122	0.274889	0.046711	0.024051
	1.0	0.282368	0.047173	0.024264	0.276844	0.047001	0.024199

TABLE 1-Continued

τ	μ	$F_1(-\mu,\tau)$	$F_3(-\mu,\tau)$	$F_5(-\mu,\tau)$	$e^{-\tau/\mu}F_1(\mu,\tau)$	$e^{-\tau/\mu}F_3(\mu,\tau)$	$e^{-\tau/\mu}F_5(\mu,\tau)$
	0	0	0	0	0	0	0
	0.010	0.046151	0.004905	0.002467	0.017420	0.004092	0.002162
	0.025	0.092529	0.011854	0.006007	0.047150	0.010406	0.005462
	0.050	0.145912	0.021196	0.010815	0.097146	0.019577	0.010205
	0.075	0.180005	0.027579	0.014117	0.135511	0.026089	0.013556
	0.10	0.202938	0.031987	0.016403	0.163411	0.030660	0.015903
	0.15	0.231381	0.037552	0.019292	0.199899	0.036492	0.018893
0.12	0.2	0.248180	0.040880	0.021022	0.222288	0.040008	0.020693
	0.3	0.267040	0.044647	0.022981	0.248069	0.044007	0.022740
	0.4	0.277337	0.046716	0.024057	0.262408	0.046212	0.023868
	0.5	0.283816	0.048022	0.024737	0.271521	0.047607	0.024581
	0.6	0.288268	0.048920	0.025205	0.277815	0.048566	0.025072
	0.7	0.291514	0.049577	0.025547	0.282432	0.049271	0.025431
	0.8	0.293986	0.050077	0.025807	0.285955	0.049806	0.025705
	0.9	0.295931	0.050471	0.026012	0.288729	0.050224	0.025918
	1.0	0.297501	0.050789	0.026178	0.290981	0.050570	0.026095
	0	0	0	0	0	0	0
	0.010	0.046151	0.004905	0.002467	0.016635	0.004023	0.002134
	0.025	0.092640	0.011881	0.006021	0.045054	0.010260	0.005407
	0.050	0.147248	0.021524	0.010990	0.094242	0.019642	0.010276
	0.075	0.183076	0.028332	0.014518	0.124954	0.026515	0.013847
	0.10	0.207594	0.033130	0.017010	0.163307	0.031536	0.016406
	0.15	0.238440	0.039285	0.020213	0.202711	0.037996	0.019725
	0.2	0.256874	0.043015	0.022156	0.227282	0.041946	0.021751
0.13	0.3	0.277746	0.047276	0.024378	0.255904	0.046486	0.024079
	0.4	0.289217	0.049633	0.025608	0.271963	0.049010	0.025372
	0.5	0.296463	0.051127	0.026388	0.282219	0.050612	0.026193
	0.6	0.301452	0.052158	0.026926	0.289329	0.051720	0.026760
	0.7	0.305097	0.052913	0.027320	0.294547	0.052531	0.027175
	0.8	0.307875	0.053488	0.027620	0.298538	0.053151	0.027492
	0.9	0.310063	0.053942	0.027857	0.301685	0.053635	0.027739
	1.0	0.311831	0.054309	0.028049	0.304241	0.054034	0.027944
	0	0	0	0	0	0	0
	0.010	0.046151	0.004905	0.002467	0.015923	0.003955	0.002106
	0.025	0.092711	0.011899	0.006031	0.043008	0.010107	0.005348
	0.050	0.148296	0.021788	0.011131	0.091252	0.019634	0.010309
	0.075	0.185651	0.028981	0.014864	0.131650	0.026919	0.014077
	0.10	0.211631	0.034147	0.017553	0.162569	0.032266	0.016835
	0.15	0.244769	0.040880	0.021064	0.204687	0.039338	0.020476
0.14	0.2	0.264799	0.045011	0.023222	0.231373	0.043724	0.022731
	0.3	0.287669	0.049776	0.025712	0.262816	0.048818	0.025347
	0.4	0.300322	0.052431	0.027101	0.280615	0.051671	0.026811
	0.5	0.308343	0.054120	0.027985	0.292036	0.053492	0.027745
	0.6	0.313940	0.055311	0.028606	0.300030	0.054816	0.028433
	0.7	0.317929	0.056146	0.029045	0.305818	0.055679	0.028867
	0.8	0.321020	0.056800	0.029387	0.310293	0.056387	0.029230
	0.9	0.323457	0.057316	0.029658	0.313830	0.056945	0.029516
	1.0	0.325427	0.057734	0.029876	0.316697	0.057398	0.029748
	0	0	0	0	0	0	0
	0.010	0.046151	0.004905	0.002467	0.015270	0.003888	0.002079
	0.025	0.092756	0.011910	0.006037	0.041126	0.009951	0.005286
	0.050	0.149120	0.022001	0.011244	0.088242	0.019568	0.010311
	0.075	0.187815	0.029539	0.015163	0.129196	0.027167	0.014253
	0.10	0.215138	0.035052	0.018038	0.161310	0.032863	0.017198
	0.15	0.250454	0.042347	0.021850	0.205935	0.040530	0.021153
0.15	0.2	0.272036	0.046879	0.024222	0.234658	0.045352	0.023636
	0.3	0.296884	0.052154	0.026986	0.268892	0.051009	0.026547
	0.4	0.310720	0.055114	0.028538	0.288439	0.054203	0.028188
	0.5	0.319522	0.057005	0.029530	0.301043	0.056249	0.029240
	0.6	0.325611	0.058317	0.030218	0.309834	0.057671	0.029970
	0.7	0.330073	0.059280	0.030723	0.316313	0.058717	0.030507
	0.8	0.333483	0.060016	0.031110	0.321284	0.059517	0.030918
	0.9	0.336173	0.060598	0.031415	0.325218	0.060150	0.031243
	1.0	0.338350	0.061069	0.031662	0.328410	0.060662	0.031506

TABLE 1-Continued

τ	μ	$F_1(-\mu,\tau)$	$F_3(-\mu,\tau)$	$F_5(-\mu,\tau)$	$e^{-\tau/\mu}F_1(\mu,\tau)$	$e^{-\tau/\mu}F_3(\mu,\tau)$	$e^{-\tau/\mu}F_5(\mu,\tau)$
	0	0	0	0	0	0	0
	0.010	0.046151	0.004905	0.002467	0.014669	0.003824	0.002052
	0.025	0.092786	0.011918	0.006041	0.039392	0.009793	0.005222
	0.050	0.149769	0.022172	0.011336	0.085258	0.019456	0.010289
	0.075	0.189636	0.030020	0.015421	0.126512	0.027324	0.014382
	0.10	0.218189	0.035857	0.018470	0.159625	0.033343	0.017501
	0.15	0.255567	0.043696	0.022575	0.206547	0.041583	0.021760
0.16	0.2	0.278656	0.048626	0.025161	0.237223	0.046837	0.024471
	0.3	0.305454	0.054415	0.028201	0.274203	0.053065	0.027681
	0.4	0.320471	0.057687	0.029921	0.295503	0.056608	0.029505
	0.5	0.330059	0.059786	0.031025	0.309303	0.058889	0.030679
	0.6	0.336706	0.061245	0.031792	0.318958	0.060478	0.031496
	0.7	0.341586	0.062318	0.032357	0.326088	0.061648	0.032098
	0.8	0.345318	0.063140	0.032789	0.331568	0.062545	0.032560
	0.9	0.348266	0.063789	0.033131	0.335910	0.063255	0.032925
	1.0	0.350653	0.064316	0.033408	0.339435	0.063831	0.033221
	0	0	0	0	0	0	0
	0.010	0.046151	0.004905	0.002467	0.014113	0.003760	0.002025
	0.025	0.092804	0.011923	0.006044	0.037791	0.009636	0.005158
	0.050	0.150280	0.022310	0.011411	0.082332	0.019307	0.010247
	0.075	0.191170	0.030433	0.015644	0.123664	0.027403	0.014469
	0.10	0.220847	0.036573	0.018857	0.157593	0.033717	0.017749
	0.15	0.260173	0.044937	0.023245	0.206605	0.042508	0.022303
0.17	0.2	0.284719	0.050260	0.026043	0.239143	0.048189	0.025240
	0.3	0.313435	0.056567	0.029362	0.278816	0.054992	0.028752
	0.4	0.329628	0.060156	0.031253	0.301864	0.058892	0.030763
	0.5	0.340003	0.062466	0.032471	0.316872	0.061414	0.032063
	0.6	0.347213	0.064077	0.033320	0.327403	0.063175	0.032971
	0.7	0.352513	0.065263	0.033946	0.335196	0.064475	0.033640
	0.8	0.356573	0.066173	0.034426	0.341194	0.065473	0.034154
	0.9	0.359781	0.066893	0.034805	0.345953	0.066264	0.034561
	1.0	0.362381	0.067477	0.035114	0.349820	0.066905	0.034892
	0	0	0	0	0	0	0
	0.010	0.046151	0.004905	0.002467	0.013597	0.003698	0.001999
	0.025	0.092817	0.011927	0.006046	0.036310	0.009480	0.005093
	0.050	0.150684	0.022421	0.011471	0.079487	0.019130	0.010189
	0.075	0.192465	0.030789	0.015837	0.120706	0.027415	0.014522
	0.10	0.223166	0.037211	0.019202	0.155283	0.033998	0.017950
	0.15	0.264327	0.046079	0.023863	0.206178	0.043313	0.022785
0.18	0.2	0.290279	0.051789	0.026870	0.240485	0.049416	0.025945
	0.3	0.320878	0.058613	0.030470	0.282789	0.056796	0.029762
	0.4	0.338239	0.062523	0.032535	0.307582	0.061060	0.031965
	0.5	0.349401	0.065050	0.033870	0.323799	0.063828	0.033394
	0.6	0.357176	0.066816	0.034803	0.335215	0.065768	0.034395
	0.7	0.362899	0.068119	0.035492	0.343681	0.067201	0.035134
	0.8	0.367288	0.069120	0.036021	0.350208	0.068304	0.035703
	0.9	0.370761	0.069912	0.036440	0.355391	0.069178	0.036154
	1.0	0.373576	0.070555	0.036780	0.359607	0.069888	0.036520
	0	0	0	0	0	0	0
	0.010	0.046151	0.004905	0.002467	0.013115	0.003637	0.001973
	0.025	0.092825	0.011929	0.006047	0.034935	0.009326	0.005029
	0.050	0.151003	0.022510	0.011519	0.076737	0.018931	0.010118
	0.075	0.193558	0.031096	0.016003	0.117684	0.027369	0.014544
	0.10	0.225191	0.037779	0.019510	0.152750	0.029195	0.018056
	0.15	0.268078	0.047131	0.024434	0.205330	0.044009	0.023211
0.19	0.2	0.295384	0.053219	0.027648	0.241309	0.050544	0.026592
	0.3	0.327826	0.060560	0.031528	0.286176	0.058481	0.030714
	0.4	0.346345	0.064795	0.033769	0.312698	0.063115	0.033111
	0.5	0.358292	0.067542	0.035224	0.330130	0.066135	0.034673
	0.6	0.366632	0.069466	0.036243	0.342438	0.068258	0.035770
	0.7	0.372782	0.070888	0.036997	0.351585	0.069829	0.036582
	0.8	0.377502	0.071982	0.037577	0.358647	0.071040	0.037207
	0.9	0.381240	0.072849	0.038036	0.364263	0.072001	0.037704
	1.0	0.384273	0.073553	0.038409	0.368835	0.072782	0.038107

TABLE 1-Continued

τ	μ	$F_1(-\mu,\tau)$	$F_3(-\mu,\tau)$	$F_5(-\mu,\tau)$	$e^{-\tau/\mu}F_1(\mu,\tau)$	$e^{-\tau/\mu}F_3(\mu,\tau)$	$e^{-\tau/\mu}F_5(\mu,\tau)$
	0	0	0	0	0	0	0
	0.025	0.092830	0.011930	0.006048	0.033655	0.009174	0.004965
	0.050	0.151255	0.022582	0.011559	0.074091	0.018806	0.010037
	0.075	0.194483	0.031359	0.016147	0.114632	0.027274	0.014539
	0.10	0.226962	0.038284	0.019786	0.150045	0.034317	0.018224
	0.15	0.271469	0.048098	0.024962	0.204115	0.044603	0.023586
	0.2	0.300076	0.054558	0.028378	0.241668	0.051521	0.027182
0.20	0.3	0.334319	0.062413	0.032538	0.289023	0.060054	0.031609
	0.4	0.353983	0.066974	0.034958	0.317258	0.065060	0.034204
	0.5	0.366712	0.069945	0.036534	0.335904	0.068339	0.035902
	0.6	0.375618	0.072030	0.037641	0.349110	0.070648	0.037097
	0.7	0.382194	0.073574	0.038461	0.358945	0.072362	0.037984
	0.8	0.387248	0.074763	0.039093	0.366550	0.073684	0.038668
	0.9	0.391254	0.075706	0.039594	0.372605	0.074734	0.039211
	1.0	0.394506	0.076473	0.040001	0.377538	0.075588	0.039653
	0	0	0	0	0	0	0
	0.025	0.092838	0.011933	0.006049	0.028372	0.008458	0.004654
	0.050	0.151917	0.022779	0.011667	0.062494	0.017499	0.009544
	0.075	0.197372	0.032220	0.016621	0.099713	0.026286	0.014233
	0.10	0.233015	0.040090	0.020780	0.135156	0.034072	0.018357
	0.15	0.284183	0.051896	0.027052	0.194068	0.046303	0.024800
	0.2	0.318317	0.060061	0.031410	0.238013	0.055056	0.029392
0.25	0.3	0.361083	0.070416	0.036943	0.296555	0.066387	0.035321
	0.4	0.386232	0.076620	0.040267	0.332976	0.073293	0.038927
	0.5	0.402782	0.080735	0.042473	0.357607	0.077911	0.041336
	0.6	0.414483	0.083658	0.044042	0.375319	0.081209	0.043056
	0.7	0.423189	0.085840	0.045213	0.388650	0.083680	0.044343
	0.8	0.429916	0.087530	0.046121	0.399039	0.085599	0.045343
	0.9	0.435271	0.088878	0.046844	0.407359	0.087132	0.046141
	1.0	0.439633	0.089977	0.047435	0.414172	0.088385	0.046794
	0	0	0	0	0	0	0
	0.025	0.092839	0.011933	0.006049	0.024393	0.007809	0.004364
	0.050	0.152127	0.022846	0.011704	0.053363	0.016240	0.008997
	0.075	0.198647	0.032629	0.016849	0.086399	0.024838	0.013652
	0.10	0.236174	0.041101	0.021345	0.120007	0.032908	0.017981
	0.15	0.292022	0.054408	0.028455	0.180235	0.046421	0.025176
	0.2	0.330878	0.064032	0.033625	0.228251	0.056665	0.030599
0.30	0.3	0.380582	0.076671	0.040439	0.295719	0.070557	0.037927
	0.4	0.410730	0.084480	0.044660	0.339482	0.079340	0.042548
	0.5	0.430875	0.089750	0.047512	0.369784	0.085340	0.045700
	0.6	0.445263	0.093536	0.049563	0.391908	0.089683	0.047980
	0.7	0.456044	0.096384	0.051107	0.408737	0.092968	0.049703
	0.8	0.464421	0.098604	0.052310	0.421954	0.095537	0.051050
	0.9	0.471114	0.100382	0.053274	0.432603	0.097600	0.052132
	1.0	0.476585	0.101838	0.054064	0.441364	0.099293	0.053019
	0	0	0	0	0	0	0
	0.025	0.092839	0.011933	0.006049	0.021259	0.007222	0.004092
	0.050	0.152194	0.022869	0.011717	0.046147	0.015041	0.008454
	0.075	0.199218	0.032822	0.016959	0.075087	0.023242	0.012960
	0.10	0.237845	0.041669	0.021666	0.105975	0.031282	0.017328
	0.15	0.296920	0.056073	0.029399	0.165072	0.045511	0.024985
	0.20	0.339272	0.066887	0.035243	0.215178	0.056881	0.031060
	0.25	0.370769	0.075132	0.039715	0.256040	0.065852	0.035836
0.35	0.3	0.394977	0.081567	0.043214	0.289307	0.073006	0.039634
	0.4	0.429584	0.090894	0.048295	0.339397	0.083571	0.045234
	0.5	0.453045	0.097293	0.051787	0.374902	0.090946	0.049133
	0.6	0.469962	0.101940	0.054326	0.401220	0.096354	0.051990
	0.7	0.482725	0.105464	0.056253	0.421451	0.100483	0.054170
	0.8	0.492691	0.108225	0.057763	0.437466	0.103735	0.055886
	0.9	0.500686	0.110446	0.058979	0.450446	0.106361	0.057271
	1.0	0.507242	0.112271	0.059978	0.461175	0.108525	0.058412

TABLE 1-Continued

τ	μ	$F_1(-\mu,\tau)$	$F_3(-\mu,\tau)$	$F_5(-\mu,\tau)$	$e^{-\tau/\mu}F_1(\mu,\tau)$	$e^{-\tau/\mu}F_3(\mu,\tau)$	$e^{-\tau/\mu}F_5(\mu,\tau)$
	0	0	0	0	0	0	0
	0.050	0.152216	0.022877	0.011722	0.040346	0.013929	0.007937
	0.075	0.199476	0.032914	0.017011	0.065622	0.021648	0.012236
	0.10	0.238737	0.041987	0.021849	0.093515	0.029459	0.016534
	0.15	0.300010	0.057177	0.030033	0.149930	0.043953	0.024418
	0.20	0.345029	0.068945	0.036424	0.200539	0.056107	0.030972
	0.25	0.379133	0.078123	0.041432	0.243406	0.066014	0.036289
0.40	0.3	0.405707	0.085405	0.045417	0.279233	0.074097	0.040613
	0.4	0.444236	0.096136	0.051305	0.334577	0.086309	0.047130
	0.5	0.470711	0.103613	0.055416	0.374727	0.095002	0.051757
	0.6	0.489974	0.109100	0.058437	0.404941	0.101468	0.055194
	0.7	0.504601	0.113291	0.060747	0.428414	0.106443	0.057837
	0.8	0.516079	0.116594	0.062568	0.447140	0.110402	0.059938
	0.9	0.525343	0.119278	0.064054	0.462409	0.113610	0.061639
	1.0	0.532924	0.121461	0.065255	0.475091	0.116266	0.063047
	0	0	0	0	0	0	0
	0.050	0.152223	0.022879	0.011723	0.035591	0.012909	0.007449
	0.075	0.199594	0.032958	0.017037	0.057724	0.020121	0.011520
	0.10	0.239217	0.042167	0.021953	0.082673	0.027589	0.015681
	0.15	0.301975	0.057911	0.030459	0.135520	0.042010	0.023610
	0.20	0.349006	0.070431	0.037288	0.185430	0.054643	0.030485
	0.25	0.385208	0.080393	0.042751	0.229261	0.065265	0.036231
0.45	0.3	0.413766	0.088417	0.047167	0.266841	0.074124	0.041006
	0.4	0.455710	0.100425	0.053797	0.326377	0.087807	0.048357
	0.5	0.484894	0.108915	0.058497	0.370572	0.097747	0.053682
	0.6	0.506311	0.115208	0.061987	0.404333	0.105238	0.057688
	0.7	0.522675	0.120048	0.064674	0.430841	0.111066	0.060801
	0.8	0.535576	0.123883	0.066805	0.452154	0.115721	0.063286
	0.9	0.546002	0.126993	0.068534	0.469639	0.119521	0.065312
	1.0	0.554602	0.129566	0.069965	0.484229	0.122679	0.066996
	0	0	0	0	0	0	0
	0.050	0.152225	0.022880	0.011724	0.031625	0.011975	0.006991
	0.075	0.199648	0.032979	0.017049	0.051098	0.018690	0.010832
	0.10	0.239476	0.042267	0.022012	0.073318	0.025756	0.014817
	0.15	0.303231	0.058399	0.030746	0.122187	0.039861	0.022656
	0.20	0.351772	0.071505	0.037919	0.170530	0.052716	0.029715
	0.25	0.389649	0.082118	0.043765	0.214468	0.063845	0.035784
0.50	0.30	0.419856	0.090783	0.048558	0.253085	0.073327	0.040933
	0.35	0.444423	0.097943	0.052530	0.286655	0.081394	0.045300
	0.4	0.464750	0.103937	0.055861	0.315805	0.088292	0.049026
	0.5	0.496351	0.113367	0.061114	0.363436	0.099382	0.055003
	0.6	0.519730	0.120423	0.065052	0.400456	0.107884	0.059570
	0.7	0.537698	0.125887	0.068106	0.429674	0.114504	0.063132
	0.8	0.551926	0.130237	0.070540	0.453422	0.119854	0.066002
	0.9	0.563466	0.133781	0.072523	0.473023	0.124245	0.068356
	1.0	0.573011	0.136721	0.074171	0.489458	0.127910	0.070320
	0	0	0	0	0	0	0
	0.050	0.152226	0.022881	0.011724	0.025390	0.010331	0.006163
	0.075	0.199684	0.032994	0.017058	0.040715	0.016134	0.009561
	0.10	0.239695	0.042356	0.022065	0.058327	0.022351	0.013150
	0.15	0.304560	0.058940	0.031068	0.099140	0.035392	0.020553
	0.20	0.355060	0.072845	0.038718	0.142798	0.048099	0.027658
	0.25	0.395316	0.084429	0.045144	0.135064	0.059706	0.034088
0.60	0.30	0.428008	0.094108	0.050542	0.224007	0.070002	0.039759
	0.35	0.454994	0.102256	0.055103	0.259089	0.079036	0.044715
	0.4	0.477597	0.109179	0.058989	0.290403	0.086947	0.049042
	0.5	0.513234	0.120258	0.065226	0.343132	0.100007	0.056164
	0.6	0.539988	0.128692	0.069987	0.385250	0.110246	0.061732
	0.7	0.560774	0.135307	0.073728	0.419380	0.118439	0.066179
	0.8	0.577371	0.140626	0.076740	0.447474	0.125121	0.069801
	0.9	0.590920	0.144991	0.079214	0.470945	0.130664	0.072802
	1.0	0.602187	0.148635	0.081282	0.490815	0.135332	0.075328

TABLE 1-Continued

τ	μ	$F_1(-\mu,\tau)$	$F_3(-\mu,\tau)$	$F_5(-\mu,\tau)$	$e^{-\tau/\mu}F_1(\mu,\tau)$	$e^{-\tau/\mu}F_3(\mu,\tau)$	$e^{-\tau/\mu}F_5(\mu,\tau)$
	0	0	0	0	0	0	0
	0.050	0.152226	0.022881	0.011724	0.020724	0.008942	0.005437
	0.075	0.199692	0.032997	0.017060	0.033030	0.013958	0.008437
	0.10	0.239761	0.042365	0.022082	0.047108	0.019372	0.011632
	0.15	0.305118	0.059181	0.031215	0.080650	0.031094	0.018423
	0.20	0.356688	0.073548	0.039146	0.118800	0.043134	0.025276
	0.25	0.398420	0.085770	0.045959	0.157819	0.054661	0.031763
0.7	0.30	0.432780	0.096170	0.051796	0.195387	0.065275	0.037691
	0.35	0.461484	0.105061	0.056809	0.230402	0.074864	0.043019
	0.4	0.485771	0.112713	0.061139	0.262504	0.083458	0.047777
	0.5	0.524528	0.125141	0.068196	0.318186	0.098015	0.055805
	0.6	0.554000	0.134751	0.073673	0.363988	0.109727	0.062240
	0.7	0.577119	0.142377	0.078029	0.401689	0.119274	0.067473
	0.8	0.595719	0.148562	0.081568	0.433580	0.127170	0.071793
	0.9	0.610994	0.153674	0.084497	0.460378	0.133792	0.075412
	1.0	0.623758	0.157966	0.086959	0.483286	0.139416	0.078482
	0	0	0	0	0	0	0
	0.050	0.152226	0.022881	0.011724	0.017121	0.007761	0.004801
	0.075	0.199694	0.032998	0.017060	0.027163	0.012106	0.007449
	0.10	0.239781	0.042394	0.022088	0.038557	0.016806	0.010279
	0.15	0.305354	0.059288	0.031281	0.068466	0.027237	0.016085
	0.20	0.357505	0.073919	0.039375	0.098681	0.038282	0.022838
	0.25	0.400139	0.086550	0.046442	0.133718	0.049349	0.029162
0.8	0.30	0.435606	0.097452	0.052589	0.168847	0.059894	0.035133
	0.35	0.465515	0.106891	0.057941	0.202669	0.069688	0.040644
	0.4	0.491033	0.115102	0.062617	0.234490	0.078663	0.045671
	0.5	0.532172	0.128612	0.070344	0.291316	0.094255	0.054362
	0.6	0.563805	0.139203	0.076428	0.339434	0.107123	0.061502
	0.7	0.588833	0.147696	0.081321	0.380091	0.117807	0.067413
	0.8	0.609105	0.154641	0.085330	0.414622	0.126767	0.072359
	0.9	0.625845	0.160418	0.088671	0.444179	0.134364	0.076546
	1.0	0.639895	0.165295	0.091495	0.469691	0.140874	0.080129
	0	0	0	0	0	0	0
	0.050	0.152226	0.022881	0.011724	0.014278	0.006752	0.004243
	0.075	0.199694	0.032998	0.017061	0.022601	0.010524	0.006582
	0.10	0.239787	0.042397	0.022090	0.031907	0.014606	0.009084
	0.15	0.305455	0.059336	0.031311	0.054473	0.023719	0.014568
	0.20	0.357918	0.074114	0.039498	0.082075	0.033765	0.020486
	0.25	0.401101	0.087005	0.046728	0.112943	0.044137	0.026503
0.9	0.30	0.437295	0.098252	0.053091	0.145058	0.054334	0.032356
	0.35	0.468042	0.108087	0.058693	0.176942	0.064054	0.037893
	0.4	0.494452	0.116720	0.063634	0.207698	0.073154	0.043047
	0.5	0.537393	0.131084	0.071898	0.264216	0.089357	0.052172
	0.6	0.570729	0.142482	0.078489	0.313464	0.103068	0.059853
	0.7	0.597305	0.151708	0.083843	0.355945	0.114663	0.066324
	0.8	0.618961	0.159309	0.088265	0.392594	0.124523	0.071813
	0.9	0.636932	0.165669	0.091972	0.424348	0.132974	0.076508
	1.0	0.652077	0.171065	0.095122	0.452026	0.140279	0.080560
	0	0	0	0	0	0	0
	0.050	0.152226	0.022881	0.011724	0.011995	0.005886	0.003753
	0.075	0.199694	0.032998	0.017061	0.018913	0.009169	0.005820
	0.10	0.239789	0.042393	0.022090	0.026640	0.012718	0.008032
	0.15	0.305499	0.059357	0.031325	0.045254	0.020689	0.012913
	0.20	0.358128	0.074217	0.039564	0.068463	0.029673	0.018294
	0.25	0.401642	0.087270	0.046897	0.095302	0.039226	0.023918
1.0	0.30	0.438312	0.098751	0.053410	0.124174	0.048886	0.029643
	0.35	0.469638	0.108870	0.059193	0.153680	0.058322	0.034976
	0.4	0.496690	0.117819	0.064335	0.182835	0.067339	0.040140
	0.5	0.540985	0.132848	0.073023	0.237930	0.083785	0.049494
	0.6	0.575654	0.144902	0.080032	0.287311	0.098048	0.057556
	0.7	0.603477	0.154740	0.085776	0.330795	0.110330	0.064468
	0.8	0.626270	0.162900	0.090555	0.368898	0.120921	0.070411
	0.9	0.645270	0.169765	0.094585	0.402316	0.130097	0.075548
	1.0	0.661341	0.175616	0.098025	0.431730	0.138098	0.080018

TABLE 2

τ	G_{11}	G_{11}	G_{12}	G_{12}	G_{13}	G_{13}	G_{14}	G_{14}
0	0	0	0	0	0	0	0	0
0.005	0.168785	0.168811	0.028209	0.028118	0.014244	0.014232	0.009507	0.009501
0.01	0.263256	0.246906	0.049063	0.048819	0.024942	0.024894	0.016664	0.016639
0.02	0.397343	0.364841	0.083120	0.082286	0.042704	0.042515	0.028585	0.028488
0.03	0.496273	0.447813	0.111327	0.109634	0.057683	0.057267	0.038681	0.038464
0.04	0.575484	0.511260	0.135736	0.132959	0.070841	0.070118	0.047584	0.047204
0.05	0.641593	0.561795	0.157345	0.153289	0.082643	0.081537	0.055599	0.055013
0.06	0.698207	0.603022	0.176755	0.171247	0.093369	0.091807	0.062908	0.062075
0.07	0.747557	0.637171	0.194367	0.187252	0.103204	0.101118	0.069633	0.068513
0.08	0.791142	0.665739	0.210469	0.201607	0.112284	0.109610	0.075862	0.074417
0.09	0.830028	0.689788	0.225279	0.214543	0.120711	0.117386	0.081660	0.079853
0.10	0.865001	0.710104	0.238964	0.226240	0.128564	0.124531	0.087080	0.084876
0.11	0.896665	0.727287	0.251662	0.236843	0.135908	0.131111	0.092163	0.089529
0.12	0.925492	0.741807	0.263482	0.246473	0.142795	0.137182	0.096944	0.093846
0.13	0.951860	0.754040	0.274518	0.255229	0.149271	0.142791	0.101451	0.097858
0.14	0.976076	0.764292	0.284847	0.263196	0.155372	0.147979	0.105708	0.101590
0.15	0.998397	0.772816	0.294535	0.270448	0.161131	0.152780	0.109738	0.105066
0.16	1.019034	0.779823	0.303640	0.277049	0.166577	0.157224	0.113557	0.108304
0.17	1.038169	0.785490	0.312212	0.283053	0.171734	0.161339	0.117183	0.111322
0.18	1.055953	0.789970	0.320296	0.288510	0.176624	0.165148	0.120630	0.114134
0.19	1.072521	0.793392	0.327929	0.293463	0.181267	0.168674	0.123909	0.116755
0.20	1.087986	0.795870	0.335147	0.297951	0.185680	0.171934	0.127033	0.119197
0.25	1.151897	0.797144	0.365978	0.314528	0.204792	0.184820	0.140649	0.129079
0.30	1.199245	0.785521	0.389965	0.323535	0.219982	0.193149	0.151578	0.135819
0.35	1.235256	0.766006	0.408958	0.327124	0.232233	0.198065	0.160474	0.140160
0.40	1.263184	0.741645	0.424196	0.326762	0.242224	0.200376	0.167788	0.142638
0.45	1.285172	0.714391	0.436550	0.323491	0.250443	0.200679	0.173852	0.143651
0.5	1.302696	0.685535	0.446652	0.318074	0.257252	0.199425	0.178912	0.143504
0.6	1.328250	0.626250	0.461861	0.302940	0.267681	0.193566	0.186735	0.140643
0.7	1.345309	0.568008	0.472400	0.284483	0.275057	0.184794	0.192335	0.135453
0.8	1.356967	0.512808	0.479829	0.264568	0.280351	0.174383	0.196395	0.128850
0.9	1.365081	0.461539	0.485138	0.244333	0.284192	0.163162	0.199371	0.121451
1.0	1.370811	0.414509	0.488975	0.224475	0.287007	0.151682	0.201570	0.113678

τ	G_{15}	G_{15}	G_{22}	G_{22}	G_{23}	G_{23}	G_{24}	G_{24}
0	0	0	0	0	0	0	0	0
0.005	0.007133	0.007129	0.004846	0.004845	0.002449	0.002449	0.001635	0.001635
0.01	0.012507	0.012491	0.009457	0.009453	0.004814	0.004814	0.003217	0.003217
0.02	0.021470	0.021405	0.018122	0.018099	0.009335	0.009329	0.006251	0.006249
0.03	0.029072	0.028927	0.026170	0.026106	0.013609	0.013593	0.009132	0.009124
0.04	0.035786	0.035531	0.033694	0.033564	0.017665	0.017631	0.011877	0.011859
0.05	0.041840	0.041445	0.040759	0.040535	0.021524	0.021463	0.014498	0.014465
0.06	0.047369	0.046806	0.047415	0.047069	0.025202	0.025104	0.017004	0.016951
0.07	0.052463	0.051706	0.053701	0.053203	0.028713	0.028566	0.019404	0.019326
0.08	0.057188	0.056209	0.059650	0.058970	0.032068	0.031861	0.021706	0.021594
0.09	0.061593	0.060366	0.065291	0.064399	0.035277	0.034999	0.023914	0.023763
0.10	0.065716	0.064217	0.070647	0.069512	0.038351	0.037989	0.026036	0.025838
0.11	0.069587	0.067793	0.075739	0.074331	0.041296	0.040837	0.028074	0.027822
0.12	0.073233	0.071120	0.080586	0.078876	0.044120	0.043552	0.030034	0.029721
0.13	0.076675	0.074221	0.085205	0.083163	0.046830	0.046139	0.031921	0.031537
0.14	0.079930	0.077113	0.089610	0.087207	0.049433	0.048606	0.033737	0.033276
0.15	0.083015	0.079815	0.093815	0.091023	0.051933	0.050957	0.035486	0.034939
0.16	0.085943	0.082339	0.097832	0.094623	0.054335	0.053197	0.037171	0.036531
0.17	0.088725	0.084698	0.101673	0.098019	0.056646	0.055333	0.038795	0.038054
0.18	0.091373	0.086905	0.105347	0.101222	0.058869	0.057367	0.040362	0.039511
0.19	0.093896	0.088968	0.108864	0.104242	0.061008	0.059305	0.041873	0.040904
0.20	0.096302	0.090897	0.112233	0.107089	0.063067	0.061150	0.043331	0.042237
0.25	0.106821	0.098793	0.127110	0.119001	0.072290	0.069113	0.049902	0.048059
0.30	0.115310	0.104313	0.139264	0.127665	0.079987	0.075255	0.055440	0.052657
0.35	0.122253	0.108005	0.149282	0.133752	0.086450	0.079897	0.060133	0.056230
0.40	0.127989	0.110264	0.157597	0.137774	0.091902	0.083292	0.064125	0.058940
0.45	0.132766	0.111386	0.164539	0.140131	0.096520	0.085650	0.067532	0.060920
0.5	0.136768	0.111600	0.170362	0.141142	0.100446	0.087143	0.070449	0.062283
0.6	0.142992	0.109983	0.179416	0.140107	0.106654	0.088078	0.075106	0.063520
0.7	0.147479	0.106472	0.185927	0.136207	0.111212	0.086988	0.078566	0.063249
0.8	0.150754	0.101772	0.190662	0.130485	0.114585	0.084510	0.081154	0.061911
0.9	0.153169	0.096364	0.194136	0.123662	0.117099	0.081106	0.083101	0.059831
1.0	0.154964	0.090583	0.196704	0.116237	0.118984	0.077114	0.084573	0.057253

TABLE 2-Continued

τ	G_{25}	G_{25}	G_{33}	G_{33}	G_{34}	G_{34}	G_{35}	G_{35}
0	0	0	0	0	0	0	0	0
0.005	0.001226	0.001226	0.001238	0.001238	0.000826	0.000826	0.000620	0.000620
0.01	0.002415	0.002415	0.002451	0.002451	0.001638	0.001638	0.001230	0.001230
0.02	0.004696	0.004694	0.004809	0.004808	0.003221	0.003220	0.002420	0.002419
0.03	0.006865	0.006860	0.007080	0.007076	0.004751	0.004749	0.003572	0.003570
0.04	0.008935	0.008923	0.009266	0.009258	0.006231	0.006226	0.004688	0.004685
0.05	0.010915	0.010893	0.011374	0.011357	0.007662	0.007653	0.005769	0.005763
0.06	0.012811	0.012775	0.013407	0.013379	0.009047	0.009032	0.006817	0.006806
0.07	0.014629	0.014576	0.015367	0.015324	0.010388	0.010365	0.007832	0.007816
0.08	0.016375	0.016299	0.017259	0.017196	0.011686	0.011652	0.008817	0.008794
0.09	0.018053	0.017950	0.019086	0.018999	0.012942	0.012895	0.009771	0.009739
0.10	0.019666	0.019531	0.020849	0.020733	0.014160	0.014096	0.010697	0.010654
0.11	0.021219	0.021047	0.022552	0.022403	0.015339	0.015256	0.011595	0.011539
0.12	0.022714	0.022500	0.024198	0.024009	0.016481	0.016376	0.012466	0.012395
0.13	0.024154	0.023892	0.025788	0.025554	0.017588	0.017458	0.013312	0.013223
0.14	0.025543	0.025227	0.027325	0.027041	0.018660	0.018502	0.014132	0.014023
0.15	0.026882	0.026507	0.028812	0.028470	0.019700	0.019509	0.014928	0.014797
0.16	0.028173	0.027735	0.030249	0.029845	0.020708	0.020481	0.015700	0.015545
0.17	0.029420	0.028911	0.031639	0.031166	0.021685	0.021419	0.016450	0.016267
0.18	0.030624	0.030038	0.032984	0.032436	0.022633	0.022323	0.017179	0.016965
0.19	0.031786	0.031119	0.034285	0.033656	0.023552	0.023195	0.017885	0.017639
0.20	0.032909	0.032154	0.035544	0.034828	0.024444	0.024035	0.018572	0.018290
0.25	0.037986	0.036706	0.041262	0.040015	0.028517	0.027794	0.021719	0.021217
0.30	0.042288	0.040344	0.046137	0.044203	0.032025	0.030888	0.024444	0.023650
0.35	0.045950	0.043211	0.050305	0.047536	0.035052	0.033402	0.026807	0.025649
0.40	0.049081	0.045425	0.053880	0.050134	0.037670	0.035413	0.028859	0.027268
0.45	0.051765	0.047081	0.056953	0.052103	0.039936	0.036985	0.030645	0.028554
0.5	0.054072	0.048263	0.059599	0.053530	0.041903	0.038176	0.032201	0.029549
0.6	0.057777	0.049472	0.063857	0.055057	0.045097	0.039605	0.034742	0.030804
0.7	0.060550	0.049495	0.067047	0.055213	0.047519	0.040031	0.036682	0.031277
0.8	0.062637	0.048664	0.069451	0.054374	0.049363	0.039708	0.038170	0.031157
0.9	0.064218	0.047227	0.071270	0.052826	0.050772	0.038836	0.039314	0.030596
1.0	0.065420	0.045373	0.072653	0.050786	0.051852	0.037568	0.040196	0.029710

τ	G_{44}	G_{44}	G_{45}	G_{45}	G_{55}	G_{55}	$E_1^{(2)}$
0	0	0	0	0	0	0	∞
0.005	0.000551	0.000551	0.000414	0.000414	0.000310	0.000310	11.139404
0.01	0.001095	0.001095	0.000822	0.000822	0.000617	0.000617	8.924688
0.02	0.002157	0.002157	0.001620	0.001620	0.001217	0.001217	6.362987
0.03	0.003188	0.003187	0.002397	0.002396	0.001802	0.001802	5.083102
0.04	0.004190	0.004187	0.003152	0.003150	0.002372	0.002370	4.271850
0.05	0.005162	0.005157	0.003886	0.003883	0.002926	0.002924	3.697389
0.06	0.006106	0.006098	0.004600	0.004595	0.003466	0.003463	3.263197
0.07	0.007022	0.007010	0.005295	0.005286	0.003992	0.003987	2.920528
0.08	0.007913	0.007894	0.005970	0.005958	0.004505	0.004496	2.641609
0.09	0.008777	0.008752	0.006627	0.006610	0.005004	0.004992	2.409252
0.10	0.009617	0.009583	0.007266	0.007243	0.005490	0.005474	2.212149
0.11	0.010433	0.010388	0.007888	0.007857	0.005963	0.005942	2.042502
0.12	0.011226	0.011169	0.008492	0.008453	0.006424	0.006397	1.894734
0.13	0.011997	0.011925	0.009081	0.009031	0.006873	0.006840	1.764732
0.14	0.012745	0.012657	0.009653	0.009592	0.007311	0.007270	1.649385
0.15	0.013473	0.013366	0.010210	0.010137	0.007737	0.007687	1.546292
0.16	0.014180	0.014052	0.010752	0.010664	0.008153	0.008093	1.453564
0.17	0.014867	0.014716	0.011279	0.011176	0.008557	0.008486	1.369694
0.18	0.015535	0.015359	0.011792	0.011671	0.008952	0.008869	1.293459
0.19	0.016184	0.015981	0.012292	0.012152	0.009336	0.009239	1.223859
0.20	0.016815	0.016582	0.012778	0.012617	0.009710	0.009599	1.160064
0.25	0.019717	0.019298	0.015020	0.014729	0.011443	0.011241	0.907304
0.30	0.022242	0.021572	0.016981	0.016513	0.012966	0.012639	0.729650
0.35	0.024440	0.023456	0.018696	0.018006	0.014305	0.013821	0.598701
0.40	0.026356	0.024996	0.020199	0.019240	0.015483	0.014807	0.498831
0.45	0.028028	0.026232	0.021517	0.020244	0.016521	0.015620	0.420678
0.5	0.029490	0.027201	0.022672	0.021044	0.017435	0.016277	0.358275
0.6	0.031886	0.028458	0.024579	0.022121	0.018952	0.017190	0.265984
0.7	0.033724	0.028985	0.026052	0.022631	0.020133	0.017663	0.202258
0.8	0.035139	0.028955	0.027193	0.022701	0.021053	0.017790	0.156636
0.9	0.036230	0.028504	0.028079	0.022435	0.021772	0.017650	0.123071
1.0	0.037074	0.027741	0.028768	0.021916	0.022335	0.017304	0.097843

where $\gamma = 0.5772156\ldots$ is the Euler-Mascheroni constant. The functions of higher order can then be found from F_1 in accordance with the recursion formula

$$F_{j+1}(\tau, \mu) = \mu\left[F_j(\tau, \mu) - \frac{1}{j} + e^{\tau/\mu}E_{j+1}(\tau)\right].$$

The function $G_{n,m}(\tau)$ is expressible in terms of the exponential integrals and the F-functions. We have

$$(m+n-1)G_{n,m}(\tau) = \tau E_n(\tau)E_m(\tau) + F_n(\tau,-1) + F_m(\tau,-1).$$

The function G'_{11} is given by

$$G'_{11}(\tau) = 2\,[E_1(\tau) + (\log\tau + \gamma)E_2(\tau) - \tau E_1^{(2)}(\tau)\,],$$

where

$$E_1^{(2)}(\tau) = \int_\tau^\infty E_1(t)\frac{dt}{t}.$$

(This function, $E_1^{(2)}(\tau)$ is also included in Table 2.) The functions $G'_{n,m}$ of higher order can be derived from G'_{11} by successive applications of the recursion formula

$$G'_{n,m}(\tau) = G'_{n-1,m+1}(\tau) - \frac{1}{n-1}E_{m+1}(\tau) + \frac{1}{m}E_n(\tau)$$

$$= G'_{n+1,m-1}(\tau) - \frac{1}{m-1}E_{n+1}(\tau) + \frac{1}{n}E_m(\tau).$$

The calculations were carried out with eight decimals; the six decimals retained in our tabulations should therefore be reliable.

Finally, we wish to acknowledge that our calculations were enormously facilitated by G. Placzek's extensive tabulations of the exponential integrals.[13]

[13] *The Functions* $E_n(x) = \int_1^\infty e^{-xu}u^{-n}du$ (National Research Council of Canada, Division of Atomic Energy, Doc. No. MT − 1 [1946]).

ON THE LINE-ABSORPTION COEFFICIENT DUE TO DOPPLER EFFECT AND DAMPING

DANIEL L. HARRIS III
YERKES OBSERVATORY
Received April 12, 1948

ABSTRACT

A table is provided to facilitate the computation of the line-absorption coefficient.

The line-absorption coefficient, which combines the Doppler effect due to thermal and turbulent motions and natural and collision damping, is of importance in the theory of the formation of lines in stellar atmospheres and in interstellar space. As is well known, this may be written in the form[1]

$$\frac{\kappa_v}{\kappa_0} = H(a, v) = \frac{a}{\pi}\int_{-\infty}^{+\infty} \frac{e^{-y^2}dy}{a^2 + (v-y)^2}, \tag{1}$$

where

$$a = \frac{\Delta\nu_N}{\Delta\nu_D} = \frac{\gamma_c + \gamma_N}{\Delta\nu_D}$$

is the ratio of the effective natural line width $(\gamma_c + \gamma_N)$, to the Doppler width, $\Delta\nu_D$; v is the deviation from the center of the line in units of the Doppler width; and

$$\kappa_0 = \frac{\sqrt{\pi}\, e^2}{m\, c} f \frac{1}{\Delta\nu_D}$$

is the absorption coefficient at the center of the line in the limit of vanishing damping.

F. Hjerting[1] has evaluated the integral defined $H(a, v)$ by numerical quadratures for values of $v = 0.0(0.25)5.00$ and for $a = 0.00(0.01)0.20$ and with less accuracy for $a = 0.3, 0.4$, and 0.5. A. C. G. Mitchell and M. W. Zemansky[2] have given the coefficients of the first two terms in a series expansion in a for $v = 0.0(0.2)12.0$.

In this paper we shall provide certain tables which will facilitate still further the evaluation of this integral for more values of v than those given by Hjerting and for larger values of a than is possible with Mitchell and Zemansky's tables.[3]

Writing the integral $H(a, v)$ as the real part of the error function for complex arguments in the form

$$H(a, v) = \frac{2}{\sqrt{\pi}} R\, e^{(a+iv)^2}\int_{a+iv}^{\infty} e^{-t^2}dt = \frac{2}{\sqrt{\pi}} R\, e^{(a+iv)^2}\left[\frac{\sqrt{\pi}}{2} - i\int_0^{v-ia} e^{t^2}dt\right], \tag{2}$$

we can obtain, for small values of a, the Taylor series

$$H(a, v) = H_0(v) + aH_1(v) + a^2H_2(v) + a^3H_3(v) + a^4H_4(v) + \ldots \tag{3}$$

[1] F. Hjerting, *Ap. J.*, **88**, 508, 1938.

[2] *Resonance Radiation and Excited Atoms* (Cambridge: At the University Press, 1934), p. 322.

[3] Errors in $1 - 2vF(v)$ in Mitchell and Zemansky's table exceeding one unit in the last decimal place are:

for $v = 2.0$	*read*	-0.2054	*instead of*	-0.2052
4.0		$-.03478$		$-.03480$
4.8		$-.02330$		$-.02336$
8.0		-0.008003		-0.008000

where

$$H_0(v) = e^{-v^2},$$

$$H_1(v) = -\frac{2}{\sqrt{\pi}}[1 - 2vF(v)],$$

$$H_2(v) = (1 - 2v^2)\, e^{-v^2}, \tag{4}$$

$$H_3(v) = -\frac{2}{\sqrt{\pi}}[\tfrac{2}{3}(1 - v^2) - 2v(1 - \tfrac{2}{3}v^2)F(v)]$$

and

$$H_4(v) = (\tfrac{1}{2} - 2v^2 + \tfrac{2}{3}v^4)\, e^{-v^2}.$$

In the above expressions we have used the abbreviation

$$F(v) = e^{-v^2}\int_0^v e^{t^2}dt. \tag{5}$$

Table 3 gives the numerical values of these coefficients. These have been computed from the table of $F(v)$ given by W. Lash Miller and A. R. Gordon[4] and the table of e^{-x} given by F. W. Newman.[5] The values of $F(v)$ for $v \leqslant 2.0$ have been checked with H. M. Terrill and L. Sweeney's table of $e^{v^2}F(v)$.[6]

TABLE 1

$10^6 a^5 H_5(v)$

v	a			v	a		
	0.1	0.2	0.3		0.1	0.2	0.3
0	−3.0	−96	−730	3	0.0	+0.8	+6.4
1	+1.9	+59	+450	4	.0	− .1	−0.9
2	−0.5	−15	−110	6	0.0	+0.0	+0.0

TABLE 2

THE MAXIMUM "ROUNDING-OFF" ERROR

v	a			v	a		
	0.1	0.2	0.3		0.1	0.2	0.3
0.0–1.9	2.5	16	60	4.0– 6.8	0.1	0.1	0.3
1.9–3.9	0.2	0.8	2	7.0–12.0	0.0	0.1	0.2

The number of significant figures obtainable by using these coefficients is, of course, dependent on the size of a and is limited (i) by the error introduced by neglecting higher-order terms in the expansion (3) and (ii) by the error introduced by "rounding off" the coefficients. The error arising from the first source can be estimated from the contribution arising from $a^5H_5(v)$, which is indicated in Table 1. The maximum error arising from the second source is indicated in Table 2 in units of the sixth decimal place.

[4] *J. Phys. Chem.*, **35**, 2877, 1931.

[5] *Trans. Cambridge Phil. Soc.*, **13**, 145, 1883.

[6] *J. Franklin Inst.*, **238**, 220, 1944.

TABLE 3

THE FUNCTIONS H_0, H_1, H_2, H_3, AND H_4

v	$H_0(v)$	$H_1(v)$	$H_2(v)$	$H_3(v)$	$H_4(v)$
0.0	+1.000 000	−1.128 38	+1.000 0	−0.752	+0.50
0.1	+0.990 050	−1.105 96	+0.970 2	− .722	+ .48
0.2	+0.960 789	−1.040 48	+0.883 9	− .637	+ .40
0.3	+0.913 931	−0.937 03	+0.749 4	− .505	+ .30
0.4	+0.852 144	−0.803 46	+0.579 5	− .342	+ .17
0.5	+0.778 801	−0.649 45	+0.389 4	− .165	+ .03
0.6	+0.697 676	−0.485 52	+0.195 3	+ .007	− .09
0.7	+0.612 626	−0.321 92	+0.012 3	+ .159	− .20
0.8	+0.527 292	−0.167 72	−0.147 6	+ .280	− .27
0.9	+0.444 858	−0.030 12	−0.275 8	+ .362	− .30
1.0	+0.367 879	+0.085 94	−0.367 9	+ .405	− .31
1.1	+0.298 197	+0.177 89	−0.423 4	+ .411	− .28
1.2	+0.236 928	+0.245 37	−0.445 4	+ .386	− .24
1.3	+0.184 520	+0.289 81	−0.439 2	+ .339	− .18
1.4	+0.140 858	+0.313 94	−0.411 3	+ .280	− .12
1.5	+0.105 399	+0.321 30	−0.368 9	+ .215	− .07
1.6	+0.077 305	+0.315 73	−0.318 5	+ .153	− .02
1.7	+0.055 576	+0.300 94	−0.265 7	+ .097	+ .02
1.8	+0.039 164	+0.280 27	−0.214 6	+ .051	+ .04
1.9	+0.027 052	+0.256 48	−0.168 3	+ .015	+ .05
2.0	+0.018 3156	+0.231 726	−0.128 21	− .010 1	+ .058
2.1	+0.012 1552	+0.207 528	−0.095 05	− .026 5	+ .056
2.2	+0.007 9071	+0.184 882	−0.068 63	− .035 5	+ .051
2.3	+0.005 0418	+0.164 341	−0.048 30	− .039 1	+ .043
2.4	+0.003 1511	+0.146 128	−0.033 15	− .038 9	+ .035
2.5	+0.001 9305	+0.130 236	−0.022 20	− .036 3	+ .027
2.6	+0.001 1592	+0.116 515	−0.014 51	− .032 5	+ .020
2.7	+0.000 6823	+0.104 739	−0.009 27	− .028 2	+ .015
2.8	+0.000 3937	+0.094 653	−0.005 78	− .023 9	+ .010
2.9	+0.000 2226	+0.086 005	−0.003 52	− .020 1	+ .007
3.0	+0.000 1234	+0.078 565	−0.002 10	− .016 7	+ .005
3.1	+0.000 0671	+0.072 129	−0.001 22	− .013 8	+ .003
3.2	+0.000 0357	+0.066 526	−0.000 70	− .011 5	+ .002
3.3	+0.000 0186	+0.061 615	−0.000 39	− .009 6	+ .001
3.4	+0.000 0095	+0.057 281	−0.000 21	− .008 0	+ .001
3.5	+0.000 0048	+0.053 430	−0.000 11	− .006 8	.000
3.6	+0.000 0024	+0.049 988	−0.000 06	− .005 8	.000
3.7	+0.000 0011	+0.046 894	−0.000 03	− .005 0	.000
3.8	+0.000 0005	+0.044 098	−0.000 01	− .004 3	.000
3.9	+0.000 0002	+0.041 561	−0.000 01	− .003 7	.000
4.0	+0.000 0001	+0.039 250	0.000 00	−0.003 3	0.000

v	$H_1(v)$	$H_3(v)$	v	$H_1(v)$	$H_3(v)$
4.0	+0.039 250	−0.003 29	8.0	+0.009 0306	−0.000 15
4.2	+ .035 195	− .002 57	8.2	+ .008 5852	− .000 13
4.4	+ .031 762	− .002 05	8.4	+ .008 1722	− .000 12
4.6	+ .028 824	− .001 66	8.6	+ .007 7885	− .000 11
4.8	+ .026 288	− .001 37	8.8	+ .007 4314	− .000 10
5.0	+ .024 081	− .001 13	9.0	+ .007 0985	− .000 09
5.2	+ .022 146	− .000 95	9.2	+ .006 7875	− .000 08
5.4	+ .020 441	− .000 80	9.4	+ .006 4967	− .000 08
5.6	+ .018 929	− .000 68	9.6	+ .006 2243	− .000 07
5.8	+ .017 582	− .000 59	9.8	+ .005 9688	− .000 07
6.0	+ .016 375	− .000 51	10.0	+ .005 7287	− .000 06
6.2	+ .015 291	− .000 44	10.2	+ .005 5030	− .000 06
6.4	+ .014 312	− .000 38	10.4	+ .005 2903	− .000 05
6.6	+ .013 426	− .000 34	10.6	+ .005 0898	− .000 05
6.8	+ .012 620	− .000 30	10.8	+ .004 9006	− .000 04
7.0	+ .011 8860	− .000 26	11.0	+ .004 7217	− .000 04
7.2	+ .011 2145	− .000 23	11.2	+ .004 5526	− .000 04
7.4	+ .010 5990	− .000 21	11.4	+ .004 3924	− .000 03
7.6	+ .010 0332	− .000 19	11.6	+ .004 2405	− .000 03
7.8	+ .009 5119	− .000 17	11.8	+ .004 0964	− .000 03
8.0	+0.009 0306	−0.000 15	12.0	+0.003 9595	−0.000 03

A comparison of the results obtained from the series expansion with Hjerting's table at a few representative points showed no differences exceeding 0.6 units in his last place. A comparison at $a = 0.5$ (which is, of course, beyond the limit of usefulness of the series expansion for small values of v) did not agree with M. Born's values;[7] but the differences found by comparison with Mitchell and Zemansky's tabulation,[8] amounting to 0.007 at $v = 0.0$, -0.005 at $v = 1.0$, and 0.001 at $v = 2.0$, can be completely accounted for by the contribution of the higher-order terms, which we have neglected.

For values of v larger than 12 the asymptotic forms,

$$H_1(v) = 0.56419v^{-2} + 0.846v^{-4}, \quad \text{and} \quad H_3(v) = -0.56v^{-4}, \tag{6}$$

can be used to give four-figure accuracy.

For most astronomical applications only the first two terms in the expansion (3) are required, but it is a simple matter to determine the number of terms required to obtain the accuracy desired in any particular case.

I am indebted to Dr. Chandrasekhar for his helpful suggestions and advice regarding these computations.

[7] *Optik* (Berlin: J. Springer, 1933), p. 486.

[8] *Op. cit.*, p. 329.

THE EFFECT OF ELECTRON SCATTERING ON THE LINE SPECTRUM OF HIGH-TEMPERATURE STARS

GUIDO MÜNCH
Yerkes Observatory
Received May 4, 1948

ABSTRACT

In this paper the problem of the transfer of radiation in an atmosphere of free electrons in thermal motion is considered. Proper allowance is made for the noncoherency of the scattered radiation, but the Compton shifts in frequency of the scattered quanta are ignored. By using a Fourier integral transformation over the frequency, the equation of transfer and the relevant boundary conditions are reduced to subsidiary forms. It is shown, further, that the transformed equation of transfer can be solved, in the space of the auxiliary variable, by the standard methods of transfer theory. The explicit solution found in a first approximation is inverted, and the dependence on frequency of the emergent radiation is studied.

The final solution to the problem is written down as the sum of two terms: one representing the fraction of the incident radiation which emerges without having suffered any scattering process and the other representing the diffuse radiation which has arisen after one or more scattering processes. This diffuse radiation for incident monochromatic light has been evaluated numerically and its values tabulated for four optical thicknesses of the electron atmosphere. The numerical examples studied for hypothetical absorption lines reveal that the main effect of the noncoherency of the electron scattering is to fill the center of the lines with radiation from the neighboring continuum and to produce very extended and shallow wings.

Finally, some general remarks are made concerning the relationship between the properties of the solutions found and certain characteristics of the line spectrum of high-temperature stars.

1. *Introduction.*—The scattering of radiation by free electrons plays an important role in the atmospheres of high-temperature stars. Thus it is now generally accepted[1] that electron scattering is one of the main sources of continuous opacity in main-sequence stars of types O and early B. And it has been pointed out by J. L. Greenstein[2] that it is probably electron scattering which is responsible for the absolute-magnitude effect shown by the Balmer discontinuity in the spectra of B and early A supergiants. More recently, S. Chandrasekhar[3] has studied the polarization effects in an electron-scattering atmosphere and has shown that a degree of polarization, to the extent of 11 per cent at the limb, should be expected in a star in which electron scattering is the only source of opacity. This prediction, according to a preliminary announcement by W. A. Hiltner,[4] seems to be confirmed by the observations of the eclipsing B-type star RY Persei, the light of which shows some degree of polarization during the phases of the eclipse close to totality. In view of these investigations on the part played by electron scattering in the atmospheres of early-type stars, S. Chandrasekhar[5] has drawn attention to the possibility of broadening and shifts and to the importance, in these connections, of an early paper by Dirac[6] on the effect of Compton scattering by free electrons, in which allowance is also made for the thermal motions of the electrons. Indeed, Dirac's paper provides the basic physical foundations for all these developments. In this paper we shall discuss the transfer of monochromatic radiation through an assembly of free electrons in thermal

[1] A. Unsöld, *Zs. f. Ap.*, **21**, 229, 1942; M. Rudkjøbing, *On the Atmospheres of B Stars* (dissertation; Copenhagen, 1947); Anne B. Underhill, *Ap. J.*, **107**, 349, 1948.

[2] *Ap. J.*, **95**, 299, 1942.

[3] *Ap. J.*, **103**, 351, 1946.

[4] *Ap. J.*, **106**, 231, 1947.

[5] In a discussion held at the Yerkes Observatory (unpublished).

[6] *M.N.*, **85**, 825, 1925.

motion, on the basis of the results obtained by Dirac and following the modern methods used in transfer theory.[7]

2. *The formulation of the problem and the equation of transfer.*—According to Dirac,[8] when monochromatic radiation of intensity $I(\nu')d\nu'$, of frequency ν', is scattered by N_e electrons having a Maxwellian distribution of velocities at a certain temperature T, the intensity of radiation $j(\nu)$ (per unit frequency range and unit solid angle) scattered in the frequency ν and in a direction making an angle Θ to the direction of $I(\nu')$ is given by an equation of the form

$$j(\nu) = \int_{(\omega)} \frac{d\omega}{4\pi} N_e \int_0^\infty \sigma(\nu')\, p(\Theta, \nu')\, I(\nu')\, \psi(\Theta; \nu, \nu')\, d\nu', \tag{1}$$

where the integral over the solid angles ω is to be carried out over the whole sphere. In equation (1), $\sigma(\nu')$ denotes the cross-section of an electron for radiation of frequency ν'; $p(\Theta, \nu')$ is the phase function for scattering; and $\psi(\Theta; \nu, \nu')$ is the probability distribution that a quantum originally of frequency ν' will have the frequency ν when scattered in the direction Θ. In a first approximation, for radiation in the visible region, we may neglect the quantum effects associated with the Compton effect and departures from the classical Thomson scattering coefficient. In this approximation we may take $\sigma(\nu')$ and $p(\Theta, \nu')$ the Thomson values

$$\sigma = \sigma_e = \frac{8\pi}{3} \frac{e^4}{m^2 c^4} \tag{2}$$

and

$$p(\Theta, \nu') = \tfrac{3}{4}(1 + \cos^2\Theta), \tag{3}$$

while $\psi(\Theta; \nu, \nu')$ takes the simple form

$$\psi(\Theta; \nu, \nu') = \left[\frac{mc^2}{4\pi kT(1-\cos\Theta)}\right]^{1/2} \frac{1}{\nu} \exp\left\{-\frac{mc^2(\nu-\nu')^2}{4kT(1-\cos\Theta)\nu^2}\right\}. \tag{4}$$

Equation (4) is due to Dirac. In higher approximations the distribution function, $\psi(\Theta; \nu, \nu')$, becomes much more complicated; but, in general, we may describe the situation by saying that, superimposed on a broadening of the type given by equation (4), there is a shift in frequency of the scattered radiation, which is of the order of magnitude of the Compton wave length (0.024 angstrom units), but which may be either to the red or to the violet, depending on the temperature T and the frequency ν. It would appear that the solution of a transfer problem involving the most general laws of the scattering process would be difficult to obtain. But it would seem that we may get a reliable picture of what may be expected to happen by separating, first, the problem of the shift from the problem of the broadening. The former effect has been considered by Chandrasekhar;[9] the latter will be examined in this paper. With this understanding, we shall now formulate the problem that we intend to study.

A plane-infinite surface S emits radiation in the outward direction with a known distribution in frequency and in angle. Above this radiating surface there is an atmosphere of free electrons, stratified in layers parallel to S and of finite optical thickness τ_1. Under the assumption that the electrons scatter radiation according to the laws expressed by equations (1)–(4), we are required to find the dependence in frequency and angle of the emergent radiation.

If we denote by z the distance from S to any point in the atmosphere, by N_e the num-

[7] For a summary of these methods see S. Chandrasekhar, "Josiah Willard Gibbs Lecture," *Bull. Amer. Math. Soc.*, **53**, 641–711, 1947.

[8] *Op. cit.*, eqs. (8)–(13).

[9] *Proc. R. Soc. London, A*, **192**, 508, 1948.

ber of electrons per unit volume, and by ϑ $(= \cos^{-1}\mu)$ the direction to the outward normal, the equation of transfer for our problem can be written in the form

$$-\mu \frac{\partial I(z,\mu,\nu)}{\sigma_e N_e \partial z} = I(z,\mu,\nu) - \mathcal{J}(z,\mu,\nu). \tag{5}$$

According to equations (1)–(4), the source function is given by

$$\mathcal{J}(z,\mu,\nu) = \frac{j(z,\mu,\nu)}{\sigma_e N_e} = \frac{3}{16\pi}\int_0^{2\pi}\int_{-1}^{+1}(1+\cos^2\Theta)\,d\mu'd\varphi\int_0^{\infty} I(z,\mu',\nu')\,\psi(\Theta;\nu,\nu')\,d\nu', \tag{6}$$

where it may be noted that

$$\cos\Theta = \mu\mu' + (1-\mu^2)^{1/2}(1-\mu'^2)^{1/2}\cos\varphi. \tag{7}$$

Equation (4) has to be solved with the boundary conditions

$$I(z=0,\mu,\nu) = I^{(0)}(\mu,\nu) \qquad \text{for} \qquad \mu > 0 \tag{8}$$

and

$$I(z=z_1,\mu,\nu) \equiv 0 \qquad \text{for} \qquad \mu < 0, \tag{9}$$

indicating, respectively, that the outward intensity at the radiating surface, $I^{(0)}(\mu,\nu)$ is assigned and that there is no radiation incident on the atmosphere from above. In order to reduce equation (5) to a form appropriate for solution, we shall introduce the optical depth, τ, as the variable

$$d\tau = -\sigma_e N_e dz. \tag{10}$$

Further, we shall measure the frequencies in units of the quantity $\nu_0(4kT/mc^2)^{1/2}$ from the fixed frequency ν_0, and write

$$\alpha = \left(\frac{mc^2}{4kT}\right)^{1/2}\frac{\nu-\nu_0}{\nu_0}. \tag{11}$$

In terms of these new variables we re-write our equation of transfer in the form

$$\mu\frac{\partial I}{\partial\tau} = I(\tau,\mu,\alpha) - \frac{3}{16\pi}\int_0^{2\pi}\int_{-1}^{+1} H(\tau,\Theta,\alpha)(1+\cos^2\Theta)\,d\mu'd\varphi, \tag{12}$$

where

$$H(\tau,\Theta,\alpha) = \frac{1}{\sqrt{\pi}}\int_{-\infty}^{\infty} I(\alpha')\frac{e^{-(\alpha-\alpha')^2/(1-\cos\Theta)}}{(1-\cos\Theta)^{1/2}}\,d\alpha'. \tag{13}$$

It will be noticed that, in writing the source function as it appears in equations (12) and (13), the quantity $\nu(4kT/mc^2)^{1/2}$ has been replaced by $\nu_0(4kT/mc^2)^{1/2}$; but this substitution is entirely justified in the present problem.

The boundary conditions under which we have to solve equation (12) are, in terms of the new variables,

$$I(\tau=\tau_1,\mu,\alpha) = I^{(0)}(\mu,\alpha) \tag{14}$$

and

$$I(\tau=0,-\mu,\alpha) \equiv 0 \qquad \text{for} \qquad \mu \geqslant 0. \tag{15}$$

3. *The solution of the equation of transfer.*—The equation of transfer (12), as it stands, cannot be solved by the methods usually employed in transfer theory, because in the source function the frequencies appear mixed. It is possible, however, to reduce it to an

equation for the intensity depending on only one subsidiary variable, by applying to the equation of transfer and the boundary conditions an integral transformation with respect to the frequency. The form of equation (13) and of the boundary conditions are such that a Fourier transformation is the most advantageous. Thus, multiplying equation (12) by $e^{i\alpha\xi}d\alpha/(2\pi)^{1/2}$ and integrating over all α's, we get, formally,

$$\mu\frac{\partial\mathfrak{I}}{\partial\tau}=\mathfrak{I}(\tau,\mu,\xi)-\frac{3}{16\pi}\int_0^{2\pi}\int_{-1}^{+1}\mathfrak{H}(\tau,\Theta,\xi)(1+\cos^2\Theta)\,d\mu'd\varphi, \tag{16}$$

where

$$\mathfrak{I}(\tau,\mu,\xi)=(2\pi)^{-1/2}\int_{-\infty}^{+\infty}I(\tau,\mu,\alpha)\,e^{i\alpha\xi}d\alpha \tag{17}$$

and

$$\mathfrak{H}(\tau,\Theta,\xi)=(2\pi)^{-1/2}\int_{-\infty}^{+\infty}H(\tau,\Theta,\alpha)\,e^{i\alpha\xi}d\alpha. \tag{18}$$

Simultaneously, we transform the boundary conditions (14) and (15) to the forms

$$\left.\begin{aligned}&\mathfrak{I}(\tau=\tau_1,\mu,\xi)=\mathfrak{I}^{(0)}(\mu,\xi)\qquad(19)\\ \text{and}\qquad&\mathfrak{I}(\tau=0,-\mu,\xi)\equiv 0\qquad(20)\end{aligned}\right\}(\mu\gtrless 0).$$

We shall now (again formally) evaluate the integral appearing in equation (18) from the definition given in equation (13). We have

$$\mathfrak{H}(\tau,\Theta,\xi)=\int_{-\infty}^{+\infty}\frac{e^{i\alpha\xi}}{\pi\sqrt{2}}\left\{\int_{-\infty}^{+\infty}I(\tau,\mu',\alpha')\frac{e^{-(\alpha-\alpha')^2/(1-\cos\Theta)}}{(1-\cos\Theta)^{1/2}}\,d\alpha'\right\}d\alpha. \tag{21}$$

Assuming the validity of the interchange in the order of the integrations over α and α', we obtain

$$\mathfrak{H}(\tau,\Theta,\xi)=\int_{-\infty}^{+\infty}\frac{I(\tau,\mu',\alpha')}{\pi\sqrt{2}}\times\left\{\int_{-\infty}^{+\infty}\frac{\exp\{i\alpha\xi-(\alpha-\alpha')^2/(1-\cos\Theta)\}}{(1-\cos\Theta)^{1/2}}\,d\alpha\right\}d\alpha'. \tag{22}$$

Now, introducing $\beta=\alpha-\alpha'$ in place of α as variable of integration, we have

$$\begin{aligned}\mathfrak{H}(\tau,\Theta,\xi)&=\frac{1}{\pi\sqrt{2}}\int_{-\infty}^{+\infty}I(\tau,\mu',\alpha')\,e^{i\alpha'\xi}d\alpha'\\&\qquad\times\int_{-\infty}^{+\infty}\frac{\exp\{-\beta^2/(1-\cos\Theta)+i\beta\xi\}}{(1-\cos\Theta)^{1/2}}\,d\beta\\&=\mathfrak{I}(\tau,\mu',\xi)\,e^{-\xi^2(1-\cos\Theta)/4}\,\frac{1}{\sqrt{\pi}}\int_{-\infty}^{+\infty}\exp\left\{-\left[\frac{\beta}{(1-\cos\Theta)^{1/2}}\right.\right.\\&\left.\left.-\frac{i\xi(1-\cos\Theta)^{1/2}}{2}\right]^2\right\}\frac{d\beta}{(1-\cos\Theta)^{1/2}}=\mathfrak{I}(\tau,\mu',\xi)\,e^{-\xi^2(1-\cos\Theta)/4}.\end{aligned} \tag{23}$$

Using this result, we may write the transformed equation of transfer (16) in the form

$$\mu\frac{\partial\mathfrak{I}}{\partial\tau}=\mathfrak{I}(\tau,\mu,\xi)-\frac{3}{8}\int_{-1}^{+1}\mathfrak{I}(\tau,\mu',\xi)\,p(\xi,\mu,\mu')\,d\mu', \tag{24}$$

where

$$p(\xi,\mu,\mu')=\frac{1}{2\pi}\int_0^{2\pi}(1+\cos^2\Theta)\,e^{-\xi^2(1-\cos\Theta)/4}d\varphi \tag{25}$$

plays formally, in equation (24), the role of a phase function. Equation (25) can be evaluated in terms of the Bessel functions $I_n(x)$ with an imaginary argument, by substituting according to equation (7) and making use of the relation

$$I_n(x) = \frac{1}{\pi}\int^{\pi} e^{x\cos\varphi}\cos n\varphi\, d\varphi \qquad (n \text{ integer}) . \quad (26)^{10}$$

We thus obtain

$$\begin{aligned} p(\xi,\mu,\mu') = {} & e^{-\xi^2(1-\mu\mu')/4} \\ & \times \{ [1+\mu^2\mu'^2+\tfrac{1}{2}(1-\mu^2)(1-\mu'^2)]\, I_0(\tfrac{1}{4}\xi^2[1-\mu^2]^{1/2}[1-\mu'^2]^{1/2}) \\ & + 2\mu\mu'(1-\mu^2)^{1/2}(1-\mu'^2)^{1/2} I_1(\tfrac{1}{4}\xi^2[1-\mu^2]^{1/2}[1-\mu'^2]^{1/2}) \\ & + \tfrac{1}{2}(1-\mu^2)(1-\mu'^2)\, I_2(\tfrac{1}{4}\xi^2[1-\mu^2]^{1/2}[1-\mu'^2]^{1/2}) \}. \end{aligned} \quad (27)$$

The justification of the process of Fourier transformation of the equation of transfer which we have followed is likely to be a difficult matter, as we cannot write down the exact solution of equation (24). However, we can solve equation (22) by the approximate methods now employed in transfer theory, and within any particular approximation (with respect to μ) we can justify the dependence on frequency of the solution, as given by the Fourier transforms. Accordingly, we replace the subsidiary equation of transfer by the system of linear differential equations,

$$\mu_i \frac{\partial \mathfrak{I}_i}{\partial \tau} = \mathfrak{I}_i(\tau,\xi) - \frac{3}{8}\sum_{j=-n}^{+n} a_j p(\xi,\mu_i,\mu_j)\,\mathfrak{I}_j(\tau,\xi) \quad (i = \pm 1, \pm 2, \ldots, \pm n), \quad (28)$$

where the μ_i's are the zeros of the Legendre polynomial $P_{2n}(\mu)$ and the a_j's are the appropriate weights in Gauss's formula for numerical quadratures. Moreover, in equation (28), we have written $\mathfrak{I}(\tau, \mu_i, \xi) = \mathfrak{I}_i(\tau, \xi)$.

In principle there is no essential difficulty in solving equation (28) in any given approximation. In practice, however, the amount of numerical work involved in obtaining solutions in approximations higher than the first would be very great. In any event, in a first survey of the problem such as this one, it is sufficient to restrict one's self to the first approximation, because we know, from other problems of radiative transfer, that the first approximation gives at least the right order of magnitude for the solution.

For $n = 1$ the system of equations (28) reduces to the pair

$$\frac{1}{\sqrt{3}}\frac{\partial \mathfrak{I}_{+1}}{\partial \tau} = \mathfrak{I}_{+1} - [M(\xi)\,\mathfrak{I}_{+1} + N(\xi)\,\mathfrak{I}_{-1}] \quad (29)$$

and

$$-\frac{1}{\sqrt{3}}\frac{\partial \mathfrak{I}_{-1}}{\partial \tau} = \mathfrak{I}_{-1} - [N(\xi)\,\mathfrak{I}_{+1} + M(\xi)\,\mathfrak{I}_{-1}], \quad (30)$$

where $M(\xi)$ and $N(\xi)$ have the values (cf. eq. [27])

$$M(\xi) = \tfrac{1}{2}\, e^{-\xi^2/6}\left[I_0\left(\frac{\xi^2}{6}\right) + \tfrac{1}{3} I_1\left(\frac{\xi^2}{6}\right) + \tfrac{1}{6} I_2\left(\frac{\xi^2}{6}\right)\right] \quad (31)$$

and

$$N(\xi) = \tfrac{1}{2}\, e^{-\xi^2/3}\left[I_0\left(\frac{\xi^2}{6}\right) - \tfrac{1}{3} I_1\left(\frac{\xi^2}{6}\right) + \tfrac{1}{6} I_2\left(\frac{\xi^2}{6}\right)\right]. \quad (32)$$

[10] Cf. G. N. Watson, *Treatise on the Theory of Bessel Functions* (Cambridge: At the University Press, 1944), eq. (6.22.4), p. 181. In order to preserve a standard notation, we designate the Bessel functions of imaginary argument by $I_n(x)$; there is no real danger of confusing them with our intensities $I(\tau, \mu, \alpha)$.

The general solution of equations (29) and (30) can be written down immediately in the form

$$\mathfrak{I}_{+1}(\tau, \xi) = A(\xi)\, e^{\chi\tau} + B(\xi)\, e^{-\chi\tau} \tag{33}$$

and

$$\mathfrak{I}_{-1}(\tau, \xi) = \frac{A(\xi)}{N}\left(1 - M - \frac{\chi}{\sqrt{3}}\right) e^{\chi\tau} + \frac{B(\xi)}{N}\left(1 - M + \frac{\chi}{\sqrt{3}}\right) e^{-\chi\tau}, \tag{34}$$

where $A(\xi)$ and $B(\xi)$ are two arbitrary functions of their argument and

$$\chi = \chi(\xi) = [1 - M(\xi) - N(\xi)]^{1/2}[1 - M(\xi) + N(\xi)]^{1/2}\sqrt{3}\,. \tag{35}$$

The functions $A(\xi)$ and $B(\xi)$ are determined from the boundary conditions, which in the first approximation are

$$\mathfrak{I}_{+1}(\tau = \tau_1, \xi) = \mathfrak{I}^{(0)}(\mu_1, \xi) = \mathfrak{I}^{(0)}(\xi) \tag{36}$$

and

$$\mathfrak{I}_{-1}(\tau = 0, \xi) \equiv 0\,. \tag{37}$$

From equations (36) and (37) we find that

$$A(\xi) = \frac{(1 - M + \chi/\sqrt{3})\,\mathfrak{I}^{(0)}(\xi)}{(1 - M + \chi/\sqrt{3})\, e^{\chi\tau_1} - (1 - M - \chi/\sqrt{3})\, e^{-\chi\tau_1}} \tag{38}$$

and

$$B(\xi) = \frac{-(1 - M - \chi\sqrt{3})\,\mathfrak{I}^{(0)}(\xi)}{(1 - M + \chi/\sqrt{3})\, e^{\chi\tau_1} - (1 - M - \chi/\sqrt{3})\, e^{-\chi\tau_1}}. \tag{39}$$

Our solutions for $\mathfrak{I}_{+1}(\tau, \xi)$ and $\mathfrak{I}_{-1}(\tau, \xi)$ are therefore

$$\mathfrak{I}_{+1}(\tau, \xi) = \frac{(1 - M + \chi/\sqrt{3})\, e^{\chi\tau} - (1 - M - \chi/\sqrt{3})\, e^{-\chi\tau}}{(1 - M + \chi/\sqrt{3})\, e^{\chi\tau_1} - (1 - M - \chi/\sqrt{3})\, e^{-\chi\tau_1}}\,\mathfrak{I}^{(0)}(\xi) \tag{40}$$

and

$$\mathfrak{I}_{-1}(\tau, \xi) = \frac{N(\xi)(e^{\chi\tau} - e^{-\chi\tau})}{(1 - M + \chi/\sqrt{3})\, e^{\chi\tau_1} - (1 - M - \chi/\sqrt{3})\, e^{-\chi\tau_1}}\,\mathfrak{I}^{(0)}(\xi). \tag{41}$$

We are primarily interested in the emergent flux, which in the first approximation is simply proportional to $I_{+1}(\tau = 0, a)$. From equation (4) we can write $\mathfrak{I}_{+1}(\tau = 0, \xi) = \mathfrak{I}_{+1}(\xi)$ in the form

$$\mathfrak{I}_{+1}(\xi) = \Gamma(\tau_1, \xi)\,\mathfrak{I}^{(0)}(\xi)\,, \tag{42}$$

where

$$\frac{1}{\Gamma(\tau_1, \xi)} = \cosh \chi\tau_1 + \frac{(1 - M)\sqrt{3}}{\chi}\sinh \chi\tau_1\,. \tag{43}$$

Formally, we can obtain our solution for the emergent intensity by applying the inverse Fourier transformation to the solution (42). Thus

$$I_{+1}(a) = (2\pi)^{-1/2}\int_{-\infty}^{+\infty}\Gamma(\tau_1, \xi)\,\mathfrak{I}^{(0)}(\xi)\, e^{-ia\xi}d\xi\,. \tag{44}$$

Now we shall consider very briefly how the purely formal process that we have carried so far can be justified. In order to be able to apply the fundamental proposition of the theory of Fourier integrals (Plancherel's theorem),[11] we require the square integrability of the given function $I^{(0)}(\mu, a)$, for all values of μ:

$$\int_{-\infty}^{+\infty} |\, I^{(0)}(\mu, a)\,|^2 da < \infty\,. \tag{45}$$

[11] Cf. E. C. Titchmarsh, *Introduction to the Theory of Fourier Integrals* (Oxford: Clarendon Press, 1937), Theorem 48, p. 69. Also R. E. Paley and N. Wiener, "Fourier Transforms in the Complex Domain," *Coll. Pub. Amer. Math. Soc.*, **19**, 2.

Under this condition, the transform $\mathfrak{I}^{(0)}(\mu, \xi)$ exists and is integrable square. On the other hand, as we shall show later, the function $\Gamma(\tau_1, \xi)$ is bounded for every ξ and τ_1. From equation (42) it then follows that $\mathfrak{I}_{+1}(\xi)$ is also integrable square, and therefore the inversion of the Fourier integral carried out in equation (44) is justified.

4. *General properties of the emergent radiation.*—In order to study the properties of our solution for $I_{+1}(a)$, given by equation (44), we need to analyze, first, the general character of the function $\Gamma(\tau_1, \xi)$ defined by equation (43). According to equations (31), (32), (35), and (43), $\Gamma(\tau_1, \xi)$ is an even function of ξ, continuous for every value of ξ. Moreover, from the properties of the Bessel functions of imaginary argument, it can be readily proved that $\Gamma(\tau_1, \xi)$ decreases monotonically from the value

$$\Gamma(\tau_1, \xi = 0) = \frac{1}{1 + \frac{1}{2}\tau_1\sqrt{3}} \tag{46}$$

to the limit

$$\Gamma(\tau_1, \xi) \to e^{-\tau_1\sqrt{3}} \qquad \text{as} \qquad \xi \to \pm\infty\ . \tag{47}$$

More particularly, the asymptotic expansion, of which relation (47) represents the dominant term, is

$$\begin{aligned}\Gamma(\tau_1, \xi) &\to e^{-\mathfrak{x}(\xi)\tau_1} \\ &\simeq e^{-\tau_1\sqrt{3}} \exp\left\{\frac{9\tau_1}{4\sqrt{\pi}}\left(\frac{1}{|\xi|} - \frac{5}{4}\frac{1}{|\xi|^3} + \frac{129}{32}\frac{1}{|\xi|^5} + \frac{1665}{128}\frac{1}{|\xi|^7} + \cdots\right)\right\}.\end{aligned} \tag{48}$$

From this we conclude that $\Gamma(\tau_1, \xi)$, as stated at the end of the preceding paragraph, is a bounded function of ξ, for every real ξ.

It seems unlikely that the integral appearing in equation (44) could be evaluated in an explicit form, for functions $\mathfrak{I}^{(0)}(\xi)$ which are of practical interest. Therefore, it is convenient to transform it to a form suitable for numerical calculations. With this point in mind, we shall re-write equation (44) in the form

$$\begin{aligned}I_{+1}(a) = {} & \frac{e^{-\tau_1\sqrt{3}}}{(2\pi)^{1/2}}\int_{-\infty}^{+\infty}\mathfrak{I}^{(0)}(\xi)\left(1 + \frac{9\tau_1/4\sqrt{\pi}}{1+|\xi|}\right)e^{-ia\xi}d\xi \\ & + \frac{1}{(2\pi)^{1/2}}\int_{-\infty}^{+\infty}\mathfrak{I}^{(0)}(\xi)\left[\Gamma(\tau_1, \xi) - e^{-\tau_1\sqrt{3}}\left(1 + \frac{9\tau_1/4\sqrt{\pi}}{1+|\xi|}\right)\right]e^{-ia\xi}d\xi\ .\end{aligned} \tag{49}$$

With the definitions

$$\Gamma(\tau_1, \xi) - e^{-\tau_1\sqrt{3}}\left(1 + \frac{9\tau_1/4\sqrt{\pi}}{1+|\xi|}\right) = \mathfrak{G}(\tau_1, \xi) \tag{50}$$

and

$$\frac{9\tau_1 e^{-\tau_1\sqrt{3}}}{4\sqrt{\pi}} = K(\tau_1) \tag{51}$$

and, noticing that by Plancherel's theorem we have

$$\frac{1}{(2\pi)^{1/2}}\int_{-\infty}^{+\infty}\mathfrak{I}^{(0)}(\xi)\, e^{-ia\xi}d\xi = I^{(0)}(a)\,, \tag{52}$$

we can re-write equation (49) in the form

$$I_{+1}(a) = e^{-\tau_1\sqrt{3}}I^{(0)}(a) + \frac{1}{(2\pi)^{1/2}}\int_{-\infty}^{\infty}\mathfrak{I}^{(0)}(\xi)\left[\mathfrak{G}(\tau_1, \xi) + \frac{K(\tau_1)}{1+|\xi|}\right]e^{-ia\xi}d\xi\ . \tag{53}$$

We now apply to the integral appearing in equation (53) one of Parseval's formulae,[12] according to which, if $F(x)$ and $G(x)$ are Fourier transforms of $f(u)$ and $g(u)$, respectively, we have

$$\int_{-\infty}^{+\infty} F(t)\,G(t)\;e^{-ixt}dt = \int_{-\infty}^{+\infty} f(u)\;g(x-u)\;du\,. \tag{54}$$

Thus we obtain, finally,

$$I_{+1}(a) = e^{-\tau_1\sqrt{3}}I^{(0)}(a) + \int_{-\infty}^{+\infty} I^{(0)}(\beta)\,\Delta(\tau_1;\, a-\beta)\,d\beta\,, \tag{55}$$

where

$$\Delta(\tau_1,\, a) = \frac{1}{2\pi}\int_{-\infty}^{+\infty}\left[\mathfrak{G}(\tau_1,\,\xi) + \frac{K(\tau_1)}{1+|\xi|}\right]e^{-ia\xi}d\xi\,. \tag{56}$$

Our solution, written in the form of equation (55), admits of a very simple physical interpretation. The first term, $e^{-\tau_1\sqrt{3}}I^{(0)}(a)$, represents that part of the radiation incident at $\tau = \tau_1$ which emerges without having suffered any scattering process in the atmosphere, while the second term represents the emergent diffuse radiation, which has been scattered one or more times.

From the form of equation (55) it would appear that the exact solution for the emergent intensity will have the general form

$$I(\mu,\, a) = e^{-\tau_1/\mu}I^{(0)}(\mu,\, a) + \int_{-\infty}^{+\infty} I^{(0)}(\mu,\,\beta)\,\Phi(\tau_1,\,\mu,\, a-\beta)\,d\beta\,, \tag{57}$$

where $\Phi(\tau_1, \mu, a)$ is a certain function which has probably, in its dependence on τ_1 and a, the same form as $\Delta(\tau_1, a)$.

5. *The scattered radiation from incident monochromatic light. Verification of the flux integral.*—The form of the term representing the diffuse radiation in equation (55) allows us to conclude that the function $\Delta(\tau_1, a)$ describes the spectral distribution of the emergent radiation for incident monochromatic light of unit total intensity, i.e., for an incident δ-function. The function $\Delta(\tau_1, a)$ has therefore an immediate physical significance. We shall now evaluate $\Delta(\tau_1, a)$ numerically in accordance with equation (56). Since $\Gamma(\tau_1, \xi)$ is an even function of ξ (cf. eq. [50]), we may write equation (56) in the form

$$\Delta(\tau_1,\, a) = \frac{1}{\pi}\int_0^{\infty}\mathfrak{G}(\tau_1,\,\xi)\cos a\xi\,d\xi + \frac{K(\tau_1)}{\pi}\int_0^{\infty}\frac{\cos a\xi}{1+\xi}\,d\xi\,. \tag{58}$$

The second integral of the right-hand side can be evaluated in terms of the sine and cosine exponential integrals,

$$Si\,a = \int_0^a \frac{\sin t}{t}\,dt \qquad \text{and} \qquad Ci\,a = \int_{\infty}^a \frac{\cos t}{t}\,dt\,, \tag{59}$$

in the form

$$\frac{K(\tau_1)}{\pi}\int_0^{\infty}\frac{\cos a\xi}{1+\xi}\,d\xi = \frac{K(\tau_1)}{\pi}\left[\left(\frac{\pi}{2} - Si\,a\right)\sin a - Ci\,a\cos a\right]. \tag{60}$$

The function $\mathfrak{G}(\tau_1, \xi)$, according to equations (50) and (48), is bounded for every ξ and, as $\xi \to \infty$, tends to zero as $1/\xi(1+\xi)$. Therefore, its cosine transform is finite for every a (including $a = 0$). The second term of $\Delta(\tau_1, a)$, however, has a logarithmic singularity at $a = 0$, according to the series development[13]

$$Ci\,a = \log a + \gamma - \frac{a^2}{2!2} + \frac{a^4}{4!4} - \cdots\,, \tag{61}$$

[12] Cf. Titchmarsh, *op. cit.*, eq. (2.1.8), p. 51.

[13] Cf. E. Jahnke and F. Emde, *Tables of Functions* (New York: Dover Press, 1943), pp. 2–3.

where γ ($=0.57721\ldots$) is the Euler-Mascheroni constant, and $\log a$ stands for the natural logarithm of a. In view of this circumstance, it is convenient to isolate the singularity and compute numerically the function $\Delta_0(\tau_1, a)$ defined by

$$\Delta_0(\tau_1, a) = \begin{cases} \Delta(\tau_1, a) + \dfrac{K(\tau_1)}{\pi} \log a & \text{for} \quad 0 \leqslant a \leqslant 1 \\ \Delta(\tau_1, a) & \text{for} \quad a \geqslant 1 \end{cases}. \tag{62}$$

The integral appearing in the expression (58) for $\Delta(\tau_1, a)$ has been evaluated numerically following standard procedures, up to a certain $\xi = \xi^*$, chosen in such a way that, for $\xi \geqslant \xi^*$, $\mathfrak{G}(\tau_1, \xi)$ could be evaluated accurately by means of the asymptotic series obtained from equations (50) and (48). From the point ξ^* to ∞, the integral was evaluated by integrating, term by term, the asymptotic series for $\mathfrak{G}(\tau_1, \xi)$. The results of the calculations are given in Table 1. It is believed that the values listed in Table 1 are accurate to three significant figures.

TABLE 1

THE FUNCTION $\Delta_0(\tau_1, a)$

τ_1	a							
	0.00	0.25	0.50	1.0	1.5	2.0	3.0	4.0
0.1.....	−0.0029	−0.0013	+0.0024	+0.0087	+0.00274	+0.00078	+0.000065	+0.0000056
.2.....	− .0002	+ .0023	+ .0069	+ .0170	+ .00596	+ .00189	+ .000213	+ .000023
.4*.....	+ .0175	+ .0189	+ .0214	+ .0314	+ .01165	+ .00483	+ .000916	+ .000171
0.8.....	+0.0609	+0.0567	+0.0532	+0.0516	+0.02438	+0.01149	+0.002657	+0.000571

* The entries in this line are, strictly, for $\tau_1 = 0.3960$; but we shall refer to it throughout as "0.4."

The values of $\Delta_0(\tau_1, a)$ given in Table 1 enable us to compute, from equation (62), the function $\Delta(\tau_1, a)$. In Figure 1 we have plotted the function $\Delta(\tau_1, a)$, in a wave-length scale, for the case $\lambda_0 = 5000$ A and $T = 30000°$ K.[14]

The results of our numerical calculations should, of course, satisfy the integrals admitted by the original equation of transfer. Thus it is readily verified that if we define $W(\tau, \mu)$ as

$$W(\tau, \mu) = \int_{-\infty}^{\infty} I(\tau, \mu, a)\, da, \tag{63}$$

then the solution of equation (12), integrated over all frequencies a, and which satisfies the relevant boundary conditions (eqs. [13] and [14]), in the first approximation is

$$W(\tau = 0, \mu_1) = \frac{W_0}{1 + \frac{1}{2}\tau_1\sqrt{3}}, \tag{64}$$

where W_0 is the incident radiation $I^{(0)}(\mu_1, a)$, integrated over all frequencies.[15] According to equation (64), for an incident monochromatic radiation, the result of integrating equation (55) over all frequencies must be

$$W = e^{-\tau_1\sqrt{3}} + 2\int_0^{\infty} \Delta(\tau_1, a)\, da = \frac{1}{1 + \frac{1}{2}\tau_1\sqrt{3}}, \tag{65}$$

[14] Cf. eq. (67) below.

[15] We recognize, in eq. (64), the solution in the first approximation of the well-known Schuster problem in line formation (see S. Chandrasekhar, *Rev. Mod. Phys.*, **17**, 138, eq. [130], 1945).

or, in terms of the function $\Delta_0(\tau_1, a)$ defined by equation (62),

$$e^{-\tau_1\sqrt{3}} + \frac{2K(\tau_1)}{\pi} + 2\int_0^\infty \Delta_0(a, \tau_1)\, da = \frac{1}{1+\frac{1}{2}\tau_1\sqrt{3}}. \tag{66}$$

The numerical verification of this equation has been done by integrating graphically the values of the function $\Delta_0(\tau_1, a)$ given in Table 1. In Table 2 we give the values of the different terms appearing in equation (66); and from a comparison of the last two columns of this table we conclude that our numerical determination of $\Delta_0(\tau_1, a)$ satisfies the flux integral accurately enough for our purposes. It is of interest also to notice in Table 2 how the percentage of the radiation which is scattered varies between 57 per cent for $\tau_1 = 0.8$ and 8.6 per cent for $\tau_1 = 0.1$.

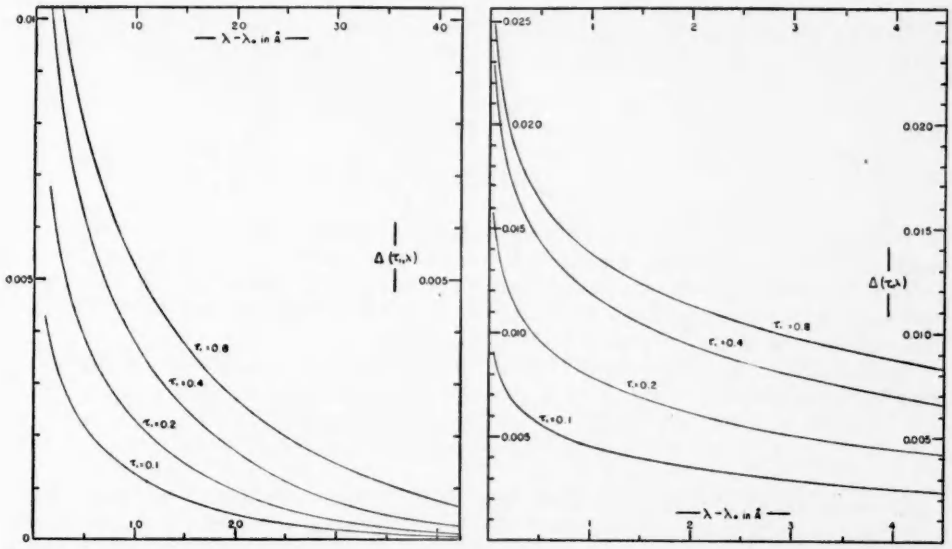

FIG. 1.—The spectral distribution $\Delta(\tau_1, \lambda)$ of the scattered radiation from incident monochromatic light of unit total intensity. (Since the curves are symmetrical about $\lambda = \lambda_0$, only one-half the curves has been illustrated.)

TABLE 2

VERIFICATION OF THE FLUX INTEGRAL

τ_1	$e^{-\tau_1\sqrt{3}}$	$\frac{2K(\tau_1)}{\pi}$	$2\int_0^\infty \Delta_0 da$	Diffuse Radiation		W	$\frac{1}{1+\frac{1}{2}\tau_1\sqrt{3}}$
0.1.....	0.8410	0.0680	0.0112	0.0792	0.0861 W	0.9202	0.9203
.2.....	.7072	.1143	.0299	.1342	.1576 W	.8514	.8534
.4.....	.5036	.1612	.0769	.2381	.3210 W	.7417	.7447
0.8.....	0.2502	0.1617	0.1740	0.3357	0.5730 W	0.5859	0.5907

6. *Numerical examples.*—With the solution of the problem given in a form suitable for numerical calculations, we can now use equation (55) for the computation of some examples. We shall take, as a representative case, an absorption line centered at $\lambda_0 =$ 5000 A and a kinetic temperature of the electrons of 30000° K. From equation (11) we

obtain the relation between our dimensionless variable a and the wave length $\Delta\lambda = \lambda - \lambda_0$:

$$a = \frac{\Delta\lambda}{22.5} \qquad (\Delta\lambda \text{ in angstroms}). \tag{67}$$

Now suppose that the residual intensity, $r(\Delta\lambda)$, of the absorption line, before it is scattered by the electrons, is given in the form

$$r(\Delta\lambda) = 1 - \psi(\Delta\lambda). \tag{68}$$

Then the residual intensity, $R(\Delta\lambda)$, in the contour after scattering, is obtained by substituting $r(\Delta\lambda)$ in place of $I^{(0)}(a)$ in equation (55). According to equation (65), we obtain

$$R(\Delta\lambda) = 1 - (1 + \tfrac{1}{2}\tau_1\sqrt{3})\Psi(\Delta\lambda), \tag{69}$$

where

$$\Psi(\Delta\lambda) = e^{-\tau_1\sqrt{3}}\psi(\Delta\lambda) + \int_{-\infty}^{+\infty} \psi(\Delta\lambda')\Delta(\tau_1, \Delta\lambda - \Delta\lambda')\frac{da}{d(\Delta\lambda')}\,d(\Delta\lambda'). \tag{70}$$

We write the scattered contour in the form of equation (69), in order to follow the usual practice of expressing the residual intensities in units of the continuum. It is of interest to notice at this point that equations (69) and (70), taken together with the result expressed by equation (65), imply that the equivalent width or total intensity of any line is preserved in the process of scattering.

Specifically, let us now suppose that the original line had the form of a Doppler contour of half-width a,

$$\psi(\Delta\lambda) = \frac{W_0}{a(2\pi)^{1/2}}\, e^{-(\Delta\lambda)^2/2a^2}. \tag{71}$$

If we introduce this function into equation (70), it is not difficult to carry out the integrations numerically, by means of the function $\Delta_0(\tau_1, a)$ defined in equation (62) and given in Table 1. The results of such calculations are given graphically in Figure 2, where we have plotted two incident contours of the form (71), with $a = \frac{1}{2}$ A and 1 A and equivalent widths $W_0 = 1$ A and 2 A, respectively. For the sake of clearness we have drawn only the respective emergent contours, after having been scattered by layers of electrons with thickness $\tau_1 = 0.4$ and 0.8. Similar calculations have also been carried out for lines of the form

$$\psi(\Delta\lambda) = \frac{\gamma}{\pi}\frac{W_0}{\gamma^2 + (\Delta\lambda)^2}. \tag{72}$$

The results are exhibited in Figure 3, for the cases $\gamma = 1$ A, $W_0 = 3.14$, and $\gamma = 3$ A, $W_0 = 9.42$.

An inspection of the contours drawn in Figures 2 and 3 reveals that, qualitatively, the main effects of the redistribution in frequency which takes place during the process of scattering can be described as follows: (1) The central parts of the absorption lines are filled in quite appreciably by radiation of the neighboring continuum; the lines, therefore, appear more shallow than those scattered coherently. (2) The removal of energy from the continuum produces very extended and shallow wings. The extent of these wings is approximately the same as the extent of the broadened contours for incident monochromatic light given in Figure 1, since all the lines which we consider in practice are narrow compared with the spectral distribution $\Delta(\tau_1, a)$. For this same reason, the intensity in the wings is proportional to the total intensity of the line (and to $1 + \frac{1}{2}\tau_1\sqrt{3}$) and, for unit equivalent width, is again approximately equal to the intensity of the functions of Figure 1. (3) As mentioned earlier in this paragraph, the scattering process, strictly speaking, does not change the equivalent widths of the scattered lines. However, from

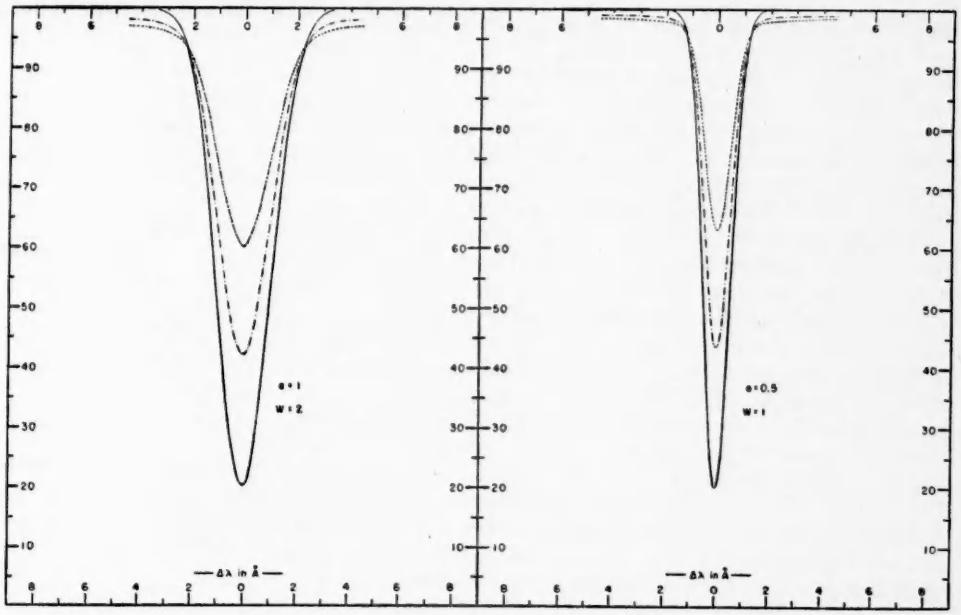

FIG. 2.—The emergent radiation for two incident Doppler contours (*full lines*) of half-widths a and equivalent widths W, after scattering by layers of electrons of optical thicknesses $\tau_1 = 0.8$ (*dotted lines*) and $\tau_1 = 0.4$ (*dot-and-dash lines*).

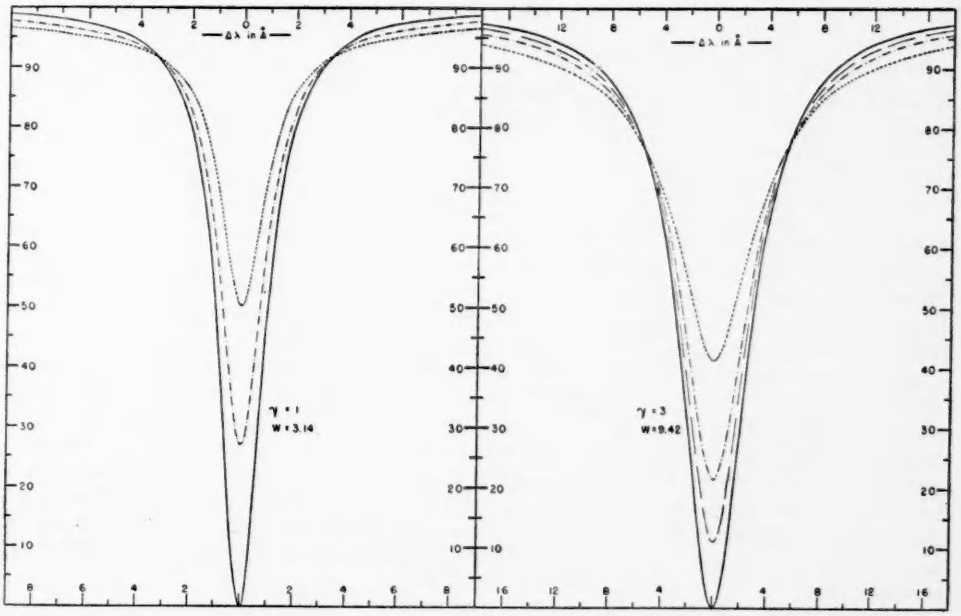

FIG. 3.—The emergent radiation for two incident damping contours (*full lines*) of half-breadths γ and equivalent widths W, after scattering by layers of electrons of optical thicknesses $\tau_1 = 0.8$ (*dotted lines*), and $\tau_1 = 0.4$ (*dot-and-dash lines*), and $\tau_1 = 0.2$ (*dashed lines*). (Notice the difference in the wave-length scale of the two contours.)

an observational point of view, it is apparent that it would be a difficult problem to detect, by the usual methods of photographic spectrophotometry, the faint and extended wings which the scattering produces. Consequently, a significant fraction of the equivalent width W would be missed by an observer trying to measure the total intensity of the line after scattering. In this context we may notice also that lines of different equivalent widths would be affected differently. While for a strong line the extended wings probably could be traced and measured out to a certain distance from the center of the contour, for a weak line the wings would be completely missed.

7. *General remarks.*—We shall briefly consider in this section the possible applications of the effects disclosed by this investigation to the interpretation of the line spectra of high-temperature stars. The first point which should be noticed is that our model, consisting of a layer of electrons superimposed on the layers in which the lines are supposed to have been formed, is likely to be quite adequate to represent the situation in the case of supergiant stars of types earlier than A0 and main-sequence stars earlier than B0. In the outer layers of these stars we may expect the material to be completely ionized as a result of the high temperature and low pressure. To illustrate the point, we may estimate the total number of electrons above the layers in which the lines are principally formed. We shall use for this purpose one of the model atmospheres recently constructed by Miss Underhill.[16] The model represents, approximately, the case of a B2 supergiant. Since in the outer layers the hydrogen is mostly ionized, the scattering coefficient of the electrons, per gram of stellar material, can be taken as having the constant value $\sigma = 0.4$. The optical depth τ_e in electron scattering is therefore given by

$$\tau_e = \int_\infty^z \sigma \rho \, dz = 0.4 \int_\infty^z \rho \, dz \,. \tag{73}$$

The equation of gravitational equilibrium, on the other hand, gives the relation

$$\frac{dp}{g} = -\rho \, dz \tag{74}$$

between ρdz and the pressure p. (As usual, g denotes the surface gravity.) Hence, by combining equations (73) and (74), we obtain the relation

$$\tau_e = \frac{0.4p}{g} = \frac{0.8p_e}{g} \tag{75}$$

between the optical depth in electron scattering at a given point, the electron pressure prevailing at that point, and the surface gravity of the star. For the B2 supergiant ($g = 100$ cm/sec^{-2}), Miss Underhill gives the value $p_e \simeq 20$ bars at the "representative layer" in which the hydrogen lines arise. Equation (75) then gives an optical $\tau_e = \tau_1 \simeq 0.16$. This value, however, should be taken as a lower limit for the true value of τ_1. In a more refined model, in which account is also taken of the opacity produced by helium and the hydrogen absorption beyond the Lyman limit, τ_1 would increase significantly. Also, it should be kept in mind that this estimate refers to the center of the hydrogen lines of the Balmer series (in particular $H\gamma$). The values of τ_1 for lines of other elements will obviously be different. From the estimate of the optical depth τ_1 for hydrogen and from the numerical examples given in the preceding paragraph,[17] we can conclude that the intensity distribution within the profiles of the hydrogen lines observed in early B supergiants is modified appreciably by electron scattering in the manner indicated by observations.

[16] Cf. *op. cit.*, p. 366, Table 7.

[17] See particularly Fig. 3, where the lines illustrated have equivalent widths of the same order of magnitude as the expected total intensity of $H\gamma$ in the B supergiants.

If we now apply equation (75) to compute the optical depth τ_1 for the layer in which $H\gamma$ is formed in a B2 main-sequence star, we will obtain a value not higher than 0.04. This value is too small to produce observable effects in the lines of the emergent spectrum. However, we may expect that, when the star is partially eclipsed and we observe only radiation arising from parts of the disk near the limb, the scattered radiation will become high enough (relative to the total light) to be observable. In equation (57) we see that the direct radiation tends to zero exponentially as the limb is approached, while the scattered radiation remains finite out to the extreme limb. Thus the scattering by electrons in the extreme outer layers may provide a clue to the general weakening of the absorption lines in the spectrum of RZ Scuti at mid-eclipse, to which O. Struve and F. J. Neubauer[18] have directed attention. And if it be assumed that this effect is the same as that observed by O. Struve[19] and O. R. Redman[20] in the absorption lines of the B-type component of the eclipsing star U Cephei, it is possible that the phenomenon is common to all B-stars with favorable eclipse conditions. In order to find the correct interpretation of this interesting phenomenon, it is apparent that the subject must be analyzed in a manner which is beyond the scope of this paper.

It is a pleasure to acknowledge my indebtedness to Dr. S. Chandrasekhar for his constant advice and helpful discussions. My thanks are also due to Dr. Otto Struve for illuminating suggestions concerning the spectroscopic problems related to high-temperature stars.

[18] *Ap. J.*, **101**, 240, 1945.

[19] *Ap. J.*, **99**, 229, 1944.

[20] *M.N.*, **96**, 488, 1936.

SUPERTHERMIC PHENOMENA IN STELLAR ATMOSPHERES

I. SPICULES AND THE SOLAR CHROMOSPHERE

RICHARD N. THOMAS
HARVARD COLLEGE OBSERVATORY
Received December 15, 1947

ABSTRACT

An interpretation of the chromospheric spicules as a system of superthermic jets is presented. It is suggested that the spicules may thus be the source of the energy needed to give the observed high chromospheric kinetic temperature. The possible configuration of the spicules, discussed on a hydrodynamic basis, is interpreted to obtain an estimate of the energy put into the chromosphere.

I have suggested[1] the need for a more literal interpretation of Doppler broadening of spectral-line contours. The so-called "turbulent velocity" represents the excess of the observed velocity, determined from Doppler broadening or the curve of growth, over the thermal velocity, computed on the basis of a radiation temperature. This turbulent velocity forms a self-contradictory concept. The more literal interpretation requires the admission of kinetic temperatures, in the stellar atmosphere, much higher than the photospheric temperatures inferred from the star's color or general radiation field. From this admission results the necessary conclusion that the true mechanical structure of the stellar atmosphere does not follow from the usual equilibrium relations built upon the general stellar radiation field. In contrast, I have suggested that we must look for a mechanical supply of energy. Drawing upon the suggestive observations of solar prominences, I proposed that the necessary mechanical transport phenomenon lies in a process of ejection of material from the photosphere in the form of jets. This jet transport differs from the usual turbulent-convective transport in that the velocity of transport exceeds the velocity of small disturbance. The directed mechanical energy of the jet becomes converted to random thermal energy, in part, as the jet moves through the atmosphere. Thus the kinetic temperature of the atmosphere rises above that of the photosphere. In general, however, one does not expect an excitation temperature equal to the kinetic temperature. Indeed, one does not, in general, expect the *existence* of an excitation temperature. To this subject we shall return in the second paper of this series.

In the original discussion, cited above, I laid stress upon the so-called "coronal streamers" as the immediate cause of the higher kinetic temperature in the outer solar atmosphere. Since the presentation of these earlier remarks, Wildt's analysis[2] and summary of Mitchell's eclipse data have appeared. The values of the hydrogen chromospheric density gradient obtained by Wildt agree with the chromospheric temperature of about 35,000° obtained by Redman[3] from careful measures of the Doppler widths in the flash spectrum. In my original remarks the lack of any boundary values hampered the presentation of quantitative calculations. Using the 6000° photospheric temperature as an initial value and the 35,000° chromospheric temperature as a final value, one readily computes the speed of a jet, all of whose initial energy is converted into random thermal energy. The velocity is about 30 km/sec. With this simple calculation in mind, it becomes a matter of some interest to read Roberts' account[4] of his observations of chromospheric "spicules." Roberts gives the velocity of a "typical" spicule as about 30 km/sec.

[1] *A.J.*, **52**, 158, 1947 (abstr.).
[2] *Ap. J.*, **105**, 36, 1947.
[3] *M.N.*, **102**, 140, 1942.
[4] *Ap. J.*, **101**, 136, 1945.

An estimate of Mohler, quoted in the paper, places the number of spicules present on the solar surface at any one time at about 2×10^6. It thus seems more likely to seek the source of the mechanical energy needed to sustain the chromosphere in these spicules than in the more spectacular, but less frequent, large-scale prominence ejections.

There arise two problems when we consider a mechanical field of energy transport; namely, that of establishing the high kinetic temperature and that concerning the distinction between kinetic and excitation temperatures. In the present paper we shall consider the first of these, in its application to the solar chromosphere. The second will be treated in a following paper. The maintenance of the high solar chromospheric temperature, in turn, forms but part of the general problem of high kinetic temperature in the general stellar atmosphere.

At this point I should like to emphasize just what is the plan of attack, so to speak, on this concept of a mechanical-energy field in the stellar atmosphere. I think the general viewpoint can best be termed "kinematic," in contrast to the generally deductive equilibrium theory of the stellar atmosphere. That is, we start from certain observed *surface* features, anomalous under the equilibrium theory, and inquire what consequences can be deduced from the *simple fact of the existence* of these phenomena. Thus, initially, the first phenomenon was the so-called "turbulence velocity." The simple existence of such a velocity greater than the thermal velocity determined from the radiation temperature of the star leads, as I have shown, to the requirement of the existence of a kinetic temperature considerably in excess of the radiation temperature. To establish such a high kinetic temperature, one infers the existence of a field of mechanical-energy transport; and I have suggested one possibility to be a system of jet ejections from the stellar interior. Now, however, we turn to the *observation* of a system (apparently) of jets—the spicules. We inquire the consequences attending the existence of such a system. We embark on a purely kinematic analysis of the spicule system in regard to its interaction with the atmosphere. While in the following we may at points consider various alternatives as to the conditions antecedent to the formation of the jets, we must not forget the primary observation—the simple existence of the spicules. This simple existence demonstates that energy in some form other than the general solar-radiation field is being supplied to the atmosphere. The question is the relation of this energy to the general discussion of high kinetic temperature, etc.

I. GENERAL CONSIDERATIONS RELATIVE TO THE SPICULE PHENOMENON

According to Roberts' paper, we may distinguish two phases in the life of a typical spicule. First occurs a period during which the spicule appears and elongates to maximum height. Next, there exists a period during which the spicule remains more or less stationary, gradually fading out. The total lifetime of an average spicule is 4–5 minutes. Of this time, 1 or 2 minutes occupies the first phase, during which the typical spicule reaches a height of some 10″. The transverse dimension is some 3″ or 4″. If we regard the spicule as a hydrodynamic jet, we may probably consider the first phase as one of nonsteady state, during which the jet progresses toward quasi-equilibrium, which characterizes the second phase.

We have spoken of the spicule as though it actually were a hydrodynamic jet. That is, we assume that the apparent motion of a luminous region outward corresponds in reality to an actual motion of matter, and not simply to the propagation of a region of luminosity through a static atmosphere. There exist three observations that seem to indicate the validity of the jet viewpoint: the appearance, the velocity, and the "magnitude" of disturbance involved in the spicule phenomenon. One would expect a "wave" propagation to be roughly hemispherical in shape, with perhaps a slight elongation in the direction of any existing temperature gradient. The spicule phenomenon resembles

a rectangle or triangle, however, more suggestive of a "jet." Second, "sonic" disturbances must be propagated with the velocity of small disturbance in the medium. The velocity given by Roberts—30 km/sec—corresponds to a wave traversing a medium characterized by a kinetic temperature of 65,000°, which seems rather high. The last point presents the most powerful evidence, the "amplitude" of the disturbance. If we are to view the progress of the spicule as the progress of a region of disturbance in a static atmosphere, we must explain the visibility of the region. We expect either a great and sudden increase of the excitation of the region of the atmosphere traversed by the wave—with an increase in radiation—or a correspondingly great increase in density of the region, so that the concentration of emitting atoms becomes sufficient to provide visibility. In either of these alternatives the magnitude of the disturbance, i.e., the rise of temperature or of density, is so great as to negate the assumption of acoustic (or vanishingly small) disturbance.

One should note that none of the three points of the preceding paragraph touches on the lag between the onset of kinetic and thermodynamic equilibrium that was earlier mentioned. The question of this lag must enter if one wishes to consider an increase in *excitation* by mechanical exchange of energy. Here, however, we simply consider the observed spread of the region of visibility, which is called the "spicule," and do not ask whether the wave is actually at the edge of the visible region at the time of observation. The observations would seem to indicate a disturbance too large to be acoustic, and therefore momentum considerations require the motion of matter in the manner indicated. We therefore conclude that the observations of the spicule system are, in reality, observations of a system of superthermic jets. ("Superthermic" implies a velocity greater than the thermal velocity. I prefer this term to "supersonic," which has unfortunately an ambiguity in physics, where it is used to refer both to frequency and to velocity; but the aerodynamic meanings of the two terms are the same.) We now proceed to consider the probable hydrodynamic configuration of the spicule.

II. CONSIDERATION OF THE HYDRODYNAMIC CONFIGURATION OF THE SUPERTHERMIC SPICULE-JET

The observational parameters available to describe the jet-spicule are essentially the velocity and the geometrical dimensions. We have agreed to adopt a "kinematic attitude," i.e., to accept the presence of the jet and to inquire into the attendant consequences. Nevertheless, we must raise the question of the "previsibility" configuration of the spicule as a necessary guide to the kinematic interpretation. Although the spicules are designated by the term "chromospheric," we recognize them as entities because they protrude *above* the chromosphere. The "typical" dimensions cited refer to the portion of the spicule protruding above the chromosphere. Thus, at least in the photographs, we study the motion outside the chromosphere to predict the behavior within the chromosphere. We have now two alternatives as to conditions within the previsibility stage, the two alternatives posing real differences in the basic physics of the motion. On the one hand, we may interpret the jet motion as stemming from some local irregularity in the hydrostatic pressure field at the photospheric level, the jet motion arising as a purely mechanical consequence of this irregularity. We here inquire into the existence of small, high-pressure regions at the photospheric level. On the other hand, we may look for the source of the original mass motion in some cause that is other than mechanical. We allow the "creation" of a high-velocity stream of matter without the existence of an antecedent high-pressure area. Such, for example, might be the result of an induction action arising from an electromagnetic field. We proceed to indicate the general characteristics of the two cases.

1. According to the first alternative, we assume the region from which the spicule

arises to be characterized by a sudden increase in pressure relative to the surrounding photosphere. The source of the pressure rise we ignore. In any event there occurs a high-pressure region, with the steepest pressure gradient an outward one. If we idealize the case, so that we may consider a zero epoch in time at which there exists as yet no motion of the material in the high-pressure region, the dynamic configuration is that to be expected in the expansion of a gas from rest into a region of lower pressure. If the temperature of the high-pressure region were known, an upper limit to the velocity of expansion could be set by the velocity of expansion into a vacuum. We have the energy equation, if we assume that radiation, heat conduction, and viscosity can be neglected, as follows:

$$\frac{v^2}{2}+\frac{\gamma}{\gamma-1}\frac{p}{\rho}=\text{Constant}\,, \tag{1}$$

where v, p, ρ, and γ are, respectively, the gas velocity, pressure, density, and ratio of specific heats. Assuming a monatomic gas with $\gamma = \frac{5}{3}$ and recognizing $\gamma p/\rho$ as the velocity of small disturbance, a, we have an upper limit of $\sqrt{3}\,a$ for v. Thus we must have an initial temperature of 20,000° to give an initial velocity of 30 km/sec (or 80,000° if 30 km/sec be the average velocity and 60 km/sec the initial). Since the expansion is not

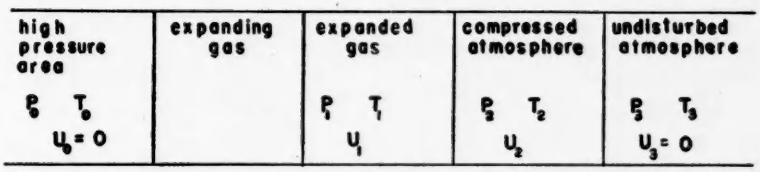

FIG. 1.—Schematic relation for jet from local high-pressure area

into a vacuum, we cannot attain this upper limit. Furthermore, we cannot identify the velocity of the spicule "front" with the velocity of the matter within the spicule. At this point the concept of the spicule as a superthermic phenomenon enters, and we see that the velocity of the spicule front must be larger than the velocity of mass motion. The spicule front is actually a shock wave. Across this shock occurs an abrupt rise in pressure, temperature, and density; and thus the spicule becomes visible. Let us consider the matter in more detail.

Initially, we have assumed a static state. As soon as the gas in the high-pressure region begins to expand, we shall have a set of "small disturbance" waves set up in the adjoining region. Since each wave slightly raises the temperature of the region that it traverses, the next wave behind will move with a slightly greater velocity, and there occurs a "catching-up" of the waves and hence the creation of a shock wave. Across the shock occurs a jump in pressure and temperature as the shock moves into the undistrubed atmosphere. Schematically, we have the situation shown in Figure 1. We see thus that the spicule expands, decreasing in temperature, until the pressure reaches a value equal to that attained by the gas from the undisturbed atmosphere upon passing through the shock wave. Just behind the shock the temperature rises. All the unknown quantities are determined from a knowledge of the pressure and temperature in the original, high-pressure photospheric region and those in the atmosphere into which the spicule moves. Or the observed velocity of the spicule front may be used as one parameter, the parameters relating to the undisturbed atmosphere may be assumed known, and we have remaining one unknown parameter to fix the conditions in the photospheric region. That

is, we have the following set of equations relating the parameters of Figure 1 (cf. Appen. A).

$$\frac{U_2}{a_3} = \sigma - \frac{\sigma^2(\gamma-1)+2}{\sigma(\gamma+1)}; \tag{2}$$

$$\sigma = \frac{V}{a_3}; \tag{2a}$$

$$\frac{p_2}{p_3} = \frac{2\gamma\sigma^2 - (\gamma-1)}{\gamma+1}; \tag{3}$$

$$p_2 = p_1; \tag{4}$$

$$\frac{\rho_2}{\rho_3} = \frac{\sigma^2(\gamma+1)}{\sigma^2(\gamma-1)+2}; \tag{5}$$

$$\frac{U_2^2}{2} + \frac{\gamma p_2}{(\gamma-1)\rho_2} = \frac{\gamma}{\gamma-1}\frac{p_0}{\rho_0}; \tag{6}$$

$$\frac{p_1}{p_0} = \left(\frac{\rho_1}{\rho_0}\right)^{\gamma}; \tag{7}$$

$$p = k\rho T; \tag{8}$$

k = Boltzman's constant.

NOTE:
$$\frac{p_3}{p_2} \neq \left(\frac{\rho_3}{\rho_2}\right)^{\gamma}$$

If we know either p_0 or ρ_0, we have a complete solution. Lacking either, all we can find is the ratio p_0/ρ_0, i.e., the temperature T_0. We can, however, solve explicitly for σ in terms of the ratio $r = a_0/a_3$. We readily obtain

$$\sigma^2 = \left([(\gamma-3) + r^2(\gamma+1)] + \left[\{(\gamma-3) + r^2(\gamma+1)\}^2 + \frac{16(\gamma-1)^2}{\gamma+1} \right]^{1/2} \right) \frac{1}{4(\gamma-1)}. \tag{9}$$

Since the concept of a shock wave requires $\sigma^2 > 1$, we see that equation (9) places a minimum value on r. For $\gamma = \frac{5}{3}$ we obtain

$$\sigma^2 = \tfrac{1}{2}\{[2r^2-1] + [(2r^2-1)^2 + \tfrac{3}{2}]^{1/2}\} \tag{10}$$

and

$$r > \sim 0.9;$$

that is, the temperature of the original photospheric region must be nearly the same as, or greater than, that of the atmosphere into which the expansion occurs if we are indeed to have superthermic velocities. From equation (9) we see also that the limiting value for σ and V, that is, the high-velocity limit, is

$$\sigma^2 = r^2 \frac{\gamma+1}{2(\gamma-1)}; \tag{11}$$

or, for $\gamma = \frac{5}{3}$,

$$V = \sqrt{2}\, a_0. \tag{11a}$$

Likewise

$$U_2 = \frac{3\sqrt{2}}{4} a_0 \tag{11b}$$

to the same approximation.

Thus we have the important result that, if this method of description involving an initial photospheric high-pressure region is valid, we must have $a_0 \gtrsim a_3$, i.e., $T_0 \gtrsim T_3$. That is, we must have regions of very high kinetic temperature at the photospheric level. (For a V of 60 km/sec, eq. [11a] would indicate a kinetic temperature of about 100,000°.)

A priori, we note that the existence of such regions of high kinetic temperature should not be an inconspicuous phenomenon. If we adopt Mohler's estimate of $2'' \times 11''$ for the average dimension of a spicule, and 2×10^6 as the number of such spicules occurring at any given time, we conclude that half the solar surface should be covered by such regions of very high kinetic temperature. Mohler's estimate is somewhat larger than one would infer from Roberts' statement that he has observed, at a given moment, some twenty-five of his "typical" spicules within a 60° arc. We should thereby set the total number of typical spicules (neglecting variation with latitude) at some 1×10^4, and so obtain an estimate that some 1 per cent of the solar surface should be covered by these high-kinetic-temperature regions. The figure is still appreciable.

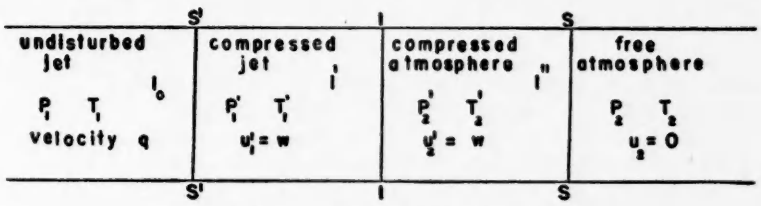

FIG. 2.—Schematic relation for "kinetic" jet

To complete the first method of description, we turn to consider the steady-state phase. In the foregoing we have treated the spicule as though it were one-dimensional. Actually, we should expect any locally high-pressure region to expand in all directions in a homogeneous atmosphere. Since, in the present case, we do have a radial gradient (i.e., radius of the sun) of pressure, density, and temperature, we might expect some sort of asymmetry in the outward propagation of the disturbance. To proceed in a rigorous manner, therefore, we should have set up the hydrodynamic equations of motion for a disturbance of finite amplitude, characterized by a shock wave, in a nonhomogeneous medium. However, to my knowledge, this problem has never been solved. Nevertheless, the essential details concerning the nonsteady case that we have reached via the one-dimensional treatment will not be disturbed. That is, the high-pressure region must be characterized by high initial kinetic temperature. Further, if a steady-state configuration exists that gives the "spikelike" spicule, it cannot, far away from the original source, be too unlike the steady-state solution for the case of the second method of description, where we simply assume an initial stream of gas moving with high velocity. We therefore turn to the second method of description.

2. For several reasons, this is the more attractive procedure. The simplest method of insuring pressure gradient that forces the motion to be essentially radial is to make the pressure a dynamic one. That is, we assume that the jet arises somewhere below the visible surface, but we do not inquire too closely into the cause of the motion. In spite of any difficulties as to its source, we must recognize the existence of the gas stream.

Consider the dynamical configuration involved in the collision of a gas jet and a stationary atmosphere. If we again idealize the case by considering the jet to be bounded laterally, we obtain the configuration sketched in Figure 2. The interface I separates the

gas in the jet from that in the atmosphere and moves forward with a velocity w. In addition, a shock, SS, moves forward into the atmosphere; and another, $S'S'$, moves backward into the jet. Each shock has its characteristic velocity. Given the pressure and temperature in the atmosphere, that in the jet, and the jet velocity, then the velocities of the shocks, of the interface, and of the matter in the compressed regions I', I'' are determined. Indeed, denoting by the indices 1 and 2 the regions in the undisturbed jet and the atmosphere, respectively, and letting the initial jet velocity be q, we have the pair of equations to solve:

$$q - a_1 \cdot \frac{2(\sigma_1^2 - 1)}{\sigma_1(\gamma + 1)} = w, \tag{12}$$

$$\frac{\rho_1 a_1^2}{\rho_2 a_2^2} = \frac{2\gamma\sigma_2^2 - (\gamma - 1)}{2\gamma\sigma_1^2 - (\gamma - 1)}. \tag{13}$$

In the case of large velocity, these reduce to the relations

$$w = \frac{q}{1 + \sqrt{\frac{\rho_2}{\rho_1}}}, \qquad \sigma_1 = \frac{\gamma + 1}{2} \frac{w}{a_1} \sqrt{\frac{\rho_2}{\rho_1}}, \qquad \frac{\sigma_2 a_2}{\sigma_1 a_1} = \sqrt{\frac{\rho_1}{\rho_2}}. \tag{14}$$

If we assume the jet to have been moving before it comes into view, we must see only the compressed region I' of the jet and not the original region, since the shock $S'S'$ has passed down below the edge of the visible disk. We are then interested in the equations describing the visible regions. These we can write as follows:

$$w = a_2 \frac{2(\sigma_2^2 - 1)}{\sigma_2(\gamma + 1)}, \tag{15}$$

and for high velocity:

$$w \to \left(\frac{2}{\gamma + 1}\right) \sigma_2 a_2, \tag{15a}$$

$$\frac{\rho_i'}{\rho_i} = \frac{\sigma_i^2(\gamma + 1)}{\sigma_i^2(\gamma - 1) + 2}, \tag{16}$$

$$\frac{T_i'}{T_i} = \frac{2\gamma\sigma_i^2 - (\gamma - 1)}{\gamma + 1} \frac{\sigma_i^2(\gamma - 1) + 2}{\sigma_i^2(\gamma + 1)}. \tag{17}$$

These equations indicate that we may have a situation considerably different from that considered in Section I. If the jet were moving into a uniform atmosphere, equations (12)–(17) would completely describe the situation. Actually, the spicule moves into the chromosphere, which has, presumably, a negative density gradient and a positive temperature gradient. The spicule must then "adjust" itself continually to the atmosphere. This it does by rarefaction waves moving back from the shock SS. There exists, thus, a lag of conditions within the spicule behind what we would calculate if we assumed for p_2, ρ_2, and T_2 the values characterizing the atmosphere at the shock front SS. The important feature of the lag is that it acts in the direction to give slightly higher values of p, ρ, and T in the compressed regions than would be the case without the lag. Now consider a spicule whose "initial" configuration consisted of a rather low kinetic tempera-

ture but a high density and a high velocity. The high velocity, q, reduces to the velocity w as shock $S'S'$ forms and moves down the spicule. The "matter" within the spicule then proceeds into the atmosphere with the velocity w, constant except for whatever adjustment the density gradient in the atmosphere requires. If we neglect, for the moment, the gravitational field, the spicule emerges into sight, at the top of the chromosphere, with characteristic parameters determined by equations (12)–(17), using the initial velocity q, the initial density and temperature at the photospheric level for ρ_1 and T_1, and the values at the top of the atmosphere for ρ_2 and T_2. What difference there is from the results of the predictions of these equations, with these initial values (apart from the gravitational loss of energy), results from the lag mentioned; and the lag gives higher density, etc., in the compressed region than that predicted. We see here the difference from that condition treated in Section I. Irrespective of the kinetic temperature in the original spicule, at the photospheric level the density in the compressed region to the *left* of the interface I, i.e., in the original matter of the spicule, is of the same order, or higher, than before passing through shock $S'S'$ at the photospheric level. In the region to the *right* of the interface I, or the matter "picked up" in the atmosphere, the density may be considerably smaller. The pressure balance is achieved by a high kinetic temperature in the region to the right, and a low kinetic temperature to the left, of the interface I. In all probability, the spicule front in this case is the interface I, which represents a vortex sheet. Thus the observed velocity of the spicule corresponds to the velocity w rather than to the velocity $\sigma_2 a_2$ of the shock front.

The modification introduced by the existence of a gravitational field in this one-dimensional case is not serious. We simply realize that the term involving the gravitational energy reduces the mass velocity, w, by the amount corresponding to the height at the particular point in the spicule and hence reduces the dynamic pressure. If, in equations (12)–(17), we simply substitute the w corresponding to the initial velocity and the height above the initial point, we obtain the results for the case which includes the gravitational field.

The foregoing considerations would hold for a spicule that was bounded laterally, i.e., one-dimensional motion. If we "remove" the lateral bound, we see that the initial configuration behind the shock $S'S'$ is simply a high-temperature, high-pressure region very similar to that considered in Section I, with the exception that the region is moving with a high speed into the atmosphere. The considerations that we developed in Section I now apply to the *lateral* expansion of the spicule. From equation (11*b*) we see that the initial velocity of expansion is essentially a_1'. Thus, for example, if we pick a value of 90 km/sec for w and an initial temperature of 6000° for the spicule ($T_1 = 6000°$), we see from equations (14) and (17) that the jet expands at about 35 km/sec. Thus in its initial stages the spicule should appear as a spot enlarging laterally as well as radially. This behavior corresponds to that actually observed.[5]

The lateral expansion must continue until the pressure at the boundary of the spicule reaches that of the atmosphere. Again using the numerical values of the last paragraph, we find that the pressure in region I' is about fifty-five times that in region I_0, and the density ratio about 4 times. If we assume that the pressure in region I_0 is the atmospheric value, the *final* value after expansion on the spicule boundary fixes the density at about one-third the initial value in region I_0. We note now that this lateral expansion has produced a diverging jet. If the divergence continues, the jet will overexpand. Therefore, the contour of the spicule must bend back toward the axis. A series of stages in the initial phase of the spicule phenomenon might resemble those sketched in Figure 3, *a*.

Clearly, as the spicule cross-section once again narrows, the pressure rises, and we should expect the phenomenon to repeat the contraction and expansion periodical y. In-

[5] *Ibid.*, p. 136.

deed, if we should proceed by analogy with a laboratory jet,[6] we should obtain just this periodic structure so long as q was not too large—say, a value corresponding to a w of 10 or 15 km/sec. For the higher velocities characteristic of the spicules, we obtain, instead, a shock-wave across the jet shortly after the cross-section begins to decrease. Thereafter, the jet moves more or less in the original direction of motion. Thus the configurations after those of Figure 3, *a*, might be similar to those sketched in Figure 3, *b*. As, indeed, from Roberts' observations one does find qualitative agreement with these predictions, one must infer the essential correctness of the interpretation. More accurate quantitative reduction of the spicule observations, which Dr. Roberts tells me are now in progress, should permit more accurate quantitative values than the ones used in the rough description above.

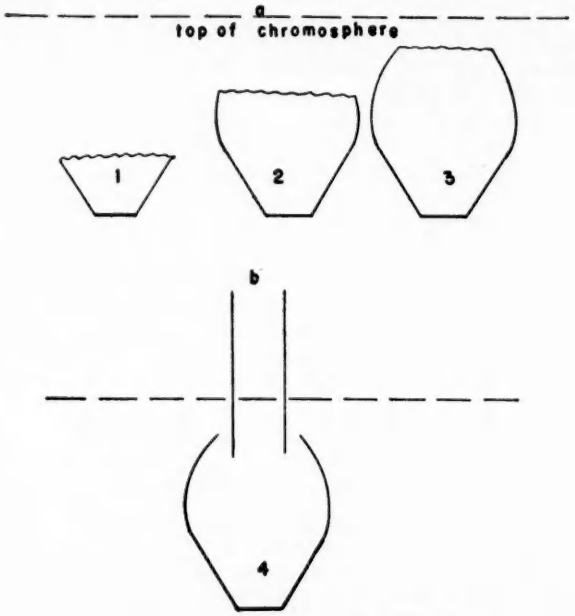

FIG. 3.—Successive stages in spicule development

The steady-state phase of the jet phenomenon sets in when the point of occurrence of the last shock-wave, across the narrowed-down section of the spicule, ceases to move up into the atmosphere. Further consideration of this point tells no more of the physical state of the spicule; so we pass on to consider the transfer of energy to the atmosphere from the spicule.

The general conclusion from this section on the hydrodynamic configuration of the spicule is a strong preference for the method of description in Section II rather than that of Section I. That is, we do not look for the source of the spicule phenomenon in regions of high pressure at the photospheric level but rather in small regions, whose thermodynamic properties may be not much different from the surrounding photosphere but which are placed in rapid motion outward. Given these regions, we expect the resulting hydrodynamic configuration, by the time the spicules become visible near the top of the chromosphere, to be that observed in the spicules themselves.

[6] Hartman and Lazarus, *Phil. Mag.*, ser. 7, **31**, 35, 1941.

III. THE TRANSFER OF ENERGY TO THE ATMOSPHERE

This problem has two parts. First, we inquire whether there is sufficient energy in the spicule system to maintain a high kinetic temperature in the chromosphere. Second, we ask after the method of energy transfer.

a. THE ENERGY SUPPLY

Let us simply compute the kinetic energy in a "typical" spicule at the base of the chromosphere. Naïvely balancing the initial velocity of the jet against the observed height that it reaches (10″ above the chromosphere) against the solar gravitational field, we obtain an estimate of 90 km/sec for the initial velocity (that is, w in the previous notation; note that we do *not* use q). Assuming that the observed maximum width of the typical spicule—4″—corresponds to the expanded portion of the jet, we use a width of 2″ for the initial value. And we take as an estimate of the density simply Wildt's value[2] for the density at the base of the chromosphere, $N = 10^{15.23}$. We then find that 2×10^{28} ergs/sec cross the base of the chromosphere in the form of mechanical energy in each spicule. Taking the total number of typical spicules as 10^4, we obtain an energy for the whole system of "typical" spicules to be about 2×10^{32} ergs/sec. This is an appreciable energy supply, about one-twentieth of the solar constant. All, of course, does not go into heating the atmosphere. Nonetheless, there is an energy supply quite sufficient to balance the energy lost by radiation from the chromosphere. In the paper following this one in the present series (Paper II), we shall consider the energy necessary to maintain a hydrogen chromosphere at a kinetic temperature of 35,000° if the illuminating radiation field is characteristic of a black body at 6000°. We can then compare directly the energy needed with the energy furnished by the spicules, to obtain some idea of the numerical validity of the ideas of the next section. At present, we simply estimate the fraction of the original kinetic energy of the jet that goes into heating the chromosphere by making assumptions as to the density of the spicule.

b. MODE OF TRANSFER OF ENERGY TO THE ATMOSPHERE FROM THE SPICULE

In Section II we tacitly assumed that the spicule becomes visible because of a higher density. If we regard the boundary of the spicule as a vortex sheet across which the pressure remains constant but the density and temperature change, we must have a lower kinetic temperature within the spicule than in the atmosphere. Since the spicule velocity is superthermic with respect to the atmosphere, we can safely neglect the thermal energy of the spicule atom compared with the kinetic energy that it possesses by virtue of the spicule velocity. The transfer of the energy to the atmosphere is, then, essentially equal to the loss of atoms from the spicule multiplied by the energy of a single jet atom. We proceed to calculate the loss.

We readily find that the transfer of atoms from the jet into the atmosphere proceeds at the following rate:[7]

$$dN = \tfrac{1}{4} N_s \bar{c}_s dS dt \,, \tag{18}$$

where dS is the surface element at the spicule boundary, dt the time interval considered, N_s the atoms per cubic centimeter in the spicule, and $\bar{c}_s$ the mean velocity in the spicule. We have:

$$\bar{c}_s = 2 \left(\frac{2kT_s}{\pi m} \right)^{1/2} . \tag{19}$$

[7] Jeans, *The Dynamical Theory of Gases* (4th ed.; Cambridge: At the University Press, 1925), p. 307.

The total loss around the circumference of the spicule, for a strip 1 cm high, then, is (R_s is the spicule radius)

$$\frac{dN}{dt} = \tfrac{1}{4} N_s \bar{c}_s 2\pi R_s . \tag{20}$$

Equation (18) also holds for the rate of entry of chromospheric atoms into the spicule, if we substitute the subscript c for s. Since the pressure is assumed constant across the spicule boundary, the ratio of the number of atoms entering the spicule to that leaving is proportional to the square root of the density ratio within the spicule to that in the atmosphere. Thus considerably more atoms enter than leave (for example, ten times more leave than enter for a density ratio of 100). We note that the entry of atoms into the spicule causes the outer layers of the spicule to lose momentum and so tends to "wash out" the vortex sheet, which we have idealized to a plane surface. At the same time, however, the loss of atoms from the spicule tends to cause the spicule radius to decrease. Since the latter effect far exceeds the first, equation (18) may be used to estimate that the radius decreases at a rate of about $\bar{c}_s/4$. If we assume a spicule density of about 10^{15} atoms/cc, then at least in the upper regions of the chromosphere (where we take a kinetic temperature of 35,000°) we have a density ratio of about 100 and a radius decrease of 0.7 km/sec. Because of the uncertainty as to the actual contour of the spicule in the chromosphere, this change in radius may be neglected in estimating the total loss of atoms while the spicule passes through the chromosphere.

Taking a t of 110 seconds (corresponding to the initial velocity 90 km/sec and a chromosphere $h = 10''$ high), a mean spicule radius of $1''.5$, a chromospheric temperature of 35,000°, a density ratio between spicule and chromosphere of 100, and a spicule density of 10^{15} (assumed constant), we have for the loss of atoms, from equation (20),

$$dN = 4.5 \times 10^{30} \text{ atoms} . \tag{21}$$

This compares with the initial total number of atoms in the small segment of the spicule considered:

$$N = \pi R_s^2 N_0 = 2.8 \times 10^{31} . \tag{22}$$

Roughly, then, some 16 per cent of the spicule atoms are lost to the chromosphere during the passage through the atmosphere. Weighting this number by the ratio of mean square velocity to initial square velocity, or by the ratio 57/81, we have about 10 per cent of the initial kinetic energy of the spicule going into heating the chromosphere. Or we have about 2×10^{31} ergs/sec put into the chromosphere by the whole spicule system. The amount would seem to be sufficient to maintain the chromosphere. We shall return to the point in the next paper of the series.

IV. SUMMARY

The chromospheric spicules, discussed by Roberts, are here identified with a system of superthermic jets. The previsibility configuration of the spicule has been considered on a hydrodynamic basis. Of two possible alternatives for this configuration, one depending upon initial high-pressure regions at the chromospheric level and the other upon some nonmechanical source for the spicule velocity, the latter seems preferable. The essential observational features of the spicule agree with the interpretation. The energy transferred from the spicule system to the chromosphere appears adequate to maintain the 35,000° kinetic temperature.

I wish to thank Dr. Donald Menzel and Dr. Walter Roberts for discussions on several phases of the spicule phenomenon.

APPENDIX A

The equations pertaining to shock-waves in the text are based on the so-called "Rankine-Hugoniot shock-wave equations." Setting

ρ = Density	a = Velocity of small disturbance
p = Pressure	c = Shock-wave velocity
T = Temperature	C_v = Specific heat at constant volume
E = Specific energy	γ = Ratio of specific heats
u = Gas velocity	R = Gas constant ;

and, denoting the high-pressure side of the shock by subscript 2, the low by subscript 1, we have the equations:

Conservation of mass : $$\rho_1 (u_1 - c) = \rho_2 (u_2 - c) = m \; ; \tag{A-1}$$

Conservation of momentum : $$m (u_1 - u_2) = p_2 - p_1 \; ; \tag{A-2}$$

Conservation of energy : $$m \{ \tfrac{1}{2} (u_1^2 - u_2^2) + (E_1 - E_2) \} = p_2 u_2 - p_1 u_1 \; . \tag{A-3}$$

If we neglect viscosity and heat conduction, we obtain

$$E = C_v T = \frac{RT}{\gamma - 1} \; . \tag{A-4}$$

Whence, if we set

$$\frac{p_2}{p_1} = \xi \; , \qquad (u_1 - c) \frac{1}{a_1} = \sigma \; ,$$
$$\frac{\rho_2}{\rho_1} = \eta \; , \qquad (u_2 - c) \frac{1}{a_1} = \tau \; , \tag{A-5}$$

we obtain the Rankine-Hugoniot equations:

$$\xi = \frac{2\gamma\sigma^2 - (\gamma - 1)}{\gamma + 1} ; \qquad \eta = \frac{\sigma^2 (\gamma + 1)}{\sigma^2 (\gamma - 1) + 2} ; \qquad \tau = \frac{\sigma^2 (\gamma - 1) + 2}{\sigma (\gamma + 1)} . \tag{A-6}$$

From these equations, considering the geometrical configuration of Figures 1–3 of the text, the equations of the text may be written down immediately.

SUPERTHERMIC PHENOMENA IN STELLAR ATMOSPHERES

II. DEPARTURE FROM THERMODYNAMIC EQUILIBRIUM IN AN IDEALIZED CHROMOSPHERE

RICHARD N. THOMAS
Harvard College Observatory
Received December 15, 1947

ABSTRACT

The steady-state condition of a hydrogen chromosphere, characterized by a kinetic temperature of 35,000° and illuminated by a radiation field of temperature 6000°, is determined. The hydrogen is found to be 99 per cent ionized. On the basis of these results, the *He* I, *He* II chromospheric observations cease to be anomalous. The net energy supply needed to maintain this chromosphere falls within the range that present observations of the spicule system indicate may be expected to come from a mechanical-energy supply. Transfer problems arising from the chromospheric emission are explicitly neglected.

In the initial paper of this series,[1] hereafter designated as "Paper I," I discussed the chromospheric spicules as a source of energy for the solar chromosphere. In the sun these spicules form a specific example of a general phenomenon of mechanical-energy transport into the stellar atmosphere. I have suggested that such a general phenomenon of mechanical-energy transport is the cause for the observed departures from the predictions made on the basis of the general "equilibrium" models. We turn, then, to the concept of an atmosphere whose properties may be largely determined by a field of mechanical-energy transport rather than by the general radiation field of the star. In the present series of papers, I have proposed to discuss this problem on the basis of an identification of the mechanical-energy field with a system of superthermic jet ejections from a subatmospheric layer in the star. (In using the term "superthermic," we imply that the velocity of the jet exceeds the thermal velocity of the atoms in the atmosphere.)

In Paper I we took the spicule to be the observed phenomenon, discussed the hydrodynamic configuration of the spicule while it moves through the chromosphere, and computed the order of magnitude of the energy transfer from the spicule to the chromosphere on the basis of this hydrodynamic configuration and Roberts' spicule observations. There is an alternative procedure. One may start with the observed "anomalies" in the atmosphere and compute the energy input needed to maintain them. The most pronounced of these anomalies are the existence of the "turbulent" velocity, the density gradient in the atmosphere, and the atmospheric density itself. The density and the density gradient may be used directly from the observations. In certain cases, however, the "turbulence" parameter introduces a certain ambiguity. That is, the "turbulence" is compounded of the thermal motions of the atmospheric atoms and the larger-scale motion of the material in the jets. Where the jets contain an appreciable fraction of the material in the atmosphere, one must analyze the observations simultaneously for the kinetic temperature and the jet velocity. (In the past, difficulties arose because of an insistence on identifying the kinetic temperature with the temperature of the radiation field of the star.) Such an ambiguity arises, apparently, in the giant stars, where the result is a spurious radial velocity, and in the Wolf-Rayet stars, where both a spurious radial velocity and an abnormal spectral-line broadening result. To these applications we shall return in a later paper of the series. For the chromosphere, we possess independent measures of the density gradient[2] and the kinetic temperature.[3] These measures agree in fixing the kinetic temperature of the lower chromosphere at about 35,000°. We shall,

[1] Thomas, *Ap. J.*, **108**, 130, 1948.

[2] Wildt, *Ap. J.* **105**, 36, 1947.

[3] Redman, *M.N.*, **102**, 140, 1942.

therefore, take this kinetic temperature of 35,000° as the observational anomaly and seek the amount of mechanical energy necessary to maintain it.

In the present paper we shall thus consider the problem of an atmosphere, illuminated by a radiation field of intensity $I(\nu)$ and characterized by a kinetic temperature $T_e > T_1$, where T_1 is the temperature characterizing the continuum of the radiation field. We shall idealize the problem and the chromosphere by considering a composition of pure hydrogen. We examine the distribution of the atoms over the various energy levels. We shall obtain numerical results for the case $T_e = 35{,}000°$; $T_1 = 6000°$.

A somewhat similar problem has previously been studied by Menzel, Aller, Baker, and Goldberg in a series of papers.[4] Hereafter, we denote this work by "MABG." In each case, MABG and the present, one has a hydrogen atmosphere losing energy by radiation. The energy loss may be balanced in two ways—by an external radiation field or by an external source of mechanical energy. If the mass of the system remains statistically constant, radiative excitation assumes predominant importance in the first case and collisional excitation in the second. MABG neglected collisional excitation and assumed the radiation field to be extremely "dilute." Clearly, this earlier treatment is but a special case of the problem now treated. References to this earlier work will be denoted by symbols such as "MABG IV," referring to Paper IV of that series.

I. FORMULATION OF THE EQUATIONS OF ANALYSIS

In general, we adopt the notation of MABG I. Our notation is as follows:

$F_{nn'}$ = Number of transitions from state n to n' per second per cubic centimeter;

$F_{nn'} = \bar{F}_{nn'} + C_{nn'}$;

$\bar{F}_{nn'}$ = Spontaneous and radiation-induced transitions ;

$C_{nn'}$ = Collisional excitation or de-excitation ;

$$\nu_n = \frac{(RZ^2)}{n^2} ; \qquad \text{for hydrogen, } Z = 1 .$$

We adopt the convention: $n'' > n > n'$;

$g_{nn'}$ = Gaunt factor, tabulated in MABG III ;

$\kappa \rightarrow -in$ and is real but not necessarily an integer, permitting extension of the formal expressions for discrete transitions to the continuum ;

$Q_{nn''}$ = Collisional cross-section, for excitation from level n to n'', in atomic units (i.e., πa_0^2 with $a_0 = 0.53 \times 10^{-8}$ cm) ;

$$K = \frac{h^3}{(2\pi m k)^{3/2}} \frac{8\pi^2 e^2 R^2}{m c^3} \frac{2^4}{3\sqrt{3}\pi} = 3.2 \times 10^{-6};$$

$$X_n = \frac{h\nu_n}{kT_e}; \qquad Y_n = \frac{h\nu_n}{kT_1}.$$

[4] "Physical Processes in Gaseous Nebulae." Beginning with Paper I, *Ap. J.*, **85**, 330, 1937; ending *Ap. J.*, **102**, 239, 1945. General Index in last paper.

The other symbols are conventional: m is the mass of the electron; m_H, that of the hydrogen atom.

We assume that there exists a kinetic temperature, T_e, defined by a Maxwellian distribution of velocities in the continuum. Since we have assumed that the source of the energy supply is chiefly mechanical, this assumption is trivial. We can then write down the equation for a steady-state population in level n as follows:

$$\sum_{n+1}^{\infty} F_{n''n} + \int_{\nu_n}^{\infty} F_{\kappa n}\, d\nu + \sum_{1}^{n-1} F_{n'n} = \sum_{n+1}^{\infty} F_{nn''} + \int_{\nu_n}^{\infty} F_{n\kappa}\, d\nu + \sum_{1}^{n-1} F_{nn'} . \tag{1}$$

We proceed to write down the explicit expressions for the F's. As a more convenient parameter than the number N_n of atoms in level n, we introduce b_n, which measures the relative departure of the population of level n from that characterizing a Boltzmann distribution at temperature T_e. That is, we write for N_n

$$N_n = b_n N_i N_e \left\{ \frac{h^2}{2\pi m k T_e} \right\}^{3/2} \frac{\varpi_n}{2}\, e^{X_n} . \tag{2}$$

We note $b_n \xrightarrow[n \to \infty]{} 1$, since we have assumed the existence of T_e. In terms of the b_n, we write down the equations for the F's. For the spontaneous transitions we have (cf. MABG I)

$$\sum_{n+1}^{\infty} \bar{F}_{n''n} = \sum_{n+1}^{\infty} N_i N_e \frac{K}{T_e^{3/2}}\, b_{n''}\, \frac{g_{n''n}}{n^3}\, \frac{2}{n''^3}\, \frac{e^{X_{n''}}}{\dfrac{1}{n^2} - \dfrac{1}{n''^2}} , \tag{3}$$

$$\int_{\nu_n}^{\infty} \bar{F}_{\kappa n}\, d\nu = N_i N_e \frac{K}{T_e^{3/2}} \frac{1}{n^3}\, e^{X_n} [\, -E_i(-X_n)\,] , \tag{4}$$

where

$$-E_i(-X) = \int_X^{\infty} \frac{e^{-x}}{x}\, dx ; \tag{5}$$

and we have set $g_{n\kappa}$, averaged over κ, equal to unity. For the induced transitions we have

$$\sum_{1}^{n-1} \bar{F}_{n'n} = \sum_{1}^{n-1} N_i N_e \frac{K}{T_e^{3/2}} S_\nu \left[\frac{b_{n'}\, e^{X_{n'n}} - b_n}{e^{Y_{n'n}} - 1} \right] \frac{g_{nn'}}{n'^3}\, \frac{2}{n^3}\, \frac{e^{X_n}}{\dfrac{1}{n'^2} - \dfrac{1}{n^2}} , \tag{6}$$

$$\int_{\nu_n}^{\infty} \bar{F}_{n\kappa}\, d\nu = N_i N_e \frac{K}{T_e^{3/2}} \frac{e^{X_n}}{n^3}\, \bar{S} \left\{ b_n \sum_{a=1}^{\infty} [\, -E_i(-a\,Y_n)\,] - \sum_{a=1}^{\infty} \left[-E_i\left(-Y_n \left\{ a + \frac{T_1}{T_e} \right\} \right) \right] \right\} , \tag{7}$$

where

$$\bar{g}_{n\kappa} = 1 \qquad \text{and} \qquad X_{nn'} = X_n - X_{n'} . \tag{8}$$

The expression for $\bar{F}_{nn'}$ follows from equation (3) if we interchange n'' with n, and n with n', etc. Further, we have considered the induced emissions as negative absorptions and hence have placed them in equations (6) and (7) rather than in equations (3) and (4). The quantity S_ν is a factor intended to account for the presence of absorption lines, which cause the radiation to depart from a true black-body distribution. (Note that S_ν could also be introduced as a dilution factor.)

A comment of some interest may be made on the bracketed factor in equation (6). In

thermodynamic equilibrium the factor reduces to unity. In the present case, however, $T_e = 35{,}000°$ and $T_1 = 6000°$. Thus we write the bracket as follows:

$$D = \frac{b_{n'} \exp\left[4.42\left(\frac{1}{n'^2} - \frac{1}{n^2}\right)\right] - b_n}{\exp\left[25.8\left(\frac{1}{n'^2} - \frac{1}{n^2}\right)\right] - 1}. \tag{9}$$

For $n' = 1$, this factor is essentially $5 \times 10^{-10}\, b_1$ for the higher n values. For $n' > 1$, the factor decreases. The bracket evidently behaves, in some respects, like a "pseudo-dilution factor," which varies with frequency. Thus we may well expect some of the same physical characteristics that would be present if the radiation field were, indeed, "dilute." We note that as n and n' become large, $b_n \to b_{n'} \to 1$, so that the bracket approaches $b_n \cdot T_1/T_e$ or about $b_n/6$ in the present case. Thus the asymptotic, low-frequency value of the pseudo-dilution factor is about $\frac{1}{6}$.

We proceed to consider the $C_{nn'}$. In general, it would appear that we might neglect collisional excitation by atoms relative to that by electrons. For the case of hydrogen, at least, this approximation seems valid. Considered as part of the spicule-jet, the hydrogen atom has a maximum velocity of about 90 km/sec. In a center-of-mass co-ordinate system, the corresponding energy is only about 20 e.v., the wrong order of magnitude to excite even the lowest level of hydrogen by collision with another *atom*. (The case of helium may provide an interesting exception to this question of excitation by atomic collision, and we shall return to the subject in another paper of the series.) Thus we consider electronic excitation only. Further, the electrons are thermal electrons, since the 90-km/sec velocity component by virtue of the jet motion is trivial compared with the thermal energy at 35,000°.

We have for the number of collisions per second per cubic centimeter, in which the atom is raised from level n to n'',

$$C_{nn''} = \pi a_0^2 N_n N_e 4\pi \left(\frac{m}{2\pi kT_e}\right)^{3/2} \int_{v_0}^{\infty} v Q_{nn''}(v, n, n'')\, v^2\, e^{-mv^2/2kT_e} dv, \tag{10}$$

where v is the electron velocity and v_0 corresponds to the lowest energy at which Q is not zero. Equations (10) include only excitations to higher levels; but, recalling the definition of the b_n, we may write the expression to include collisional de-excitations. We have

$$C_{nn''} = 4\pi^2 a_0^2 N_n N_e \left(\frac{m}{2\pi kT_e}\right)^{3/2} \left(1 - \frac{b_{n''}}{b_n}\right) \int_{v_0}^{\infty} v^3 Q_{nn''}\, e^{-mv^2/2kT_e} dv, \tag{11}$$

or, completely eliminating N_n and substituting $E = mv^2/2$,

$$C_{nn''} = \frac{4\pi^2 a_0^2}{m^2} N_i N_e^2 \left(\frac{h}{2\pi kT_e}\right)^3 b_n \left(1 - \frac{b_{n''}}{b_n}\right) \varpi_n\, e^{X_n} \int_{E_n}^{\infty} E Q_{nn''}(E, n, n'')\, e^{-E/kT_e} dE. \tag{11a}$$

We now proceed to consider the value of $Q_{nn''}$.

We wish to consider collisional excitation by thermal electrons at $T_e = 35{,}000°$. In the literature few values exist for the collisional cross-section at these relatively low energies. From experiment,[5] we have values for ionization from the ground state. There exists a rather complete set of theoretical calculations for excitation from the ground state by electrons of such high energies that the Born first-order approximation holds.[6] Mott and Massey[7] state that this first-order approximation should no longer give results

[5] Mott and Massey, *Theory of Atomic Collisions* (1st ed.; Oxford, 1933), p. 180.

[6] Bethe, *Handbuch der Physik* (2d ed.; Berlin: Springer, 1933), p. 519. [7] *Op. cit.*, p. 129.

as good as 10 per cent accuracy below about 100 e.v. An expression for slower electrons, taking into account exchange phenomena, has been given by Mohr and Massey.[8] They have evaluated a few cross-sections, but hardly enough for our present needs. Actually, by applying the first-order Born approximation to an electron having just the excitation energy of the level, we calculate a cross-section of 4.1 for Q_{12}. The value drops to 1 at 95 e.v. We use Mott and Massey's equation (40).[7] The more exact value of Massey and Mohr rises initially to about 2, then drops to 1 between 20 and 30 e.v. and thereafter decreases slowly. For the lower-velocity electrons, Massey and Mohr's values suffer from error in the same direction as did the original Born treatment, neglecting exchange, namely, the values are too high. If we may judge from the ionization cross-section, the error seems, however, less than about 70 per cent. It would seem, then, that if we simply adopted a cross-section of 1 out to 95 e.v., we should be well within a factor of 2 for the cross-section Q_{12}. For the higher levels, I have simply adopted the Born first-order dependence of Q_{1n}'' on n''. (Thus I have neglected the exchange term.) We have

$$Q_{1n}'' = \frac{16\pi^2}{v^2h^2a_0^2} |\, z_{1n} \,|^2 \, ln \, \frac{2mv^2}{E_n - E_1}, \tag{12}$$

where $|z|$ is the matrix element of z. Hence, apart from the logarithmic term, the dependence on n'' is that on the electric dipole moment. If we set

$$x' = \frac{E}{kT_e} \tag{13}$$

and evaluate the matrix element, we finally obtain

$$Q_{1n}'' = \frac{h^2}{3mkT_e 2\pi^2 a_0^2} \left[\frac{2^8 n^7 (n-1)^{2n-5}}{(n+1)^{2n+5}}\right] \frac{1}{x'} \, ln \left(\frac{4kT_e}{E_n - E_1} \, x'\right). \tag{14}$$

Use of equation (14) in equation (11*a*) will give a value of C_{nn}'' that is too high; so we simply take $Q_{12} = 1$ out to an energy of 95 e.v. (where the value 1 agrees with the predictions of eq. [12]) and use equation (14) thereafter. That is, we have

$$Q_{1n}'' = \frac{h^2}{3mkT_e 2\pi^2 a_0^2} \left[\frac{2^8 n^7 (n-1)^{2n-5}}{(n+1)^{2n+5}}\right] \frac{T_e}{35{,}000} \frac{ln4}{4.08 \cdot 3.32} \tag{15a}$$

$$\text{for } x' > \frac{1.55 \cdot 10^{-5}}{T_e}\left(1 - \frac{1}{n^2}\right) = X_{1n}$$

and equation (14) for

$$x' > 31.5 \, . \tag{15b}$$

We note that the factor $T_e/35{,}000$, in equation (15*a*), is introduced to retain the true independence of Q_{1n}'' of T_e. The apparent explicit dependence results only from the introduction of the parameter x'.

Essentially, energies above 95 e.v. contribute nothing to the integral (11*a*) for this case of $T_e = 35{,}000°$, so that equation (15*b*) may be ignored and the upper limit of the integral involving equation (15*a*) may be taken to be infinity. Using equation (15*a*), we obtain for equation (11*a*)

$$C_{1n}'' = b_1 \left(1 - \frac{b_n''}{b_1}\right) N_i N_e^2 \frac{A}{T_e} \left[\frac{n^{10}(n-1)^{2n-5}}{(n+1)^{2n+5}}\right] [X_{1n} + 1] \frac{e^{X_n}}{n^3} \varpi_1 , \tag{16}$$

$$A = \frac{h^5}{m^3k^2} \frac{2^6}{3\pi^3} \frac{ln4}{4.08 \cdot 3.32} \frac{1}{35{,}000} = 1.73 \cdot 10^{-24}.$$

[8] *Proc. R. Soc. London, A*, **132**, 605, 1931.

In a similar manner we evaluate the number of ionizations from the ground level. From the experimental results[5] we find that Q may be well represented by

$$Q = \frac{(E - 13.52)}{36.5} \qquad \text{for} \qquad E \leqslant 50 \text{ e.v.}, \tag{17a}$$

$$Q = 1.05 - 10^{-3}E \qquad \text{for} \qquad E \geqslant 50 \text{ e.v.} \tag{17b}$$

Hence we obtain

$$C_{1\kappa} = G(2 + X_1) N_i N_e^2 b_1 \left(1 - \frac{1}{b_1}\right), \tag{18}$$

$$G = \frac{a_0^2 h^3}{2\pi m^2} \frac{0.0274}{1.6 \cdot 10^{-12}} = 2.7 \cdot 10^{-32}.$$

Equations (16) and (18) account for the collisional transitions involving the ground level. Inclusion of collisional excitations from levels other than the first would necessitate an unwarranted amount of labor. On the basis of the foregoing comments on pseudo-dilution effects, we expect b_1 to be quite large, three or four orders of magnitude, at least, larger than the other b_n. Thus the contribution of the lower levels, by collisional excitation, is quite small relative to that from the ground level. For the higher levels, since b_n must approach 1 asymptotically, we expect detailed balancing to hold very nearly. Thus we do not expect an appreciable error to arise by a neglect of collisional excitation from levels other than the first.

We may inquire whether we are justified in retaining terms involving radiation excitation from levels $n > 1$ in view of the collisional-excitation neglect. Actually, the appreciable terms for both collisional and radiative excitation are those from the higher n. While in the collisional excitation we assume detailed balancing to hold, this assumption is not valid for the radiative case. There is thus some justification for retaining the radiative terms.

We have, then, for equation (1), substituting values from equations (2)–(18),

$$\frac{2N_i N_e K e^{X_n}}{T_e^{3/2} n^3} \left[\left\{ \sum_{n+1}^{\infty} \left[\left(b_{n''} - S_\nu \frac{b_n e^{X_{nn''}} - b_{n''}}{e^{Y_{nn''}} - 1} \right) \frac{g_{nn''}}{n''^3} \frac{e^{-X_{nn''}}}{\frac{1}{n^2} - \frac{1}{n''^2}} \right] \right.\right.$$

$$- \sum_{1}^{n-1} \left[\left(b_n - S_\nu \frac{b_{n'} e^{X_{n'n}} - b_n}{e^{Y_{n'n}} - 1} \right) \frac{g_{n'n}}{n'^3} \frac{1}{\frac{1}{n'^2} - \frac{1}{n^2}} \right] + \tfrac{1}{2} [-E_i(-X_n)] \tag{19}$$

$$\left.\left. + \bar{S}_\nu \left(-\frac{b_n}{2} \sum_{a=1}^{\infty} [-E_i(-a Y_n)] + \frac{1}{2} \sum_{a=1}^{\infty} \left[-E_i \left(-Y_n \left\{ a + \frac{T_1}{T_e} \right\} \right) \right] \right) \right\} + J \right] = 0,$$

where, for level n,

$$J = \frac{b_1 N_e A T_e^{1/2}}{K} \left\{ \frac{n^{10}(n-1)^{2n-5}}{(n+1)^{2n+5}} \right\} \{ X_{1n} + 1 \}$$

and, for level 1,

$$J = -\frac{b_1 A e^{-X_1} T_e^{1/2} N_e}{K} \left\{ \sum_{2}^{\infty} \left[\frac{n^{10}(n-1)^{2n-5}}{(n+1)^{2n+5}} \right] [X_{1n} + 1] \frac{e^{X_n}}{n^3} + \frac{G T_e}{A} (X_1 + 2) \right\}.$$

For computing purposes, these equations (19) may be re-written thus:
For b_n:

$$
\begin{aligned}
b_n \left\{ \frac{{}_g t_n}{2} - \frac{G_{1n}}{n^3}\tau_n + \frac{\bar{S}_\nu}{2}\sum_{a=1}^{\infty}\left[-E_i(-aY_n)\right]\right\} e^{X_n} \\
= \left\{ \frac{1}{2}\left[-E_i(-X_n) + \bar{S}_\nu \sum_{a=1}^{\infty}\left(-E_i\left[-Y_n\left(a+\frac{T_1}{T_e}\right)\right]\right)\right.\right. \\
\left.\left. + \left\{-E_i(-X_1) + \bar{S}_\nu \sum_{a=1}^{\infty}\left(-E_i\left[-Y_1\left(a+\frac{T_1}{T_e}\right)\right]\right)\right\}\tau_n e^{X_{1n}}\right] e^{X_n} \right. \\
\left. + \sum_{2}^{n-1} b_{n'}\left[G_{1n'}P_{n'}\tau_n + S_\nu \frac{e^{X_{n'n}} - \dfrac{b_n}{b_{n'}}}{e^{Y_{n'n}}-1} G_{n'n}\frac{e^{X_n}}{n'^3}\right] \right. \\
\left. + \sum_{n+1}^{\infty} b_{n''}\left\{\left[G_{nn''} + G_{1n''}\tau_n\right]P_{n''} - S_\nu \frac{\dfrac{b_n}{b_{n''}}e^{X_{nn''}} - 1}{e^{Y_{nn''}}-1} G_{nn''}P_{n''}\right\}\right\}
\end{aligned}
\tag{20}
$$

For b_1:

$$
\begin{aligned}
b_1 = \frac{1.85\cdot 10^{18}}{N_e T_e^{1/2}} \frac{1}{F(T_e, N_e)} \left\{ \sum_{2}^{\infty} b_{n''} G_{1n''} P_{n''} + \frac{1}{2}\left[-E_i(-X_1)\right.\right. \\
\left.\left. + \bar{S}_\nu \sum_{a=1}^{\infty}\left(-E_i\left[Y_1\left(a+\frac{T_1}{T_e}\right)\right]\right)\right] e^{X_1}\right\},
\end{aligned}
\tag{21}
$$

where we have used the symbols

$${}_g t_n = 2\sum_{1}^{n-1}\frac{G_{nn'}}{n'^3},$$

$$f(n) = \left[\frac{n^{10}(n-1)^{2n-5}}{(n+1)^{2n+5}}\right], \qquad \tau_n = \frac{q(n)}{F(T_e, N_e)},$$

$$g(n) = \left\{ f(n)[X_{1n}+1] + \frac{1.85\cdot 10^{18}}{N_e T_e^{1/2}} S_\nu G_{1n} \frac{e^{X_{1n}}}{e^{Y_{1n}}-1}\right\} e^{X_n},$$

$$\frac{g_{nn'}}{\dfrac{1}{n'^2} - \dfrac{1}{n^2}} = G_{n'n}, \qquad \frac{e^{X_n}}{n^3} = P_n,$$

$$
\begin{aligned}
F(T_e, N_e) = \left\{ \sum_{2}^{\infty}\left(f(n)[X_{1n}+1]P_n\right) + 1.54\cdot 10^{-8} T_e [X_1 + 2]\right. \\
\left. + \frac{1.85\cdot 10^{18}}{N_e T_e^{1/2}} e^{X_1}\left[\sum_{2}^{\infty}\frac{G_{1n''}S_\nu}{n''^3(e^{Y_{1n''}}-1)} + \frac{\bar{S}}{2}\sum_{a=1}^{\infty}\left[-E_i(-Y_1 a)\right]\right]\right\}.
\end{aligned}
$$

The system of equations (20) may be solved by successive approximation. The convergence is reasonably rapid, and the asymptotic value of b_n is clearly 1. Before considering the actual numerical solution, we may draw some rather important conclusions from equations (20) and (21).

Consider the four terms that contribute to $F(T_e, N_e)$. In the order in which they are

written above, these terms are: (*a*) collisional excitation to the discrete levels, (*b*) collisional ionization, (*c*) radiative excitation to discrete levels, and (*d*) radiative ionization. Consider the case where T_1 is held constant at the solar value of 6000°, and $S_\nu = 1$. Then for T_e about 35,000°, the term (*d*) is insignificant. Consider the value of F and b_1 as N_e varies. For sufficiently large N_e, term (*c*) is much smaller than (*a*). In the present instance, where we shall take for N_e the value at the base of the chromosphere,[2] 2×10^{11}, term (*c*) is about 2 per cent of (*a*). As N_e becomes sufficiently large, b_1 approaches closer to the order of magnitude unity. (We note that, if b_1 becomes much below about 100, our approximation of neglecting collisional excitations from levels lower than the first becomes invalid.) If, now, N_e decreases, term (*c*) gradually takes over the control of F. For example, at the top of the chromosphere, N_e is probably about 10^{-3} times its value at the bottom, and term (*c*) is about thirty times term (*a*). That is, the radiative excitation from level (1) far predominates, and F becomes about thirty times larger. From equation (21) we see that the result is also a decrease in b_n.

If we do not assume $S_\nu = 1$, the situation changes only in that much smaller values of N_e are required to make term (*c*) predominant. The value of S_ν depends, of course, on the depth of the absorption line. Clearly, a complete neglect of the radiation field, i.e., $S_\nu = 0$, assumes wholly black lines and neglects emission within the chromosphere. The quantity $S_\nu = 1$ assumes no absorption lines. The true situation must be intermediate between the two extreme cases.[9] We shall therefore carry out a numerical solution under the two assumptions to indicate the range of solution for b_n.

We may here comment on the solution by MABG. Their efforts were directed toward illuminating the problem of the planetary nebulae. In MABG XII, the N_e are determined for some typical planetaries and found to be about 10^4; T_e is 10,000° or less. S_ν, however, arises as a dilution factor, of the order of 10^{-15}. Also, $T_1 > T_e$ here, although it is probably not more than ten times greater than the 6000° value used in the calculations of the present paper. If we use these values to compute the relative magnitude of terms (*a*) and (*c*), we see that MABG were probably justified in neglecting term (*a*), collisional excitation, so long as T_1 has indeed the high value cited. If, however, this value drops by about half, the neglect of the term (*a*) is dubious. It is quite clear, however, that a direct application to the Wolf-Rayet stars of the MABG results for planetary nebulae is not justified. If we accept the results of Mrs. Shapley and Kopal for V 444 Cygni as typical,[10] we obtain for N_e a value of about 10^{12} for these stars. We must then include collisional-excitation terms in the theory before applying it to the Wolf-Rayet stars.

Returning to the problem at hand, we consider the manner of maintenance of the high T_e. From the discussion of Paper I, the high kinetic temperature is maintained by mechanical energy furnished by the spicule. From Paper I we see that the rate of supply of mechanical energy, per unit *volume* of the chromosphere, does not decrease so rapidly with height of penetration of the spicule into the chromosphere as does the chromospheric density. Thus the energy per gram of chromospheric material supplied by the spicule actually increases with chromospheric height. Consequently, we expect a rise of kinetic temperature with chromospheric height. Wildt's results indicate a mean T_e of some 35,000° up to about 2000 km. Hence, we shall confine our calculations to this region and

[9] In the present problem we carry through the treatment on the assumption that the radiation field is either not present or is characteristic of a black body at 6000°. We do *not* consider the problem of radiative transfer arising from the conversion of the mechanical energy of the spicule into energy radiated by electron capture. A completely exact treatment would include the energy radiated by the chromosphere. The energy clearly builds up in the lines, particularly in Lyman α. If, initially, the lines are black, we must obtain emission cores. Corresponding to the assumption of the 6000° black-body curve, we must obtain a greater radiation toward the violet than the black-body curve. The treatment of the present paper clearly assumes the effect to be negligible. The validity of the assumption is open to question. In any event, however, the direction of the effect is to cause the b_n to increase, $n > 1$.

[10] *Ap. J.*, **104**, 160, 1946.

shall return to the question of the chromospheric temperature gradient at another time. In the present paper, we simply seek to ascertain whether the order of magnitude of the energy furnished by the spicules agrees with the order of magnitude of the energy needed to support the 35,000° kinetic temperature.

II. NUMERICAL SOLUTION

In the final remarks of the preceding section we have indicated how the mechanical energy input of the spicule system may be expected to result in a chromospheric temperature gradient. We should expect to apply the method of Paper I directly to obtain the energy furnished by the spicule; to solve equations (20) and (21) of the present paper for the b_n values and hence obtain the energy radiated; and, finally, to balance the mechanical energy available against the net radiation in order to fix the steady-state kinetic temperature. Unfortunately, the numerical properties of the spicule system[11] are not yet well enough known to complete such a set of calculations. So we simply solve the set of equations (20) and (21), with the kinetic temperature 35,000° taken as applying to some region of the atmosphere. We shall obtain the physical conditions, as given by the b_n values, in that region. More elaborate calculations may be made by using the spicule system rather than the kinetic temperature as given, when more complete data become available for the spicules.

TABLE 1

	b_1	b_2	b_3	b_4	b_5	b_6	b_7	b_8	b_9	b_{10}
$S=1$.....	2.1×10^6	10.9	4.67	3.45	2.93	2.62	2.42	2.27	2.17	2.08
$S=0$.....	2.3×10^6	12.3	5.33	3.92	3.31	2.96	2.75	2.60	2.47	2.36

As stated above, we solve equations (20) and (21) under two assumptions. First, we neglect absorption lines or emission in the lines exceeding the black-body value and set $S = 1$. For the second case, we set $S = 0$. Here we assume that all the energy comes from the mechanical source. We use throughout the following values: $T_1 = 6000°$; $T_e = 35{,}000°$; and $N_i = N_e = 2 \times 10^{11}$. (The assumption $N_i = N_e$ does not, of course, enter into the determination of the b_n values.) We obtain the b_n values given in Table 1.

III. COMMENT ON THE b_n VALUES AND CONDITIONS WITHIN THE CHROMOSPHERE

The most immediately significant result follows from the value of b_1. Substituting back in equation (2), we see that there are only about 4×10^8 atoms in the ground level. Comparing this with the value 2×10^{11} for the number of ions, we find that the hydrogen is about 99.5 per cent ionized and that the density of hydrogen is essentially the ion density. These figures differ considerably from those obtained by Wildt.[2] We may, however, make several comments. First, the existence of the kinetic temperature forces the conclusions of the present paper upon us. The disagreement with Wildt's values results simply from the assumptions made. Wildt uses throughout an excitation temperature of 4830°. The choice of such a value in the regions where the density gradient indicates a kinetic temperature of 35,000° seems highly dubious, since the kinetic and electron temperatures must be identical. As Wildt points out, the choice of the excitation temperature does not alter the computed density gradient and hence the kinetic temperature; for these quantities are essentially fixed by the higher series members. The values of these latter are relatively insensitive to the temperature. The chief effect lies in the values computed for the absolute density and degree of ionization. Wildt has further shown that the 35,000° value must set in between about 200–500 km elevation. Hence our results must apply above, say, 500 km. If we take them directly at the 500-km

[11] Roberts, *Ap. J.*, **101**, 136, 1945.

level and apply a density gradient corresponding to a 6000° photospheric temperature, we obtain densities at the height 0 of about 10^{13} for hydrogen. This value is somewhat low; but, on the other hand, the values 10^{15}–10^{16} given by Wildt seem rather high. Since, of course, the values are highly sensitive to the particular height chosen—here 500 km—too strict an interpretation of the 10^{13} value would be unjustified. If, for example, we increase our height by 50 per cent, we raise the value to 10^{14}. On the other hand, if we realize that there must be at least a small region where the density gradient shifts from the 6000° value to the 35,000° value, we lower the absolute density value.

The predictions as to the high state of ionization of hydrogen in the chromosphere should hardly cause much concern. Indeed, observing the anomalous behavior of *He* I and *He* II in the chromospheric spectrum, one might be pleased by these results for hydrogen; for they indicate that an analysis similar to the present, carried out for helium, might be expected to "predict" the anomaly. Certainly, the rise to the 35,000° kinetic temperature indicates that the appearance of *He* I lower (in height) than *He* II is no anomaly.

We might consider this computation of the b_n values the essential result of the paper. While the value 35,000° that we have adopted might be altered (Redman suggests[3] 30,000° might be better), the 6000° value changed, and factors of 2 or so put into the electron density and collisional cross-section, etc., still the main qualitative features of the paper must stand. Thus, even though it should prove necessary to conclude that but 10 per cent of the hydrogen was ionized, the main features of the high-kinetic-temperature chromosphere are shown to require parameters quite different from the chromospheric thermodynamic equilibrium ones, particularly at 6000° or less.

We may, finally, perform a calculation of the energy needed to sustain the chromosphere at this high kinetic temperature. We note that the chief danger lies in an overestimation of the energy needed, for we have neglected the radiation from, and absorption within, the chromosphere itself. Thus, even though the energy radiated by the photosphere is completely null in Lyman α and violet-ward, still the chromosphere will build up energy in this region. In our computations we have, however, assumed that this energy can never exceed that of a 6000° black body. Again, however, we demonstrate an important consequence of this high chromospheric kinetic temperature—the increase of energy in the ultraviolet due to the conversion of mechanical energy into radiant.

IV. EMISSION OF RADIATION FROM THE CHROMOSPHERE

With the values of the parameters already given, we can compute the net radiation emitted (see Table 2).

TABLE 2

	$S=1$ (Ergs/Cm²Sec)	$S=0$ (Ergs/Cm²Sec)
Emission	2.85	3.20
Absorption	0.05	0
Net emission	2.8	3.2

We then compute the total emission from a shell 1 cm thick at the chromosphere base. We have

$$\text{Emission} = (4\pi R_{\odot}^2)\,(1)\,(\text{Emission/cm}^3\text{sec})$$

$$= 17 \cdot 10^{22}\ \text{erg/sec} \quad \text{for} \quad S = 1 \tag{22}$$

$$= 20 \cdot 10^{22}\ \text{erg/sec} \quad \text{for} \quad S = 0\ .$$

This emission we may compare with the energy input discussed in Paper I, where we computed the energy input into the whole chromosphere, taking broad averages. We see how sensitive is the determination of the energy radiated to the electron density, and so we cannot consider the chromosphere as a whole. Thus we consider the shell 1 cm thick. From equation (20) of Paper I we obtain

$$\text{Energy input} = \tfrac{1}{4} n_s \bar{c}_s 2\pi R_s \frac{v^2}{2} m_H N_s \,, \tag{23}$$

where the symbols denote, in order of occurrence: the spicule density, mean thermal velocity of the jet atoms, spicule radius, spicule velocity, mass of the hydrogen atom, and number of spicules over the solar surface of the "typical" type discussed in Paper I. The quantity $\bar{c}_s$ is proportional to the square root of the ratio of chromospheric density to spicule density and is 1.37×10^6 cm/sec for $T_e = 35{,}000°$ and a density ratio of unity. In Paper I we used a density ratio of 1/100. We also used a value 10^{15} for n_s; but, from the results of the present paper and the ratio 1/100, we should here use the value 2×10^{13}. Writing explicitly the values used, in the order of equation (23), we have

$$\begin{aligned} \text{Emission} &= \tfrac{1}{4}\,(2 \cdot 10^{13})\,(1.4 \cdot 10^5)\,(2\pi)\,(\tfrac{3}{2}\,725 \cdot 10^5)\,(\tfrac{81}{2}\,10^{12})\,(1.7 \cdot 10^{-24})\,10^4 \\ &= 3.10^{20}\ \text{erg/sec} \,. \end{aligned} \tag{24}$$

From these calculations, the spicule system would appear to fall short by about a factor of 600 of providing the energy needed to support the chromosphere. The discrepancy in these calculations is not, however, serious. First, we have neglected the transfer problem. Not only the effect of the chromospheric emission but also that of the chromospheric absorption of the "excess" radiation, which we have assumed entirely escapes the atmosphere, has been neglected. We note that this atmospheric absorption acts to decrease the discrepancy between the results of Table 2 and equation (24). We shall return to this problem in the next paper of the series.

We note also that the parameters of equation (24) are not too accurately known because of our lack of detailed knowledge of the spicule system. The results of these first two papers of the series seem to indicate the value of a more careful study of the spicule system. Dr. Roberts tells me that these additional observations will be carried out at Climax. We must recognize, of course, that any other supply of mechanical energy will satisfy the requirements of the present paper as well as will the spicule system. Thus the large prominences, etc., must contribute to the energy supply. The question simply is one of relative importance. If nothing more, these first two papers of the series should provide a useful guide to the phenomenological pattern to be expected if this interpretation of mechanical-energy supply for the solar chromosphere is correct.

In the next paper of the series, as mentioned, we return to consider the chromospheric radiation field. A consideration of the variance of the b_n values under a change in N_e and T_e will be presented, and the hydrogen density gradient, which differs from the emission gradient in as highly ionized an atmosphere as the present, will be considered.

I am indebted to Dr. Payne-Gaposchkin and to Dr. Menzel, who have read the paper and discussed with me several aspects of the problem. Again, I am indebted to Dr. Roberts for discussions over the general chromospheric problem.

NOTES

THE SPECTRUM OF THE ECLIPSING BINARY UX URSAE MAJORIS

This remarkable system has a period of only 4^h43^m. The spectrum was observed by Kuiper as that of a B3 subdwarf.[1] Since the apparent magnitude of the binary is 12.7 at maximum and the depth of the principal minimum is 1.0 mag., the star can be observed only with small dispersion. A new series of spectrograms was obtained at the McDonald Observatory with a Cassegrain quartz spectrograph whose linear dispersion is 220 A/mm at λ 3933. The spectrum undergoes remarkable changes in appearance. The velocities have been measured differentially against spectrogram Q*f*/1 10879, which has fairly strong *H* absorption lines. Later, this spectrogram was measured against another star whose radial velocity is about zero. In this manner the velocity of the standard plate of UX UMa was found to be about +245 km/sec. The velocities are subject to large errors, not only because of the small dispersion, but especially because of the varying intensity of the absorption lines. The results are presented in Table 1 and are intended to give only the order of magnitude of the radial velocities. The phases were computed with Krat's elements (*Poulkovo Obs. Circ.*, No. 30, 1940). Principal minimum = JD 2427341.222+0.19667138E.

TABLE 1

OBSERVATIONS OF UX URSAE MAJORIS

Plate Q*f*/1	Date 1948	U.T.	Phase	Vel. (Km/Sec)	Description		
					H Abs.	*He* I Abs.	*Hβ* Em.
10872	May 6	3^h21^m	3^h11^m	+245	Weak	Absent	Present
73	6	4 16	4 06	+261	Strong	Strong	Absent
74	6	5 07	0 13	−135	Weak	Weak	Absent
75	6	5 49	0 55	−325 (?)	Very weak	Very weak	Strong
79	7	2 58	3 12	+245	Fairly strong	Weak	Strong
80	7	3 47	4 01	+120	Very strong	Strong	Absent
81	7	4 42	0 13	−235	Very weak	Very weak	Absent
82	7	5 24	0 55	− 55 (?)	Very weak	Very weak	Strong
83	7	6 04	1 35	+145 (?)	Weak	Weak	Weak

These elements satisfactorily represented the photometric observations from 1933, when S. Beliavsky discovered the variation, to 1939, when Krat's observations were made. An observation of principal minimum by Lange[2] on JD 2430960.171 fits these elements well. It is probable that the elements are still quite reliable. From the velocities we see that minimum occurred at about phase 1 hour, with $V = -250$ km/sec, and maximum at phase 3 hours, with $V = +250$ km/sec. Disregarding the eccentricity and adopting $V_0 = 0$ km/sec, we have, roughly, $K_1 = 250$ km/sec and, consequently,

$$a_1 \sin i = 7 \times 10^5 \text{ km}; \quad \frac{m_2^3}{(m_1 + m_2)^2} \sin^3 i = 0.3 \odot .$$

[1] *Pub. A.A.S.*, **10**, 206, 1941.

[2] *Kasan Astr. Circ.* No. 26, p. 6, 1944. I am indebted to Dr. N. L. Pierce for this reference.

From the photometric solution we know that sin $i \sim 1.0$. Hence $a_1 = 7 \times 10^5$ km; and, if we arbitrarily assume $m_1 = m_2$, we find $m_1 = 1 \odot$. It must be remembered, however, that the mass function is very sensitive to K_1 and that this latter has been determined only very roughly. Nevertheless, the character of this system is fairly well established.

The spectral variations are especially noteworthy. The *H* and *He* I absorption lines are strong and not particularly broad or shallow at phase 4 hours, or about 1 hour before principal mid-eclipse. The Balmer series can be seen as far as *H*15. Unless the ephemeris based upon Krat's elements is no longer accurate, this cannot be due to the spectrum of the secondary. It may be caused by a mass of gas at relatively low pressure on that hemisphere of the primary which is visible when this component is receding. Emission lines are present when the absorption lines are almost invisible. Only $H\beta$ is clearly seen as a rather diffuse, bright line of slightly greater intensity than that of the neighboring continuous spectrum. At these phases $H\gamma$, $H\delta$, etc., are completely invisible, and only the barest traces of the higher Balmer lines can be seen in absorption. The corresponding radial velocities are especially difficult to measure. The emission lines are too elusive for measurement.

OTTO STRUVE

McDONALD OBSERVATORY
May 1948

PECULIAR FEATURES IN THE SPECTRUM OF α VIRGINIS

In June and July, 1945, Dr. Carlos U. Cesco obtained a series of coudé spectrograms of α Virginis at the McDonald Observatory. Most exposures were made on Eastman II-O emulsion, with a dispersion of 3.8 A/mm at λ 4405. An examination of these spectrograms has brought out several interesting features.

On July 1.159 and 5.128 the phases, as computed with the elements by Struve and Ebbighausen,[1] were 0.660 and 0.615 days. Thus both plates were taken close to the epoch of conjunction, with the principal component behind the secondary component. Since the period is 4.014160 days, they were separated by a single revolution. Both spectra show a peculiar central reversal in *He* I 4472 and *Mg* II 4481. Such reversals, or tendencies to appear double, have been suspected on some previous occasions, but they were not sufficiently pronounced to justify an announcement. The present evidence is much more reliable, despite the fact that the dark reversal in *He* I 4472 on July 1 looks slightly bent. The reversals of *Mg* II 4481 are quite normal. This phenomenon is not always present at superior conjunction of the principal component. It represents a temporary phenomenon, perhaps in the nature of a large area of disturbance on that side of the primary which is directed toward the secondary. This area was present in two successive revolutions It was not definitely observed on June 27 or on July 13 and 17. There were no observations at similar phases in other revolutions. In this connection it is of interest to point out that the greatly broadened rotational profile of the primary acts somewhat like a spectroheliogram in one co-ordinate: it distinguishes between differences of surface brightness of different strips on the apparent disk of the star having different projected velocities of rotation.

The rest of the observations illustrated in Figure 1 confirm and extend our previous knowledge of the two components. The secondary lines are even more narrow than was known from the Yerkes three-prism spectrograms. They are stronger when they are displaced toward the violet than when they are displaced toward the red. There is an indication that these sharp lines are superposed over broad and exceedingly faint lines

[1] *Ap. J.*, **80**, 365, 1934.

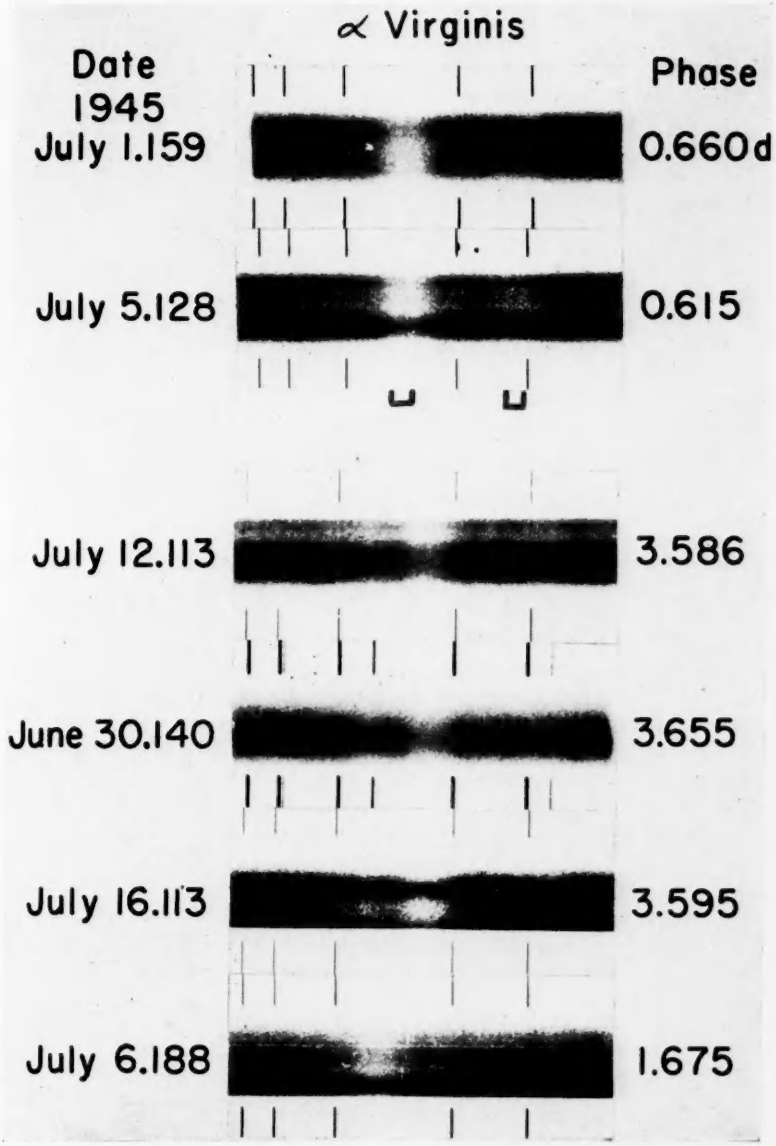

FIG. 1.—The spectrum of α Virginis. The spectrograms of July 1 and 5 were taken near the phase of superior conjunction of the primary component. The strong line *He* I 4472 and the weak line *Mg* II 4481 appear double. This phenomenon was not observed at inferior conjunction.

whose profiles are similar to those of the primary. The narrow profile may be caused by reflection.[2] The narrow secondary component of *Mg* II 4481 is relatively much stronger than that of *He* I 4472. Thus the spectral type of the secondary, or at least its narrow-lined "hot spot," has a spectral type which is later than that of the primary—B5 as against B2.

OTTO STRUVE

McDONALD OBSERVATORY
May 8, 1948

AN ATTEMPT TO DETECT POLARIZATION IN THE *Ca* II EMISSION LINES OF AR LACERTAE

A Wollaston prism was mounted in front of the slit of the Cassegrain spectrograph of the McDonald Observatory, so that both plane-polarized beams could enter the slit. Since the beams are deviated from their original direction by almost equal angles, they fall upon the collimator some distance apart. Each beam fills approximately half the aperture, so that on the plate there are formed two separate strips, corresponding to the planes of polarization that are parallel and perpendicular to the slit. The entire spectrograph could be turned in position angle in order to record different orientations. The spectrograph was equipped with quartz prisms and with a 500-mm UV camera giving a linear dispersion of 40 A/mm at λ 3933.

The eclipsing variable AR Lac has bright lines of *Ca* II in the spectrum of its secondary, K0, component.[1] Since these lines are probably produced by fluorescence in a localized cloud[2] at the extremities of the tidal bulges of the K0 star, it was interesting to determine whether the light of these lines is polarized. In harmony with R. W. Wood's[3] experiments with the vapors of sodium, iodine, and other gases illuminated from a direction which makes an angle of 90° with the direction of observation, we might expect a maximum of about 20 per cent of polarization at phases 0.25*P* and 0.75*P*.

Observations were obtained at three different phases, and with two different orientations of the slit, as shown in the accompanying tabulation. There was no evidence of

Plate	Date 1947	Phase	P.A. of Slit	Exposure (Minutes)
CQ 6120	Oct. 15.135	0.380P	90°	60
6121	Oct. 15.190	.407P	45	85
6122	Oct. 16.124	0.878P	90	197

polarization on any of the plates. Figure 1 shows the profiles of *Ca* II K in the two spectra of October 16. The abscissae are angstrom units, the ordinates are percentages of absorption. The two emission components are very nearly identical: the measured total energies are in the ratio of 1.00 to 0.85. This difference is within the probable error of measurement. The other two exposures, although obtained at other phases, show no measurable differences. If we estimate that the errors of measurement prevent us from

[2] *Ap. J.*, **86**, 198, 1937.

[1] A. B. Wyse, *Lick Obs. Bull.*, **17**, 39, 1934; W. A. Hiltner, *Ap. J.*, **106**, 481, 1947.

[2] The localization of the *Ca* II emission areas has not been investigated in AR Lac but is inferred from the fact that it has been found in RZ Cnc and RW UMa.

[3] *Physical Optics* (3d ed.; New York: Macmillan Co., 1934), p. 634.

finding a ratio of the intensities larger than $r = 0.85$, then we would find that the corresponding ratio of polarized to total light is

$$\frac{\text{Polarized}}{\text{Total}} = \frac{1 - r}{1 + r} = 8 \text{ per cent}.$$

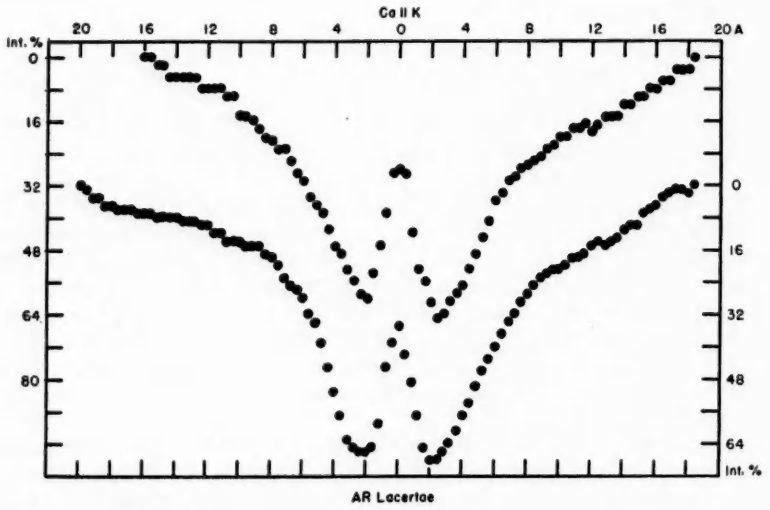

FIG. 1.—Profiles of *Ca* II K in AR Lacertae

Our test suggests that the degree of polarization of the *Ca* II emission lines cannot be much larger than about 10 per cent.

OTTO STRUVE

McDONALD OBSERVATORY
May 6, 1948

THREE Be STARS SHOWING BRIGHT LINES OF *Fe* II

In the course of an investigation of the rotational velocities of the brighter Be stars of spectral types B2–B5, three stars have been found to have spectra showing bright lines of *Fe* II, similar to the bright-line spectrum of φ Persei (see Table 1).

TABLE 1

NEW *Fe* II EMISSION STARS

HD	MWC	α(1900)	δ(1900)	m	Sp	*Fe* II Int. (φ Per = 4)	Date of Plate
45995	146	6^h25^m6	+11° 19′	5.8	B2ne	2	Mar. 4, 1948
60855	565	7 31.4	−14 16	5.6	B5ne	1	Jan. 27, 1948
208682	381	21 52.9	+64 52	5.8	B3ne	1	Sep. 1, 1947

A plate of HD 45995, taken by W. W. Morgan on December 23, 1943, shows *Fe* II emission to be present but considerably weaker than that shown on recent plates. $H\beta$ is also weaker in emission in 1943 than in 1948.

A comparison of the recent plate with one obtained by Merle Tuberg on February 1, 1944, indicates that the emission spectrum of HD 60855 has not changed noticeably during this interval of time.

The spectrum of HD 208682 fails to show any trace of *Fe* II emission on a plate taken by Morgan on August 13, 1943, although the strength of $H\beta$ emission is about the same.

The spectrograms of 1947–1948 were obtained with a small spectrograph attached to the 40-inch, which gives a dispersion of 60 A/mm at $H\gamma$; they were greatly widened to bring out diffuse emission and absorption features.

ARNE SLETTEBAK

YERKES OBSERVATORY
April 1948

THE PURITY OF INTERSTELLAR *Hα* EMISSION*

In 1938 Struve and Elvey[1] used the McDonald nebular spectrograph[2] to measure the intensity of *Hα* emission from interstellar hydrogen clouds. From these results the density of interstellar hydrogen has been estimated[3] as 3 atoms per cubic centimeter. However, W. H. Wright pointed out[4] that the intensity measurements might be in error because of the blending of *Hα* (λ 6563) with the forbidden *N* II doublet (λ 6548, λ 6584). On the prism spectrograms of Struve and Elvey, with a dispersion of 1000 A/mm at *Hα*, these lines could not be resolved.

The recently completed B-spectrograph of the McDonald Observatory, a fast grating instrument to be described in detail elsewhere, has been used in a nebular-spectrograph arrangement to separate and measure the relative intensities of *Hα* and [*N* II] λ 6584 in six of the emission regions observed by Struve and Elvey. The spectrograph was originally designed by Horace W. Babcock and consists of an *f*/4 parabolic collimator mirror of 2 inches aperture and 7.65 inches focal length; a plane aluminum-on-glass grating of 15,000 lines per inch, ruled by H. D. Babcock; and a solid *f*/0.65 UV glass Schmidt camera of 1.33 inches effective focal length, made by D. O. Hendrix.

Spectra were taken on Eastman 103*a*-F film, hypersensitized in an ammonia bath, cut to 5/8 × 5/8 inch and pressed into contact with an oiled concave surface (radius of curvature 2 inches) on the front of the solid Schmidt block. Another part of each hypersensitized sheet of film was exposed for an equal time in a spot sensitometer with a filter transmitting λλ 6300–6900 (the limit of the 103*a*-F emulsion sensitivity) and developed with the spectrogram. With *Hα* centered, the spectra are in good definition from λ 5900 to λ 6900, with an approximately linear dispersion of about 350 A/mm.

In order to reproduce the wide-angle coverage of the McDonald nebular spectrograph, a small *f*/3.5 quartz-fluorite lens of 77.7-mm focal length was mounted in front of the slit. This focused on the slit a strip of the sky 10° long and 13′ wide (for slit width of 0.30 mm), the central portion, 5° long, being unvignetted. The scale on the spectrograms is 4°.16 per millimeter, perpendicular to the dispersion.

The spectrograph and "telescope" were mounted as a unit, with the slit east-west, on the frame of the 20-inch Schmidt telescope of the McDonald Observatory and were lined up with the guide telescope, with the aid of a bright star.

Table 1 shows pertinent data on spectra obtained with this arrangement. The co-ordinates of the center of the slit are estimated to be accurate to ±20′. Guiding was accurate to ±10′.

* *Contributions from the McDonald Observatory, University of Texas*, No. 152.

[1] *Ap. J.*, **88**, 364, 1938; **89**, 119, 517, 1939.

[2] *Ap. J.*, **87**, 559, 1938.

[3] O. Struve, *Proc. Nat. Acad. Sci.*, **25**, 36, 1939; B. Strömgren, *Ap. J.*, **89**, 526, 1939.

[4] *Ap. J.*, **89**, 525, n. 14, 1939.

Figure 1 is an unretouched 30× enlargement of spectrum TB 187 beside its microphotometer tracing to the same scale. From this and other tracings, the intensity ratios of Table 1 were determined. They have an internal probable error of ±20 per cent. It is at once apparent that the intensity of *Hα* measured by Struve and Elvey is not appreciably affected by the [*N* II] λ 6548, λ 6584 doublet. The intensity of the fainter line, λ 6548, is theoretically[5] one-third that of λ 6584, a value confirmed by measured line intensities in bright gaseous nebulae,[6] although λ 6548 has not been measured on these spectrograms.

TABLE 1

SPECTRA OF *Hα* EMISSION REGIONS

Film No. (TB)	Region	Center of Slit (1950)		Slit Width*	Exposure	Date (January 1948)	Length of *Hα* (E–W)	Intensity *Hα*/λ 6584
		α	δ					
162.....	NGC 1499	3^h57^m	+36°04′	0.20	1 hr.	9/10	1°.2	.....
166.....	NGC 1499	3 57	+36 04	.20	2 hr.	10/11	2.1	2.1
190.....	NGC 1976	5 32.8	− 5 25	.30	1, 2, 5 min.	14/15	0.15	5.9
173.....	NGC 1977	5 32.7	− 4 52	.20	3 hr.	11/12	0.25	3.6
183.....	NGC 1977	5 32.9	− 4 52	.30	2½ hr.	12/13	4.5	2.4
172.....	IC 434	5 37.6	− 2 37	.20	3 hr.	11/12	1.4	1.5
179.....	IC 434	5 37.5	− 2 32	.30	2½ hr.	12/13	6.3	3.2
165.....	NGC 2024	5 38.3	− 1 51	.20	2 hr.	10/11	2.0	2.0
187.....	Struve 41	5 44.2	+ 1 09	.30	8½ hr.	13/14	3.5	4.3
189.....	Struve 41	5 44.9	+ 1 09	.30	4 hr.	14/15	4.8	.....
178.....	NGC 2237	6 29.3	+ 4 57	.20	2½ hr.	11/12	1.7	10.
189.....	NGC 2237	6 29.3	+ 4 57	.30	1½ hr.	12/13	1.5	6.
191.....	NGC 2237	6 30.4	+ 7 00	0.30	4 hr.	14/15	0.6	.....

* 0.20-mm slit width corresponds to 8′. 0.30-mm slit width corresponds to 13′.

The relative intensities of the [*N* II] and [*S* II] λ 6717, λ 6731 doublets in these faint emission clouds will be discussed in more detail elsewhere.

I am grateful to Professor Bengt Strömgren for suggesting this investigation, and to Professor Struve for discussing the results.

THORNTON PAGE

McDONALD OBSERVATORY
March 15, 1948

[5] I. S. Bowen, *Rev. Mod. Phys.*, **8**, 68, 1936.

[6] W. H. Wright, *Pub. Lick Obs.*, **13**, 193, 1918.

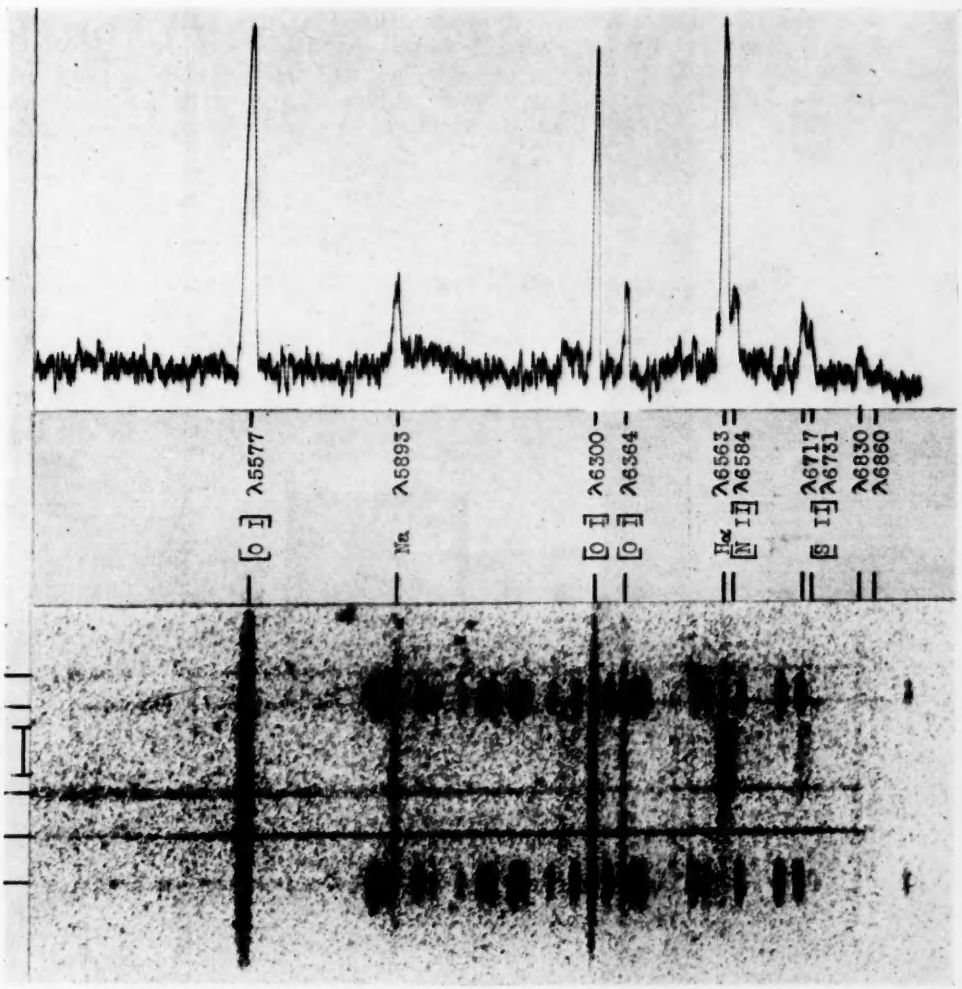

FIG. 1.—Spectrum of the "outer loop" of Orion. TB 187 enlarged 30×. Slit east-west, center $\alpha 5^h44^m2$; $\delta+1°09$; Star *A:* BD+1°1168; *B:* BD+0°1208; *C:* BD+1°1126; *D:* BD+1°1105; *E:* BD+0°1138 (*Ne* comparison spectrum).

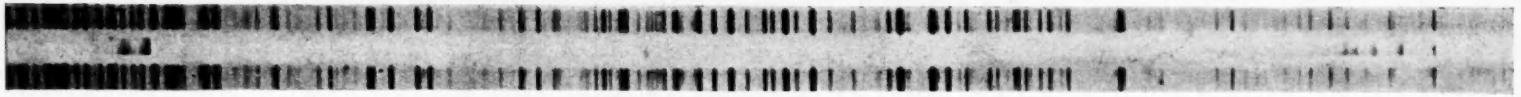

a

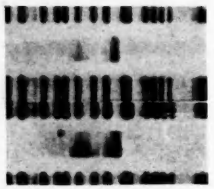

b

FIG. 1.—*a*, the spectrum of Comet 1947n taken on December 13.033, 1947 (U.T.). *b*, the band of *CN* ($\Delta v=0$) on the two spectrograms obtained in Bosque Alegre

THE SPECTRUM OF COMET 1947n

The spectrum of the head of Comet 1947n has been obtained with the Wood grating spectrograph attached to the 60-inch reflecting telescope at the Bosque Alegre Astrophysical Station of the Córdoba Observatory, which gives a dispersion of 40 A/mm. Two spectrograms (S 701 and S 708) were taken on December 12.029 and December 13.033, 1947 (U.T.) on Eastman 103 *a*-O emulsion with equivalent slit-widths of 1.5 A and 1.8 A and exposure-times of 45 and 59 minutes, respectively. The heliocentric distances of the comet, at the times of mid-exposure, were 0.410 and 0.442 A.U., according to Bobone's preliminary parabolic elements.[1] The estimated diameter of the head was about 10″.

TABLE 1

THE SPECTRUM OF COMET 1947n

Measured Wave Lengths	Estimated Intensities	Measured Wave Lengths	Estimated Intensities
3854.6	0–1	3881.9, 3883.6	Overexp.
3858.6	1	4215.8	2
3862.4	2	4677.6	6
3864.8	3	4684.7	7
3866.2	10	4696.9	7
3867.7, 3869.9	3	4715.0	8
3873.2	3	4736.7	8
3877.8	5		

The spectrum of the comet (Fig. 1) shows a fairly weak reflected solar spectrum and conspicuous bands of *CN* corresponding to $\Delta v = 0$ and of C_2 corresponding to $\Delta v = 1$ (Swan bands). There are also present the band at λ 4216 due to *CN* ($\Delta v = -1$), relatively weak, and extremely faint features belonging to the λ 4050 group and to the $\Delta v = 2$ sequence of C_2.

The structure of the *CN* band at λ 3883 is also shown in Figure 1, and the measured wave lengths and the estimated intensities are listed in Table 1.

JORGE SAHADE

OBSERVATORIO ASTRONÓMICO NACIONAL
CÓRDOBA, ARGENTINA
February 24, 1948

THE LUMINOSITIES OF TRUMPLER'S STARS

Since Trumpler[1] published his investigation concerning the red shifts in class O stars, the effective temperature of B0 stars has become better known.[2]

The analysis of the atmospheres of B0 stars which has recently been carried out indicates that the radiation emitted in wave lengths to the red of the limit of the Lyman series is large enough to raise the effective temperature of the star to at least 35,000° K with a boundary temperature of 25,000° K.[3] Nevertheless, the radiation in the photographic region of the spectrum corresponds to a temperature of about 28,000° K, which

[1] Harvard Announcement Card No. 865.

[1] *Pub. A.S.P.*, **47**, 249, 1935.

[2] A. Unsöld, *Zs. f. Ap.*, **21**, 229, 1942; M. Rudkjøbing, *Publ. Medd. Københavns Obs.*, No. 145, 1947.

[3] Rudkjøbing, *op. cit.*, p. 57.

is not very different from the effective temperature of 26,000° K assumed by Trumpler for a B0 star. Consequently, the radius and the mass as calculated by Trumpler from the absolute photographic magnitude and the red shift will not change their orders of magnitude by a calculation based on the revised values of the temperatures. However, the effective temperature being 35,000° K instead of 26,000° K, the star will be about 1.3 mag. brighter bolometrically. A change in luminosity of this order of magnitude will just bring the Trumpler stars on the mass-luminosity-curve (cf. the diagram on p. 255 of Trumpler's paper). It would therefore seem that these stars are not so "underluminous" as they have been generally considered to be.

MOGENS RUDKJØBING

YERKES OBSERVATORY
July 23, 1948

EMISSION LINES OF *Ca* II IN X CYGNI

The star X Cygni is now being observed spectrographically at the McDonald Observatory for the purpose of redetermining its radial velocity-curve. The plates are being obtained at the Cassegrain focus of the 82-inch telescope with two quartz prisms and a 500-mm camera. This combination gives a dispersion of 40 A/mm at λ 3930.30. Particulars for the plates already available are given in Table 1. For the computation of the phases the following expression was used: Phase = JD 2421511.892 + 16^d.385680E. Phase 0.000P then corresponds to maximum brightness.

TABLE 1

SPECTROGRAPHIC OBSERVATIONS OF X CYGNI

No.	Date (1948)	U.T.	Phase	Emission of *Ca* II
CQ 6942	May 16	10^{h}13^m	0.061P	Strong
43	May 16	10 35	.062	Strong
44	May 16	11 10	.063	Strong
48	May 17	9 54	.121	?
49	May 17	10 06	.122	?
51	May 17	10 38	.123	?
54	May 19	8 29	.240	None
62	May 28	10 33	.796	None
63	May 28	10 59	.797	?
65	May 29	10 30	.857	?
66	May 29	10 58	.858	?
69	May 30	10 27	.918	Strong
70	May 30	10 51	.919	Strong
73	May 31	10 12	.978	Faint?
74	May 31	10 41	.979	Faint?
77	June 2	11 29	.103	Faint
78	June 3	9 21	0.159	None

An inspection of these plates showed the following remarkable peculiarities: those of May 16, taken shortly after maximum, at phase 0.062P, exhibited strong H and K lines of *Ca* II, with a pronounced emission line on the violet wing; these emission lines had almost disappeared on the plates taken on May 17, at phase 0.121P. A close inspection revealed, however, that the violet wing of the absorption lines was somewhat more abrupt than was the red one, as if a remnant were left of the emission of the night before.

Figure 1 shows these features clearly. The gradual fading-out of the emission lines was checked by plate CQ 6977, June 2, phase 0.103P, which showed a faint but unmistakable

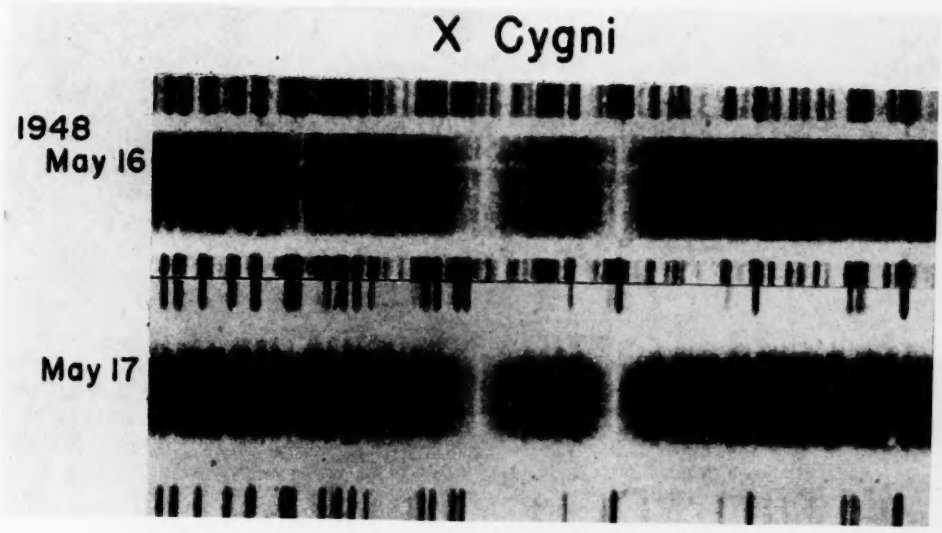

FIG. 1.—The *Ca* II lines of X Cygni

emission. No emission is visible at phases farther down the descending branch of the light-curve.

As for the ascending branch of the light-curve, there is again strong emission at phase 0.918*P* (plates CQ 6969 and 6970), while this was still absent on the plate CQ 6965, taken the night before at 0.857*P*. The emission lines again fade away on the steep portion of the ascending branch of the light-curve; the two plates of May 31 at 0.978*P* show only faint remnants of the strong lines of the night before.

Summarizing, we can say that, from the material now available, the emission seems to occur shortly after a sharp increase in brightness has come to a standstill (primary maximum) or has been slowed down (end of the hump on the ascending branch of the light-curve). With respect to the observed radial velocities derived from the absorption lines, the phenomenon can perhaps also be described in this way: the emission occurs whenever the outer layers, where the emission is believed to originate, undergo an expansion.

In order to find a provisional value of the difference in radial velocity between the emission and the absorption lines, rough measurements were made on plates CQ 6942, 6943, and 6944 of mean phase 0.062*P* and on plates CQ 6969 and 6970 of phase 0.918*P*.

The *Fe* I lines λλ 4005.25, 4045.82, 4063.60, and 4071.74 were used for this comparison. The result of these measurements was:

Phase 0.062*P:*

$$\overline{V_{em}} - \overline{V_{abs}} = -89 \text{ km/sec} \pm 8 \text{ km/sec (m.e.)};$$

Phase 0.917*P:*

$$\overline{V_{em}} - \overline{V_{abs}} = -84 \text{ km/sec} \pm 4 \text{ km/sec (m.e.)}.$$

Thus the difference in radial velocity between the two kinds of lines seems to be almost constant, but the excess of one velocity over the other measures about four times the semiamplitude of the radial velocity derived from the absorption lines.[1] The difference in the corresponding velocities of expansion should be even greater, as allowance must be made for differential limb darkening.

I wish to express my gratitude to the Belgian American Educational Foundation, Inc., in New York, for the grant of a fellowship advanced by the Commission for Relief in Belgium, and to Dr. O. Struve for his assistance and encouragement.

A. Van Hoof

McDonald Observatory
Fort Davis, Texas
June 5, 1948

[1] J. C. Duncan, *Ap. J.*, **53**, 95, 1921.

REVIEWS

L'Espace interstellaire. By HENRI MINEUR. Paris: Presses Universitaires de France, 1947. Pp. 276. Fr. 220.

The task of writing a truly popular book is by no means easy; Dr. Mineur has performed this task in an admirable way. Starting from elementary matters like the definition of stellar magnitudes and the wave length of light, he proceeds to spectroscopy and the Bohr atom and gradually develops the whole field of gaseous nebulae and interstellar matter. A clear style, many examples, and the constant emphasis on the main line of the exposition make the book pleasant reading. As an inspiring survey for the layman, this book may certainly be called successful.

Some popular books are also suitable as introductory textbooks for students. In this respect the book is less useful, because it is not up to date. Several sections seem to be inspired by the conference at Paris in 1937,[1] and subsequent discoveries have received comparatively little attention. For instance, the interstellar absorption coefficient is still estimated at 0.7 mag/kpc, and the interstellar particles are called "metallic." Stebbins' work on color excesses is not mentioned, nor is there any discussion of the multiplicity of interstellar lines. The list of molecules identified in interstellar space does not yet include CH^+. On page 211 it is surprising to find the final explanation of the "nebulium problem," which is one of the main themes of the book, followed by the statement that the mystery of coronium still remains. (Edlén published the identifications in 1941.) Such a time lag does not, however, affect the merits of the book as a popular work.

Some points of actual confusion were noted. All galactic nebulae are consistently called "gaseous nebulae." This leads to the queer description of a reflection nebula as a gaseous nebula consisting of solid particles. On the central stars of planetary nebulae we read that they are the "so-called white dwarfs" (p. 29) and that a nova after explosion becomes a Wolf-Rayet star surrounded by a planetary nebula (p. 221). The formula on page 245 gives twice the correct value of the energy density of diluted radiation.

The book is printed attractively and has good illustrations. It is one of a popular series: "La Science vivante."

H. C. VAN DE HULST

Yerkes Observatory

[1] *Ann. d'ap.*, 1, 1, 1938.